ST. ANTHONY FALLS LABORATORY

Engineering, Environmental and Geophysical Fluid Dynamics

SAFL Project Report No. 611

A Field Study of Recreational Powerboat Hydrodynamics and their Impacts on the Water Column and Lakebed.

By:

Andrew Riesgraf, Jeffrey Marr, William Herb,

Matthew Lueker, Jessica Kozarek

St. Anthony Falls Laboratory, University of Minnesota, 2 Third Ave SE, Minneapolis, MN 55414

Prepared for:

St. Anthony Falls Laboratory

July 2025

Minneapolis, Minnesota

(This page intentionally left blank)

ACKNOWLEDGEMENTS

The first research report to come from SAFL's Healthy Water Initiative Program characterized the divergent wake waves produced by various recreational boats, including wakeboats (Marr et al. 2022). This first phase of research was fully funded by crowdfunding and its success was the catalyst for the second phase of research reported here. This second research phase on water column and lake bottom impacts caused by recreational powerboats, including wakeboats, was funded via crowdfunding and the Minnesota Environment and Natural Resources Trust Fund (ENRTF) as recommended by the Legislative-Citizen Commission on Minnesota Resources (LCCMR).

We want to thank everyone who made contributions to this second round of crowdfunding. We are grateful to all the donors who supported our research team at the University of Minnesota to execute high-quality, independent, and unbiased research. It is important to note that crowdfunding donors had no input in the design, methods, analysis, results, or recommendations of this study.

We want to thank the ENRTF for funding a third phase of research that will run for three years (2023-2026). The Trust Fund is a permanent fund constitutionally established by the citizens of Minnesota to assist in the protection, conservation, preservation, and enhancement of the state's air, water, land, fish, wildlife, and other natural resources. Currently, 40% of net Minnesota State Lottery proceeds are dedicated to growing the Trust Fund and ensuring future benefits for Minnesota's environment and natural resources. Year one of this funding enabled our team to complete additional fieldwork that was needed to publish this phase 2 report.

Thank you to Professor Kimberly Hill (UMN-SAFL Affiliated Faculty) for her valuable input during the project design and data analysis phases of the project. We also want to thank those who made the fieldwork campaigns possible. Thank you to the captains of the test boats, who were also the owners of the boats. We are grateful to the Jabbour and Bendt families for allowing their properties on Lake Minnetonka to serve as home bases for this study. Having access to their property, shoreline, and docks was essential in executing a field study of this magnitude and

complexity. We want to thank our fellow SAFL colleagues Bryce Daniels, Chris Milliren, Chris Feist, Erik Steen, Tyler Novotny, Matilde Pratas Fernandes, and Matt Hernick for their vital help during the fieldwork campaigns, and Joe Miller and Michelle Andruss for reviewing a near final draft of this report.

Finally, a big thank you to Dr. Maricarmen Guerra Paris (Assistant Professor, Departamento de Ingeniería Civil, Universidad de Concepción), Dr. Catherine L. Hein (Research Scientist, University of Wisconsin-Madison, Center for Limnology), and Dr. Danielle Wain (Lake Science Director, 7 Lakes Alliance) for volunteering their time to independently review this report. Their expertise in the subject matter and willingness to provide thorough and constructive comments greatly improved this report.

INDEPENDENT TECHNICAL REVIEW PROCESS

This report has undergone an independent technical review by subject matter experts not affiliated with the University of Minnesota. The reviewers were Dr. Maricarmen Guerra Paris (Assistant Professor, Departamento de Ingeniería Civil, Universidad de Concepción), Dr. Catherine L. Hein (Research Scientist, University of Wisconsin-Madison, Center for Limnology), and Dr. Danielle Wain (Lake Science Director, 7 Lakes Alliance). The authors sent the reviewers the draft report and associated materials (appendix, videos) in April 2025. The three reviewers provided detailed feedback as comments and markup. The authors integrated the feedback into a revised report that was then sent to each reviewer individually. The reviewers were provided with the opportunity to review the revised report and each concurred that the authors had sufficiently considered and incorporated their feedback. Each reviewer approved the publishing of the final version presented here. The final version was published through the University of Minnesota's Digital Conservancy in July 2025.

(This page intentionally left blank)

TABLE OF CONTENTS

(This page intentionally left blank)

EXECUTIVE SUMMARY

Background

In 2020, The University of Minnesota (UMN), St. Anthony Falls Laboratory (SAFL) launched a research program titled “Healthy Waters Initiative” with a mission of establishing multi-year research efforts focused on issues that have the potential to adversely affect Minnesota lakes and rivers. The first research topic under this initiative was focused on characterizing boat-generated surface waves, specifically the divergent waves generated by powerboats, including wakeboats. The research output was a report titled “A Field Study of Maximum Wave Height, Total Wave Energy, and Maximum Wave Power Produced by Four Recreational Boats on a Freshwater Lake” that was published in February 2022. Since its publication it has been downloaded over 17,000 times and shared many more, which is a testament to the importance of this research topic. This led to the second research topic reported here, focused on characterizing the hydrodynamic phenomena that occur beneath the water surface as a powerboat moves about, and their potential impacts to the aquatic environment. With funding secured through a crowdfunding campaign and the Minnesota Environment and Natural Resources Trust Fund (ENRTF), fieldwork started in the fall of 2022, with a second fieldwork campaign completed in the fall of 2023.

Purpose

Powerboats are a ubiquitous component of recreation on lakes, rivers, and water storage reservoirs. In some locations, recreational boating is a significant economic driver that continues to grow. The increase in powerboat popularity, along with increasing boat size, horsepower, and newer wake-enhancing technologies, has led to increasing concerns for the health of these aquatic environments. More specifically, wakeboats and the mode in which they are operated during wakesurfing is a topic of intense public interest.

The motivation of this study was the need to better understand the environmental impacts within the water column and at the lakebed as different types of recreational powerboats traverse under their typical modes of operation. The objectives of this study were to:

- Clarify and define the various hydrodynamic phenomena that are created by a recreational powerboat in motion, and how these phenomena vary with water depth and mode of operation.
- Investigate the depth of penetration and duration of emission gases (e.g., engine exhaust bubbles).
- Investigate the water column velocities and depth of penetration of the bow, stern, and transverse waves and their potential to resuspend lakebed sediment.
- Investigate the propeller wash velocity and depth of penetration, and the potential to resuspend lakebed sediment.
- Investigate the effects of repeated boat passage on thermal stratification and mixing in the water column.
- Capture underwater and aerial video of the hydrodynamic phenomena and any subsequent impacts (e.g., sediment resuspension).

Methodology

Over two field campaigns (Fall 2022 and Fall 2023), seven recreational powerboats were tested, including two deck boats, three bowriders, and two wakeboats. The boats were driven over bottom mounted acoustic-based velocity sensors at four water depths (9, 14, 16, and 27 ft) while traversing under their typical modes of operation. For the non-wakeboats (deck and bowrider) this was displacement mode and planing mode. For the wakeboats this was semi-displacement mode (surfing) and planing mode. Each boat was driven over the sensors five times for each operational mode to gather replicate data sets for analysis. Additional data sets were collected including various water quality parameters, underwater and aerial videos, and lakebed sediment samples.

Key Findings and Recommendations

This report identifies three distinct hydrodynamic phenomena produced by common recreational powerboats that have the potential to impact the water column and lakebed: 1) bow and stern pressure waves, 2) transverse gravity waves, and 3) propeller wash.

Bow and stern pressure waves are associated with water being displaced by the boat's hull during motion. The pressure wave that forms at the bow forces water forward and downward, while

the stern pressure wave is a restorative motion immediately abaft where water moves upward and backward. The bow and stern waves couple together to form a short-duration orbital wave motion that can extend deep into the water column. However, the individual contributions of the bow and stern waves were clearly discernable in our datasets and therefore were evaluated separately. The bow and stern waves were found to be the primary hydrodynamic phenomena that initiate the movement of lakebed sediments but were not sufficient to cause sustained sediment resuspension.

Transverse waves are gravity waves that result from the constructive interference of the bow and stern waves. Transverse waves are only produced at slower displacement and semi-displacement speeds where the boat is primarily supported by buoyancy forces. Transverse waves travel at approximately the same speed and in the same direction as the boat, so they appear, from a passenger's perspective, to be a stationary feature of the wake. The data showed that transverse waves can penetrate deep into the water column, can persist for several minutes after the boat has passed, and can generate velocities large enough at the lakebed to resuspend and entrain sediment.

Propeller wash is a highly complex, 3-dimensional phenomena formed from the high velocity rotational jet produced by the boat propeller(s). The initial propeller wash jet projects along the same alignment as the propeller shaft. The jet expands and slows as it moves farther from the rotating propeller. For all the boats tested here, and most recreational boats operating today, exhaust gas from the internal combustion engine is injected into the propeller wash jet as entrained bubbles. These bubbles interact with the propeller wash by dampening energy and providing buoyancy. As the boat and propeller are moving along the water surface, the direction of the propeller wash is altered by the crossflow effect of the quiescent water, bending the pathway of the propeller wash away from the bottom. The cumulative effect of the exhaust bubbles and crossflow limit the penetration depth of the propeller wash. Propeller wash was shown to impact the water column for several minutes after the boat pass and, under certain modes of operation, contributed to the resuspension and entrainment of bottom sediment. It was further observed that propeller wash can directly cause shearing and complete uprooting of submerged aquatic vegetation under certain operating conditions.

The three hydrodynamic phenomena described above occur simultaneously and move with the boat. The velocity magnitudes and their extent (penetration depth and duration) are tightly linked to boat displacement and mode of operation. The bow and stern pressure waves are the primary phenomena initiating the movement of lakebed sediments, while the transverse waves and propeller wash are the phenomena that lift and entrain sediment into the water column.

The data generated by this study can be used to inform science-based guidance for the minimum operational water depth that recreational powerboats under typical modes of operation should maintain to minimize water quality impacts to lakes, rivers, and reservoirs. Taken individually each data set has limitations, but collectively, there are multiple lines of evidence that support the following recommendations:

- When operating in planing mode, it is recommended that recreational powerboats similar to the ones studied here, should operate in 10 ft of water or greater to minimize impacts on the lakebed.
- When operating in sustained displacement mode (e.g., slow cruising), recreational powerboats similar to the ones studied here, should operate in 10 ft of water or greater to minimize impacts on the lakebed.
- For most recreational boat users, traveling in waters less than 10 ft deep is unavoidable (e.g., going through channels, getting to and from boat lifts, docks, and launches, etc.). In these scenarios it is recommended to go as slow as possible (i.e., slower than the displacement speeds tested here or no wake) to minimize the magnitude of the bow and stern pressure waves.
- Wakeboats should operate in 20 ft of water or greater when in semi-displacement (surfing) mode to minimize impacts on the lakebed.
- All boats have the potential to damage aquatic vegetation. The depth recommendations provided above are specified relative to the lakebed but could also be interpreted as relative to the top of submerged vegetation. Since vegetation grows throughout the open-water season, this is a more difficult recommendation to specify. In general, boats should avoid areas of the lake with aquatic vegetation to minimize damage.

(This page intentionally left blank)

TERMINOLOGY

Acoustic Doppler Current Profiler (ADCP) – An instrument that uses multiple diverging high frequency pulsed sound beams to measure the velocity field over an area in the water column.

Acoustic Doppler Velocimeter (ADV) – A device that measures three-dimensional velocity within a small volume of water by emitting short acoustic pulses and measuring the shift in the frequency (Doppler shift).

Amplitude (Signal Amplitude) – A data quality parameter recorded by the Nortek ADCP and the Nortek ADV to indicate the strength of the acoustic return signal. This parameter can be used to identify poor-quality data and is related to the quality of acoustic reflections from particles in the water.

Baseline Attenuation Profile – The attenuation of the ADCP signal as it travels through the water column in the absence of strong acoustic reflectors (e.g., sediment, bubbles, etc.).

Bubble Depth Limit – Greatest depth where significant bubble influence was observed in the ADCP data.

Bowrider – A powerboat with a narrow deep V-shaped planing hull design with an open bow area for seating. The bowriders tested in this study were powered by inboard/outboard (sterndrive) engines.

Bow Wave – The pressure wave that forms at the bow of a boat hull as it displaces water during motion.

Correlation – A data quality parameter recorded by the Nortek ADCP and the Nortek ADV that indicates the similarity of the signal transmitted by the sensors to the signal received after echoing back from reflectors. This parameter can be used to identify poor-quality data.

Crossflow – A flow pattern where the direction of a stationary fluid jet is perpendicular to a moving fluid. For propeller wash discussed here, the crossflow effect is produced by the propeller and boat moving relative to the stationary water within the lake.

Deck Boat – A powerboat with a wide V-shaped planing hull design that allows for more deck space and seating. The deck boats tested in this study were powered by outboard engines.

Deep Water Waves – Classification of a type of gravity wave where the water depth is greater than ½ the wavelength. Here the wave has minimal to no interaction with the bottom.

Depth Froude Number – A non-dimensional number, often used in naval architecture, defined as: $F_{rH} = \frac{V}{\sqrt{gH}}$, where V is the boat velocity, H is water depth, and g is the acceleration of gravity. The depth Froude number can be used to predict the characteristics of divergent and transverse waves produced by a boat hull and provides an indication if the resistance to motion of the boat hull is impacted by the depth of water.

Displacement Mode – The weight of the boat is fully supported by hydrostatic forces (buoyancy) whether at rest or traveling at slow speeds. Here the boat can be said to be floating or moving through the water. **Referred to as Condition 2 for the non-wakeboats tested.**

Divergent Waves – Gravity waves produced by the hull of a moving boat that travel at an oblique angle to the boat's direction of travel.

Gravity Waves – Surface water waves formed by the disturbance and displacement of the water surface and gravity acting to restore the water back to an equilibrium position. In this report, gravity waves are produced at the bow and stern of a powerboat resulting in divergent and transverse gravity waves.

Hull Speed –The speed at which the bow wavelength is equal to the wetted length of the boat hull.

Intermediate Water Waves – Classification of a gravity wave where the water depth is between $^1/_2$ and $^1/_{20}$ the wavelength. Here the wave has some interaction with the lake bottom.

Length Froude Number – In the context of boats and naval architecture, a non-dimensional number defined as: $F_{rL} = \frac{V}{\sqrt{gL}}$, where V is the boat velocity, L is the boat length, and g is the acceleration of gravity. The length Froude number can be used to describe the wave-making resistance of all boats.

Measurement Bin – A discrete volume of water along an ADCP beam path where a measurement is made. Each beam path is segmented into many measurement bins.

Neutral Trim – Standard drive unit position where the angle of the propeller shaft is parallel relative to the water surface.

Operating Condition – Set of boat parameters selected and used within a test condition. The parameters included: speed, engine trim, ballast weight, wake shaper setting, and trim tab/hydrofoil setting.

Pad – ADCP or ADV deployment structure placed on the lake bottom during testing.

Pass – A single instance of a test boat driven along the track line under one of the operating conditions.

Penetration Depth – The depth from the water surface that is reached by either exhaust bubbles or a hydrodynamic phenomenon (i.e., bow/stern waves, transverse waves, propeller wash).

Pitch – The angle of a boat's hull in relation to the water surface.

Planing Hull – A boat hull design that generates hydrodynamic lift with speed.

Planing Mode – A boat is planing when its weight is predominantly supported by hydrodynamic lift, rather than hydrostatic forces (buoyancy). Here the boat can be said to be moving on top of the water. **Referred to as Condition 1 for all boats tested.**

Powerboat (Boat) – A watercraft propelled by an internal combustion engine.

Propeller Wash – The turbulent water that is thrust aft (or fore when in reverse) by a powerboat in motion. The thrust created by the blades of a boat propeller accelerates water astern in a manner that resembles a turbulent jet-like flow. For the recreational boats studied here, engine emissions are injected into the propeller wash as exhaust bubbles.

Sediment Resuspension Limit – The water depth, measured from the lakebed, of where the mean ADCP echogram amplitude of resuspended sediment exceeded a sound intensity of 10 decibels.

Semi-Displacement Mode – A boat traveling in the transition period between displacement mode and planing mode where some hydrodynamic lift occurs, but the weight of the boat is predominately supported by hydrostatic forces (buoyancy). This causes maximum drag on the hull that results in large divergent and transverse waves. Here the boat can be said to be plowing through the water at intermediate speeds. **Referred to as Condition 2 for the wakeboats when tested in surfing mode.**

Shallow Water Waves – Classification of a gravity wave where the water depth is less than $^{1}/_{20}$ of the wavelength. Here the wave strongly interacts with the bottom.

Stern Wave – The pressure wave that forms at the stern of a boat generated by the restorative upward motion of the water as it fills the volume previously displaced by the hull.

Thermocline – a sharp temperature gradient in a body of water between the warmer mixed water at the surface and colder deep water below.

Track Line – A straight line marked by a start and end buoy that ensured the test boats traversed over the ADCP and ADV sensors when making a pass.

Transverse Wave – A set of wake waves that extend astern and move in the same direction as the powerboat itself, with crests oriented perpendicular to the direction of boat travel.

Turbidity – A water clarity measurement. Measures the level of water cloudiness or haziness caused by suspended particles such as sediment, plankton, or detritus.

Wakeboat – A powerboat with a deep V-shaped planing hull and technologies specifically designed to increase wake wave size for wakesports.

Wakesports – Refers to the sports of wakeboarding and wakesurfing in this report.

Wave-making resistance – The resistance a boat encounters due to the waves it creates as it moves through the water. This is separate from skin friction resistance of the boat hull.

1.0 INTRODUCTION

The use of lakes, rivers, and water storage reservoirs for recreational purposes continues to grow and has led to concerns about increasing anthropogenic pressures on these aquatic environments. Many of the lakes in Minnesota are public waters and citizens cherish these aquatic resources while acknowledging that their recreational use has some level of impact on the water environment. Through personal decision-making and resource management, such as those implemented by local lake associations, watershed districts, or state and federal agencies, society generally sets guidance and laws that help maintain a balance between the usage of resources and environmental protection, preservation, and restoration.

Since the emergence of powerboats in the early 1900s, people have found enjoyment in a range of activities such as exploring, cruising, fishing, tow sports, and more. Recreational boating is also a significant economic driver in many states. The design and technology of powerboats have advanced over the decades including hull shape, engine size and efficiency, propeller performance, safety, interior comfort, and more. As boat technologies have evolved, so have their usage and modes of operation. For example, the emergence of new recreational sports and activities.

Just as recreational boating continues to evolve and grow, so has our understanding of aquatic ecosystems and the anthropogenic influences imposed on them. Concerning powerboats specifically, multiple literature reviews have been completed that document strong connections between powerboat usage and environmental impacts such as shoreline erosion, sediment/nutrient resuspension and turbidity, invasive species transport, and disturbance to flora and fauna (Asplund 2000, Bilkovic et al. 2017). Knowledge of these linkages, and furthering the science, is fundamental to effective management of recreational and environmental resources.

This report summarizes a multi-year research effort to characterize the hydrodynamic phenomena that occur directly beneath powerboats as they travel under various operating conditions. Through field research conducted in 2022 and 2023, we identify and characterize three primary phenomena: bow and stern waves, transverse waves, and propeller wash. We

present measured and visual data on how these phenomena influence the water column and lake bottom for different boat types, usage scenarios, and water depths.

2.0 BACKGROUND

2.1 Hydrodynamic phenomena produced by recreational powerboats

Multiple literature reviews have been completed that document strong connections between powerboat usage and environmental impacts such as shoreline erosion, decreased water clarity and quality (e.g., sediment/nutrient resuspension), aquatic invasive species transport, disturbance to flora and fauna, pollutants, and more (Asplund 2000, Beachler and Hill 2003, Bilkovic et al. 2017, Mosisch and Arlington 2004). More specifically, there is a growing base of literature regarding wakeboats and their effects on aquatic ecosystems (Francis et al. 2023, Ortiz et al. 2024). In this report, a *wakeboat* is defined as a powerboat specifically designed to increase wake wave size for wakesports, where *wakesports* refer to wakeboarding and wakesurfing.

Wakeboats, described in more detail in Section 5.4.3, enhance their wake waves via hull shape, a powerful engine (some greater than 600 horsepower), added ballast water weight, trim/hydrofoil plates, and wake shapers. Most important, however, is the constant speed at which wakeboats operate while wakesurfing. Where most powerboats travel at either slow displacement or fast planing speeds, wakesurfing is performed at semi-displacement speeds (10-12 mph) associated with the maximum wave-making resistance. It has long been known that environmental effects, like lakebed sediment resuspension, increase when boats move slowly under heavy loads at high engine RPMs, as this scenario induces maximum wave-making (Gucunski 1982). Beachler and Hill (2003) demonstrate that boats operating at slow displacement speed have no greater impact on the lake bottom than boats traveling at high planing speed, but the greatest impact was seen by boats traveling at the intermediate semi-displacement speed. While it is true that all boats pass through the semi-displacement condition when accelerating to planing or decelerating to a slow displacement condition, it tends to be a quick transition period on the order of a few seconds. However, wakeboats continuously operate in this semi-displacement condition while wakesurfing, often for long periods of time. It is important to

understand that this is a wholly new boat usage scenario that creates hydrodynamics that lakes, rivers, and reservoirs have not historically encountered.

The authors of this report published a report in 2022 that characterized the divergent waves (i.e., the waves that travel at an oblique angle relative to the boat's direction of travel) produced by various recreational powerboats, including wakeboats (Marr et al. 2022). We found that wakeboats operated in wakesurfing mode created divergent waves that were 2-3 times higher, had 3-9 times more energy, and were 6-12 times more powerful than non-wakeboats operating at typical planing speeds. When watching boat-generated waves crash into the shoreline, it is typically these divergent waves that are being observed. In addition to divergent waves, all boats create additional hydrodynamic phenomena that are less apparent but may also be of significant environmental concern. These additional hydrodynamic phenomena occur directly beneath and along the boat's path and include the bow and stern waves, transverse waves, and propeller wash.

Two primary factors influence the degree of environmental impacts by a powerboat's bow and stern waves, transverse waves, and propeller wash: 1) the depth of water and thermocline (if present) directly beneath the boat, and 2) the depth that the hydrodynamic phenomena extend into the water column, termed *penetration depth*. In scenarios where the water depth and/or thermocline are deep relative to the penetration depth, there is a lower likelihood of impacts to the water column and lake bottom. On the contrary, where the water depth and/or thermocline is equal to or less than the penetration depth, there is a greater potential to impact the water column and lake bottom. Therefore, it follows that the water column and lake bottom along a boat's path is a region of concern.

2.1.1 Bow and stern waves

A powerboat in forward motion produces a local high pressure under the wetted portion of the hull, defined as the *bow wave* in this report. For the same boat, just behind the stern, water rebounds upward from the hull producing a local low pressure that fills the volume displaced by the hull, defined as the *stern wave* in this report. Figure 1 is a conceptual schematic of the bow and stern pressure waves that a powerboat hull produces when in motion. Note that the term

wave is used for both the bow and stern because these phenomena are localized to the hull and therefore translate with the boat. While bow and stern waves appear like waves, they are technically not gravity waves. *Gravity waves* are defined here as surface water waves formed by the disturbance and displacement of the water surface and gravity acting to restore the water back to an equilibrium position. The bow and stern waves of a powerboat induce velocity and pressure fluctuations directly under the boat, which is the source of divergent waves and, if present, transverse waves (BAW 2011, Savitsky and Morabito 2010, Tavakoli et al. 2022).

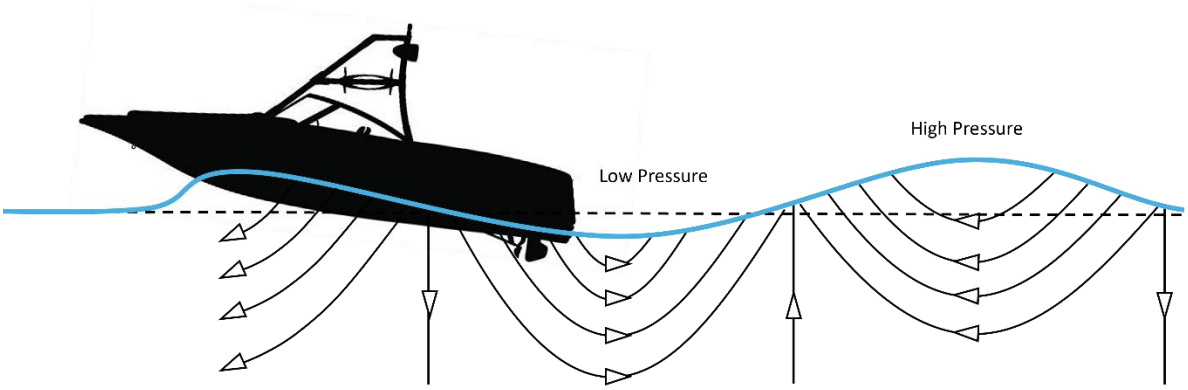

Figure 1. Conceptual schematic of velocity flow lines and pressures induced directly beneath a moving boat.

As introduced in Figure 1, the forward motion of the hull forces the water to move forward and down. Immediately abaft the water moves backward and up as it rebounds to fill the volume displaced by the hull. The bow and stern waves are two distinct and separate disturbances, however, the two interact with one another through constructive or destructive interference (Larsson and Raven, 2010). Additionally, the wavelength of the bow wave changes with the speed of the boat, increasing with greater speed. In terms of boat wakes, the maximum constructive interference occurs when the boat length is generally half of the wavelength of the bow wave. At this ratio, the stern coincides in space with the trough of the bow wave, and in this situation, the gravitational restoring force of the bow wave and the force created by the stern act in the same upward direction and resonate to create maximum wave making hull resistance. Alternatively, if the length of the boat is equal to the wavelength of the bow wave, the forcing caused by the stern acts opposite the gravitational restoring force of the bow wave, and the bow

and stern forcing tend to cancel each other (i.e., destructive interference). In reality, there is a full spectrum of behavior and interference that depends on the boat's speed and length and is also influenced by the water depth.

2.1.2 Divergent and transverse waves

The cumulative result of the bow and sterns waves created by a powerboat in motion are divergent waves and transverse waves (Figure 2). Divergent waves are gravity waves created by the moving boat hull that propagate laterally from the boat track line (Lewis 1941, Macfarlane 2018, Macfarlane 2025). Again, our previous study extensively characterized the divergent wake waves produced by various recreational boats (Marr et al. 2022). Transverse waves are gravity waves generated at sub-planing speeds (Lewis 1941, Macfarlane 2018) that propagate off the stern of a boat in the direction of the boat path (Figure 2). As a boat speeds up from displacement, the wavelength of the bow wave increases until a limit is reached when the wavelength is equal to the length of the boat, termed *hull speed*. When a boat tries to go faster than its hull speed it produces a bow wave that is longer than the boat itself. At this stage, the boat is traveling at semi-displacement speeds where the stern is sitting in the first bow wave trough and the bow is riding on the wave peak (i.e., bow wave). Fundamentally, the boat is stuck in its bow wave where the overall boat pitch angle is high with the hull resistance being substantial relative to speed. As boat speed is further increased the boat outpaces the bow wave and enters a distinctly different mode of operation called planing, where the higher speeds produce local water pressures that lift the hull out of water and onto "plane". At displacement and semi-displacement speeds in deep water, transverse waves are formed and travel at approximately the same speed as the boat (Larsson and Raven 2010); however, at planing speeds they are no longer able to be fully created (Gucinski 1982, Osborne et al. 2007).

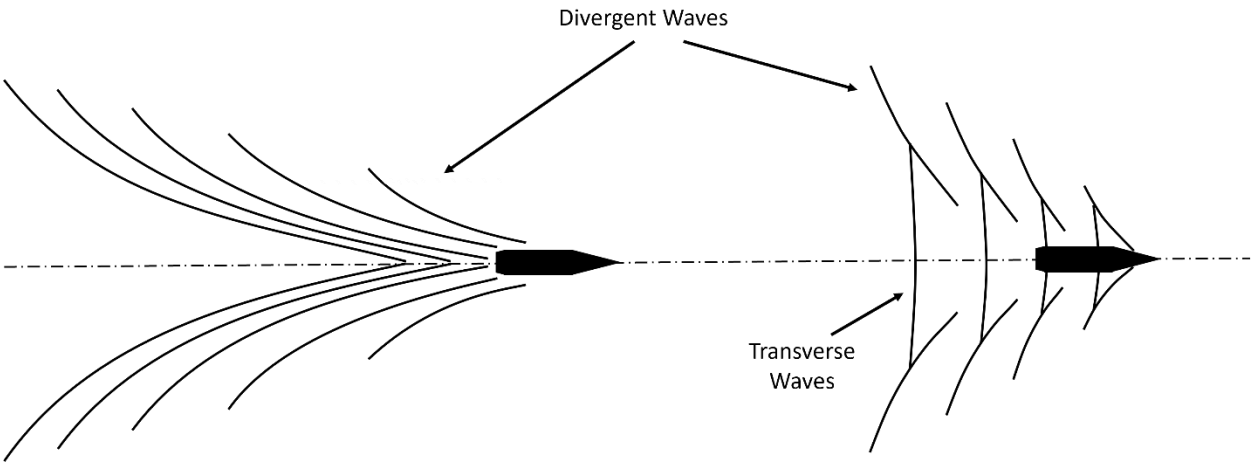

Figure 2. Wake wave patterns of a powerboat traveling at fast planing speeds (left) and slower displacement and semi-displacement speeds (right).

2.1.3 Propeller wash

The thrust created by the rotating blades of a powerboat propeller accelerates water astern in a manner that resembles a turbulent jet-like flow, termed *propeller wash*. Most studies on propeller wash impacts on water bodies have focused on large vessels (e.g., naval ships, tugboats) operating in harbors (Hamill et al. 1999, Liao et al. 2015, Wang et al. 2016, Wei et al. 2020). Numerous equations have been developed both for propeller wash velocity distributions and for corresponding rates of sediment scour (Wei et al. 2020), but their applicability to smaller recreational powerboats is unclear.

Several studies have characterized propeller wash for recreational powerboats. Beachler and Hill (2003) used an acoustic doppler velocimeter (ADV) and an optical backscatter turbidity sensor to measure subsurface velocities and sediment suspension from several boats operating in shallow lakes (3.9 – 6.2 ft depth) and found that boats operating at intermediate semi-displacement speeds had the potential to resuspend lake sediments. Although the sediment resuspension was attributed to propeller wash, the sample velocities from the ADV given in the paper resemble a bow/stern wave signal, not propeller wash. Symonds et al. (2016) studied the impact of a large recreational powerboat (43.5 ft in length) operating in a marina with depths ranging from 9.8 to 23.0 ft. An Acoustic Doppler Current Profiler (ADCP) was used to measure propeller wash velocities and multiple optical backscatter turbidity sensors were used to measure sediment

resuspension. Simple models for propeller wash velocities were successful in estimating observed velocities, but testing was only done for a fixed boat position. The effects of boat motion on the propeller wash velocities, referred to as crossflow, were not considered. Valbuena et al. (2024) studied boat-induced sediment resuspension in Lake Tahoe in comparison to wind-wave induced resuspension. Propeller wash bottom velocities for water depths in the range of 6 to 10 ft (1.8 to 3 m) were estimated using the same model as Beachler and Hill (2003) and were found to be substantially larger compared to velocities predicted by a numerical model (Valbuena et al. 2020).

The propeller wash velocity models used by Beachler and Hill (2003), Symonds et al. (2016), and Valbuena et al. (2024), are based on non-buoyant free jet theory and likely apply only to propeller wash in deep water and for stationary or slowly moving powerboats (boat velocity much less than propeller exit velocity). In shallower water, a propeller wash jet may extend the full water column, which will have different decay rates (the decrease in velocity with distance from the boat) compared to a free jet (Maynord 2000).

It is important to note that most modern recreational boats are powered by internal combustion engines that discharge their emissions (e.g., exhaust bubbles) directly into the propeller wash via vents/manifolds. The bubbles are entrained in the turbulent velocities of the propeller wash, but because bubbles naturally rise in water due to buoyancy and compressibility, there is reason to hypothesize that they influence the propeller wash hydrodynamics (e.g., upwelling effects, energy dissipation, time of sediment resuspension, etc.). This effect of buoyancy on propeller wash penetration into the water column has not been quantified in previous studies.

2.1.4 Integrating the hydrodynamic phenomena

The hydrodynamic phenomena described above occur simultaneously and move with the boat. Figure 3 is a conceptual illustration summarizing the bow and stern pressure waves, transverse gravity waves, and propeller wash for a boat traveling in displacement or semi-displacement mode. The transverse waves produce orbital velocities that can extend deep into the water column. The effects of buoyancy (exhaust bubbles) and crossflow cause the propeller wash jet to uplift and bend horizontally relative to the lake bottom. In other words, without the boat

movement and exhaust bubbles, the angle of the propeller wash jet would flow more directly towards the lake bottom (crossflow effects are discussed in detail in Section 8.1.3). The magnitude of the three hydrodynamic phenomena and their penetration into the water column are tightly linked to the type of boat and their mode of operation, which in combination with the water depth, composition of the lakebed, presence and composition of aquation vegetation, and more, play a vital role in environmental impacts to the lake environment.

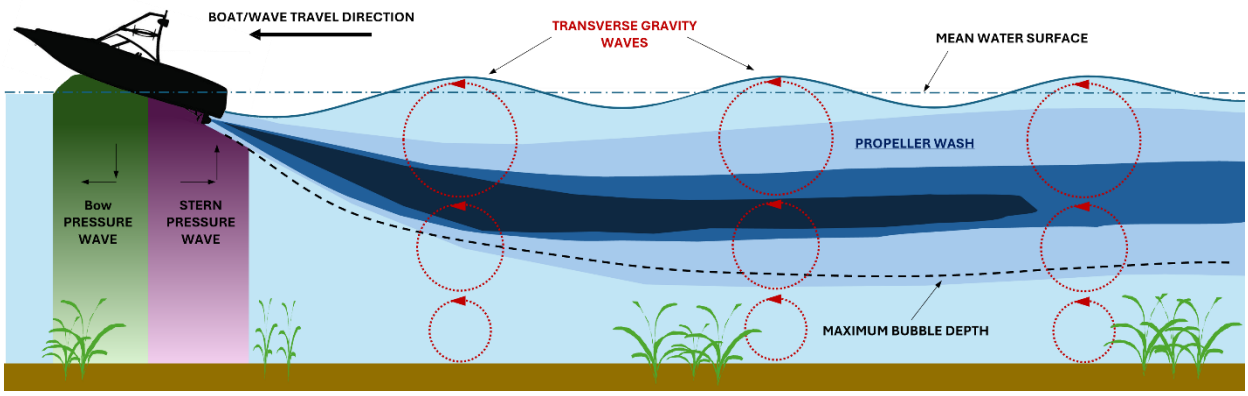

Figure 3. Conceptual illustration of the three hydrodynamic phenomena formed during displacement and semi-displacement modes of operation when transverse waves are present, that produce orbital movement in the water column. The figure represents the first ~10 seconds of time following a boat in forward motion. The arrows in the green bow and purple stern regions represent the direction that the water is moving as it is being displaced by the boat's hull.

2.1.5 Deep vs. intermediate vs. shallow waves

Gravity waves are a familiar phenomenon seen from the water surface. Waves have an extensive vertical component that decreases exponentially with depth and, depending on the water depth, waves may or may not interact with the lake bottom. Waves are often classified as deep water, intermediate water, or shallow water waves based on the wavelength (λ) to water depth (D) ratio (Figure 4, Ahmed et al. 2010). Wavelength is the distance between two consecutive wave peaks or troughs. Deep water waves are considered deep if the water depth is greater than $^1/_2$ the wavelength ($D > {}^{\lambda}/_2$). Deep water waves do not interact with the lake bottom and have an orbital motion that is circular in nature. Since these waves experience no interference from the bottom, they generally travel far distances with little energy loss. On the contrary, shallow water waves occur at depths that are less than $^1/_{20}$ of the wavelength ($D < {}^{\lambda}/_{20}$). Here, the wave interacts

strongly with the bottom causing an elliptical motion where the major axis is in the horizontal direction. As the depth decreases, the horizontal velocities become increasingly similar at the water surface and lake bottom. Intermediate water waves occur at depths between deep and shallow waves ($\lambda/_{20}$ < D < $\lambda/_{2}$), where some bottom interaction and altered orbital motion occur, although to a lesser extent than shallow water waves.

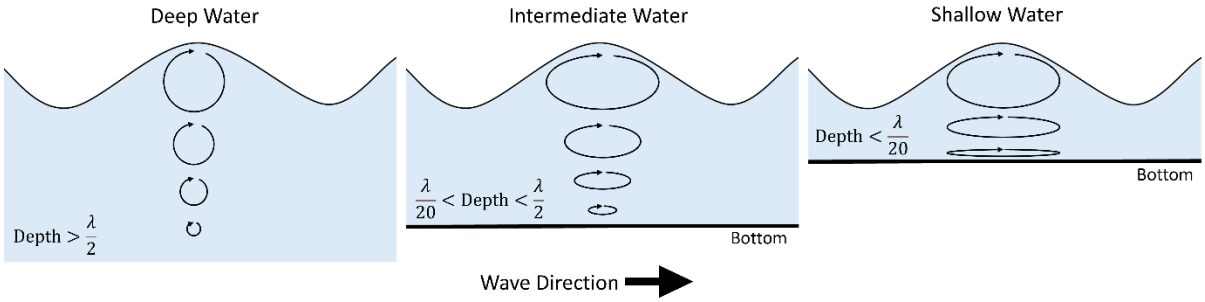

Figure 4. The orbital motion of gravity waves in deep, intermediate, and shallow water depths showing the waves become increasingly elliptical with decreasing water depth.

2.1.6 Hull resistance variation with water depth

It is well established in the literature that the depth of water beneath the boat can influence hull resistance (Schlichting 1934, Lewis 1941, Lackenby 1963, Macfarlane 2012, Kumar and Premchand 2015). Specifically, as the water depth becomes shallow relative to the speed of the boat, the resistance on the hull increases.

A common way to evaluate this phenomenon for boats of all shapes and sizes is the non-dimensional depth Froude number, F_{rH}:

$$F_{rH} = \frac{V}{\sqrt{gH}} \quad (1)$$

where V is the boat velocity, H is water depth, and g is the acceleration of gravity. The depth Froude number is the ratio of boat velocity to $\sqrt{gH}$, which is defined as the shallow water wave speed or the maximum speed a gravity wave can move at a given depth. Herein, the depth Froude number is used as an indicator of the boat hull interacting with the lakebed. Depth Froude numbers less than 0.75 are termed subcritical and indicate little or no influence of water depth on hull resistance. Depth Froude numbers between 0.75 and 1 are defined as trans-critical and a

depth Froude number equal to 1 is termed critical. At critical depth Froude the boat is traveling at a speed equal to the maximum speed of the gravity wave. In the ranges of trans-critical and critical speeds, the boat hull has measurable resistance effects due to the shallow depth, reaching a maximum level in this region. Finally, depth Froude numbers greater than 1 are defined as supercritical conditions, where the gravity wave cannot keep pace with the boat. At supercritical speeds, the boat hull experiences a reduction in hull drag similar to what is experienced in deep water situations. (Larsson and Raven 2010).

2.1.7 Non-dimensional wave-making resistance

While the production of waves by a powerboat depends on many variables, the size of the divergent and transverse waves for a given boat is largely dependent on boat length, boat speed, and water depth. The effects of these variables on wave characteristics can be greatly simplified using a second dimensionless parameter, the length Froude number, F_{rL}:

$$F_{rL} = \frac{V}{\sqrt{gL}} \tag{2}$$

where V is the boat velocity, L is the boat length, and g is the acceleration of gravity. The largest transverse waves are generated at length Froude numbers around 0.4 (Larsson and Raven 2010, Rabaud and Moisy 2014), and the smallest for length Froude numbers greater than 1. Faltinsen (2005) gives a relationship between the length Froude number and wave-making resistance (Figure 5), showing that the total resistance is highest at a length Froude number of about 0.5 for boats in deep water. In shallow water, the peak of the resistance curve may shift to lower values of the length Froude number, with higher peak resistance (Larsson and Raven 2010).

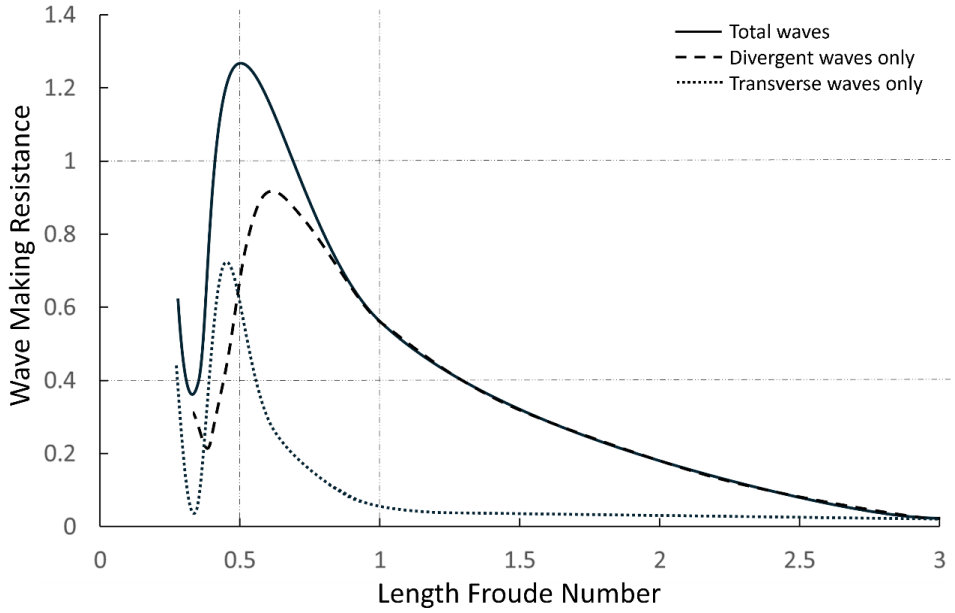

Figure 5. Wave-making resistance coefficients vs. length Froude number. From Faltinsen 2005. Reproduced with permission of The Licensor through PLSclear.

The length Froude number is a parameter that captures the important hydrodynamics of wave-making resistance for all different shapes and sizes of boats. We introduce the concept of length Froude number because it can also be used to explain the various modes of operation examined in this study (Section 5.5). Displacement mode approximately corresponds to length Froude numbers less than 0.4, semi-displacement mode corresponds to length Froude numbers ~0.5, and planing mode corresponds to length Froude numbers greater than ~0.5 (Figure 5, Faltinsen 2005). Most recreational boats operate in either displacement or planing mode, where the transitional time from one to the other is minimal. Conversely, wakeboats in wakesurfing mode operate in the transitional semi-displacement mode, where maximum wave-making resistance occurs.

2.2 Environmental impacts by recreational powerboats

2.2.1 Sediment/nutrient resuspension

Lakebed sediments are typically comprised of clastic materials (fragments of mineral and rock), organic material (plants and animals), chemical and nutrient precipitates, or combinations of these. The sediments have accumulated from the watershed over long periods of time, but land

development has generally increased the sediment accumulation rates (Baud et al. 2021). Hydrodynamic forces that mix these sediments and the superjacent water can adversely affect the aquatic ecosystem, chiefly via decreased water clarity and increased nutrient availability (Niemistö et al. 2012, Weyhenmeyer 1998). Examples include stimulation of algae growth (Qin et al. 2004, Orihel et al. 2017, Pelley 2016), shifts in depth and distribution of macrophyte growth (Canfield et al. 1985, Chambers 1985), reduced feeding efficiency of fish and benthic invertebrates (Barrett et al. 1992, Gardner 1981, Stuart-Smith et al. 2004, Trebitz et al. 2007), and changes in thermal regime and dissolved oxygen concentrations (Irvine et al. 1997). Furthermore, degraded waters can negatively impact the ecosystem services they provide, like decreased food provisions, property values, recreational opportunities, aesthetics, etc. (Mueller et al. 2016)

Turbidity is a measure of water clarity, often described as cloudiness or haziness, that is related to the quantity of particles in water. The source of turbidity can be external (e.g., soil erosion and runoff, waste discharge) or internal (e.g., resuspension of bottom sediments, algal growth). Internal turbidity sources can be natural (e.g., wind waves, organism mobility and feeding) or anthropogenic (e.g., boating, swimming) processes. The waves and mechanical action of a powerboat create water currents and turbulence that can lead to increased turbidity by directly resuspending solids and by indirectly releasing nutrients like phosphorous (P) from sediment (i.e., internal loading) that can stimulate excessive algae growth (Mosisch and Arthington 2004). Because P is usually considered the limiting factor for primary production growth (e.g., algae) in freshwater lakes (Schindler 1977), and 90-95% of P entering a lake is accumulated in the top few inches of sediment (Doig et al. 2017, Nedohin and Elefsiniotis 1996, Qin et al. 2004), any anthropogenic activity that can suspend sediment containing nutrients into the water column warrants attention. For algae growth, phosphate is the most readily available form of phosphorus (Wetzel 1983). Yousef (1977) found that phosphate constituted 41% to 55% of total phosphorus increases due to boating activities, and attribute the phosphate increases to high pore water concentrations in the lake sediment. However, several shallow lake studies have shown that while wind-waves can cause measurable increases in total phosphorus in the water column, their effect on phosphate concentrations was less clear (Hamilton and Mitchell 1997, Tang et al. 2020).

Where and how powerboats are used influences the potential for sediment resuspension (Daeger et al. 2022, Hoverson and McGinley 2007). Boating activity has been found to increase nearshore turbidity, and heavy boating activity can prevent fine sediments from settling out, resulting in sustained turbidity and suspension of P (Alexander and Wigart 2013, Anthony and Downing 2003, Asplund 2000). A powerboat's rotating propeller was found to increase aeration and disturb concentration gradients near the sediment-water interface, thereby mobilizing phosphorous and other nutrients (Yousef et al. 1980). A study of recreational boating impacts on Lake Tahoe, CA, document increases in turbidity from propeller wash, hull displacement, and boat wakes especially in depths less than 10 ft (3 m) when traveling at speeds between 6 and 20 mph (Valbuena et al. 2024).

In a study of recreational powerboats with engines up to 160 hp operating in a shallow lake (7 ft mean depth), Hoverson and McGinley (2007) demonstrated that the larger the boat, engine, and draft the more sediment is resuspended. They found even greater sediment resuspension when the angle of the boat relative to the water surface (i.e., pitch) directs the propeller wash towards the bottom. Sediment resuspension measured in the study was much higher at a 4 ft depth test site than one at 6 ft deep. Finally, they found minimal sediment resuspension at slow displacement speeds in both shallow and deep depths.

Garrad and Hey (1987) tested recreation boats of up to 42 ft (12.8 m) in length in a United Kingdom river (Norfolk Broads) and found significant increases in turbidity associated with boat passes, with a time constant on the order of a few minutes. Smarts et al. (1985) found that both commercial and recreational boats produced measurable increases in turbidity in both the main channel and side channel areas of Navigation Pool 9 in the Upper Mississippi River. Recreational boats measurably increased suspended sediment concentrations in a 4.9 to 9.2 ft (1.5 - 2.5 m) deep side channel test area, but not in a 20.0 to 24.9 ft (6.1 - 7.6 m) deep main channel test area.

In a study of three lakes in Florida, Yousef et al. (1980) found increases in turbidity and P concentrations due to recreational boats with motors up to 115 hp, documenting increases in P concentration in the range of 28 to 55% for lakes with mean depths ranging from 5.9 to 13.1 ft (1.8 - 4.0 m). Anthony and Downing (2003) estimated increases in turbidity in a shallow Iowa lake

(9.5 ft mean depth) of up to 50%. Daeger et al. (2022) measured sediment resuspension and the associated nutrient loading in an Indiana lake for a range of recreational watercraft, operating conditions, and water depths. Resuspension, as measured from water samples before and after boat passes, was observed in 5.0 ft (1.5 m) water depth for several boats at semi-displacement speeds, including a wakeboat in wakesurf mode, but no resuspension was measured for water depths of 10 ft (3 m) or greater (see Section 3.2 for more detail on this paper).

2.2.2 Water column mixing (temperature and dissolved oxygen)

Most lakes in temperate climates that can support powerboating are dimictic, meaning the water temperature follows seasonal cycles of mixing and stratification. In the spring and fall, dimictic lakes completely mix (i.e., turnover), delivering nutrients and oxygen to aquatic life at all depths. During summer there is strong thermal stratification, where a thermocline (i.e., a sharp temperature gradient with depth) separates the warm and less dense surface waters (i.e., epilimnion) from the cold and denser deep waters (i.e., hypolimnion), as illustrated in Figure 6. The thickness of the epilimnion is determined by the amount of heat energy entering the water surface, which tends to warm the surface water and stratify the lake, balanced against the amount of wind exposure on the lake, which supplies energy to mix the water column (Horne and Goldman 1994). During thermally stratified periods, bioavailable forms of phosphorus and nitrogen in the epilimnion are taken up by algae and other aquatic organisms. These organisms eventually die and sink to the hypolimnion where decomposers (i.e., bacteria, fungi, and other microorganisms) feed on their remains. This decay process subsequently consumes oxygen while releasing readily available nutrients, such as nitrogen and phosphorus. While nutrients are necessary for plant and animal health and growth, they can be deleterious in excess, or if made available at times when they otherwise wouldn’t be. During summer stratification, boat-induced wave turbulence may increase mixing across the thermocline, allowing for the nutrient-rich water from the hypolimnion to rise and mix with the nutrient-depleted epilimnion. This nutrient influx can quickly be taken up by algae contributing to algal blooms, some of which can be toxic (e.g., blue-green algae). The magnitude of this effect is difficult to quantify as it is dependent on many factors including lake depth and area, the level of nutrient loading to the lake, air and water temperature, level of boat traffic, etc. Larger lakes with more wind exposure tend to have more

wind mixing and thicker epilimnions (Ford and Stefan 1980) and are likely less susceptible to the effects of boat traffic compared to smaller wind-sheltered lakes.

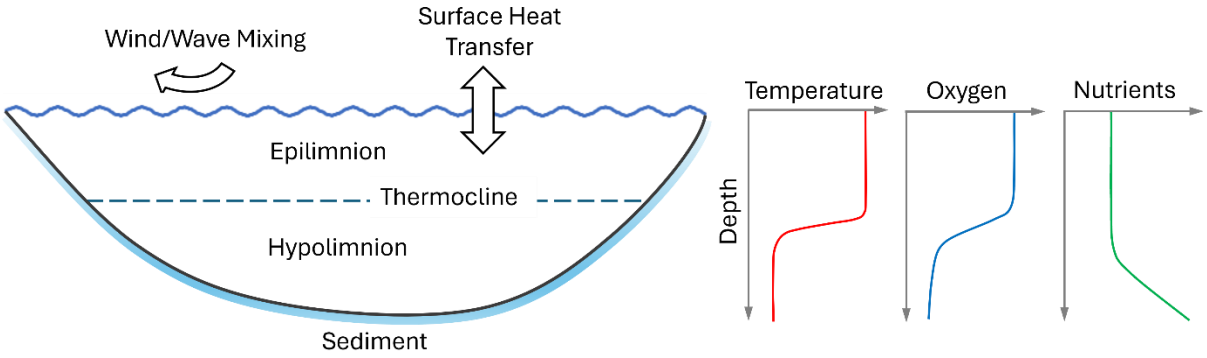

Figure 6. Diagram of the epilimnion, thermocline, and hypolimnion in a stratified lake, along with typical vertical profiles of temperature, dissolved oxygen, and nutrients.

A minimum level of dissolved oxygen (DO) is needed in lakes for fish to survive and reproduce. Oxygen enters a lake at the surface via surface reaeration and is also produced by algae and rooted aquatic plants in the epilimnion. The thermocline tends to block the transport of DO downward, and DO is consumed by decomposers in the hypolimnion and at the lake bottom. As a result, stratified lakes tend to have high DO in the epilimnion and low DO in the hypolimnion during the summer. Low hypolimnetic DO is an issue for coldwater fish species such as lake trout and cisco, because they are adapted to live in the colder temperatures of the hypolimnion (Jacobson et al. 2010). However, deep stratified lakes with good water quality and low nutrient loading can maintain sufficient oxygen in the hypolimnion for coldwater fish (Fang et al. 2012).

The impact of boating traffic on DO and fish habitat is not clear and thereby warrants research attention. Additional mixing energy in a lake from boat wakes and propeller wash may provide some additional transport of oxygen downwards, but also may transport warm water downwards, which could impact coldwater habitat. Increased mixing energy can also lead to the transport of more nutrient-rich bottom water to the surface, causing algal blooms (Riley and Prepas 1984). The thermocline could also act to dissipate mixing energy, and reduce the penetration of boat-induced velocities, however, this has not been quantified.

2.2.3 Aquatic flora and fauna

Shallow regions that extend to a water depth of about 15 ft are favorable for macrophyte growth because sunlight can penetrate to the lake bottom; however, this depth is highly dependent on water clarity. Rooted macrophytes (emergent and submerged) stabilize the lakebed and resist sediment resuspension by acting as wave breaks that reduce the force of waves (Mosisch and Arthington 2004, Sagerman et al. 2020). Macrophytes can grow to substantial heights above the lakebed. If the boat propeller or the penetration depth of the hydrodynamic phenomena reaches the macrophytes, they can be damaged, sheared, or uprooted completely, resulting in a loss of plant communities, habitat for fauna, and protection from sediment resuspension (Liddle and Scorgie 1980). Asplund and Cook (1997) documented increased macrophyte biomass, coverage, and shoot height when recreational powerboats were excluded from experimental testing plots. The authors also reported a 20% reduction in macrophyte coverage because of recreational boating. Asplund (2000) notes that increased turbidity from boats may limit light penetration and affect the distribution, species composition, and growth rate of macrophytes, and further effects may include decreased feeding efficiency and growth of invertebrates and fish (e.g., filter- and sight-based feeding). More specifically, Murphy et al. (1995) reviewed studies where it was found that silt deposition caused by powerboats can affect invertebrates and fish by clogging respiratory structures, reducing feeding rates, increasing invertebrate drift, disrupting courting and spawning behavior, and reducing hatch rates.

3.0 RESEARCH REVIEW OF WAKESPORT IMPACTS ON THE WATER COLUMN AND LAKEBED

Lake associations, lake users, shoreline property owners, and natural resource managers are promoting research, educating stakeholders, and contemplating new guidance and rules concerning wakesports like wakesurfing. For example, a citizen-led group (Responsible Wakes for Vermont Lakes) successfully petitioned the Vermont Agency of Natural Resources to implement new rules for managing wakesports on inland lakes. In 2024, Vermont passed a rule that established ‘wakesport zones’ on 30 of its lakes. Wakesports are only allowed to take place in these zones, defined as lake areas that have a minimum of 50 contiguous acres that are at least 500 ft from shore in all directions, and at least 20 ft deep (State of Vermont 2024). The Maine

state legislature also passed a bill in 2024 that specifically regulates wakesurfing, stipulating that the activity must take place more than 300 ft from shore and in at least 15 ft of water (State of Maine 2024). Vermont and Maine were the first in the country to establish state-wide laws directed at wake-enhanced sports, like wakesurfing. Here in Minnesota, the Minnesota Department of Natural Resources and Cook County approved the state's first ordinance that restricts wakesufing. The ordinance applies only to 760-acre Caribou Lake, stating that wakesurfing be contained to a specific area of the lake that is at least 20 ft deep and 500 ft or more from shore. Many other states, counties, and individual lake associations are in the process of establishing similar regulations (Ortiz et al. 2024).

In 2023, the Michigan Department of Natural Resources, Fisheries Division, published a literature review on the effects of wakeboat activity on aquatic lake ecosystems (Francis et al. 2023). The report provides recommendations for best operating practices for wakesports that include staying at least 500 ft from docks and shorelines regardless of water depth and operating in depths of at least 15 ft. In 2024, Wisconsin Green Fire published a similar literature review (Ortiz et al. 2024). The authors conclude that wakeboats creating wakesport waves should be restricted to areas that are at least 20 ft deep and at least 600 ft from any shoreline. The recent regulations and literature reviews cite many of the same publications to justify their depth and distance recommendations. However, there continue to be conflicting recommendations for an “environmentally safe” water depth for wakesports that minimize the potential for environmental impacts, like sediment resuspension. The following is a synopsis of the scientific literature that specifically pertains to operational depth for wakesports, which ranges from as shallow as 10 ft to as deep as 33 ft.

3.1 Modeling studies

Fay et al. (2022) and Ray (2020) are two modeling papers often cited when justifying the minimum water depths for wakesports activities. Fay et al. (2022) and Ray (2020) recommend minimum water depths of 10 ft and 33 ft, respectively.

Fay et al. (2022) is a computational fluid dynamics (CFD) study that, in two separate simulations, models the divergent waves and propeller wash generated by recreational boats; here we focus

only on the propeller wash simulations. The authors simulate propeller thrust and conclude that "the recommended depth for wake surf operation is conservatively set at 10 ft (3 m)". This statement is based on a single modeled scenario from a single boat without validation data to confirm that model results appropriately represent the relevant physics. It is standard practice in simulation research to provide evidence of validation of the numerical model and details of the modelling framework (numerical mesh and simulation boundary conditions) so that there can be confidence in the results. No such validation is provided or discussed warranting caution when considering the results of this paper. Additionally, there is essential technical information left out of this report. For example, the overall hull pitch used in the simulation is not provided. Our research suggests that hull pitch is an important factor in penetration depth of the propeller wash.

The figures detailing propeller wash extent in Fay et al. (2022) are difficult to interpret. While not described in the article, the authors use a moving frame of reference for the simulation - the boat is stationary and water is moving in opposite direction of boat travel at 12 mph (17.6 ft/s); this is an approach often adopted in simulation research. If we subtract the boat velocity from the velocity range shown in the figures, we transform the results to a frame of reference where the boat is moving and the water is stationary with a color map from 2 mph (3.0 ft/s) to 13 mph (19 ft/s) (referencing Figure 33 in Fay et al., 2022). Unfortunately, the authors do not plot data below 2 mph (3 ft/s), opting to show it as white space. Our research reported herein, and that of others, consider velocities as low as 0.3 ft/s to have the potential to disturb and resuspend fine lakebed sediment. It is reasonable to infer that the simulation results would show that velocities of 0.3 ft/s extend much deeper into the water column. In general, the stated conclusions from the propeller wash simulations are not supported by their simulations. Several topical experts have questioned and criticized the methodologies, analyses, and drawn conclusions of this paper (Vermont Department of Environmental Conservation – collection of critiques).

In another computational modeling effort, Ray (2020) developed slip-stream (i.e., propeller wash) velocity decay profiles and correlated them with shear forces necessary to move and suspend bottom sediments. Three wakeboats traveling at wakesurfing speeds were modeled, with results showing "wake boat slip-streams have the potential to affect bed sediments at 33 ft

of depth." The model simulates a turbulent, non-buoyant, free jet, "such as those found behind boats." It is important to clarify that this model is an oversimplification of boat-generated propeller wash. First, the model assumes a stationary water jet penetrating a quiescent fluid from a nozzle, which is not the case for a boat in motion. Second, the propeller wash jet of modern boats has some degree of buoyancy, as the engine exhaust gases are injected directly into the propeller wash. Due to the model assumptions, the reported velocities and depth of penetration are likely overestimated.

3.2 Field studies

Three field studies used common recreational watercraft, including wakeboats, to look at disturbances to the water column and lake bottom before, during, and after a pass.

Daeger et al. 2022 performed multiple experiments to test substrate resuspension by recreational watercraft. Specifically, the watercraft vs. water depth experiment sought to determine the smallest depth of water required to minimize sediment resuspension for several recreation watercraft types including a pontoon, bowrider, personal watercraft, waterski boat, and wakeboat. The watercrafts made a single pass (no replicates) through water depths of 5 ft (1.5 m), 10 ft (3.0 m), and 15 ft (4.6 m) under typical modes of operation. These were planing modes for all watercraft except the wakeboat, which traveled in semi-displacement mode (i.e., wakesurfing at 10 mph with full ballast). Water samples were collected from multiple depths pre- and post-watercraft pass to test for potential changes in depth-averaged concentrations of nutrients and suspended solids. Concentrations of ammonia (NH_3), chloride (Cl^-), sulfate (SO_4^-), nitrite (NO_2^-), nitrate (NO_3^-), silica (SiO_2), soluble reactive phosphorus (SRP), total phosphorus, (TP), total Kjeldahl nitrogen (TKN) and suspended solids (SS) were measured in water samples collected from three depths at each location. Despite potential differences in concentration with water depth, these three samples were treated as replicates for each location for pre- and post-boat pass times. After the wakeboats passed in wakesurfing mode the depth-averaged total phosphorous (TP), total nitrogen (TN), and suspended solids (SS) increased in only the 5 ft water depth, and TN was the only parameter to show a statistically significant increase. No other water quality parameters increased following the passage of any of the other watercraft in any depths. The authors average three vertical water samples to obtain a depth-averaged concentration (e.g.,

a concentration averaged over the water column). Averaging over the water column likely underestimated the impact of sediment or nutrients suspended near the lakebed, especially in deeper water where concentrations may not have been fully mixed over the water column. The authors state that their results suggest limiting “near plane” boat operations to depths ≥ 10 ft at their study lake (Lake Wawasee).

Raymond and Galvez (2015) tested various speeds (displacement, semi-displacement, and planing) using a single wakeboat. Measurements were collected by driving the boat over an Acoustic Doppler Current Profile (ADCP), like the one used in our study (Section 5.3.1). They aimed to define the depths at which the horizontal velocities of the propeller wash could resuspend bottom sediments in the water column. The sediment resuspension velocity threshold was set at 0.33 ft/s (0.1 m/s), which was expected to create conditions that can suspend coarse silts (i.e., 50 µm). During wakeboarding and wakesurfing modes, the boat traveled with full ballast at 18 mph and 12 mph, respectively. Results show velocities of 0.33 ft/s were generated down to 13 ft during wakeboarding and 15 ft during wakesurfing. For comparison, the velocity threshold did not exceed a depth of 3 ft during slow displacement or fast planing speeds.

Terra Vigilis Environmental Services Group (2022 and 2024) used subsurface video imagery to monitor the movement of fiber optic filaments and streamers mounted to rigid vertical masts within the water column. The videos available from the 2022 report show movement of the filaments at 20 ft below the water surface when a wakeboat in surfing mode passes above. In the 2024 report, the authors deployed a longer mast with streamers attached at two “deep” sites and report water movement down to 26 ft of depth. In both studies, the authors attribute the motion to propeller downwash. Our research suggests that the oscillating water in the videos is likely boat-generated waves (e.g., bow, stern, or transverse), not propeller wash.

Both Terra Vigilis Environmental Services Group studies report an increase in Total Phosphorous (TP) from water samples collected before and after testing of the wakeboat in surfing mode. The 2024 study also reports sediment re-distribution associated with the observed water motion. There is minimal information provided on the water quality sampling and analysis methodologies employed in either study. The authors do caution that the findings pertaining to TP are

preliminary in nature. Similarly, regarding the sediment re-distribution observations, there is no quantified information on the grainsize, quantity of material or where the sediment came from. The authors assume it was resuspended locally but as documented in our aerial videos (Section 7.10), it could have also been sediment re-suspended and entrained in a sediment plume that settled at the deeper site. The research provides novel information on the water motion throughout the water column associated with recreational boats, and the results show water movement down to 20 ft (2022) and 26 ft (2024) during testing of wakeboats in waksurfing mode. In their 2022 study, water movement at depths of not more than 3-5 ft were observed for the other watercraft tested while in planing mode, which included a pontoon, ski boat, and personal watercraft. The actual water velocities were not measured in the study; therefore, it is not possible to evaluate whether the movement would have resulted in sediment resuspension or other environmental impacts.

4.0 STUDY OBJECTIVES

The primary objective of this study was to investigate the hydrodynamic phenomena that are produced in the water column and at the lakebed by various powerboats, including wakeboats, during typical modes of operation. Objectives of this study include:

- Clarify and define the various hydrodynamic phenomena that are created by a recreational powerboat in motion and how these phenomena vary with water depth and boat usage.
- Investigate the water column velocities of the bow, stern, and transverse waves and their potential to resuspend lakebed sediment.
- Investigate the propeller wash velocity and the potential to resuspend lakebed sediment.
- Investigate the effects of repeated boat passages on thermal stratification and mixing in the water column.
- Investigate the depth of penetration and duration of emission gases (e.g., engine exhaust bubbles).

- Document and publish various forms of data for future analysis and information sharing, including sensor data and underwater and aerial video.

5.0 METHODS

5.1 Study location and test sites

This study was conducted in the fall of 2022 and 2023 on Lake Minnetonka, Orono, Minnesota, USA (44°57'29.09"N, 93°37'9.82"W). Lake Minnetonka is located 20 miles west-southwest of Minneapolis, Minnesota, and is one of Minnesota's most popular outdoor recreational destinations. It provides boating opportunities for crafts of all sizes, from kayaks to large yachts. The lake is comprised of many connected bays totaling more than 14,200 surface acres and 130 miles of complex shoreline (MN DNR).

Test sites were selected based on the following characteristics: two water depths (i.e., one shallow and one deeper) near each other with minimal lakebed slope, greater than 500 ft from any shoreline, and little to no vegetation. A sonar unit (Humminbird Helix 10) that displays Global Positioning System (GPS) coordinates, high-resolution bathymetry, vegetation density and height, and substrate hardness was used to locate potentially suitable sites. An underwater remotely operated vehicle (Deep Trekker DTG3) was deployed to visually explore the potential sites, and after many hours of exploring, two sites meeting the aforementioned characteristics were selected. The fall 2022 test site was in North Arm Bay (Figure 7), which is 307 acres with a maximum depth of 64 ft. The fall 2023 test site was in Maxwell Bay (Figure 7), which is 300 acres and has a maximum depth of 44 ft.

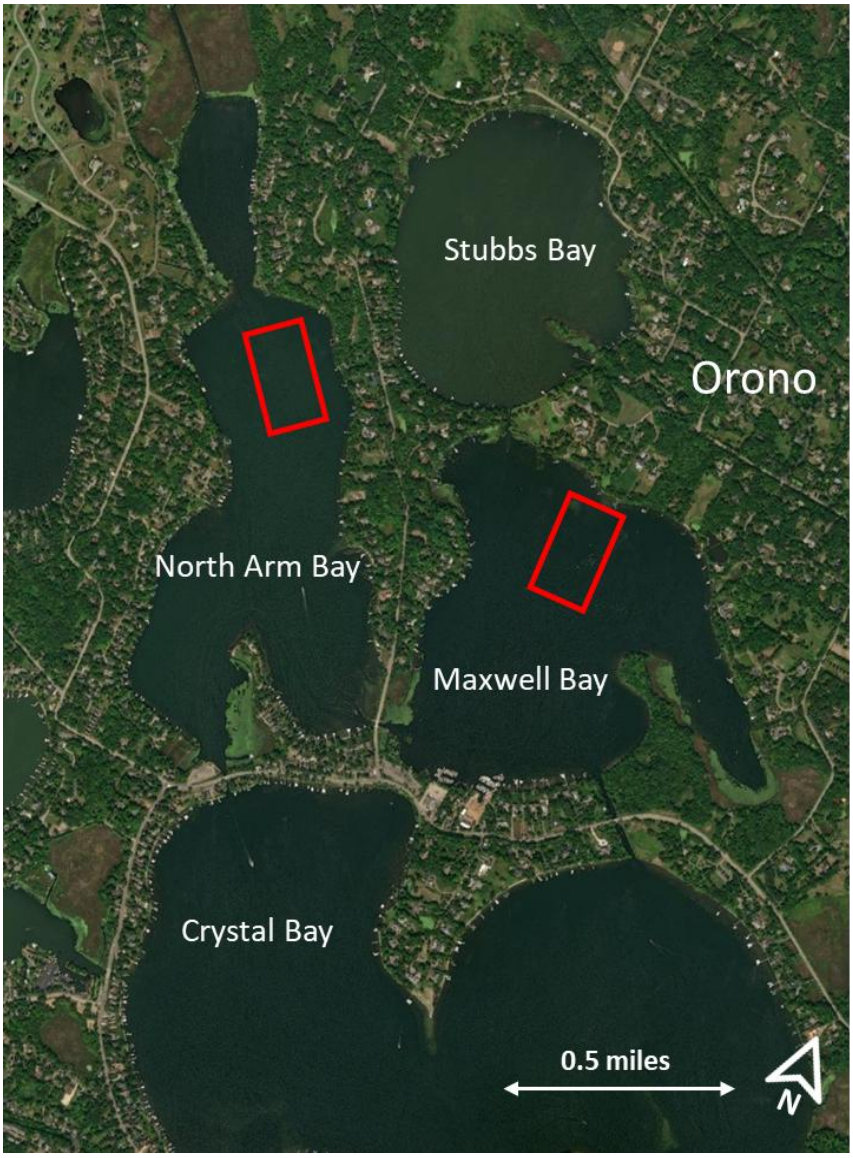

Figure 7. Lake Minnetonka, Orono, Minnesota, USA. The red boxes depict the fall 2022 test site in North Arm Bay (44°57'41.93"N, 93°37'18.59"W) and the fall 2023 test site in Maxwell Bay (44°57'41.53"N, 93°36'22.49"W).

5.2 Layout of the test sites

Figures 8 and 9 show the layout of the test sites in North Arm Bay and Maxwell Bay, respectively. Using the Humminbird GPS and bathymetry, two pads that each held various data sensors (Section 5.3), were deployed on the lake bottom at known water depths (Table 1). Taut-moored start and end buoys were deployed to define a straight track line that traversed directly over the pads. As part of the pad deployment process (Section 5.3), two taut-moored buoys were positioned 20 ft apart and perpendicular to the track line. These buoys provided a visual goalpost

for the boat operator to drive through, which ensured the boat was driven directly over the sensor pads. Before testing, a buoy perimeter was deployed to keep other watercraft well away from the study area.

Table 1. Depth of water that the sensor pads were deployed in each test year.

Year	Pad	Water Depth
Fall 2022	ADCP	27.0 ft (8.2 m)
	ADV	16.0 ft (4.9 m)
Fall 2023	ADCP	14.0 ft (4.3 m)
	ADV	9.0 ft (2.7 m)

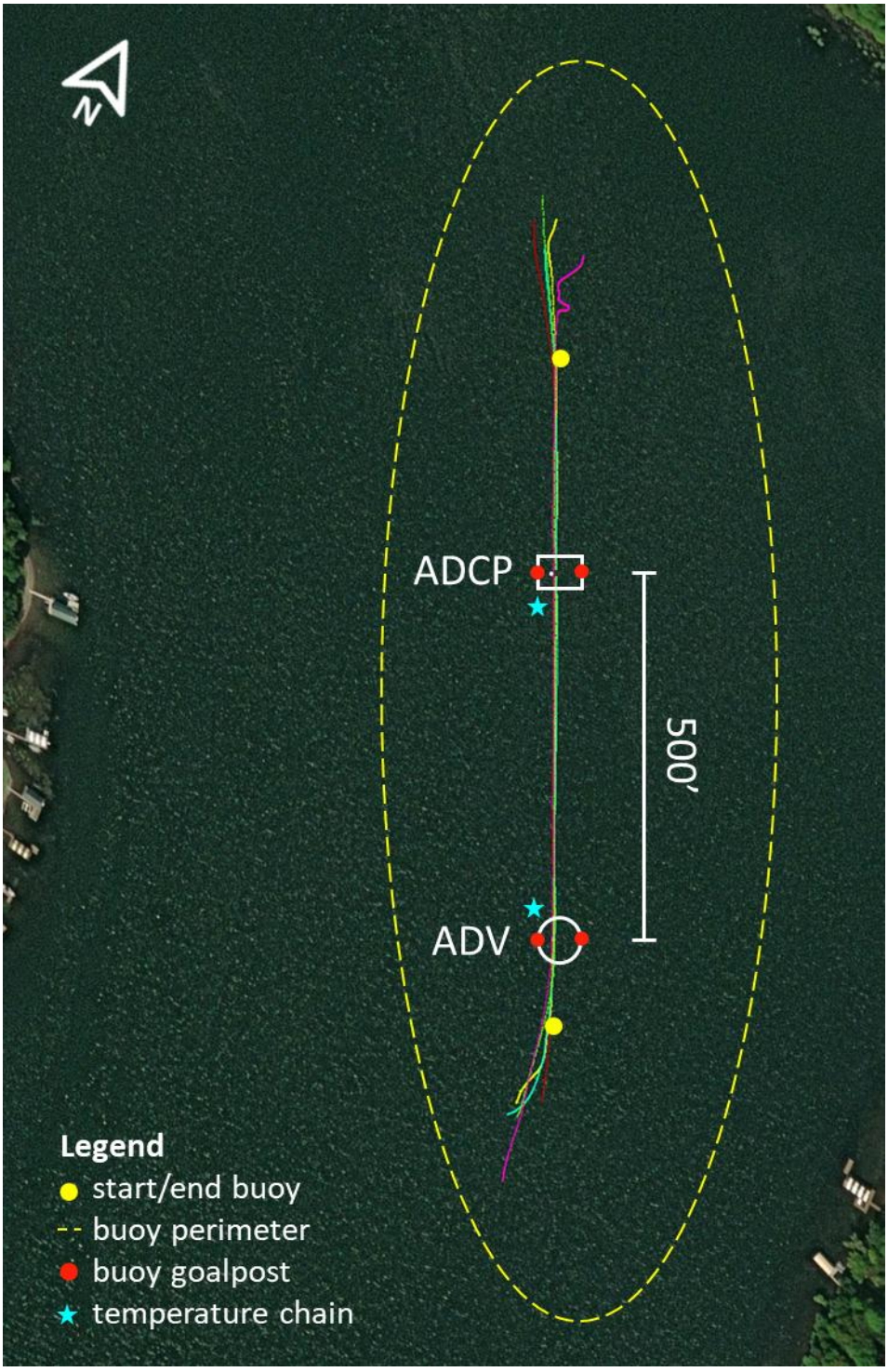

Figure 8. Layout of the fall 2022 study site in North Arm Bay. The center of the white rectangle and white circle denote the locations of the ADCP and ADV pads, respectively. The colored lines are actual boat positional data imported into ArcMap of five passes made from north to south along the track line.

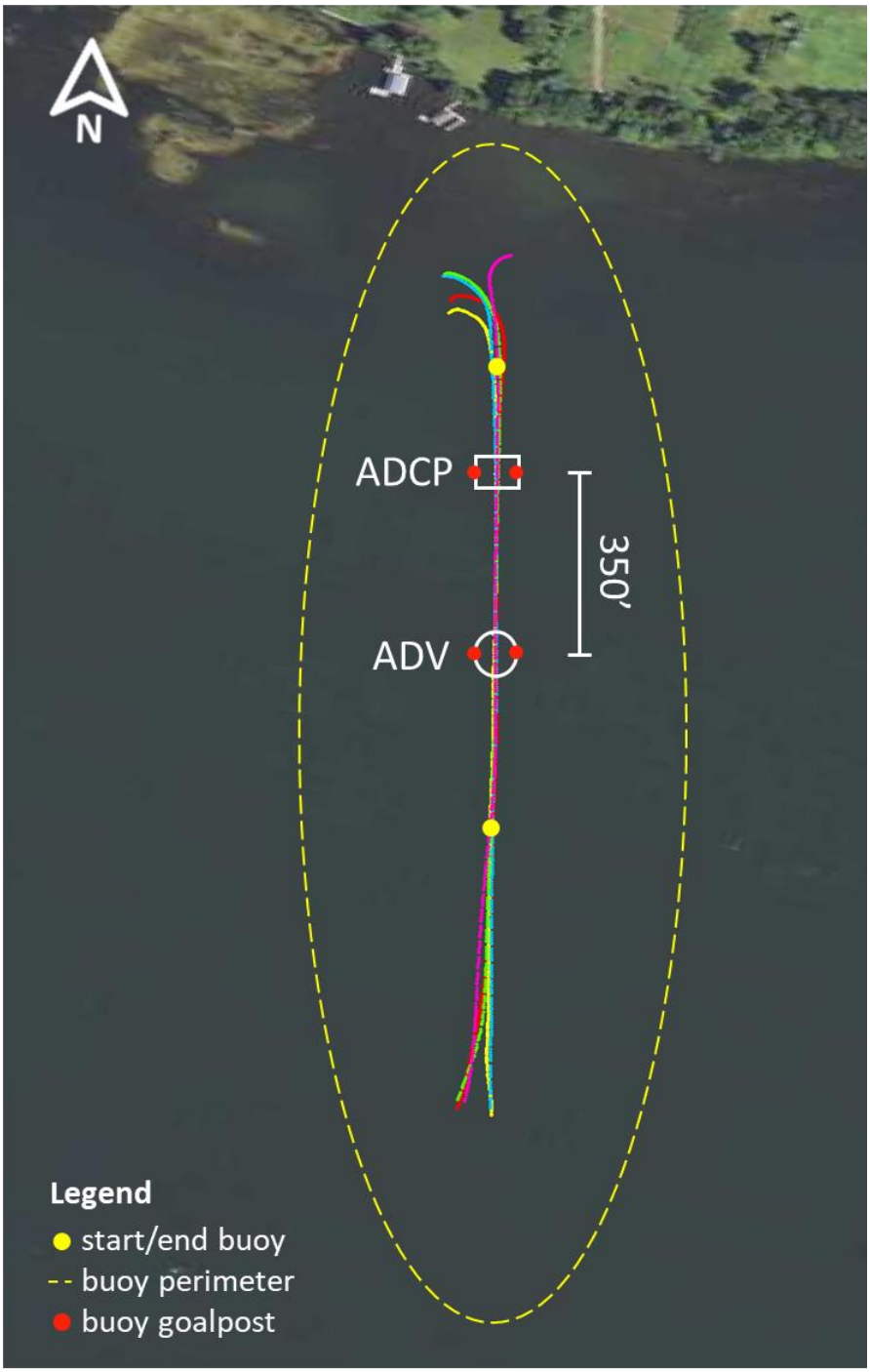

Figure 9. Layout of the fall 2023 study site in Maxwell Bay. The center of the white rectangle and white circle denote the locations of the ADCP and ADV pad deployments, respectively. The colored lines are actual boat positional data imported into ArcMap of five passes made from south to north along the track line.

5.3 Description of pads, attached data sensors, and their deployment

The two pads were 4 x 2.5 ft rectangular structures constructed of 1-5/8 in steel strut designed to be deployed and retrieved by two people on each day of testing (Figures 10 and 11). 4 ft wire ropes were secured to each corner of the pad and the two wire ropes on each end were joined to a single carabiner, which helped keep the pad level and upright during deployment and retrieval. A 4 ft nylon rope was attached to each carabiner and the other end was secured to an anchor, anchor line, and large temporary buoy. From the bow of a Jon boat, the two-person team simultaneously lowered their respective anchor line until the pad was resting on the lake bottom. Both lines were made taut with the large buoy that temporarily kept the anchors suspended in the water column while the boat was repositioned. One at a time, the large buoy was removed, and the boat slowly propelled perpendicularly away from the track line while the anchor line was gradually released until the anchor was resting on the lake bottom. The anchor line was then secured taut with a smaller buoy. Once this process was completed for both sides, the buoys provided a 20 ft wide visual goalpost for the boat to be driven through, which ensured the boat was driven directly over the sensors.

We found this method of deployment to be the least disruptive to the lake bottom because the pad and anchors only contacted the lake bottom once. The pads were deployed a minimum of one hour before testing commenced. Minimizing disturbance to the lake bottom and allowing plenty of time for any disturbance to return to a steady state was imperative because water quality samples were collected during boat testing and later analyzed in a lab (Section 5.8.2).

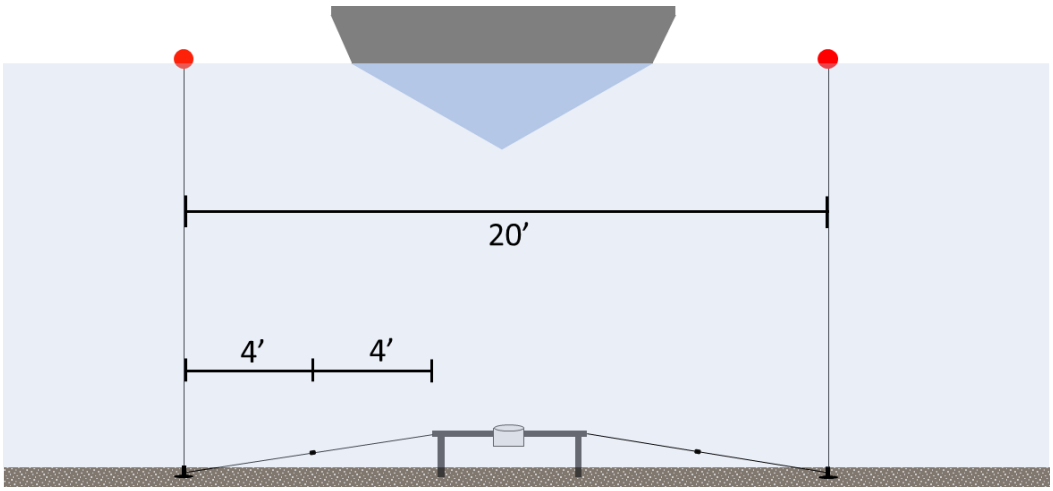

Figure 10. Schematic of a pad deployed on the lake bottom. The two 4 ft wire ropes on each end of the pad were joined to a single 4 ft nylon rope that was then attached to an anchor, anchor line, and buoy. Once the ropes were pulled perpendicular to the track line and the anchor lines were taught, the buoys established the 20 ft wide goalpost that the test boats were driven through.

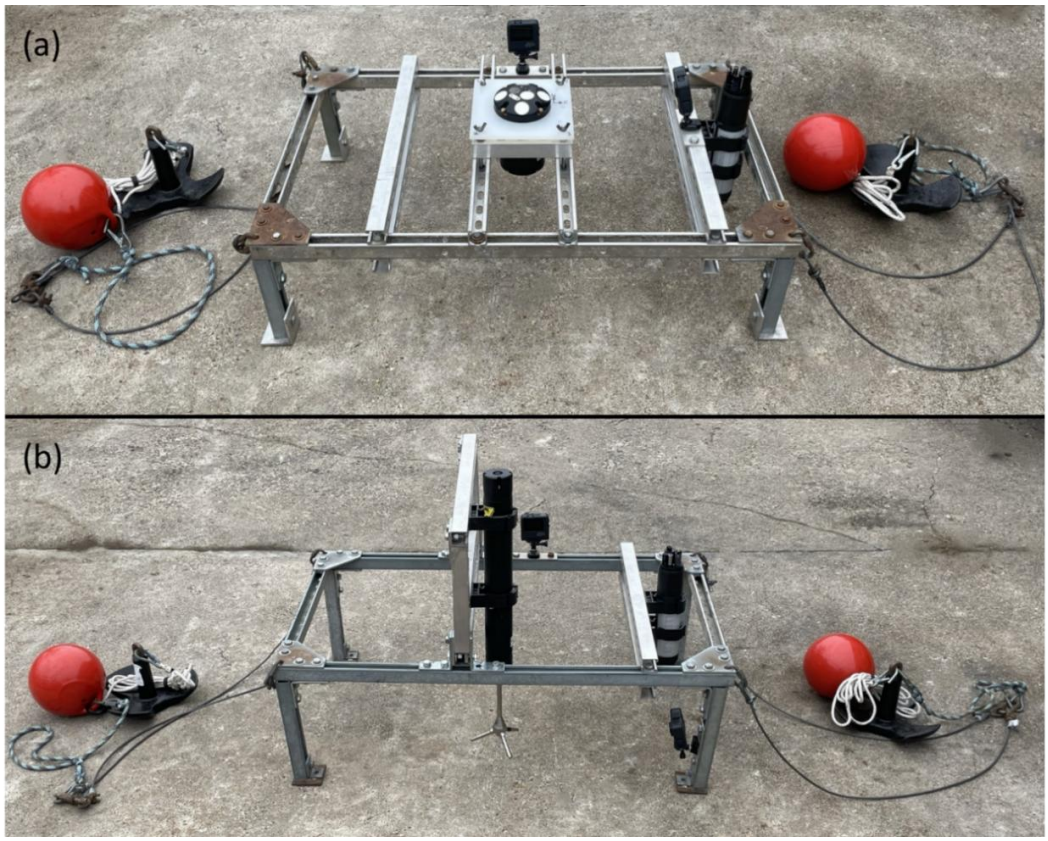

Figure 11. Rectangular pads made of steel strut that the (a) ADCP and (b) ADV were secured to. When deployed on the lake bottom the red buoys created a 20 ft wide goalpost that the test boats were driven through. The fall 2023 fieldwork also included water quality sondes and GoPro cameras mounted to the pads.

5.3.1 Acoustic doppler current profiler

An Acoustic Doppler Current Profiler (ADCP; Nortek Signature 1000) was secured to the center of one of the pads and deployed on the lake bottom in 27 ft of water in 2022, and 14 ft of water in 2023 (Figure 11a, Table 1). The ADCP is an autonomous unit with an internal clock synched to internet time, battery, and data logger. Specifically, the ADCP was mounted up-looking to collect high-resolution echogram and velocity measurements through the water column (i.e., 1.5 ft off the lake bottom to the water surface). Additionally, the ADCP measured its magnetic bearing, motion (e.g., pitch/roll), and the local water temperature and pressure at the sensor. During post-data processing, the pitch and roll orientations were examined for each deployment to verify that the ADCP wasn't excessively tilted during data collection. Additional details on tilt measurements are provided in the Appendix.

For an ADCP to operate, there needs to be particles in the water that have an acoustic impedance (i.e., resists and reflects sound waves) that are sufficiently different from the surrounding water. The ADCP in our deployment utilized five acoustic transceivers to transmit and receive "pings" of sound waves at a programmed sampling frequency of 4 Hz. Each ping travels through a focused region along the transceiver's axis, hereafter referred to as a beam. The beams pointed toward the water surface, where Beam 5 pointed vertically, and Beams 1-4 pointed at a 25° angle from vertical (Figure 12). Prior to deployment, the beams were programmed into vertical measurement bins, where the height of each bin (i.e., cell size) is a user-specified parameter. The bin height was set at 5.0 cm in 2022 and 2.0 cm in 2023. The ADCP was deployed such that Beams 1 and 3 were aligned with the boat track line and Beams 2 and 4 were aligned transverse to the track line. By precisely measuring the travel time of a beam to reflect off particles (e.g., exhaust bubbles, sediment, aquatic biota, etc.), the ADCP captured the vertical distance and intensity of reflectors in the water column. The ADCP used Beam 5 to generate the echogram data (Section 6.1), while all 5 beams were simultaneously used to calculate water column velocities (Section 6.2). Additional information on the principles of ADCP operation are included in the Appendix.

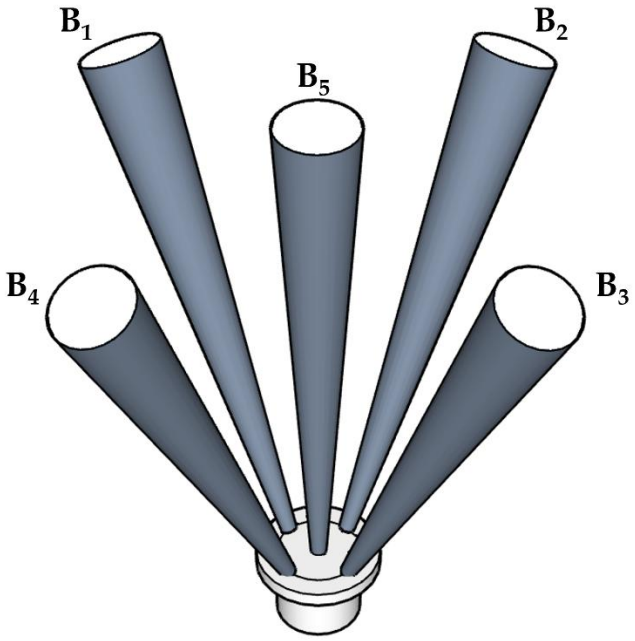

Figure 12. Conceptual illustration of the five beams that emit from the Acoustic Doppler Current Profiler (ADCP) towards the water surface where Beam 5 (B_5) points vertical and Beams 1-4 (B_1, B_2, B_3, B_4) point at a 25° angle from vertical.

5.3.2 Acoustic doppler velocimeter

An Acoustic Doppler Velocimeter (ADV; Nortek Vector – 300 m) was secured to the center of another pad and deployed in 16 ft of water in fall 2022, and 9 ft of water in fall 2023 (Figure 11b, Table 1). Like the ADCP, the ADV is an autonomous unit with an internal clock synchronized to internet time, battery, and data logger. The ADV is a high-accuracy single-point current meter that collected a small volume (i.e., 15 mm diameter x 15 mm height) of velocity measurements at a sampling rate of 32 Hz. The stated accuracy of the ADV is ±0.5% or ±1 mm/s (0.00328 ft/s). The ADV is based on the Doppler shift principle. The ADV transmits two short pulses of acoustic energy that reflect off moving particles (e.g., plankton, sediment) in the sample volume. The phase shift recorded in the reflected sound is measured by the three receiving probes (Figure 13) and used to calculate the three components of velocity along the beam coordinates, and subsequently transformed to the Cartesian XYZ coordinate system. The ADV has a defined x, y, and z orientation, where x and y are horizontal, and z is vertical. The ADV was deployed down-looking with the x direction aligned with the boat track line, and the sampling volume positioned

4 inches (10 cm) off the lake bottom. In addition to near-bed velocity measurements (Section 6.3), the ADV also collected data quality parameters including the signal-to-noise ratio (SNR), correlation, signal strength (i.e., amplitude), and the local pressure at the ADV. The use of these datasets is further described in the data analysis section (Section 6.3.1).

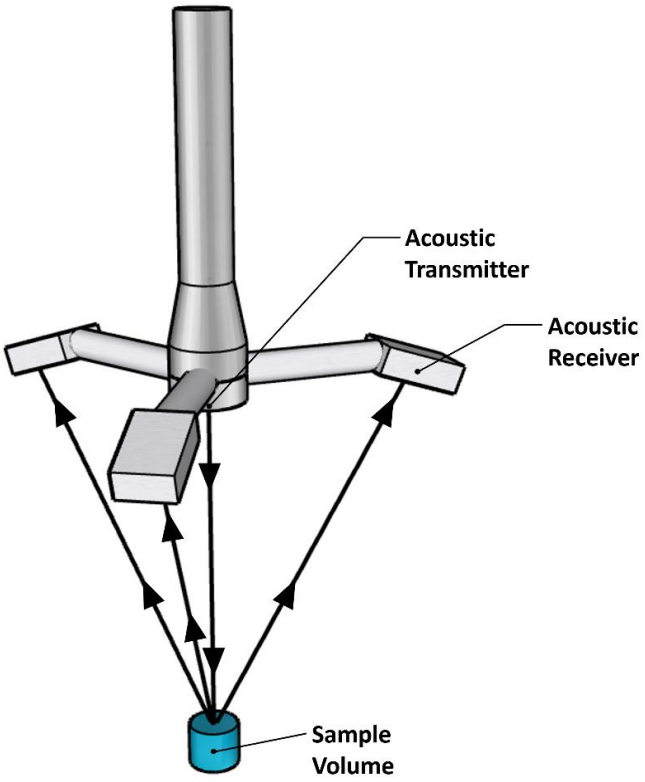

Figure 13. Conceptual illustration of an Acoustic Doppler Velocimeter (ADV)

5.3.3 Other sensors

Additional data collection sensors were deployed in the fall 2023 field campaign. Water quality sondes were deployed on each pad to continuously collect turbidity measurements (Figure 11, Section 5.8.3). Because of the complexity of boat-generated waves and wash, we also wanted to visually document these phenomena. Two video cameras (GoPro HERO9 Black) were secured to each pad that recorded timestamped video for the duration of the pad deployments (Section 6.6). One video camera was positioned so the frame of view was the sensor (i.e., ADCP or ADV), while the other looked down the boat track line (i.e., boats traveled directly above and away from the camera) with the lakebed in the frame of view.

5.4 Types of recreational powerboats tested

This study included seven recreational powerboats categorized into three common types: deck boats, bowriders, and wakeboats (Table 2). This study is not intended to highlight any specific boat manufacturer, but rather recreational powerboats in general. There are many other boat manufacturers, models, and types not considered in this study.

5.4.1 Deck boat with an outboard engine

A deck boat employs a wide V-shaped planing hull design that expands the bow section and allows for more deck space and seating. The two deck boats tested were powered by outboard engines that were controlled at the helm. Outboard engines are mounted to the outside of the transom with only the drive unit (i.e., propeller, skeg, and other components) being submerged. The entire engine can be turned and/or trimmed to change performance during various operating conditions, and this attribute makes the boat highly responsive to maneuvering at slow speeds.

We tested a 2016 Hurricane SS203 and a Starcraft Limited 2000. The 2016 Hurricane SS203 was powered by a 175-horsepower outboard engine, had a length of 20.8 ft, a beam of 8.5 ft, and weighed 2,600 lb dry (Table 2). Although powered by a slightly smaller outboard engine (i.e., 150-horsepower), the 2021 Starcraft Limited 2000 was nearly identical in terms of size. It had a length of 20.3 ft, a beam of 8.5 ft, and a dry weight of 2,715 lb (Table 2). These boats were not equipped with wake-manipulating technologies and the divergent wake waves that were produced were symmetric.

5.4.2 Bowrider with an inboard/outboard engine

A bowrider has a narrowing bow with passenger seating and a deep V-shaped planing hull that improves performance, especially handling during rough waters and high speeds. The three bowriders tested were powered by inboard/outboard (I/O) engines, also known as sterndrives, because the engine is positioned at the stern with the drive unit protruding through the transom under the waterline. When the boat operator steers and/or changes the trim angle, only the protruding drive unit responds in accordance. Similar to outboard motors, I/O engines are more responsive to slow-speed maneuvers than other powertrain types (e.g., inboard, jet). Like the

deck boats, the bowriders were not equipped with wake-manipulating technologies and created divergent wake waves that were symmetric.

We tested a 2021 Cobalt R5, 2022 Cruisers Yachts 34GLS, and 2023 Sea Ray SPX190. The Cobalt R5 had a 300-horsepower engine, a length of 25.7 ft, a beam of 8.5 ft, and weighed 4,880 lb dry (Table 2). It is important to note that this engine had contra-rotating propellers (i.e., two propellers on the same shaft that counter-rotate). The Cruisers Yachts 34GLS was the largest boat tested in terms of power and size and fits the description of a yacht because it has a cabin intended for overnight use. Two 380-horsepower engines, both having contra-rotating propellers (i.e., four total propellers), powered this 35.8 ft long, 11.7 ft wide, and 14,530 lb boat (Table 2). Boats of this size are uncommon on most Minnesota inland lakes, except for on larger lakes, like Lake Minnetonka where this study took place. The Sea Ray SPX190 was the smallest boat tested in terms of length (19.6 ft) and width (8.3 ft) and weighed 2,675 lb dry (Table 2).

5.4.3 Wakeboat with an inboard engine

Like the bowrider with an I/O engine, a wakeboat has a deep V-shaped planing hull with an engine housed at the stern. The majority of the wakeboats today, including the two tested in this study, employ a V-drive inboard powertrain configuration. Here, the drivetrain makes a V-shape before the driveshaft protrudes through the hull (i.e., under the boat) where a rotating propeller provides thrust while a rudder determines the boat's direction. Inboard engines are preferred by wakesport enthusiasts because of the increased safety with the propeller set forward of the transom. Further, having the engine weight at the stern creates greater aft trim, and thus larger wake waves. In addition to engine placement, wakeboats are specifically designed (e.g., weight, hull shape) and equipped with various technologies to generate and manipulate the large wake wave characteristics (e.g., height, length, shape, direction) needed for wakesports, like wakesurfing. In general, the technologies employed include ballast systems, wake shapers, and trim/hydrofoil plates. Ballast systems take on water that makes the boat heavier and able to displace more water, which results in increased wake wave size. Wake shapers are baffle-like tabs on either side of the transom, just below the water surface. When one side is actuated, the flow is directed to form an asymmetric wake that is larger and smoother on the opposite side of the boat. This is where the wakesurfing takes place. Finally, trim/hydrofoil plates off the boat's

transom can be deployed or stowed to change the running pitch of the boat. For example, they can aid in getting the boat on plane quicker, keep the bow down while turning, or add downward force at the stern during wakesports. Refer to Section 5.5.2 for a more detailed description of these wake-altering technologies and their use during testing.

We tested a 2022 Nautique Super Air G23 Paragon and a 2019 Malibu Wakesetter VLX. The 600-horsepower Nautique Super Air G23 Paragon was the bigger of the two wakeboats tested. It was 23 ft long with an 8.5 ft beam and weighed 7,200 lb dry (Table 2). The 450-horsepower Malibu Wakesetter VLX had a length of 21 ft, a beam of 8.2 ft, and a dry weight of 4,200 lb (Table 2).

Table 2. Summary of the seven powerboats tested.

Boat Type	Manufacturer	Model	Year	Drive	Max Horsepower	Length (ft)	Beam (ft)	Dry Weight (lb)	Max Ballast (lb)	Trim Plate/ Hydrofoil	Wake Shaper
Deck	[1] Hurricane	SS 203	2016	Outboard	175	20.8	8.5	2600	No	No	No
Bowrider	[1] Cobalt	R5	2021	Inboard/Outboard	350	25.7	8.5	4880	No	No	No
Bowrider	[1] Cruisers Yachts	34 GLS	2022	Inboard/Outboard (twin)	760	35.8	11.7	14530	No	No	No
Wake	[1,2] Nautique	Super Air G23 Paragon	2022	Inboard (V-drive)	600	23.0	8.5	7200	2200	Yes	Yes
Wake	[1,2] Malibu	Wakesetter VLX	2019	Inboard (V-drive)	450	21.0	8.2	4200	3690	Yes	Yes
Deck	[2] Starcraft	Limited 2000	2021	Outboard	150	20.3	8.5	2715	No	No	No
Bowrider	[2] Sea Ray	SPX 190	2023	Inboard/Outboard	250	19.6	8.3	2675	No	No	No

1 - Fall 2022
1,2 - Fall 2022 and 2023
2 - Fall 2023

5.5 Operating conditions tested

This study tested two operating conditions that represent typical boating activities for each boat tested. The operating conditions were defined by boat speed and if/when applicable, engine trim, ballast weight, and position of the trim/hydrofoil plate and wake shaper (Tables 3 and 4). Three occupants were aboard the boats during testing that added a combined weight of approximately 500 lb. The occupants were the driver in the helm seat, and two passengers, one in the seat adjacent the driver and the other in the stern seating area.

5.5.1 Condition 1

For Condition 1 (Table 3), all boats traveled in planing mode (i.e., 21.0 - 25.0 mph), where the weight of the boat is largely supported by hydrodynamic lift, rather than hydrostatic forces (i.e., buoyancy). Here, the boat has minimal draft and hull drag. Common activities that occur while planing include fast cruising, waterskiing, and tubing. The slight difference in boat speeds was a result of the boats' ability to reach planing mode fully. For example, the two heaviest boats (i.e., Cruisers Yacht 34 GLS and Nautique G23 Paragon) required slightly more speed than the other boats to get fully on plane.

The drive units on the deck and bowrider boats were trimmed to a neutral position, where the propeller shaft was parallel to the water surface. Both wakeboats used their trim/hydrofoil plates (i.e., Nautique's Configurable Running Surface (NCRS) and Malibu's Power Wedge III) to pass through semi-displacement mode quickly; however, the plates were automatically stowed once reaching planing mode. The ballast tanks were empty, and the wake shapers were stowed.

Table 3. Summary of the operating conditions for Condition 1. The boats traveled in planing mode with no wake-enhancing technologies deployed.

Boat	Boat Speed (mph)	Engine Speed (rpm)	Engine Trim	Ballast (lb)	Trim Plate/ Hydrofoil	Wake Shaper
[1] Hurricane SS 203	21.0	3250	Neutral	N/A	N/A	N/A
[1] Cobalt R5	21.0	3000	Neutral	N/A	N/A	N/A
[1] Cruisers Yachts 34 GLS	25.0	3650	Neutral	N/A	N/A	N/A
[1,2] Nautique G23 Pragagon	22.0	2900	N/A	0	Stowed	Stowed
[1,2] Malibu VLX Wakesetter	21.0	3800	N/A	0	Stowed	Stowed
[2] Starcraft Limited 2000	21.0	3300	Neutral	N/A	N/A	N/A
[2] Sea Ray SPX 190	21.0	2650	Neutral	N/A	N/A	N/A

1 - Fall 2022
1,2 - Fall 2022 and 2023
2 - Fall 2023

5.5.2 Condition 2

For Condition 2, the non-wakeboats traveled in displacement mode where the weight of the boat was primarily supported by hydrostatic forces (i.e., buoyancy). Boating activities that tend to occur in displacement mode include leisurely cruising, night navigation, encountering objects (e.g., other boats, docks), etc. The drive units were trimmed to a neutral position and the boats traveled 9.0 mph in 2022 and 7.0 mph in 2023 during testing.

The wakeboats traveled in semi-displacement mode (i.e., 11.6 mph), also referred to as transitional or plowing mode. Here, the boats remained in this transition period between displacement mode and planing mode where some hydrodynamic lift occurs, but the weight of the boat is predominately supported by hydrostatic forces (buoyancy). This causes maximum hull resistance which creates the large wake waves needed for wakesurfing. In addition to traveling in semi-displacement mode, the wake-altering technologies were specifically set for wakesurfing and are described hereafter.

The Nautique G23 Paragon has configurable wakesurf settings that customize the wake to the rider's preference by changing the ballast weight and its distribution, the trim position of the NCRS, and the horizontal reach of the wake shaper (referred to as the Nautique Surf System –

NSS). The settings range from 0-10, with 10 creating the tallest and steepest wake. During testing, the boat was set to general wakesurf setting number five (Figure 14a). The ballast tanks were 100% filled with 2,200 lb. of water weight, the port side wake shaper was fully deployed (Figure 14b) forming an asymmetric wake that was larger and smoother on the starboard side (Figure 14c), and the NCRS was stowed.

Figure 14. (a) Factory wakesurf setting five that was selected for Condition 2 testing, with (b) showing the NSS fully deployed, and (c) the actual asymmetric surfwake that formed during testing.

The Malibu VLX Wakesetter also had its ballast tanks 100% filled, which added 3,690 lb of water weight. Like Nautique's NSS, Malibu's version of the wake shaper, termed Surf Gate (Figure 15a), was deployed on the port side to produce an asymmetric wake that was larger and smoother on the starboard side of the boat (Figure 15b). Malibu's hydrofoil, termed Power Wedge III, can produce up to 1,500 lb of downward force, which is equivalent to 1,500 lb of aft ballast (Malibu

Boats 2020). The Power Wedge III had adjustable settings that ranged from lift to stow (Figure 15c). When in lift mode the hydrofoil creates an upward lift force that allows the boat to get on plane quickly. The wake becomes taller and steeper as the hydrofoil is raised from lower-numbered settings to higher-numbered settings. The Power Wedge III was set to position two during the testing of this operating condition (Figures 15c and 15d). Note – we added the numbers (1-6) to help explain the selected settings.

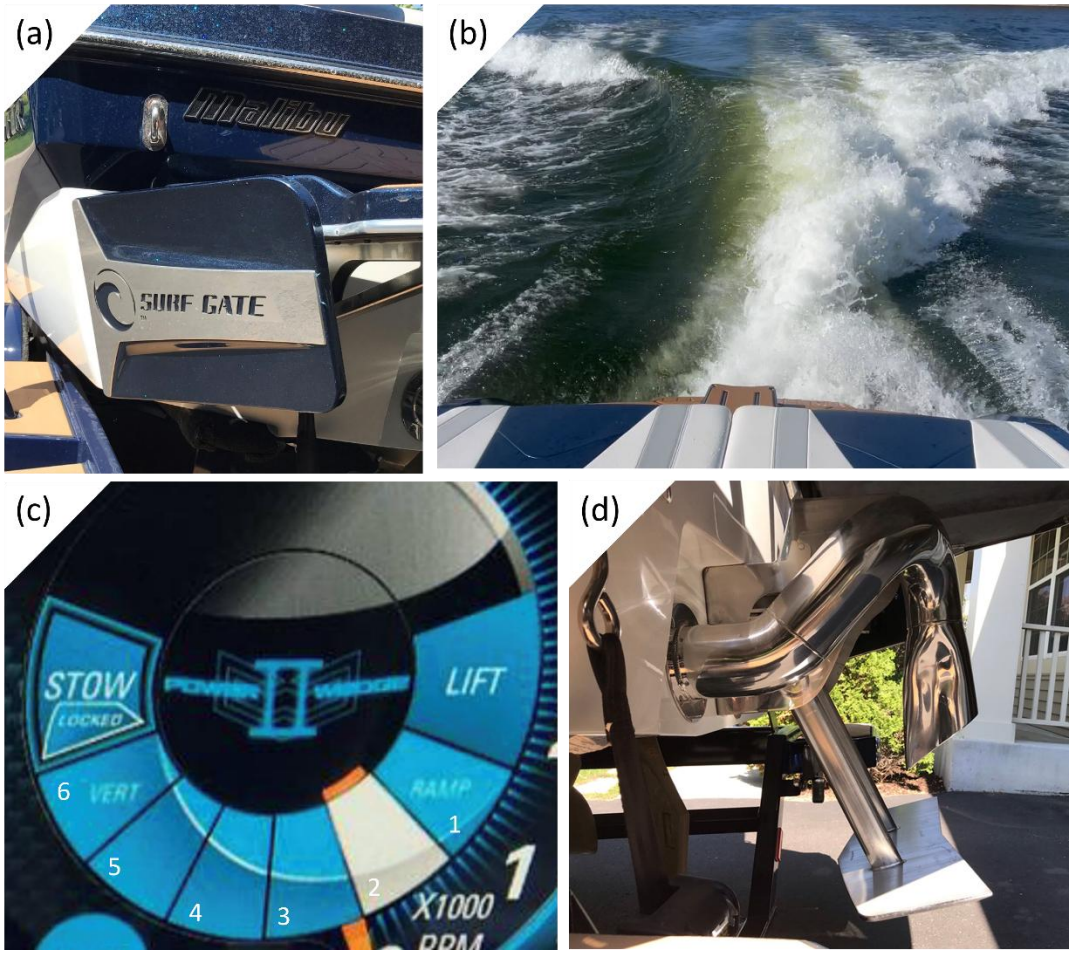

Figure 15. (a) Malibu's portside wake shaper (Surf Gate) and (b) the asymmetric surfwake that formed during testing. (c) The Power Wedge III was set to position two with (d) showing the running attitude of the Power Wedge III in said position. It also shows the engine exhaust manifold.

Table 4. Summary of the operating conditions for Condition 2. The non-wakeboats traveled in displacement mode with no wake-enhancing technologies deployed. The wakeboats traveled in semi-displacement mode with their wake-enhancing technologies specifically set for wakesurfing.

Boat	Boat Speed (mph)	Engine Speed (rpm)	Engine Trim	Ballast (lb)	Trim Plate/ Hydrofoil	Wake Shaper
[1] Hurricane SS 203	9.0	2400	Neutral	N/A	N/A	N/A
[1] Cobalt R5	9.0	2000	Neutral	N/A	N/A	N/A
[1] Cruisers Yachts 34 GLS	9.0	1650	Neutral	N/A	N/A	N/A
[1,2] Nautique G23 Pragagon	11.6	2900	N/A	2200	Stowed	Port - Position #5
[1,2] Malibu VLX Wakesetter	11.6	4400	N/A	3690	Down – Setting #2	Port - Deployed
[2] Starcraft Limited 2000	7.0	1600	Neutral	N/A	N/A	N/A
[2] Sea Ray SPX 190	7.0	1550	Neutral	N/A	N/A	N/A

1 - Fall 2022
1,2 - Fall 2022 and 2023
2 - Fall 2023

5.6 Creating boat-generated hydrodynamic disturbances

Each powerboat was tested in a single day. Wind speed, wind direction, and air temperature data were obtained from a nearby weather station for each test day. These data were averaged one-hour preceding a test condition and one-hour during a test condition (Appendix). Each boat made five passes along the track line for the two operating conditions evaluated (Section 5.5). 15 minutes transpired between each pass to allow water conditions to return to a pre-pass steady state. Planing (Condition 1) testing was in the morning, and displacement or semi-displacement (Condition 2) testing was in the afternoon. Condition 1 was performed first because there was a lower likelihood of lake bottom disturbance when the boat was in planing mode. An hour-long hiatus occurred between testing the two conditions to allow any suspended materials (e.g., sediment, detritus, etc.) to settle. To ensure the waves and wash being generated by the boats were at a steady state when passing over the pads, the boat operator reached test speed and alignment with the track line before arriving at the start buoy and continued to maintain speed and course until fully passing the end buoy (Figures 8 and 9).

5.7 Collecting real-time boat position and attitude

We used the same instrumentation as Marr et al. (2022) to continuously measure the boat's GPS position, speed, and pitch during each pass. A high-performance global navigation satellite system aided by an inertial navigation system (VectorNav 200) was mounted to the center of the test boat and a mobile Raspberry Pi-based interface running Python queried the data into a single data file at 5 Hz. The positional data for each pass were later imported into ArcMap (examples shown in Figures 8 and 9).

In the context here, pitch refers to the angle of a boat's hull in relation to the waterline. As hull pitch increases the bow lifts higher into the air and the stern sinks more into the water. No pitch (zero degrees) would indicate that the boat's hull is parallel to the waterline. The pitch of a boat's hull is important because it is directly related, amongst others (e.g., motor trim, prop shaft, propeller pitch), to the angle and penetration depth of the propeller wash.

5.8 Collecting water quality parameters

To examine the direct effects of boat passage, various water quality data were collected including water temperature profiles, total suspended solids (TSS), volatile (organic fraction) suspended solids (VSS), fixed (inorganic fraction) suspended solids (FSS), total phosphorus (TP), and turbidity.

5.8.1 Temperature profiles

The intended purpose of collecting continuous temperature profiles through the water column in 2022 was to determine if the boat wave and wash being generated caused thermally stratified waters to mix. In the case of this study, it is not so much the actual temperature (i.e., degrees) that was of interest, but the potential change with cumulative boat passes.

In the 2022 field campaign, waterproof temperature sensors (HOBO UA-002-64) were used to profile the water column temperature at each pad location. The sensors were synchronized with internet time before deployment and programmed to sample every 10 seconds (0.10 Hz). At the 27 ft pad location, 8 sensors were attached to a taught anchor/buoy line spaced vertically at 3 ft increments. At the 16 ft pad location, 10 sensors were deployed in the same fashion but spaced vertically at 1.5 ft increments. The sensor lines, referred to as temperature chains, were positioned on the west side of the boat track line immediately adjacent to the goalpost buoys

(Figure 8). The temperature chains were deployed in the morning before boat testing began and were removed in the afternoon after testing concluded.

Based on the fall 2022 water temperature data (Section 7.2.1.1) and preliminary fieldwork, it was evident the water column temperature would be well-mixed and no longer stratified during the fall 2023 field campaign in Maxwell Bay. Instead of deploying temperature chains again, we opted to use a portable sonde (YSI ProODO) to collect a single water column temperature profile at the deeper 14 ft pad on each test day to verify that there was no measurable stratification. Measurements were collected at 1 ft increments.

5.8.2 Water samples (TSS, VSS, and TP)

Water samples were collected at each pad by two-person crews in small Jon boats. One crew member was responsible for collecting the samples, while the other member maintained the boat's position using oars. Oars were used instead of a motor to minimize any disturbance to the water column (e.g., propeller wash). Moreover, having a designated rower to maintain the boat position eliminated the need to deploy an anchor that would likely disturb the lakebed. The samples were collected via custom-built Van Dorn samplers that were designed to instantly capture triplicate 1 L samples at the same water depth (Figure 16).

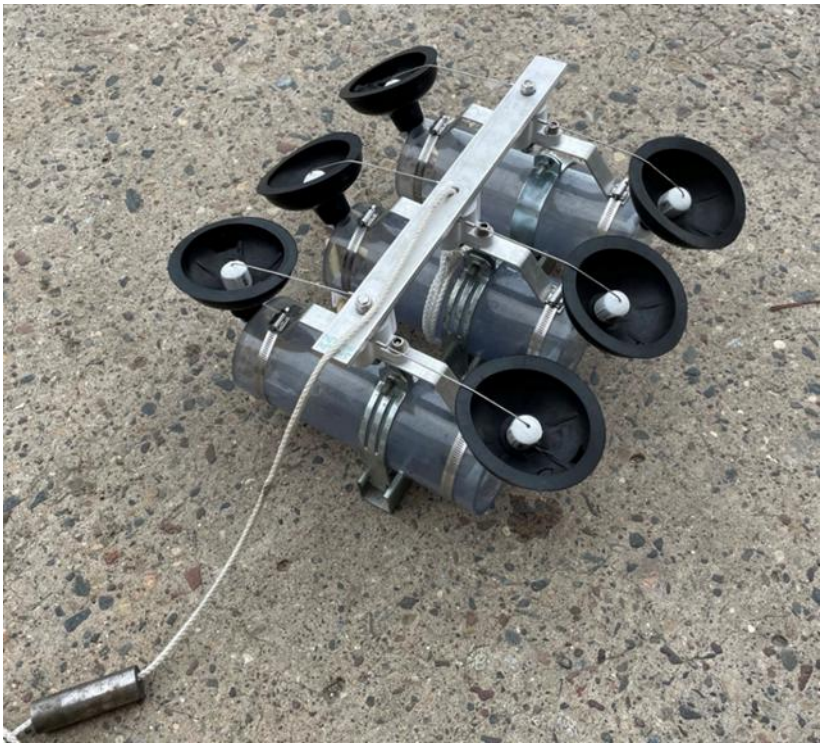

Figure 16. SAFL-built Van Dorn water sampler that instantaneously captured three one-liter samples at a selected water depth.

The samplers were deployed near the sensor pads and directly over the boat track line, fifteen minutes before each set of five passes (pre), immediately after the first pass (pass), and immediately after the fifth and final pass (post). For both field campaigns, samples were collected 3.0 ft off the lakebed at both pads (Table 5). Because the 2022 pads were deployed deeper, an additional sample was collected at the midway depth between the near bed sample and water surface (Table 5).

Table 5. Van Dorn sampling depths at each pad

Year	Pad	Sample 1 Depth	Sample 2 Depth
2022	ADCP	24.0 ft (7.3 m)	12.0 ft (3.7 m)
	ADV	13.0 ft (4.0 m)	6.0 ft (1.8 m)
2023	ADCP	11.0 ft (4.3 m)	N/A
	ADV	6.0 ft (1.8 m)	N/A

Once samples were onboard, 500 mL of each sample was transferred to a clean bottle for laboratory analysis of total suspended solids (TSS) and volatile suspended solids (VSS). In 2022, an additional 50 mL of each sample was collected in a separate sterile vial for laboratory analysis of total phosphorous (TP) concentration. All samples were immediately placed into ice-filled coolers and were transferred to the University of Minnesota's Research Analytical Laboratory (RAL) by the end of the day where they were frozen until analysis. The samplers were thoroughly rinsed with ultrapure water (Milli-Q Water System) between each deployment to prevent cross-contamination.

5.8.3 Turbidity

Turbidity datasets were only collected during the 2023 field campaign due to equipment malfunction in 2022. In 2023, water quality sondes were set to monitor turbidity levels once per minute. On the first day of testing (i.e., Starcraft Limited 2000), a single water quality sonde (In-Situ Aqua Troll 600) was deployed on the deeper (14 ft) pad because newly purchased sondes had yet to arrive. The new water quality sondes (Eureka Manta+30) were deployed on each pad during testing of the three remaining boats. The reported accuracy of this turbidity probe is ± 0.3 FNU (Formazin Nephelometric Unit). Calibration was completed in the laboratory between 0 and 400 FNU using ultrapure water and a turbidity standard. Turbidity measurements were collected 1.5 ft and 0.8 ft from the lakebed at the ADCP and ADV pads, respectively.

5.8.4 Sediment samples

A Van Veen grab sampler was used to collect consolidated lakebed sediment samples from the pad locations once per field campaign. The samples were analyzed for organic matter content, total and extractable phosphorus, and grain size distribution to quantify the characteristics of the lakebed sediment. The sediment sampling method used is prone to lakebed disturbance at the sediment-water inface (e.g., shock wave) that can washout unconsolidated material (e.g., detritus, fine sediments).

5.9 Collecting aerial video

In the 2023 campaign, a professional-grade drone (DJI Phantom 3) was deployed between 250 ft (76 m) and 400 ft (122 m) above the study site to capture video of test boat passes. In addition

to visually documenting any environmental changes (e.g., sediment resuspension), the video allowed for the examination of the wave and wash characteristics from a birds-eye view. For example, wavelengths (i.e., crest to crest) of the transverse waves were measured and used in the ADV analysis process (Section 6.3.2.3).

6.0 DATA ANALYSIS

6.1 ADCP – echogram

The ADCP was used to collect a continuous echogram of the water column during each boat pass. As previously described (Section 5.3.1), Beam 5 measured the intensity of reflected sound within the water column. By knowing the speed of sound in water and the two-way travel time for sound to be emitted and echo back, the ADCP can measure both the sound intensity level (decibel scale) and the distance of the reflector. Strong reflectors include changes in fluid density (e.g., the air-water interface at the water surface, exhaust bubbles, suspended sediments, fish, zooplankton, boat hulls, and more) (Velasco et al. 2021).

All test boats were powered by internal combustion engines, which produce emissions (e.g., exhaust gases) that are discharged into the water at the boat's stern. This is done by the manufacturer for noise suppression and to protect passengers and persons being towed (e.g., waterskiing, wakesurfing, tubing, etc.) from inhaling exhaust gases. For outboard and inboard/outboard engines, the exhaust is either vented through the center of the propeller or ports in the lower unit. For inboard engines, such as on the wakeboats evaluated in this study, the exhaust is discharged into the water just aft of the propeller via a manifold pipe (Figure 15d). Because bubbles are a strong reflector for echo sounding (Velasco et al. 2021), the echograms of the boat passes captured the extent (i.e., depth and duration) of the exhaust bubbles. The echograms were also used to measure the height and duration of sediment that was suspended off the lake bottom.

6.1.1 Analyzing raw data – correction for signal attenuation

Figure 17 is an example of a single boat pass echogram collected by the ADCP in 2023. The vertical axis is water depth where the first measurements occurred at 12.5 ft. This was 1.5 ft above the

lakebed where the ADCP was mounted to a deployment pad (Section 5.3.1). The horizontal axis is time in minutes where time zero (t=0) marks when the boat passed over the ADCP. One minute before the boat's arrival is included in the plot to show the pre-pass condition (i.e., baseline) within the water column. Eight minutes after the boat pass is also included to ensure the full extent of the bubbles was included in the analysis. The figure colors represent the intensity of reflected sound in decibels (dB) with red indicating a higher concentration of bubbles.

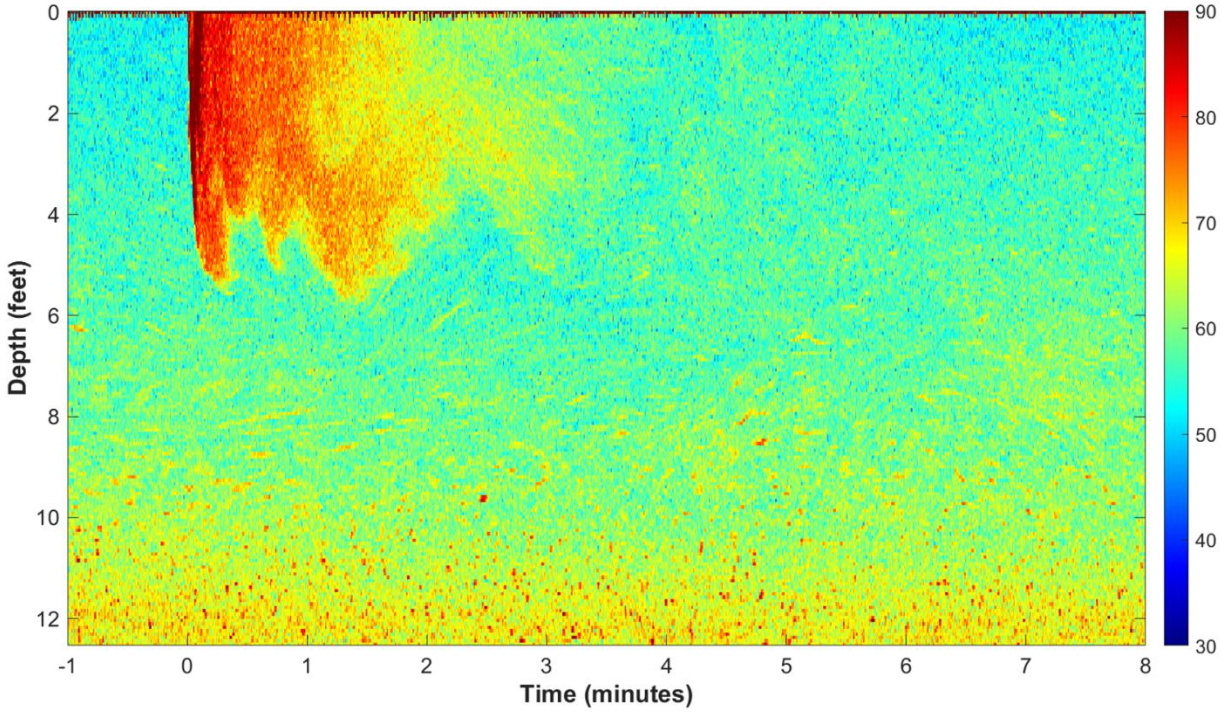

Figure 17. Echogram data from a single pass made by the Starcraft Limited 2000 in planing mode (Condition 1) during the 2023 field campaign. The y-axis is water depth with 0 being the surface. The colors represent the intensity of reflected sound in decibels (dB) with red indicating a higher concentration of bubbles.

In the absence of any strong reflectors in the water column, a loss of sound intensity with distance from the ADCP (y-axis) can be seen in the one-minute time-period before the boat arrives (Figure 17). This was caused by attenuation of the signal as it moved through the water column; we define this as the *baseline attenuation profile*. Eight minutes of pre-condition data was used to compute the baseline attenuation profile that was then subtracted from the raw signal of each boat pass. Figure 18 shows the same echogram data presented in Figure 17 after removing the baseline attenuation profile.

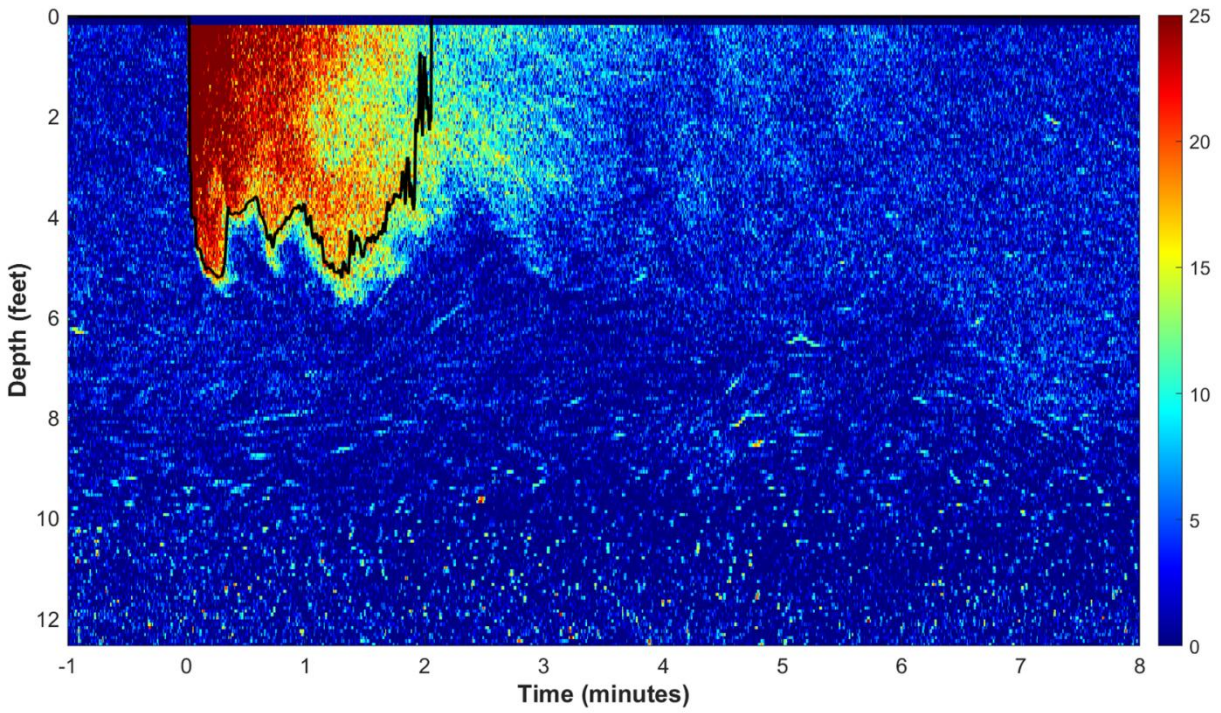

Figure 18. Echogram data from a single pass made by the Starcraft Limited 2000 in planing mode (Condition 1) during the 2023 field campaign after removing the baseline attenuation profile. The black line shows the bubble depth limit using a 15 dB threshold. The colors represent the intensity of reflected sound in decibels (dB).

6.1.2 Examining bubble extent

The echogram data were used to identify and track the extent of the bubbles that were entrained in the water column after each boat pass. This analysis presumes that the high sound intensity measured within the echograms are bubbles.

The data were processed in MATLAB. A thresholding routine was developed to search for the bubble interface, hereafter referred to as the *bubble depth limit*. For each boat pass from t=0 to eight minutes later, we identified the deepest depth where the mean return amplitude exceeded a sound intensity of 15 dB. The threshold of 15 dB was set by trial and error to yield a bubble depth limit that visually matched the filtered echogram data (Figure 18). A mean bubble depth limit was computed and then smoothed using a 5-second moving average filter, which aided in the visual assessment of trends once graphed. In another analysis, the bubble depth limit data was filtered via the 99th percentile to remove outliers before calculating a maximum bubble depth for each test condition. Statistical analysis methods (e.g., ANOVA, *t*-tests) were performed

to compare the mean maximum bubbles depths across the various boats and conditions and are discussed in the results (Section 7.1.1).

6.1.3 Examining sediment resuspension extent

Because inorganic solids (e.g., clays, silts, sands) and organic debris (e.g., detritus) suspended in the water column are also strong acoustic reflectors (Velasco et al. 2021), the echograms were used to evaluate the geometry of the resuspended sediment plumes. Visually examining the echograms of every boat pass showed that in 2023 testing, both wakeboats caused bottom sediment to resuspend above the ADCP when operated in semi-displacement mode (Condition 2). In 2023 the ADCP was deployed in 14 ft of water with the first measurements taken 1.5 ft above the lakebed (Section 5.3.1).

A MATLAB script was developed, much like the bubble depth limit script, to identify the upper depth limit of resuspended sediment using a threshold routine, defined as the *sediment resuspension limit*. The threshold level was set to 10 dB and was determined by trial and error to yield a resuspended sediment limit that visually matched the filtered echogram data (Figure 19). Because the data was highly variable between passes and over time, it was filtered via the 99th percentile before calculating a mean maximum sediment resuspension limit.

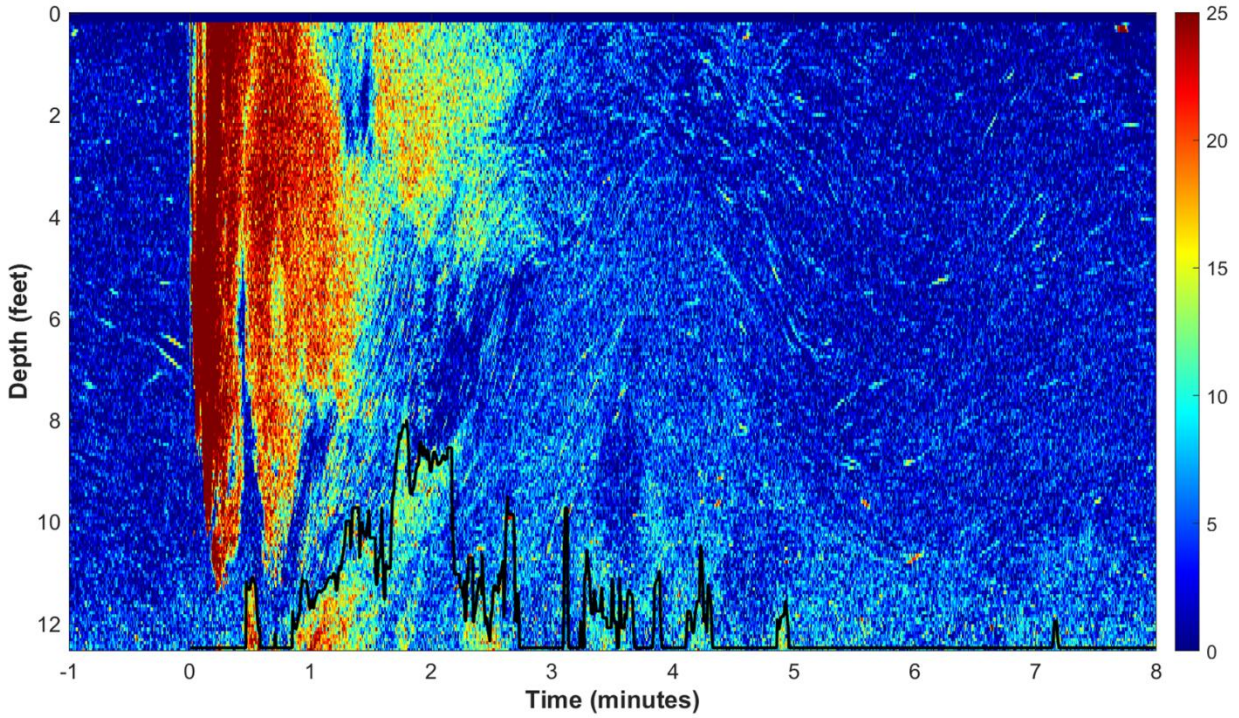

Figure 19. Echogram data from a single pass made by the Malibu VLX Wakesetter in semi-displacement mode (Condition 2) during 2023 testing. The black line shows the sediment suspension limit using a 10 dB threshold. The colors represent the intensity of reflected sound in decibels (dB).

Beyond the visual examination of each echogram, an additional step was executed to ensure no other boat or condition tested in 2023 caused sediment to resuspend above the ADCP. The two wakeboats when operated in semi-displacement mode (Condition 2) created bubbles that penetrated the deepest (Section 7.1.1) and caused sediment to resuspend. Based on the echogram data, the next boat and condition that would have logically resuspended sediment in 2023 testing was the Malibu VLX Wakesetter when operated in planing mode (Condition 1), as it had the next deepest bubble penetration depth (Section 7.1.1). These passes were run through the MATLAB sediment resuspension analysis process and the results showed no evidence (i.e., no values exceeding the 10db threshold) of sediment resuspension above the ADCP. Therefore, it was deemed unnecessary to analyze the other boats and conditions for resuspended sediment. It is important to note that this analysis method could only determine if sediment was resuspended above the ADCP (i.e., >1.5 ft off the bottom). Sediment may have been resuspended

below the ADCP for other boats and conditions; however, the underwater videos show no evidence of sediment resuspension (see results -Section 7.2.2).

6.2 ADCP – water column velocity

In addition to collecting echogram data, the ADCP also continuously collected velocity measurements through the water column, signal quality metrics, and the local water pressures at the instrument. The analysis approach described hereafter sought to isolate the various hydrodynamic phenomena associated with boat operation as described in the background section, which includes the bow and stern waves, transverse waves, and propeller wash.

6.2.1 Data quality checks for all beams (correlation, amplitude, false accelerations, and local pressure)

The first step in processing the velocity data was to remove beam-wise velocity data that was deemed poor-quality. This was done using signal quality metrics, specifically the correlation and amplitude data. Correlation is a parameter that assesses the quality of the return signal relative to the emitted signal. Per the instrument manufacturer's published recommendations, velocity data having correlation values of less than 50% were discarded (Nortek 2017). Amplitude is a measure of the strength of the return signal. Low amplitude (i.e., weak return signal) can result from a lack of particles in the water. Velocity data with amplitude values <3 dB above the noise floor is recommended to be removed from the dataset (Nortek 2017). While the data was evaluated for low amplitude, there were no instances of low amplitude values.

Two additional parameters were used to further filter the data. First, the top 12% of the water column data, 3.2 ft in 2022 and 1.7 ft in 2023, was excluded due to sidelobe interference – an effect of the sound interacting with the water surface that can result in false velocity readings (Nortek 2017). Second, spurious velocity spikes were identified and removed from the data.

After filtering the data, an interpolation strategy was implemented to estimate values within the data gaps that resulted from the filtering process. This strategy used the MATLAB *interp1gap* linear function with a maximum allowable gap distance of five cells. Figure 20 illustrates the output from the filtering and interpolation process for a single beam. This process was performed on the data for all five beams.

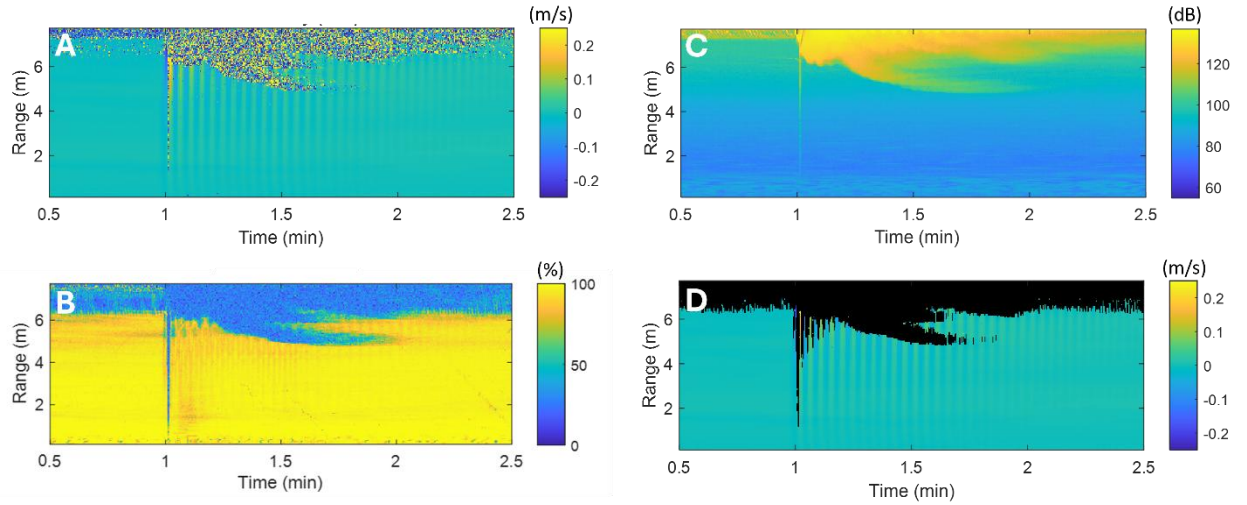

Figure 20. ADCP Beam 1 velocity from a single pass made by the Hurricane SS203 in displacement mode (Condition 2) during 2022 testing. Panels A-D illustrate the filtering processes used for each of the 5 beam-wise velocities. A) raw beam-wise velocity before filtering (m/s). B) correlation data (%). C) amplitude data (dB). D) final filtered beam-wise data after removing poor correlation, amplitude, errant accelerations, and side-lobe interference data and addition of the interpolated velocity data (m/s). The black areas represent excluded data.

6.2.2 Beam-wise velocity transformation into Cartesian coordinates

The ADCP velocity data were captured along beam-wise coordinates. During post-processing, these were transformed into the x, y, z Cartesian coordinate system using standard transformation procedures outlined by the manufacturer (Nortek 2017). During deployment, Beams 1 and 3 were aligned with the boat track line and Beams 2 and 4 were aligned transverse to the track line. Transformation of Beams 1 and 3 (X-direction and Z-direction), 2 and 4 (Y-direction and Z-direction), and 5 (Z-direction) resulted in Cartesian velocities referred to as U_{13}, W_{13}, V_{24}, W_{24}, and W_5. The horizontal (U_{13}) and vertical (W_5) velocities were the most relevant data for the objectives of this study and were thus analyzed; the other velocities are not included in this report. The Appendix includes a description of the transformation process and additional principles of operation for the ADCP.

6.2.3 Decomposition of the measured signal and extracting component velocity parameters

6.2.3.1 Determining time of peak wave velocities

The maximum horizontal (U_{13}) and vertical (W_5) velocities produced by the bow, stern, and transverse waves occur at the times associated with the maximum and minimum wave peaks of

these hydrodynamic phenomena. The first step in the Condition 2 analysis was to extract these times for each boat pass by plotting the vertically averaged velocities for the bottom half of the water column (2022: ~13-27 ft and 2023: ~7-14 ft), then manually selecting the times associated with the maximum and minimum velocities (Figure 21). The bottom half of the water column was selected because it was generally a cleaner signal, devoid of intense propeller wash. These time arrays were utilized in the data analysis steps described below.

For Condition 1, the time arrays were established a different way because transverse waves did not exist. In these cases, the time arrays were determined by the following equation (3):

$$time(n) = \Delta t * n \quad (3)$$

Where,

n was an integer ranging from 1 to 40. The maximum of 40 was determined by trial and error to provide a total duration sufficient for analysis.

Δt was computed as the time difference between the bow wave maximum and the stern wave minimum.

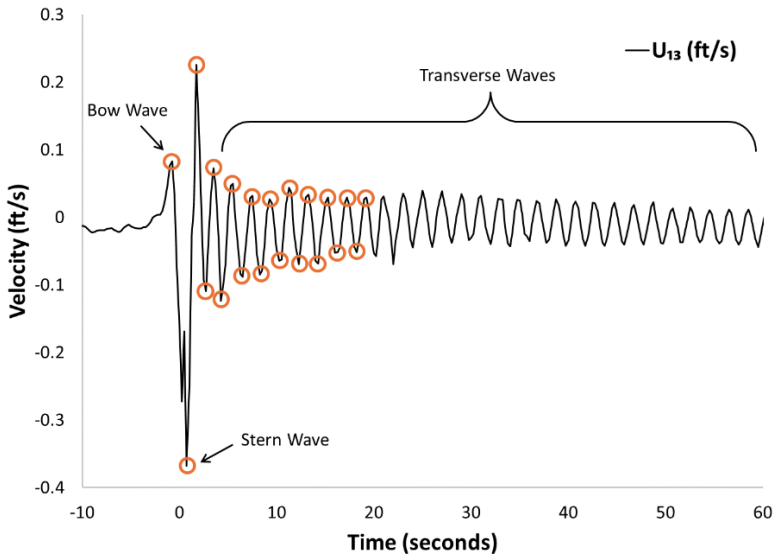

Figure 21. Vertically averaged horizontal (U_{13}) velocity of the bottom half of the water column during a single pass made by the Sea Ray SPX190 operating in displacement mode (Condition 2) during 2023 testing. The orange circles represent the manually selected times of the maximum and minimum velocities for the bow, stern, and transverse waves.

6.2.3.2 Estimating bow and stern wave velocities

The user-selected times were used to extract U_{13} and W_5 velocity profiles through the water column at the maximum value of bow and stern pressure waves for each of the five passes. These data were fed through MATLAB *filloutliers* function. Outliers were identified with a 10-cell *movmedian* function and replaced using linear interpolation of neighboring non-outlier data. A z-score was then calculated for each data point through the water column (depth intervals were 0.16 ft in 2022 and 0.07 ft in 2023) for each of the five passes, and used to identify outliers, where values greater than ± two standard deviations from the mean were removed. Figure 22 is example data for the five passes made by the Hurricane SS203 deck boat during displacement mode (Condition 2) testing in 2022, showing the individually filtered bow and stern wave velocities through the water column and the five pass mean. The mean bow and stern wave velocity profiles were computed for each test boat and condition and plotted in the results section for comparison.

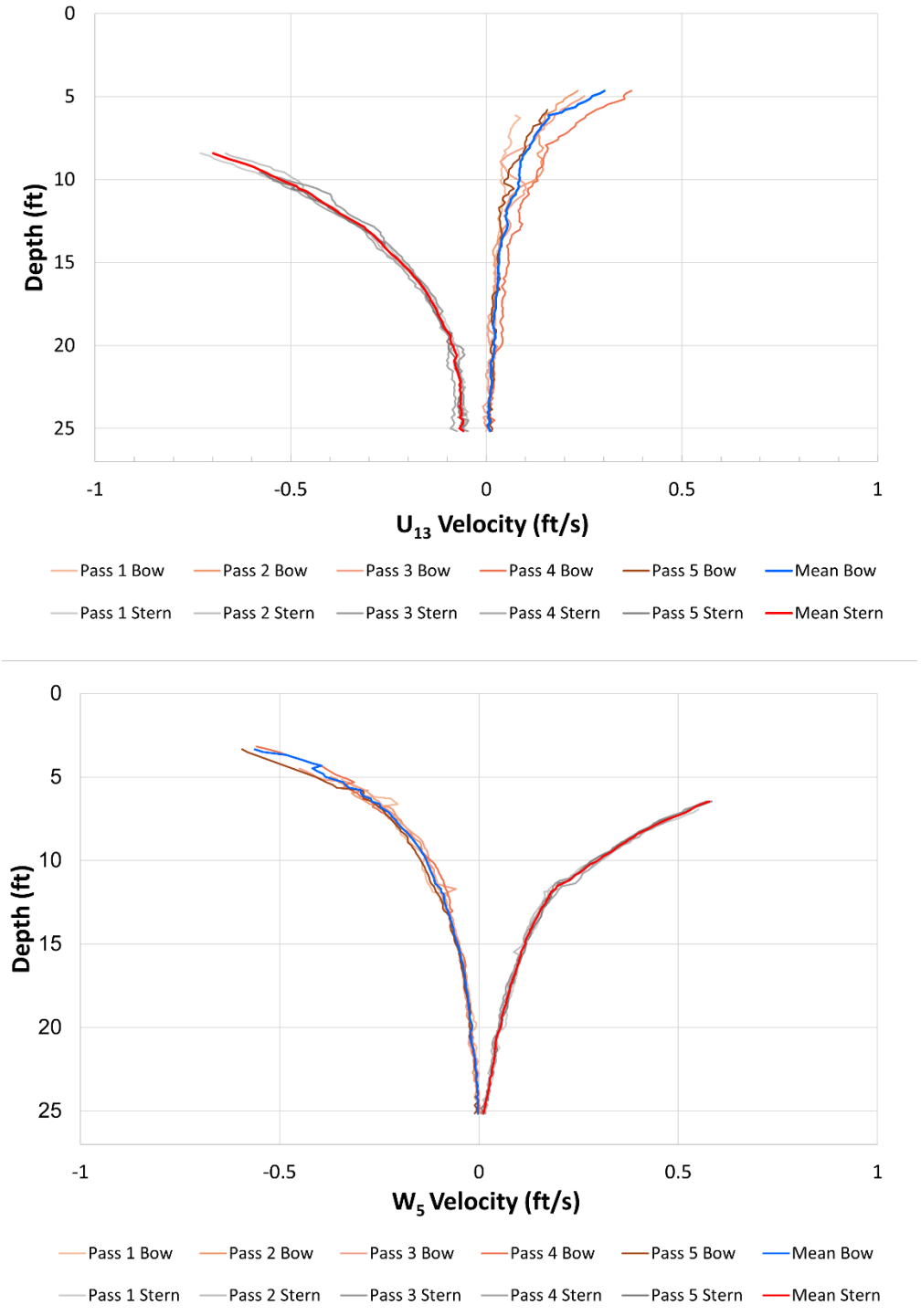

Figure 22. Horizontal (top) and vertical (bottom) velocities produced by the bow and stern pressure waves, measured for each pass of the Hurricane SS203 during Condition 2 testing in 2022. Positive U_{13} velocities indicate water moving in the same direction as the boat, and positive W_5 velocities indicate water moving vertically towards the water surface.

6.2.3.3 Estimating propeller wash velocities during planing mode (Condition 1)

The U_{13} and W_5 velocity data immediately following the stern pressure wave were used to evaluate propeller wash velocities at three discrete depths. For 2022 data, where the maximum depth at the ADCP was 27 ft, data were evaluated at depths of 10, 15, and 20 ft from the surface. For 2023, where the maximum depth was 14 ft, data were evaluated at depths of 8, 10, and 12 ft from the surface.

As described in Section 6.2.3.1, a sampling time interval was computed from the time between the bow and stern wave, Δt. This sampling time interval was used to subsample U_{13} and W_5 data. This was done to use a consistent analysis approach for datasets with and without transverse waves. Using MATLAB's *filteroutliers* function, each pass was then filtered to remove values ± two standard deviations from the mean. Figure 23 is an example of the five passes of subsampled W_5 data from the 2022 Malibu VLX Wakesetter after filtering.

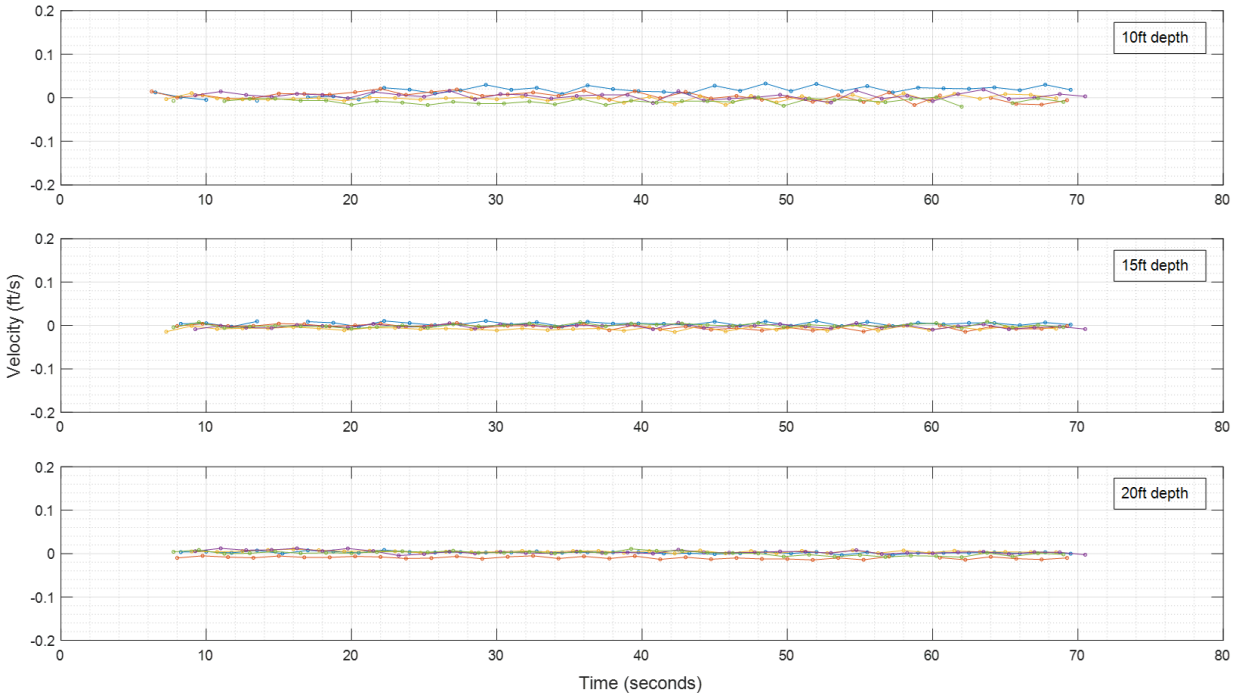

Figure 23. Example of processed and subsampled W_5 data at depths of 10, 15, and 20 ft from the surface for the Malibu VLX Wakesetter during 2022 planing mode (Condition 1).

The data were further distilled. For each evaluation depth, the data for each pass was binned into three time-bins, followed by calculating a mean for each bin. The selected time-bins were 5-10

seconds, 10-30 seconds, and 30-50 seconds and selected to roughly capture changes in velocities within 50 seconds of the boat pass. The distribution of the time-binned means for each test year, boat, and condition are shown and compared via box plots in the results.

6.2.3.4 Estimating velocities associated with transverse waves and propeller wash during displacement or semi-displacement mode (Condition 2)

When a boat travels at displacement and semi-displacement speeds the hull produces transverse waves, which travel at approximately the same speed and direction as the boat (Section 2.1.2). Additionally, the water immediately astern receives propeller wash (Section 2.1.3). The dynamics between the transverse wave and propeller wash are highly complex and dependent on the boat's operational speed, water depth, hull resistance, and more. The objective of this analysis was to isolate the individual velocity contributions of the transverse wave and propeller wash.

6.2.3.4.1 Decoupling transverse waves and propeller wash velocities

The method used to extract the horizontal (U_{13}) and vertical (W_5) velocities associated with the transverse waves took advantage of the oscillatory nature of the wave, focusing on the maxima and minima of the transverse wave. Previously, we described how the times associated with peaks and troughs in the U_{13} and W_5 dataset were manually selected and recorded. The transverse wave velocity at each of the selected times was computed as ½ the difference between consecutive maximum to minimum or minimum to maximum (e.g., peak to trough) – effectively the amplitude of the local orbital velocity. The general equations used for computing the absolute values of the transverse wave velocities are:

$$U_{Twave} = \left|\frac{\left(\widehat{U_{13}}(i)-\widehat{U_{13}}(i-1)\right)}{2}\right| \quad (4)$$

$$W_{Twave} = \left|\frac{\left(\widehat{W_5}(i)-\widehat{W_5}(i-1)\right)}{2}\right| \quad (5)$$

Where, $\widehat{U}_{13}$ and $\widehat{W}_5$ are the measured horizontal and vertical velocities and $\widehat{\ }$ indicates the baseline currents within the lake measured before the boat pass velocities have been subtracted. (*i*) represents the time of the wave maximum/minimum and (*i-1*) represents the time maximum/minimum immediately before *i*.

The method used to extract the horizontal (U_{13}) and vertical (W_5) velocities associated with the propeller wash were computed in a similar manner. Again, $\widehat{U}_{13}$ and $\widehat{W}_5$ data were used. The average of two consecutive maxima/minima were computed and represent the local velocity component of propeller wash. This approach assumes that the transverse wave is oscillatory about zero. Under this condition, the average of a consecutive transverse wave peak and trough will be approximately zero and therefore canceled out of equations 6 and 7, leaving only the portion of the velocity associated with the propeller wash. The general equations for computing the propeller wash are:

$$U_{propwash} = \frac{\left(\widehat{U_{13}}(i)+\widehat{U_{13}}(i-1)\right)}{2} \quad (6)$$

$$W_{propwash} = \frac{\left(\widehat{W_5}(i)+\widehat{W_5}(i-1)\right)}{2} \quad (7)$$

U_{Twave}, W_{Twave}, $U_{propwash}$ and $W_{propwash}$ were computed at each identified maxima/minima after the stern pressure wave and evaluated at the same three water depths as described in the planing mode (Condition 1) analysis, which were 10, 15, and 20 ft for 2022 and 8, 10, and 12 ft for 2023.

6.2.3.4.2 Estimating transverse wave velocities

Further processing of the transverse wave data (U_{Twave}, W_{Twave}) began with each pass being filtered using MATLAB's *filloutliers* function to remove values ± two standard deviations from the mean. Figure 24 is example data for the five passes made by the Hurricane SS203 deck boat in 2022 testing showing the filtered and smoothed velocities measured at the 10, 15, and 20 ft evaluation depths.

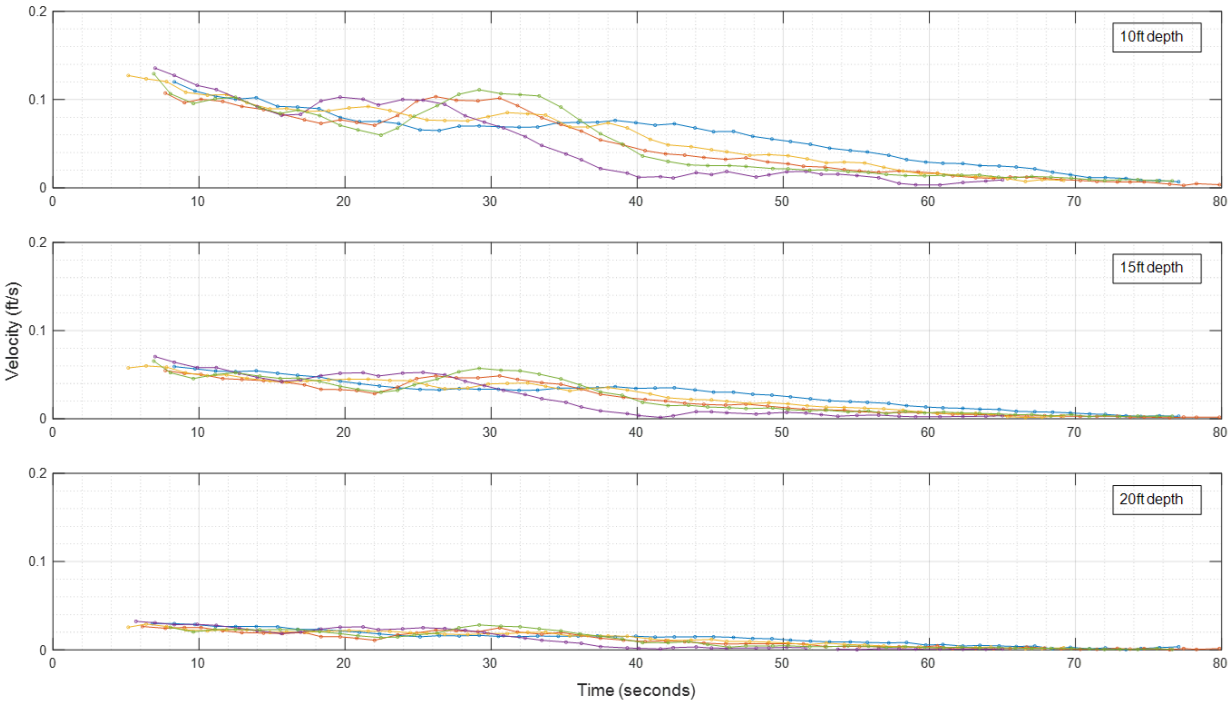

Figure 24. Example processed data from the 2022 Hurricane SS203. This figure shows the amplitude of the vertical velocity associated with the transverse waves produced by the boat. Each line represents an individual pass and data are presented at 10, 15, and 20 ft depths from the surface. Each data point is the mean of all data for that pass with a 2-second time bin.

6.2.3.4.3 Estimating propeller wash velocities

Further processing of propeller wash data ($U_{propwash}$, $W_{propwash}$) followed a similar analysis process as those described for Condition 1 planing mode. Each pass was filtered using MATLAB's *filloutliers* function to remove values ± two standard deviations from the mean. For the three evaluation depths, the mean value of data within three time-bins was computed (i.e., 5-10, 10-30, and 30-50 seconds), and the distributions for each test year, boat, and condition are shown and compared via box plots in the results.

6.3 ADV – near-bed velocity

The goal of the ADV analysis was to quantify the maximum near-bed velocities associated with the bow and stern waves, the transverse waves, and the propeller wash for each boat and condition tested. In addition, the ADV signal amplitudes were used as a qualitative measure of near-bed sediment resuspension. All ADV data processing was performed in MATLAB.

As previously described (Section 5.3.2), the ADV continuously measured velocities 4 inches above the lakebed at a sampling rate of 32 Hz. The raw output from the ADV includes three components of water velocity along the direction of the three sonic beams (Figure 13), referred to as Beam 1, Beam 2, and Beam 3. The beam velocities are in a coordinate system specific to the ADV probe, but because the orientation of the beams was known, the beam velocity information was converted to velocities in the x, y, and z Cartesian system. The associated velocities in the Cartesian system are defined as U, V, and W, respectively. In addition to velocity data, the ADV also collected data quality parameters that were used in the analysis including the single-to-noise ratio, correlation, signal strength (i.e., amplitude), and the local pressure at the ADV.

The stated accuracy of the ADV is ±0.5% or ±1 mm/s (0.00328 ft/s). However, the root-mean-square (rms) noise floor was typically 0.06 ft/s in 2022 testing and 0.02 ft/s in 2023, which placed a lower limit on measurable velocities. For measured velocities exceeding the noise floor, the standard deviation of the measured velocities between the five passes of each boat and test condition gave an estimate of the velocity uncertainty – the velocity standard deviation was typically in the range of 0.02 to 0.05 ft/s (Table 10).

6.3.1 Data quality checks (signal-to-noise ratio and correlation)

The signal-to-noise ratio and correlation were used to determine the quality of the velocity data. If the data were poor, either additional analysis methods were used, or the data was discarded. The signal-to-noise ratio (SNR), reported in decibels (dB), is a measure of the strength of the acoustic signal relative to the background noise level. A SNR below 30 dB means the signal is corrupted or obscured by noise and may be difficult to distinguish or recover. In all boat passes, the SNR exceeded 30 dB, and additional filtering was not necessary. The correlation data are a statistical measure of the relationship between how similar the transmitted acoustic signal is to the signal that is received after reflection. Correlation output is in percentage, where 100% means perfect correlation and 0% means no similarity. We used a 50% correlation threshold because it is commonly used (Nortek, 2017). The correlation values were generally quite high, except for conditions with significant propeller wash (Figure 25). A correlation value for each beam velocity was measured during each boat pass. If there was a time window where one of the three correlation values was below 50%, then that entire time window of velocity data was

discarded. The time windows of low correlation that occurred during periods of intense propeller wash may have been due to excessive turbulence, bubbles, and/or debris in the water column, or velocity readings exceeding the maximum measurement velocity of the instrument, which was 6.6 ft/s in 2022 and 3.3 ft/s in 2023.

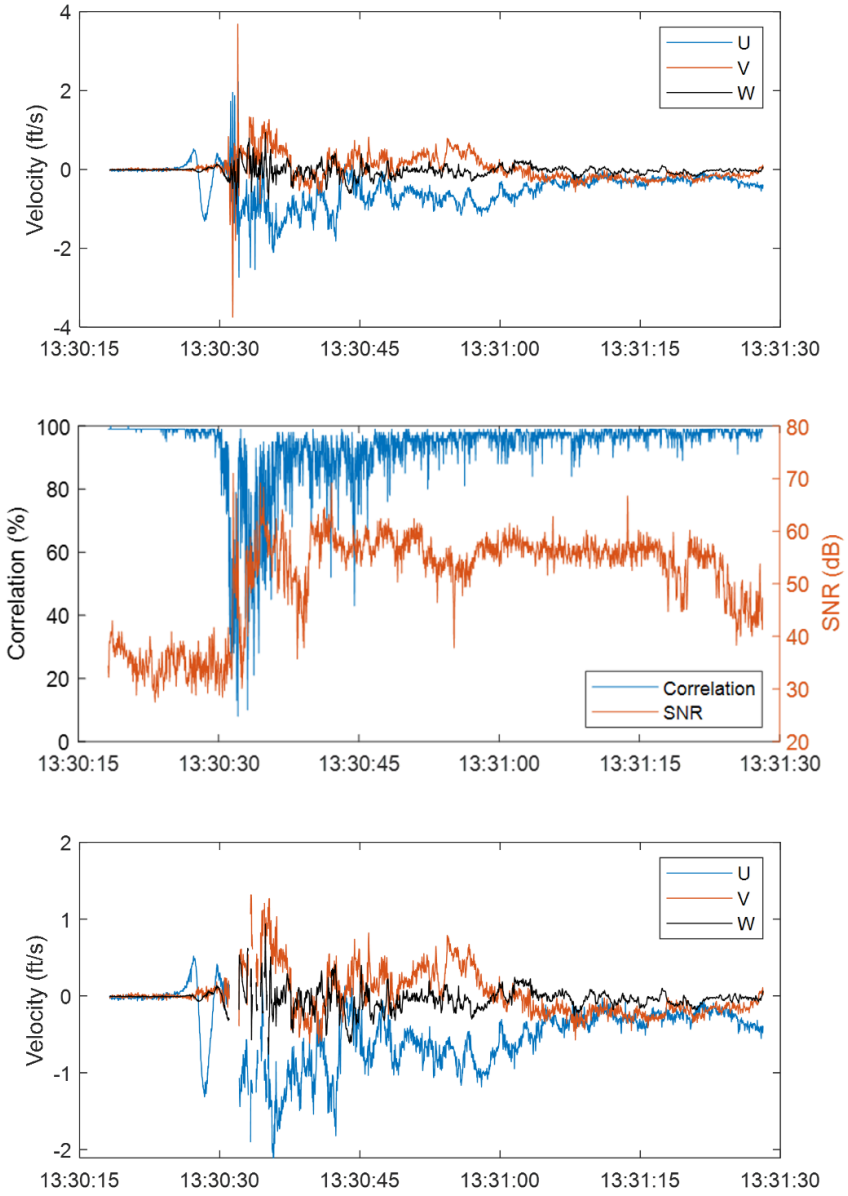

Figure 25. Time window of the raw velocity data (top panel), the corresponding correlation coefficient and signal-to-noise ratio for Beam 1 (middle panel), and the filtered velocity data (bottom panel) for a single pass by the Malibu VLX Wakesetter in 2023 during semi-displacement mode (Condition 2, 9 ft depth).

6.3.2 Decomposition of the signal and extracting velocity parameters

6.3.2.1 Estimating bow, stern, and transverse wave velocity in the absence of propeller wash

The measured velocity fluctuations at the bottom of a lake are a cumulative effect composed of individual hydrodynamic phenomena produced during a single boat pass (e.g., bow and stern waves, transverse waves, propeller wash). These interactions are complex, and the objective of the data analysis was to deconstruct the measured signal into these individual components.

Beginning with passes that had little or no propeller wash, the velocity measurements can be deconstructed into fluctuations caused by the bow wave, the stern wave, and the trailing transverse waves. To isolate the maximum and minimum velocities resulting from impulse-type phenomena (i.e., the bow and stern wave) and wave velocity amplitudes resulting from the transverse wave oscillations, the measured horizontal velocity component (U,V) were first smoothed with a 10-point moving average filter, and the horizontal velocity magnitudes were calculated using equation (8).

$$U_{mag} = \sqrt{(U^2 + V^2)} \quad (8)$$

U_{mag} was then plotted as a time series and the maximum/minimum velocity of the bow and stern waves were manually identified (Figure 26). Similarly, the maximum velocity was identified for the transverse wave, picking the highest velocity in the first five oscillations of the wave (Figures 26 and 27).

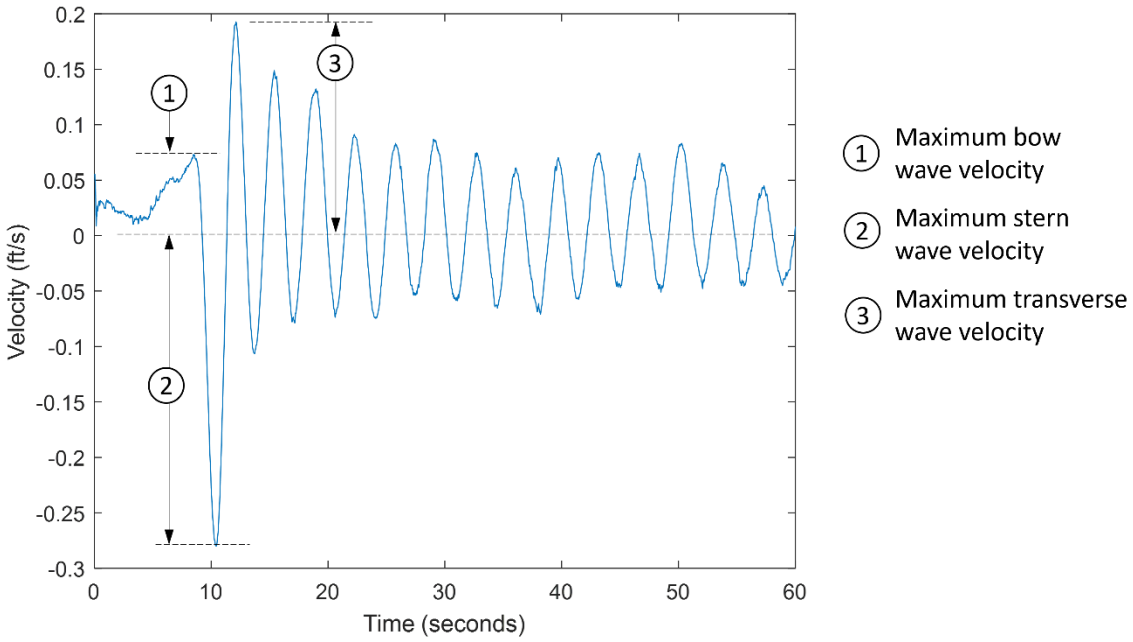

Figure 26. The velocity quantities extracted from the ADV signal for a case of negligible propeller wash (2022 data, Malibu VLX Wakesetter, semi-displacement mode - Condition 2, 16 ft depth).

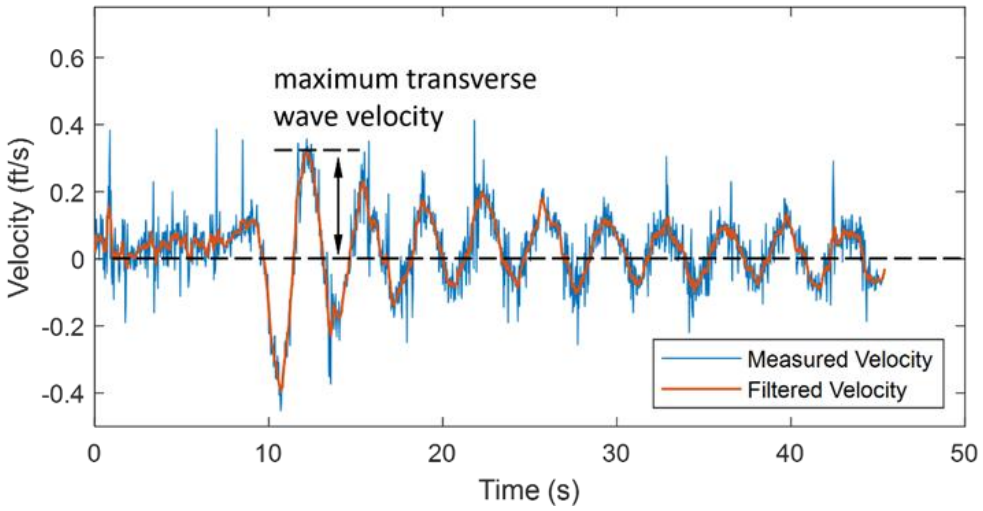

Figure 27. Measured velocity data, the filtered velocity data, and the maximum transverse wave velocity for a 2022 pass made by the Malibu VLX Wakesetter operating in semi-displacement mode (Condition 2, 16 ft depth).

6.3.2.2 Estimating propeller wash velocities

For cases with measurable propeller wash, several additional steps were needed to 1) characterize the transverse wave velocity amplitude, and 2) extract the transverse wave from the

filtered velocity data to determine the propeller wash velocity. Both steps were accomplished by using the measured pressure data, which recorded pressure fluctuations associated with changes in the water surface elevation above the sensor (i.e., waves) and were insensitive to pressures associated with the propeller wash (Figure 27). It was assumed that small density changes in the propeller wash jet due to entrained bubbles did not affect the wave-induced pressure readings near the lake bottom.

The raw pressure signal was first detrended, meaning the constant pressure offset of the water depth and any long-term variation in mean pressure were removed from the data (e.g., changing atmospheric pressure over the test day). Next, the frequency spectrum of the pressure signal was found using the Fast Fourier Transform (FFT) function, which converted the data from the time domain to the frequency domain. The primary frequency of the transverse wave, F_t, was revealed by the FFT function as typically about 0.3 Hz (Figure 28). An n-point smoothing filter was then used to remove the transverse wave from the velocity signal, where n was determined via equation (9):

$$n = 2 * \frac{F_s}{F_t} \quad (9)$$

Where, F_s is the sampling frequency (32 Hz). Solving equation (9), n was computed to be approximately 200. The n-point smoothing filter was then applied to the U, V, and W velocity data, resulting in an estimate of the slowly-varying mean velocity associated with propeller wash, and of the maximum propeller wash velocities along the x, y, and z directions. Figure 29 is an example of a U-component of velocity (blue line) and the extracted U-component of the slowly-varying mean velocity of the propeller wash (orange line) for a single boat pass.

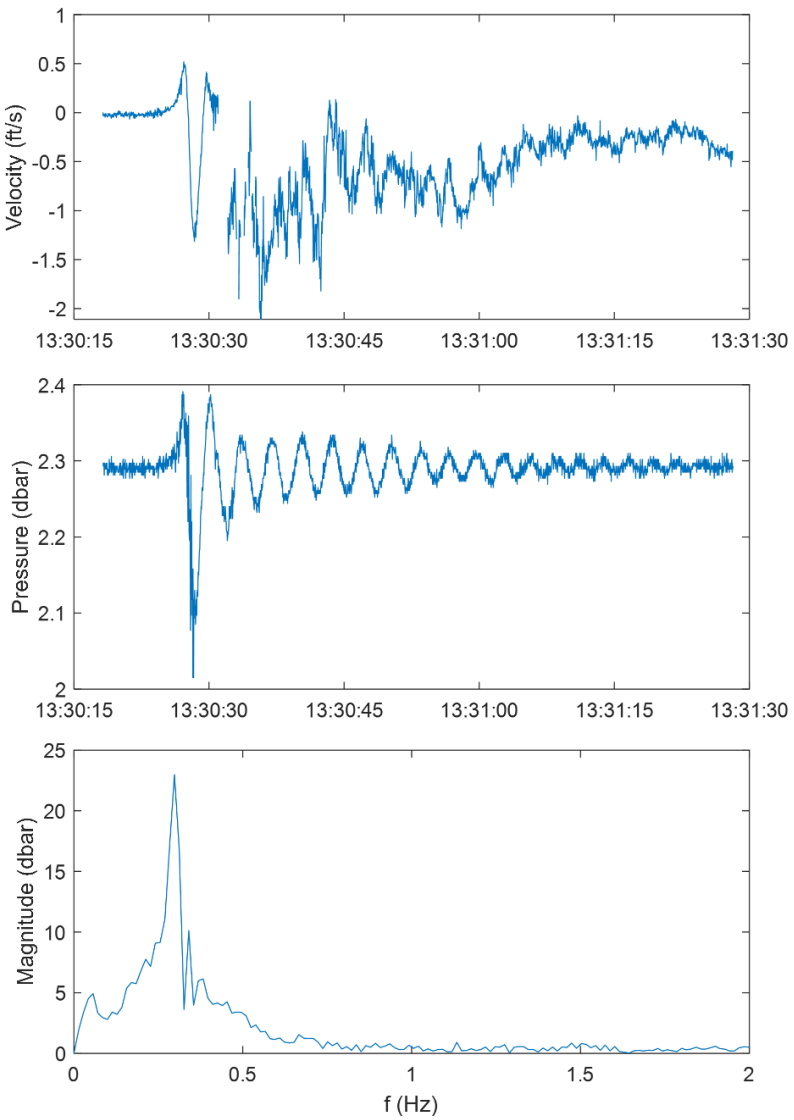

Figure 28. Time history of the velocity data, U-component, (top panel), the raw pressure signal for the same time period (middle panel), and the frequency spectra of the pressure signal (bottom panel), showing the main transverse wave frequency, F_t, at 0.298 Hz. This data is from a single pass of the Malibu VLX Wakesetter operating in semi-displacement mode (Condition 2, 9 ft depth) in 2023. Portions of the raw velocity data with correlation coefficients <50% have been removed.

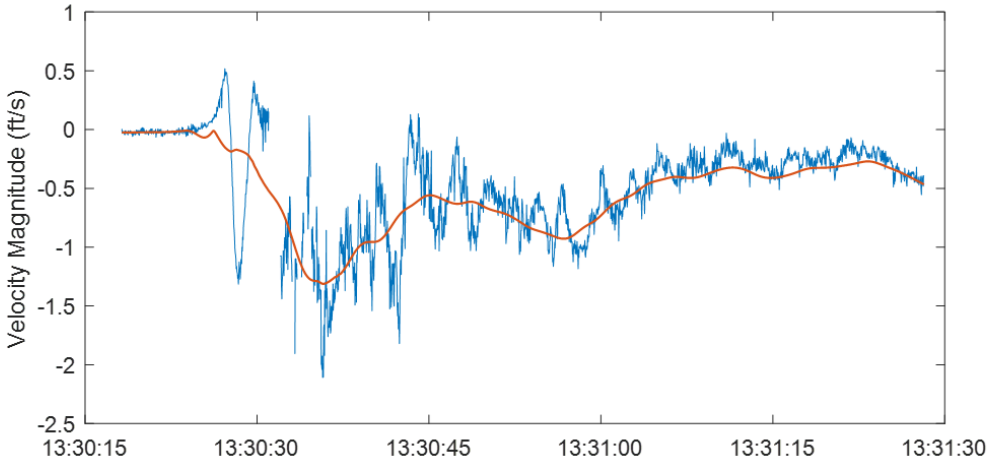

Figure 29. Time history of the U-component, raw velocity data (blue line) and the slowly-varying mean propeller wash velocity obtained using the n-point filter (orange line). The maximum velocity due to propeller wash was 1.3 ft/s for this pass made by the Malibu VLX Wakesetter operating in semi-displacement mode (Condition 2, 9 ft depth) in 2023. Portions of the raw velocity data with correlation coefficients <50% have been removed.

6.3.2.3 Estimating transverse wave velocities in the presence of propeller wash

Measured velocity signals with significant propeller wash present required extra analysis steps to extract the transverse wave velocities. This was accomplished by estimating the local transverse wave velocity from the ADV pressure data. The measured pressure fluctuations ($\tilde{p}$) can be related to velocity fluctuations ($\tilde{u}$) using the unsteady form of Bernoulli's equation (10):

$$\tilde{u} = \rho\tilde{p}\frac{T}{L} \tag{10}$$

Where, ρ is the density of water, T is the wave period, and L is the wavelength. For this analysis, the wavelengths (crest to crest) of the transverse waves produced by the Malibu VLX Wakesetter were estimated from the aerial drone videos to be 50.0 ft (15 m). This wavelength was used assumed for all boats. An example of the pressure-derived velocity and the subsequent fit of the maximum transverse wave velocity is given in Figure 30. The figure shows the measured filtered velocity data (black line) for a semi-displacement (Condition 2) pass made by the Malibu VLX Wakesetter in 2023, which includes contribution from the bow and stern waves, propeller wash, and transverse wave. The figure includes the estimated transverse velocity (blue line) from Equation (10) and represents the component of the measured velocity that is from the transverse

wave. The maximum transverse wave velocity was then selected for the first five cycles of the transverse wave time series.

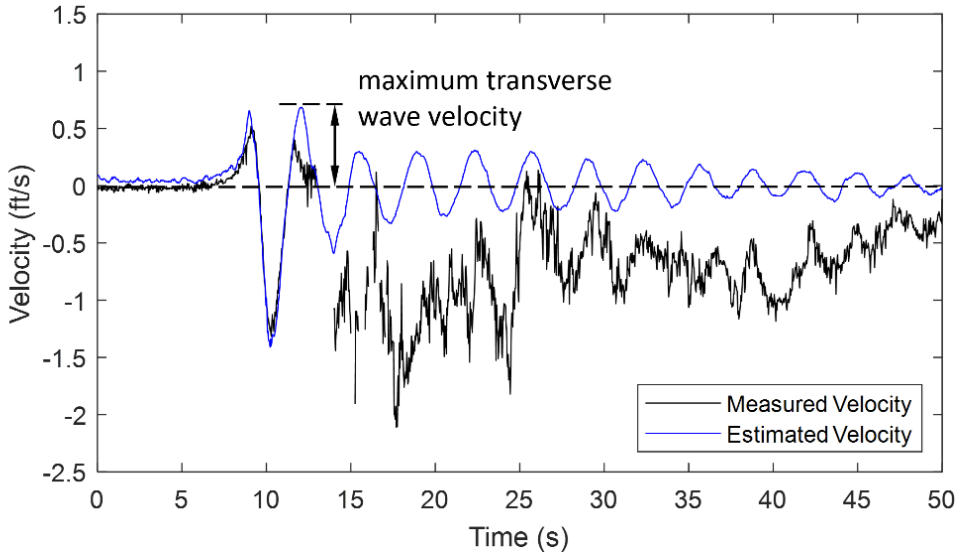

Figure 30. Measured velocity (U), estimated wave velocity from the pressure sensor data, and the transverse wave fit. 2023 data for the Malibu VLX Wakesetter, semi-displacement mode (Condition 2, 9 ft depth).

6.3.3 Relating propeller wash and wave-induced velocities to sediment resuspension

The measured velocity resulting from boat passes are complex, including oscillating velocities due to waves, slowly-varying mean flow due to propeller wash, and propeller wash turbulence. Assessing the ability of these velocity components to resuspend sediment can only be done in very approximate way, based on published studies for sediment resuspension in steady channel flows (e.g., Fischenich 2001) and in wave-driven velocity fields (e.g., Green and Coco 2013). The methods we used for relating near-bed, wave-induced velocities and propeller wash turbulence to the potential for sediment resuspension are detailed in the Appendix.

6.3.4 Qualitative measure of sediment concentration via ADV amplitude signal

The ADV uses acoustic backscatter from particles in the measurement volume to measure velocities (Section 5.3.2). The strength of the backscatter signal varies with the concentration and type of particles (e.g., sediment), so the ADV signal amplitude can be used as a measure of sediment concentration (Fleit and Baranya 2021, Nikora and Goring 2002). However, to obtain quantitative measurements, an accurate calibration curve between signal amplitudes and

sediment concentrations is required. In our case, a local calibration curve was not performed; however, the ADV signal amplitudes were still used as a qualitative measure of sediment concentration changes during the boat passes. The ADV stored a signal amplitude for each of the three acoustic beams – we used a 10-second window starting three seconds after the stern wave to calculate a simple mean of these amplitudes. The mean signal amplitudes were then plotted for each pass, followed by recording the maximum 10-second average signal amplitude. Statistical comparisons of the maximum average signal amplitudes were then made between boats and operating conditions using paired t-tests.

6.4 Boat hull pitch

For each boat pass, the real-time boat position data (Section 5.7) was used to calculate the boat's average hull pitch between the two pad locations. The average hull pitch for each boat and condition is shown as boxplots in the results (Section 7.1.5).

6.5 Water quality

6.5.1 Suspended solids

The water samples were analyzed for total suspended solids (TSS), volatile (organic fraction) suspended solids (VSS), and fixed (inorganic fraction) suspended solids (FSS, calculated as the difference between TSS and VSS). The method detection limit for TSS and VSS was approximately 1.0 mg/L. For TSS and VSS, samples that were reported as less than 1.0 mg/L were included in statistical analyses as 0.5 mg/L. The water samples in 2022 were also analyzed for total phosphorus (TP), where the method detection limit at the UMN RAL was 0.05 mg/L.

To compare the impact of boat passes on background suspended solids concentrations, the preliminary (pre) samples for each year were analyzed using a two-way ANOVA for the effect of sample date and condition (morning or afternoon). ANOVA results supported treating each condition as an independent experiment and were thus analyzed separately (see results -Section 7.2.1.2).

Mixed models were used to fit the repeated measures data for each independent dataset (for each operating condition for each boat) allowing for unequal variance at different time steps. For 2022, these models tested for the effect of sampling location (16 and 27 ft), sampling depth

(near-bed, mid-depth), boat pass (pre, pass, post), and the interactions between these factors. For 2023, these models tested for the effect of sampling location (9 and 14 ft), boat pass (pre, pass, post), and the interactions between these factors. All statistical analyses were completed in JMP Pro 17.

6.5.2 Turbidity

Due to equipment malfunction in 2022, only turbidity datasets from 2023 are available at each instrument pad. Except for the first day (Starcraft Limited 2000), all turbidity is reported in FNU (Formazin Nephelometric Units), a measure of the passage of light though water. A different water quality sonde was used only at the 14 ft site for the Starcraft Limited 2000 testing day (Section 5.8.3); therefore, these units of turbidity are slightly different, NTU (Nephelometric Turbidity Units). Because readings on the Starcraft Limited 2000 testing day were so low, (mostly 0 NTU; Figure 31) these turbidity readings were excluded from further analysis. Turbidity data were collected at 1-minute intervals.

There was a lot of variation in turbidity measurements, and spikes in turbidity were not consistently observed following boat passes. The maximum sampling rate of the instrument was one minute, and it is possible that high turbidity spikes occurred between sampling points. It is also possible that a plume of high concentration suspended material was not perfectly aligned with the instrument and thus turbidity spikes were not recorded. Therefore, instead of analyzing maximum recorded turbidity values, baseline turbidity values over 9-minute windows before and after boat passes were examined. There appears to generally be higher baseline turbidity after boat passes, especially in shallow water (Figure 31, also see results). To quantify this effect, two separate analyses were conducted.

First, to minimize the effects of individual spikes, median turbidity values were calculated for a 9-minute time period spanning one minute prior to each recorded boat pass time and eight minutes after each pass time. For each boat and condition, the post-pass median turbidity values were compared to the median turbidity values for three 9-minute time periods prior to the first boat passes (i.e., three median turbidity values collected during times when boats were not present). These values were used in a one-way ANOVA with Welch's Test to test if pre-pass and

post-pass median turbidity values were equal. Welch's test allows for unequal variances as would be expected if there was more variability after a boat pass. These tests were completed separately by boat, condition, and location, in part due to the difference in elevation from the bed for the turbidity sensors at each location. The second analysis compares the cumulative probability of turbidity readings prior to boat passage and after. Because the turbidity readings had a few apparent spikes, a Hampel filter with a threshold of 2 times the moving median absolute deviation was applied (similar to Valbuena et al. 2024). The cumulative probability was then plotted against the turbidity for each boat and operating condition at each instrumentation pad location.

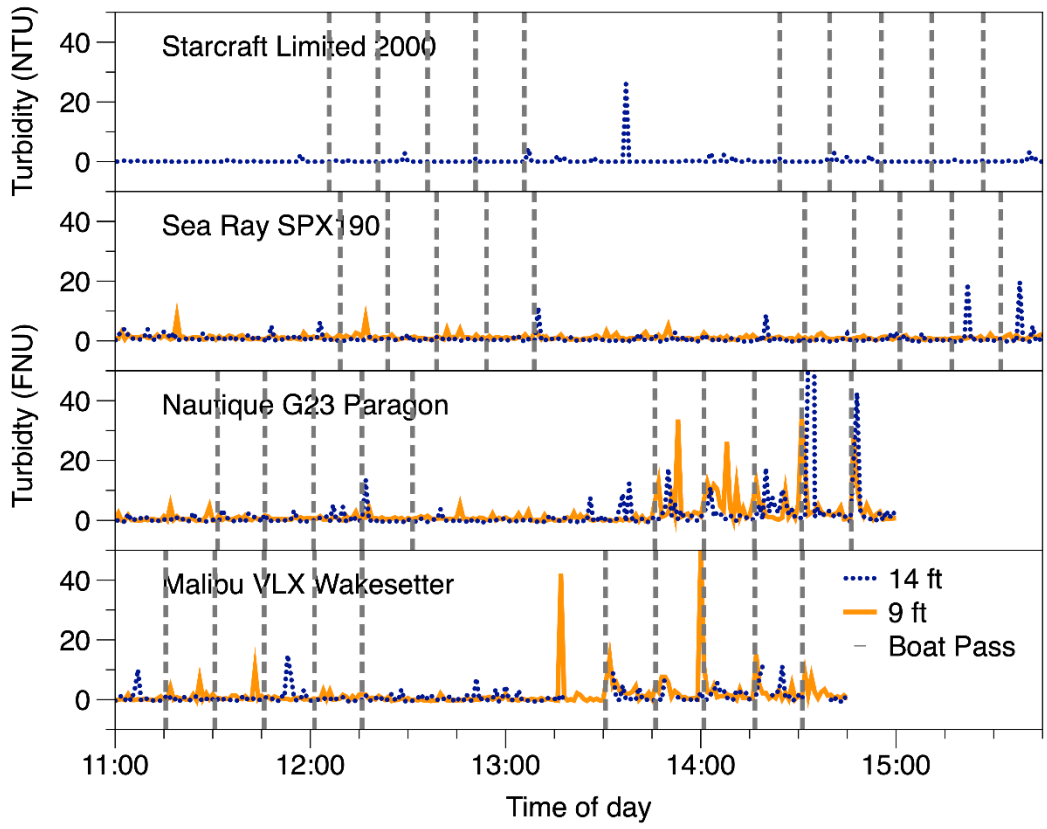

Figure 31. Measured turbidity (unfiltered) in 2023 in Maxwell Bay. Dashed vertical lines note the timing of the individual boat passes, where the first five were in planing mode (Condition 1) and the second five were in displacement mode for the non-wakeboats and semi-displacement mode for the wakeboats (Condition 2). The orange solid lines are the measured turbidity at the 9 ft ADV site, and the blue dotted lines are the measured turbidity at the 14 ft ADCP site. A single measurement for the Nautique G23 Paragon at the 14 ft sampling location was abnormally high (~400 FNU) and is not included in this graph.

6.6 Underwater and aerial video

Multiple video cameras were added to the 2023 field campaign to capture underwater footage of boat passes (Section 5.3.3). Therefore, we only have footage for the Starcraft Limited 2000 (deck boat), Sea Ray SPX190 (bowrider), Nautique G23 Paragon (wakeboat), and Malibu VLX Wakesetter (wakeboat). The four video cameras (i.e., two on each pad) started recording immediately before pad deployment and continued to record until pad retrieval. The first step in video analysis was to isolate each boat pass from the 6-plus hours of continuous footage for each camera. Short videos of the first pass for each condition were created showing the four different camera views. These videos can be downloaded at the University of Minnesota's digital conservancy/data repository (https://doi.org/10.13020/r7w9-dp20). It should be noted that on day one of testing (i.e., Starcraft Limited 2000) the video cameras lost power after planing mode (Condition 1) testing due to battery capacity issues. Therefore, there is no video of displacement mode (Condition 2) testing for this boat.

Aerial video also captured boat passes during the 2023 field campaign (Section 5.9). Due to some technical difficulties with the drone, there are no videos of the Starcraft Limited 2000, Sea Ray SPX190, or Nautique G23 Paragon during planing mode (Condition 1) testing. The videos that were created can be downloaded at the University of Minnesota's digital conservancy/data repository (https://doi.org/10.13020/r7w9-dp20).

6.7 Sediment characteristics

Lakebed sediment samples were collected (section 5.8.4) and analyzed by UMN RAL for organic matter content (loss on ignition; Combs et al. 1998) and total (Tadon et al. 1968) and extractable (Bray; Frank et al. 1998) phosphorus. A sieve analysis for particle size distribution (gradation) was completed at the UMN -St. Anthony Falls Laboratory using standard methods (ASTM D6913/D6913M-17). The two ADCP sites were characterized as fine muck (>20% organic matter, result- Section 7.2.4), and were not analyzed for grain particle size.

7.0 RESULTS

7.1 Hydrodynamic phenomena produced by recreational powerboats

7.1.1 ADCP echogram – bubble extent

The ADCP echograms captured the extent of the exhaust bubbles that were injected into the water column by the boat's engine. As described in Section 6.1.2, the echogram data was processed through a MATLAB script, with the output being the bubble depth limits for each pass. A mean bubble depth limit was calculated and smoothed with a 5-second moving average filter for each test condition (Figures 32 and 33). The 2022 and 2023 data for each wakeboat were combined because there was little variation in the data between years for both operational conditions (see Appendix).

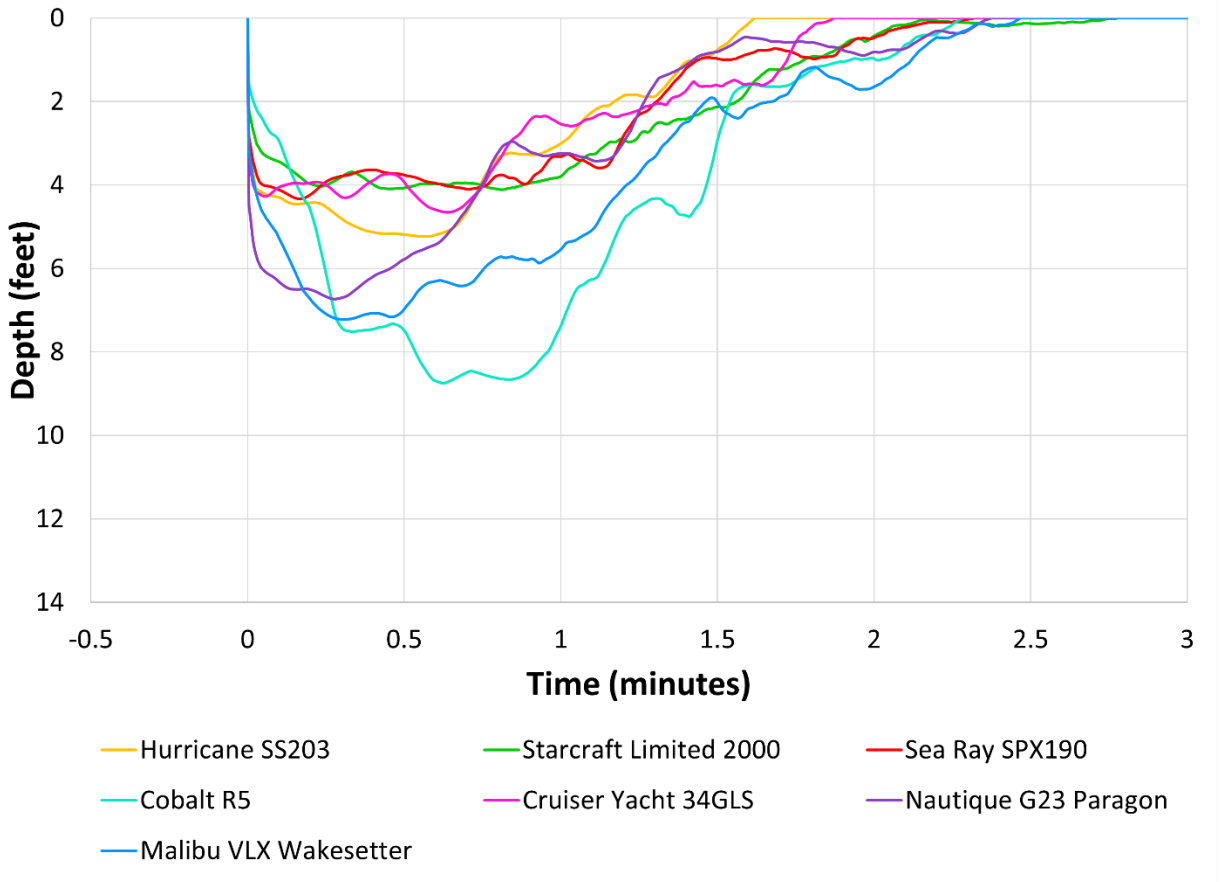

Figure 32. Mean bubble depth limit for the five passes made by the boats when operated in planing mode (Condition 1). The 2022 and 2023 data for the Nautique G23 Paragon and Malibu VLX Wakesetter are combined (n=10).

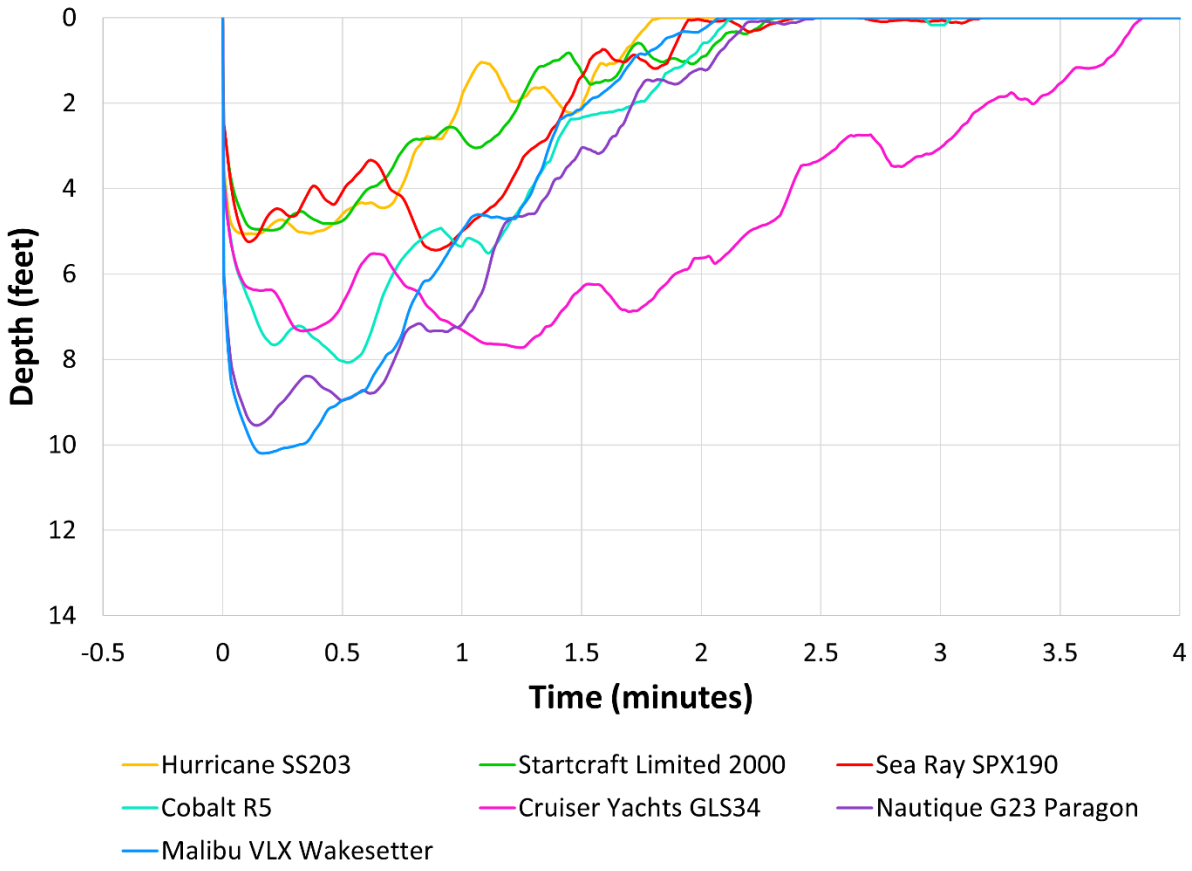

Figure 33. Mean bubble depth limit for the five passes made by the boats when operated in Condition 2. This was displacement mode for the non-wakeboats and semi-displacement for the wakeboats. The 2022 and 2023 data for the Nautique G23 Paragon and Malibu VLX Wakesetter are combined (n=10).

The seven boats tested fall into three types (deck boats, bowriders, wakeboats, Section 5.4). For all but one of the boats, the bubbles rose to the water surface within 2.5 minutes of the pass regardless of operational condition. The largest boat, the Cruisers Yachts 34GLS bowrider, did not follow this trend during displacement mode (Condition 2) testing, as the bubbles were entrained in the water column for approximately 3.75 minutes. Regardless of the condition, the extent of the bubbles was similar for the deck boats. The Sea Ray SPX190 bowrider, which was similar in size and weight to the deck boats, created bubbles that were entrained in a similar geometry to the deck boats. Interestingly, when operated in planing mode (Condition 1), the Cruisers Yachts 34GLS bowrider, which was the largest boat tested, also created a similar bubble extent.

The two wakeboats had similar bubble extent geometries; however, the bubbles were entrained deeper during semi-displacement mode (Condition 2) than in planing mode (Condition 1). Among

all boats, the deepest bubble entrainment depths were produced by the wakeboats during semi-displacement (Condition 2) testing. Perhaps one of the most interesting findings is the Cobalt R5 bowrider bubble extent during planing mode (Condition 1). Although the bubble entrainment duration was similar to the other boats, the penetration depth was the deepest for Condition 1. These same trends emerge when the mean maximum bubble depths are evaluated using statistical comparison methods.

A two-way Anova revealed that the mean maximum bubble depth was statistically significant by boats, conditions, and the interactions between these variables (p-value <0.0001). This significant effect of condition across all boats motivated further investigation into the relationships between the boats and mode of operation (i.e., test condition). A one-way ANOVA test examined the effect of all boats by operational condition on the mean maximum bubble depth, which revealed a statistically significant relationship (p-value <0.0001). Consequently, a post hoc Tukey-Kramer HSD test identified specifically which boats and conditions differ from each other (Figure 34).

A series of pooled t-tests were performed to examine the effect of the operational conditions on the mean maximum bubble depth for each boat (Table 6). The effect of condition was statistically insignificant for the Hurricane SS203 (p-value = 0.2384), Starcraft Limited 2000 (p-value = 0.4629), and Sea Ray SPX190 (p-value = 0.3008), which were the smallest boats in terms of length (<21.0 ft) and weight (<3000 lb). Regardless of condition, these boats had very similar means that ranged between 5.1 and 6.0 ft. The effect of condition was statistically significant for the four heavier (>4000 lb) and longer (≥21.0 ft) boats that include the Cobalt R5 (p-value = 0.0210), Cruisers Yachts 34GLS (p-value = 0.0028), Nautique G23 Paragon (p-value <0.0001), and Malibu VLX Wakesetter (p-value <0.0001). The wakeboats in semi-displacement mode (Condition 2) created the overall deepest mean maximum bubble depths of approximately 11.0 ft, which is about two times the penetration depth of the smaller boats operating in either displacement or planing condition.

Table 6. The mean maximum bubble depth for all boats in planing mode (Condition 1), non-wakeboats in displacement mode (Condition 2), and wakeboats in semi-displacement mode (Condition 2). Bold values indicate statistical significance between conditions.

Boat	Type	Condition 1 Mean ± SD (ft)	Condition 2 Mean ± SD (ft)	Pooled *t*-test (*p*-value)
[1]Hurricane SS203	Deck	5.1 ± 0.3	5.6 ± 0.7	0.2384
[2]Starcraft Limited 2000	Deck	5.1 ± 0.8	5.7 ± 1.5	0.4629
[2]Sea Ray SPX190	Bowrider	5.3 ± 1.0	6.0 ± 1.2	0.3008
[1]Cobalt R5	Bowrider	9.9 ± 0.3	8.9 ± 0.6	**0.021**
[1]Cruisers Yachts GLS34	Bowrider	5.3 ± 0.3	9.8 ± 2.4	**0.0028**
[1,2]Nautique G23 Paragon	Wake	7.6 ± 1.2	10.8 ± 1.4	**< 0.0001**
[1,2]Malibu VLX Wakesetter	Wake	8.3 ± 0.7	11.2 ± 1.2	**< 0.0001**

1 - 2022
1,2 - 2022 and 2023
2 - 2023

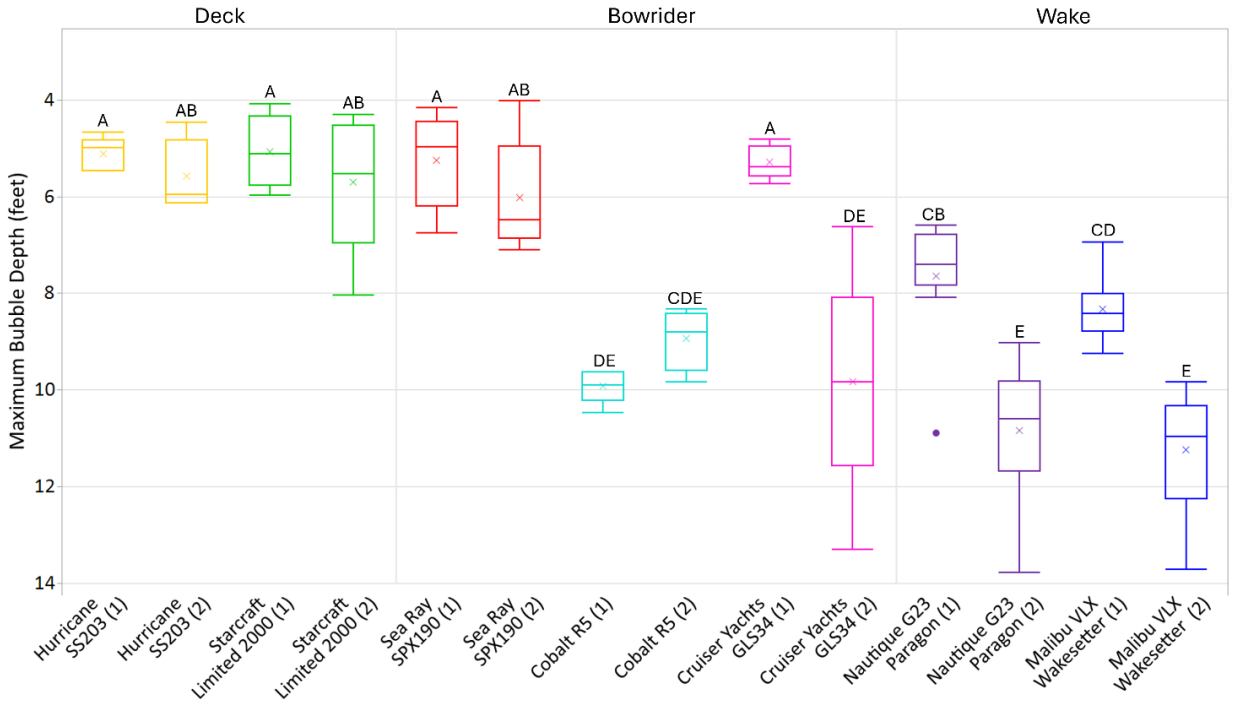

Figure 34. Boxplots (five-number summary) of the maximum bubble depth for each boat by condition. A Tukey-Kramer HSD test was used to compare the means (x) where connecting letters are not significantly different from each other. (1) and (2) in the x-axis label denote Condition 1 and Condition 2, respectively.

7.1.2 ADCP echogram – resuspended sediment extent

The 2023 ADCP was deployed in 14 ft of water and the echogram data shows resuspension of sediment for only the wakeboats during semi-displacement mode (Condition 2) testing. Section 6.1.3 describes how these data were processed through a MATLAB script to yield a sediment resuspension limit for each pass, and it is important to reiterate that this analysis method could only determine if sediment was resuspended above the ADCP (i.e., >1.5 ft off the bottom). However, based on the underwater videos (Section 7.2.2) we can confirm that no other boats or conditions caused sediment resuspension to heights that would be detected by the ADCP.

The resuspension of the bottom sediment was quite variable between passes for both wakeboats (Figure 35). The data was filtered via the 99th percentile method to remove outliers before calculating a maximum sediment resuspension height off the lake bottom for each pass (Figure 36). The mean maximum sediment resuspension was 5.7 ft $\pm$ 2.3 ft (mean $\pm$ SD) and 4.3 ft $\pm$ 1.6 ft for the Nautique G23 Paragon and Malibu VLX Wakesetter, respectively. Even though these wakeboats are different in terms of maximum horsepower, length, and weight (Section 5.4.3, Table 2), there was no significant difference (pooled *t*-test; *p*-value = 0.2894) between the mean maximum resuspended sediment heights of these boats when operated in semi-displacement mode (Condition 2).

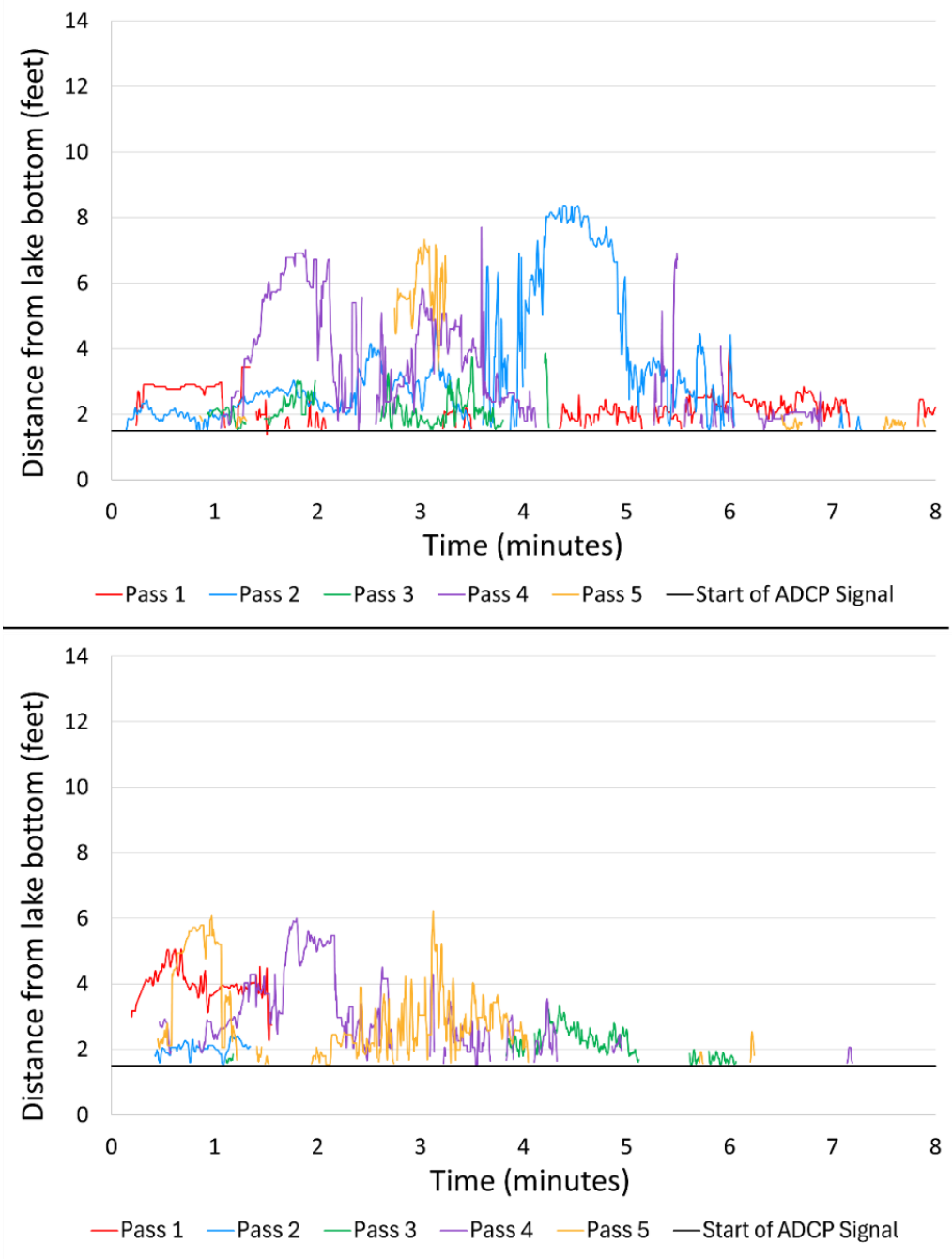

Figure 35. Sediment resuspension limit created by the Nautique G23 Paragon (top) and Malibu VLX Wakesetter (bottom) while operating in semi-displacement mode in 2023 (Condition 2, 14 ft depth). Start of the ADCP signal (black horizontal line) notes the water depth where the ADCP measurements begin, which is 1.5 ft above the lakebed.

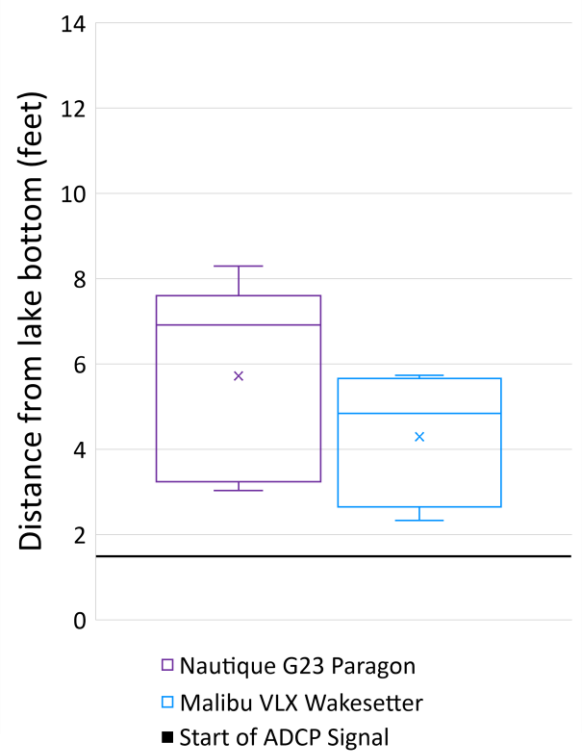

Figure 36. Boxplots (five-number summary) of the maximum sediment resuspension heights of the 99th percentile for passes made by the wakeboats in semi-displacement mode (Condition 2) in 2023, where X denotes the mean. The start of the ADCP signal (black horizontal line) notes the water depth where the ADCP measurements begin, which is 1.5 ft above the lakebed.

7.1.3 ADCP – wave velocity

7.1.3.1 Summary of overall data quality

The ADCP sensor was deployed in 27 ft of water in 2022 and 14 ft of water in 2023. The ADCP was able to collect quality velocity data throughout the water column with the following exceptions:

1. Exhaust bubbles entrained in the propeller wash caused high attenuation of the acoustic signals resulting in high data loss in this region. This impact was only seen in the transverse wave and propeller wash data since it occurred after the bow and stern pressure waves. The severity of this impact was dependent on boat type and test condition but was most prominent during the first 30 seconds after the boat had passed. After this time, the ADCP data quality improved substantially.
2. For times after the stern passed the sensor, horizontal (U_{13}) velocity data had a significant loss of data during filtering due to the data correlation requirement for accurate

transformation of beam-wise velocities to Cartesian coordinates. The vertical (W_5) velocity data was a single beam and thus did not require transformation, resulting in lower data loss from filtering.

7.1.3.2 Velocities associated with the bow and stern waves

In Figures 37 and 38, the thick solid lines (bow) and thick dashed lines (stern) are the mean outputs from the data processing procedure discussed in Section 6.2.3.2. A logarithmic regression analysis was used to forecast the data trends when possible (thin dotted lines). A logarithmic regression was used because it provided the best fit, as the bow and stern wave velocities tend to decrease quickly with depth and then level out. A trend line was not applied to situations with a poor R^2 value (<0.6). The regression analysis coefficients and associated statistics are provided in the Appendix.

In general, the velocity trends with respect to water depth were as expected, where higher velocities were generated at depths closer to the surface that attenuated towards zero with increasing depth. The velocities generated by the bow and stern waves occur quickly, on the order of a few seconds, and follow the hydrodynamics described in Section 2.1.1. Figure 37 shows the horizontal velocities (U_{13}), where the hull forces the bow wave forward (positive values) and the stern wave backward (negative values). Figure 38 shows the vertical velocity (W_5), where the hull forces the bow wave downward (negative values), while the stern wave rebounds upward (positive values). During displacement mode for the non-wakeboats and semi-displacement mode for the wakeboats (Condition 2), the stern waves had greater velocities than the bow waves. This is likely due to the slower speeds, buoyancy, and greater displacement by the hull. The results also show that the horizontal velocities (U_{13}) tend to be greater than the vertical velocities (W_5), and Condition 2 created higher overall velocities than Condition 1.

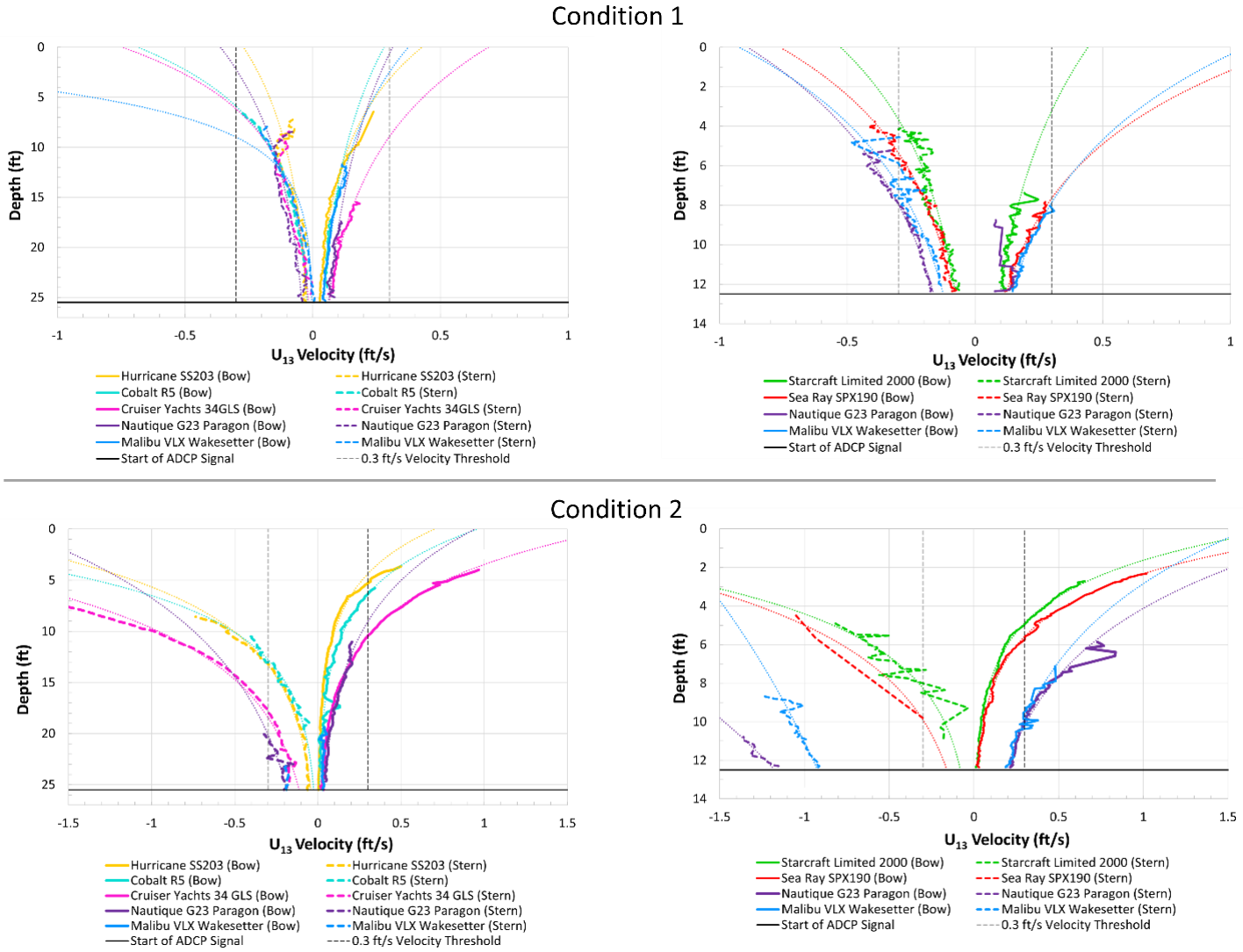

Figure 37. Horizontal (U_{13}) velocities of the bow waves (solid lines) and stern waves (dashed lines) recorded by the ADCP for Condition 1 and Condition 2 during 2022 (left panels) and 2023 (right panels). Best fit trendlines (log) are plotted as dotted lines. Positive values are in the direction of boat travel.

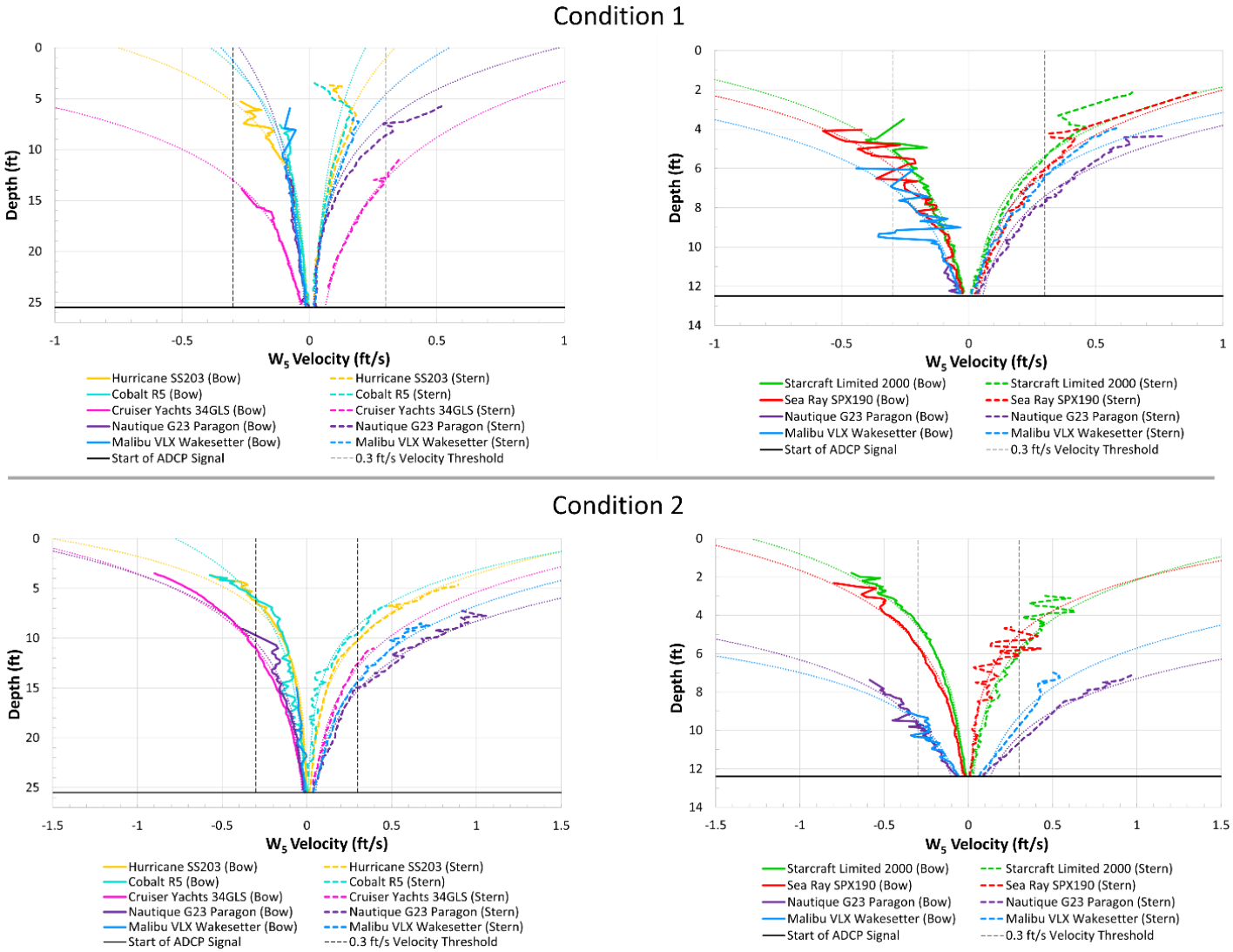

Figure 38. Vertical (W_5) velocities of the bow waves (solid lines) and stern waves (dashed lines) recorded by the ADCP for Condition 1 and Condition 2 during 2022 (left panels) and 2023 (right panels). Best fit trendlines (log) are plotted as dotted lines. Positive values are in the direction of boat travel.

Figures 37 and 38 were used to create Tables 7 and 8. A velocity threshold of 0.3 ft/s was selected to compare boats and conditions because similar velocities were shown to resuspend non-cohesive coarse silts in lakes (Section 6.3.3 analysis, Beachler and Hill 2003, Raymond and Galvez-Cloutier 2015). The values in the tables are the water depths at which the velocity threshold is met, rounded to the nearest 0.5 ft. From a water surface down perspective, this is the approximate water depth where velocities attenuate to the 0.3 ft/s velocity threshold. Since wave-driven velocity attenuation is dependent on the total water depth, the water depths given in Tables 7 and 8 are only an estimate of the penetration depth for disturbance. It is important to emphasize that these tables can be recreated with any velocity threshold that has the potential to disturb or resuspend sediment (e.g., different sediment types, organic debris).

7.1.3.2.1 Condition 1 (planing mode)

The largest test boat, the Cruisers Yachts 34GLS bowrider, generated bow and stern velocities that met the 0.3 ft/s threshold for coarse silt disturbance at a depth of 13 ft (Table 7). All other test boats reached the 0.3 ft/s velocity threshold at depths less than 10 ft.

Table 7. Planing mode (Condition 1) summary of the water depth, referenced from the surface and rounded to the nearest 0.5 ft, at which the horizontal (U_{13}) and vertical (W_5) velocities generated by the bow and stern waves are ≤ 0.3 ft/s.

		Horizontal (U_{13})		Vertical (W_5)	
	Boat	Bow Wave	Stern Wave	Bow Wave	Stern Wave
2022	Hurricane SS203	3.0∗	—	5.0∗	1.0∗
	Cobalt R5	—	6.0∗	2.0∗	—
	Cruisers Yachts 34GLS	9.0∗	6.0∗	13.0∗	13.0
	Nautique G23 Paragon	0.5∗	2.0∗	—	8.5
	Malibu VLX Wakesetter	2.5∗	9.0∗	1.5∗	4.5∗
2023	Starcraft Limited 2000	3.0∗	3.5∗	5.0	5.5
	Sea Ray SPX190	7.5∗	5.5	6.5	6.0
	Nautique G23 Paragon	NULL	8.0	NULL	8.0
	Malibu VLX Wakesetter	8.5	8.0	9.5	6.5

NULL $R^2 < 0.6$

— velocity threshold was not reached

∗ trendline used to obtain value

7.1.3.2.2 Condition 2 (displacement or semi-displacement mode)

Differences in the bow and stern wave velocities are more apparent during Condition 2 (Table 8). In 2022, the Nautique G23 Paragon generated U_{13} stern velocities that reached the 0.3 ft/s threshold for coarse silt disturbance at a depth of 22.5 ft. Unfortunately, there was not enough quality U_{13} data to obtain a depth for the Malibu VLX Wakesetter. However, the Nautique G23 Paragon and Malibu VLX Wakesetter generated W_5 stern velocities that reached the threshold at similar depths of 15.0 ft and 14.5 ft, respectively; therefore, it is likely that the Malibu VLX Wakesetter U_{13} stern velocity met the threshold at a similar depth (i.e., ~22.0 ft) as the Nautique G23 Paragon. The largest test boat, the Cruisers Yachts 34GLS, produced a U_{13} stern velocity that met the 0.3 ft/s threshold at a depth of 18.0 ft. For the Hurricane SS203 and Cobalt R5 this depth was 13.0 ft.

At the shallower test site, the wakeboats far exceeded the 0.3 ft/s velocity threshold. At a water depth of 12.5 ft, the Nautique G23 Paragon and Malibu VLX Wakesetter generated U_{13} stern wave velocities 3-4 times the velocity threshold, 1.2 ft/s and 0.9 ft/s, respectively (Figure 37). No other test boat, including 2022 boats, generated velocities on the order of 1.0 ft/s at 12.5 ft. The two smaller boats, Starcraft Limited 2000 and Sea Ray SPX190 created velocity profiles that were similar to the ones they generated in planing mode (Condition 1), where the U_{13} velocities met the 0.3 ft/s velocity threshold at depths ≤ 10 ft.

Table 8. Condition 2 summary of the water depth, referenced from the surface and rounded to the nearest 0.5 ft, at which the horizontal (U_{13}) and vertical (W_5) velocities generated by the bow and stern waves are ≤ 0.3 ft/s.

		Horizontal (U_{13})		Vertical (W_5)	
	Boat	Bow Wave	Stern Wave	Bow Wave	Stern Wave
2022	Hurricane SS203	5.5	13.0	6.0	10.0
	Cobalt R5	6.5	13.0	6.0	9.5
	Cruisers Yachts 34GLS	10.5	18.0	11.0	12.5
	Nautique G23 Paragon	9.0✳	22.5	10.5	15.0
	Malibu VLX Wakesetter	NULL	NULL	NULL	14.5
2023	Starcraft Limited 2000	5.0	8.5	4.5	6.0
	Sea Ray SPX190	5.5	10.0	5.5	6.0
	Nautique G23 Paragon	10.0	≫ 12.5	10.0	10.5
	Malibu VLX Wakesetter	10.5	≫ 12.5	10.5	10.0

NULL $R^2 < 0.6$

✳ trendline used to obtain value

7.1.3.3 Velocities associated with transverse waves

Transverse waves were only produced in Condition 2, which was displacement mode for the non-wakeboats and semi-displacement mode for the wakeboats. The ADCP was not able to collect quality transverse wave data within the region of intense propeller wash. This region contains the entrained exhaust bubbles, which caused high signal attenuation. However, quality data was successfully measured below the bubble depth limit and after the most intense propeller wash had passed. Because of the loss of data in the initial moments after the boat pass, the horizontal U_{13} velocity data was poor and not useable for transverse wave calculations. Fortunately, the vertical W_5 velocity data sets for 2022 and 2023 were less noisy, and thus the focus hereafter. Figure 39 is included to show the average bubble depth limit for each boat (Section 7.1.1), along with the three depths and time frame that these data were evaluated.

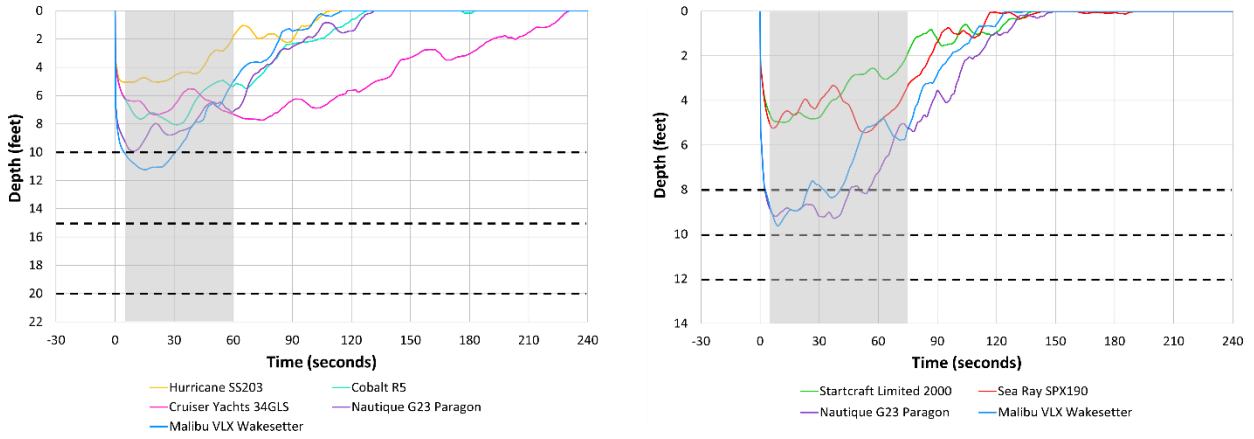

Figure 39. Condition 2 bubble depth limits determined by 2022 (left) and 2023 (right) ADCP echograms. The dashed lines (depths) and gray shaded region (time frames) that the vertical (W_5) transverse wave velocities were evaluated. Time zero (t=0) is when the boat passed over the ADCP.

These data are the absolute values of W_{Twave} (Equation 5) and do not indicate upward or downward movement but overall amplitude of vertical motion. In 2022, the first 15-20 seconds of data were sparse for the wakeboats due to propeller wash effects, so an exponential regression model (W_{Twave} = b1*exp(-b2)+b3) was fit to the data using MATLAB's *fitnlm* function (Figure 40). The regression lines were used to estimate the transverse wave velocity amplitude to within 10 seconds after the boat passed (t=10). This method yields only an estimate of velocities; a direct measurement would have been optimal but was not possible. For the non-wakeboats, velocity estimates did not require a regression model because of higher data availability.

In 2022, at 10 seconds after the boat pass, the largest transverse wave velocities were identified for the wakeboats (Figure 40). The Nautique G23 Paragon and Malibu VLX Wakesetter velocities at 10 ft were 0.22 ft/s and 0.17 ft/s, respectively. At 15 ft the velocities decreased to 0.21 ft/s and 0.12 ft/s, respectively, and by 20 ft they both decreased to below 0.1 ft/s. The non-wakeboats generated velocities at or below 0.1 ft/s at 10 ft that decreased to less than 0.06 ft/s by 15 ft, and by 20 ft had decreased to miniscule values.

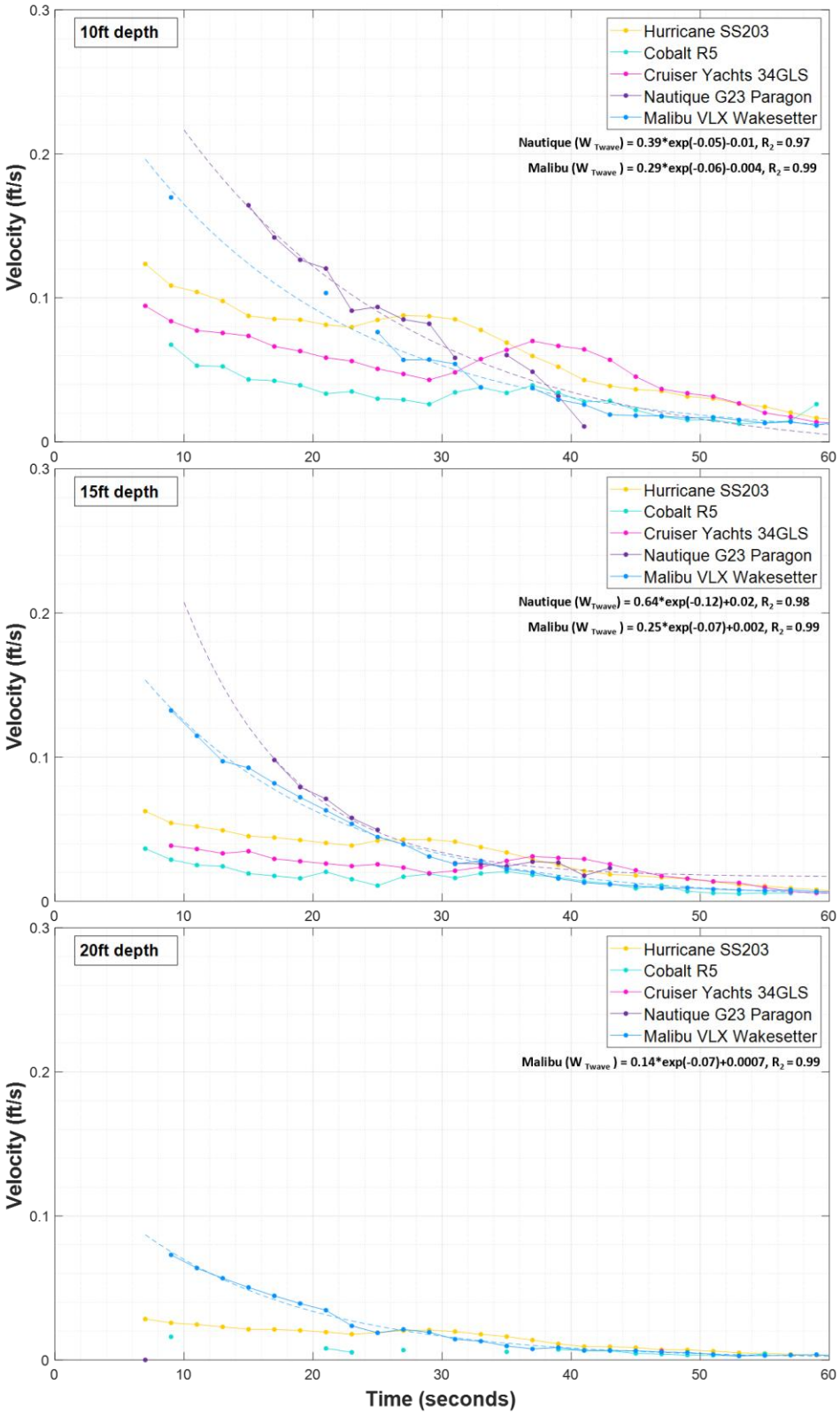

Figure 40. Vertical (W_5) transverse wave velocities calculated at 10, 15, and 20 ft depths during 2022 Condition 2 testing. Time zero (t=0) is when the boat passed over the ADCP.

In 2023, the propeller wash and associated exhaust bubbles were significant, especially for the wakeboats, where much of the water column was disrupted (Figure 39). Because of this, very little quality transverse wave data was available from the wakeboats until roughly 25 seconds after the boat pass (Figure 41). An attempt was made to fit an exponential regression model to estimate the missing velocity data, but the model produced an inaccurate fit (i.e., poor R^2) and therefore not plotted.

The wakeboats again produced higher transverse wave velocities than the non-wakeboats at the three evaluation depths. At the 8 ft depth and approximately 25 seconds after the boat pass, the wakeboats had velocities near 0.1 ft/s that decreased with time. At 10 ft and ~30 seconds, the Nautique G23 Paragon and Malibu VLX Wakesetter velocities were 0.08 and 0.04 ft/s, respectively. At the 15 ft depth the velocities were both less than 0.04 ft/s. The Starcraft Limited 2000 and Sea Ray SPX190 velocities were small and relatively unchanged with time at all depths, never exceeding 0.025 ft/s.

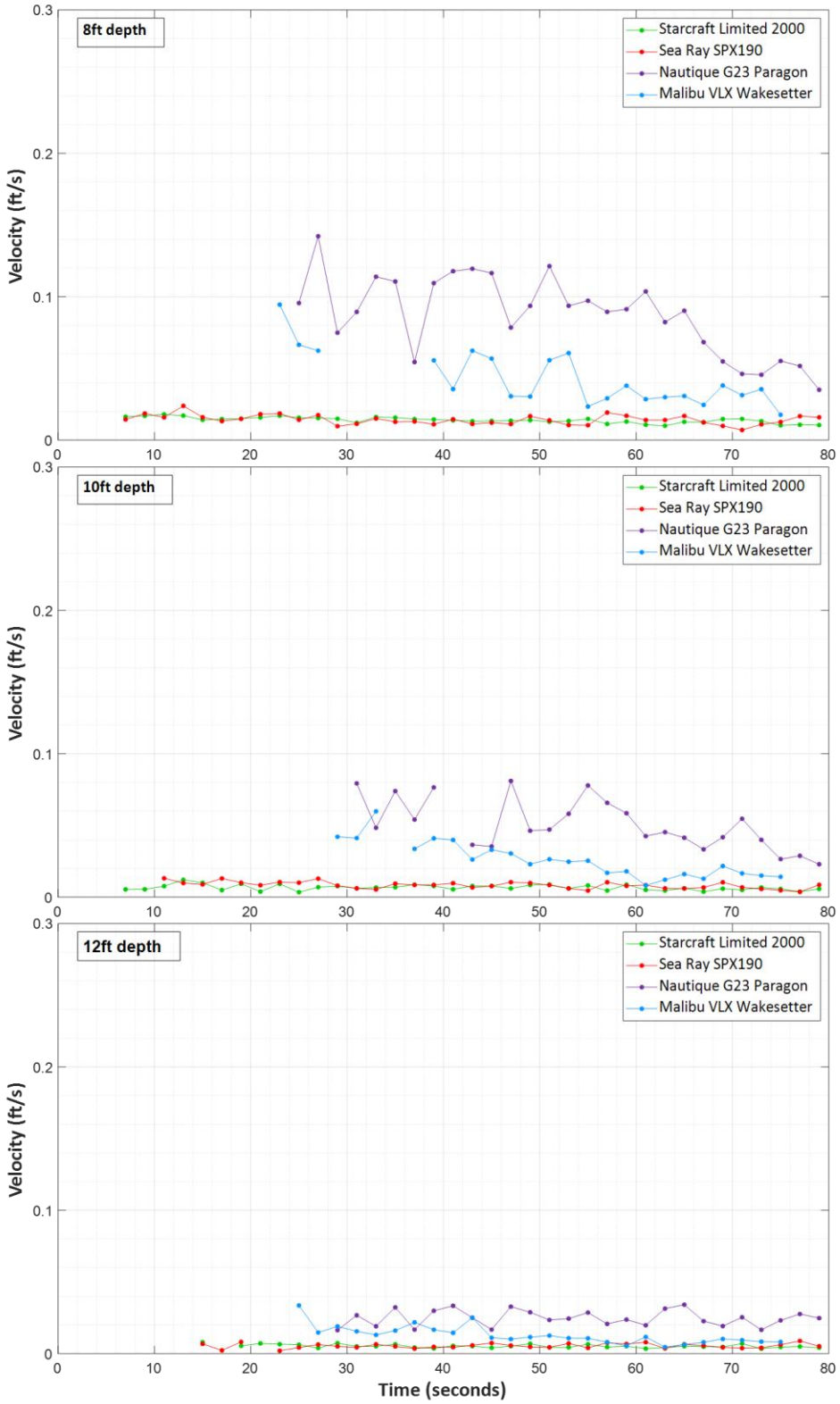

Figure 41. Vertical (W_5) transverse wave velocities calculated at 8, 10, and 12 ft depths during 2023 Condition 2 testing. Time zero (t=0) is when the boat passed over the ADCP.

7.1.3.4 Wave period associated with transverse waves

The wave period is defined as the time of one complete wave measured peak to peak or trough to trough. Since the times of each maximum transverse wave peak were manually selected (Section 6.2.3.1), the W_5 data were used to compute an average wave period for the first 60 seconds following the stern wave for each pass under Condition 2 testing (Table 9). The two wakeboats generated the greatest wave periods (average = 3.3 seconds) that were 37.5% longer than the non-wakeboats (average = 2.4 seconds).

Table 9. The average wave period of the transverse waves generated in Condition 2, which was displacement mode for the non-wakeboats and semi-displacement for the wakeboats.

	Boat	Average Wave Period (s)
2022	Hurricane SS203	2.7
	Cobalt R5	2.5
	Cruisers Yachts 34GLS	2.6
	Nautique G23 Paragon	3.2
	Malibu VLX Wakesetter	3.1
2023	Starcraft Limited 2000	2.0
	Sea Ray SPX190	2.0
	Nautique G23 Paragon	3.4
	Malibu VLX Wakesetter	3.4
	non-wakeboats (mean)	2.4
	wakeboats (mean)	3.3

7.1.3.5 Velocities associated with propeller wash

Like the transverse wave data, the ADCP was not able to collect quality propeller wash velocity data in the region directly aft of the boat. However, propeller wash velocities were successfully measured below the bubble depth limit and after the most intense propeller wash had passed. Figures 42 (Condition 1) and 46 (Condition 2) are included to show the bubble depth limits for each test condition, along with the depths and time-bins (i.e., 5-10, 10-30, and 30-50 seconds after pass) that these data were evaluated.

7.1.3.5.1 Condition 1 (planing mode)

Because the evaluation depths for 2022 were below the most intense region of propeller wash and devoid of bubbles (Figure 42), both horizontal (U_{13}) and vertical (W_5) data sets were good quality and thus analyzed. For 2023, the U_{13} data was again too noisy and not useable even though the evaluation depths were below the bubble extents; however, the W_5 data was good quality and therefore able to be analyzed.

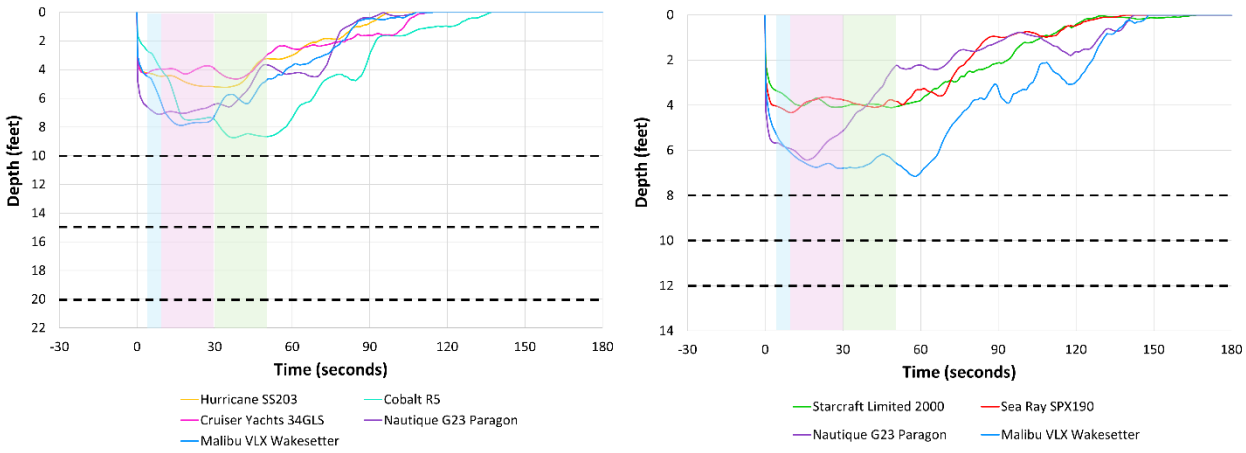

Figure 42. Condition 1 bubble depth limits determined by the 2022 (left) and 2023 (right) ADCP echograms. The blue (5-10 seconds), pink (10-30 seconds), and green (30-50 seconds) shaded regions show the three time-bins, and the dashed lines show the three depths, that the propeller wash velocities were evaluated.

In 2022, the U_{13} (Figure 43) and W_5 (Figure 44) propeller wash velocities below the most intense region were relatively small for all test boats. The mean velocity values were near zero at both 10 and 15 ft depths. At 20 ft the velocities were not measurable and are therefore not plotted in the figure. A similar trend is seen with the 2023 boats, where all boats had mean W_5 velocities near zero at 8, 10, and 12 ft depths (Figure 45).

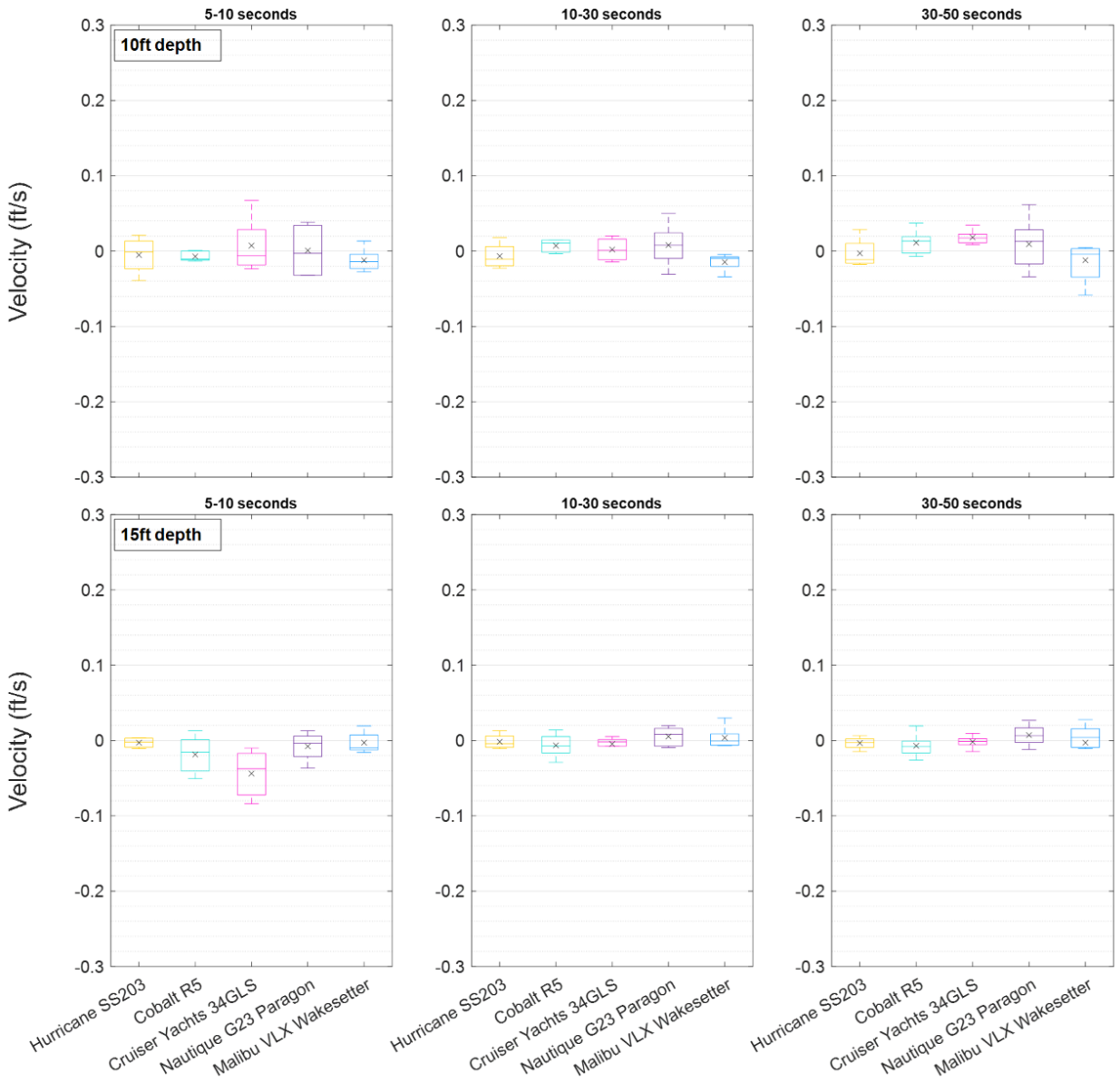

Figure 43. Boxplots (five-number summary) of the horizontal (U_{13}) propeller wash velocities measured at 10 and 15 ft during 2022 Condition 1 testing. Positive velocities indicate water movement in the same direction as the boat.

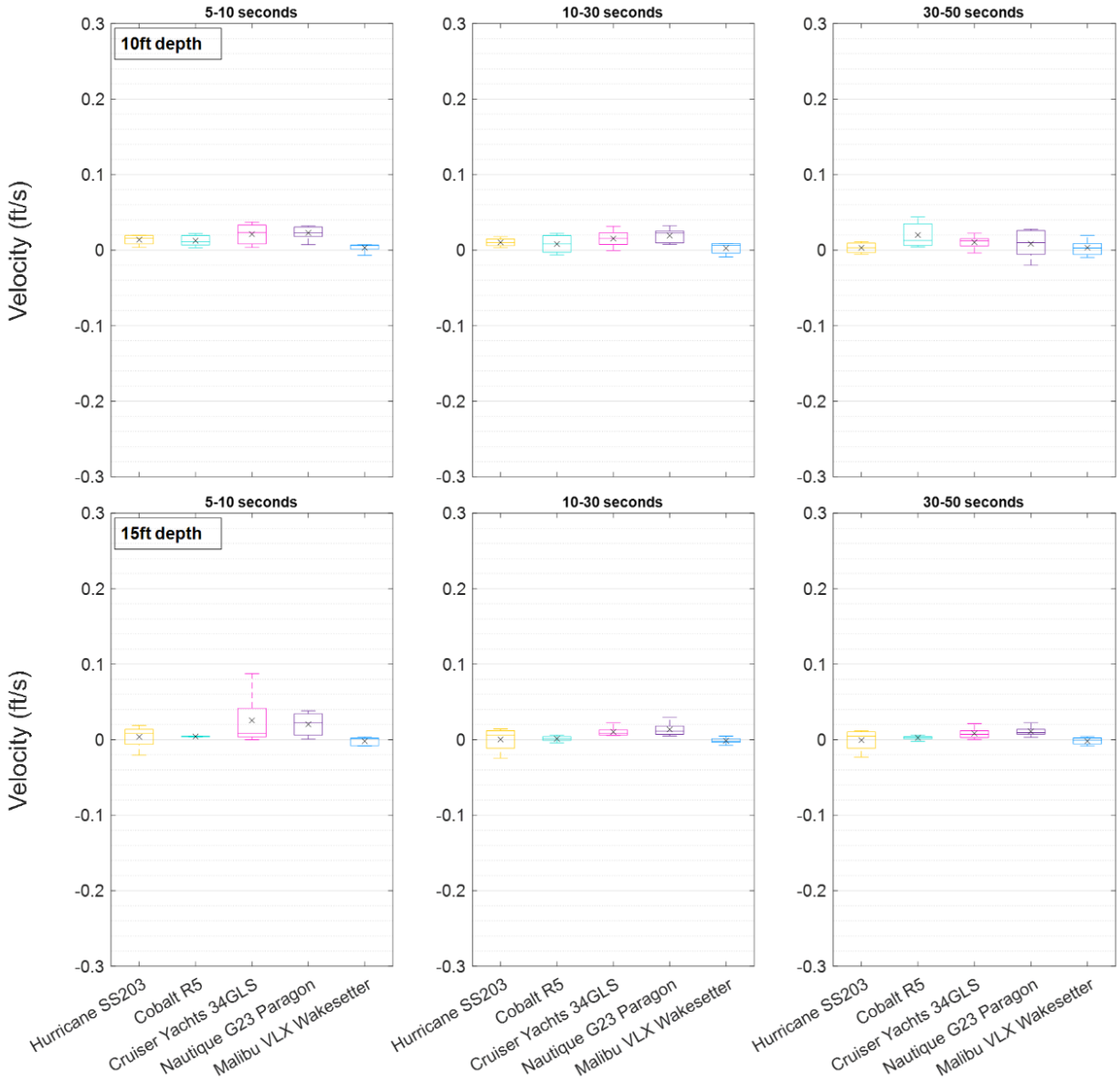

Figure 44. Boxplots (five-number summary) of the vertical (W_5) propeller velocities measured at 10 ft and 15 ft during 2022 Condition 1 testing. Positive velocities indicate water movement in the upward direction.

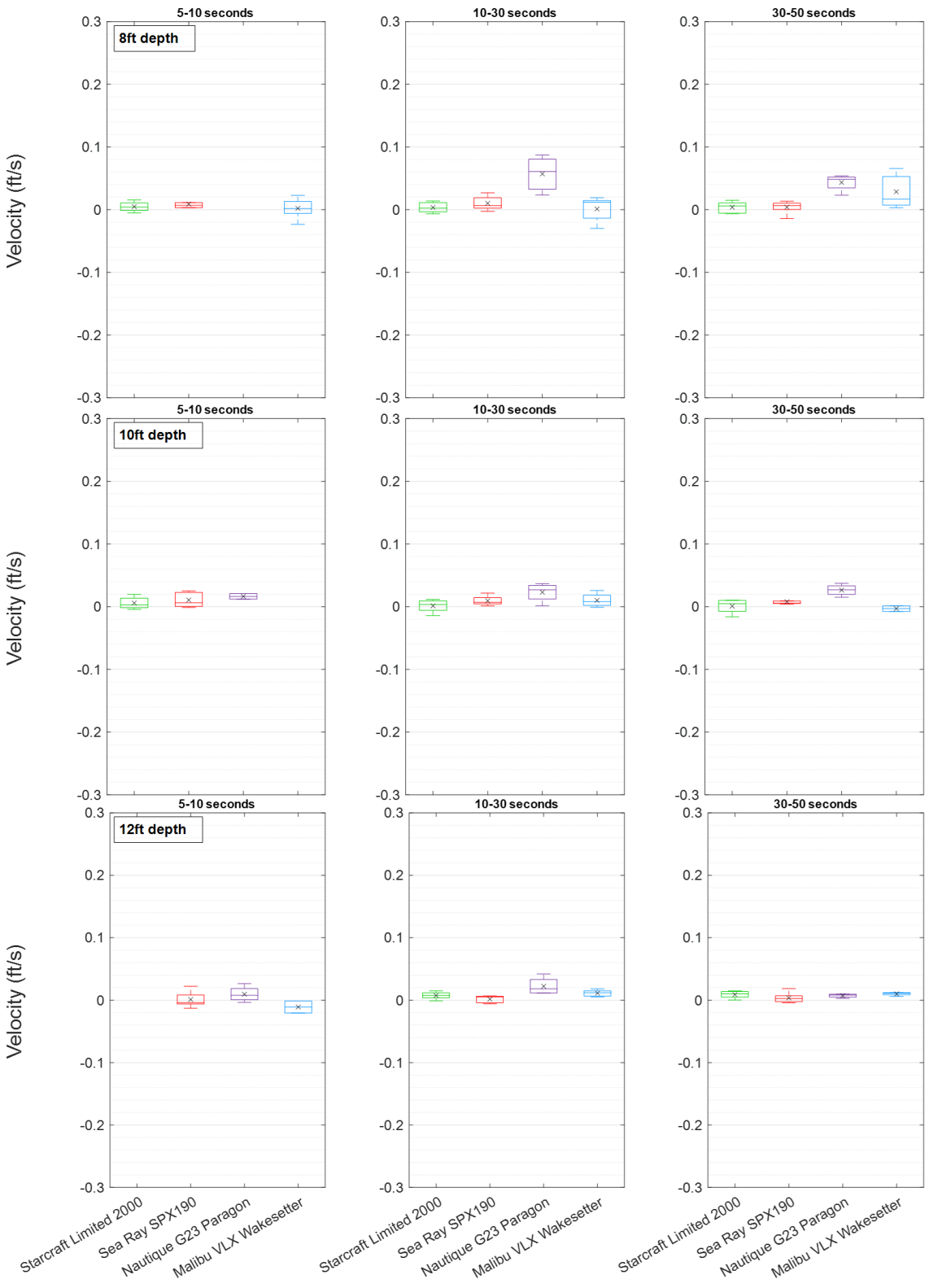

Figure 45. Boxplots (five-number summary) of the vertical (W_5) propeller wash velocities measured at 8, 10, and 12 ft during 2023 Condition 1 testing. Positive velocities indicate water movement in the upward direction.

7.1.3.5.2 Condition 2 (displacement or semi-displacement mode)

Figure 46 shows Condition 2 bubble depth limits for each year, along with the depths and time-bins (i.e., 5-10, 10-30, and 30-50 seconds after pass) that the propeller wash data were evaluated. Like the transverse wave data, the U_{13} propeller wash data for Condition 2 was deemed poor quality and not used, but the W_5 data was determined to be good quality and therefore analyzed.

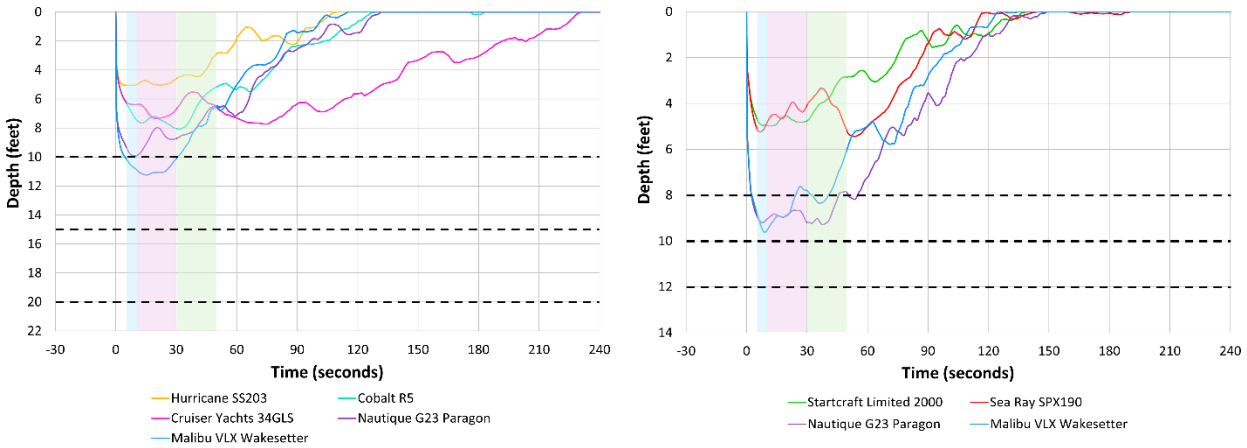

Figure 46. Condition 2 bubble depth limits determined by the 2022 (left) and 2023 (right) ADCP echograms. The blue (5-10 seconds), pink (10-30 seconds), and green (30-50 seconds) shaded regions show the three time-bins, and the dashed lines show the three depths, that the propeller wash velocities were evaluated.

In 2022, the wakeboats showed propeller wash upwelling (i.e., positive velocity values) at the 10 ft depth with mean velocities approaching 0.1 ft/s (Figure 47). The non-wakeboats also show upwelling at 10 ft, but to a lesser extent. At the 15 ft depth, the propeller wash velocities had reduced to near zero. At the 20 ft depth, the velocities were not measurable and are therefore not plotted in the figure.

In 2023, an upwelling trend is also observed (Figure 48). At the 8 ft depth, the first time-bin (5-10 seconds) had poor quality data for both wakeboats and is not plotted. At the same depth between 10-50 seconds, the wakeboats had mean propeller wash velocities between 0.12 – 0.2 ft/s. At the 10 ft depth the upwelling noticeably decreases to mean velocities between 0.02 – 0.13 ft/s. The velocities further decreased to near zero at the 12 ft depth. The non-wakeboats had mean velocities that were less than 0.02 ft/s at all three depths.

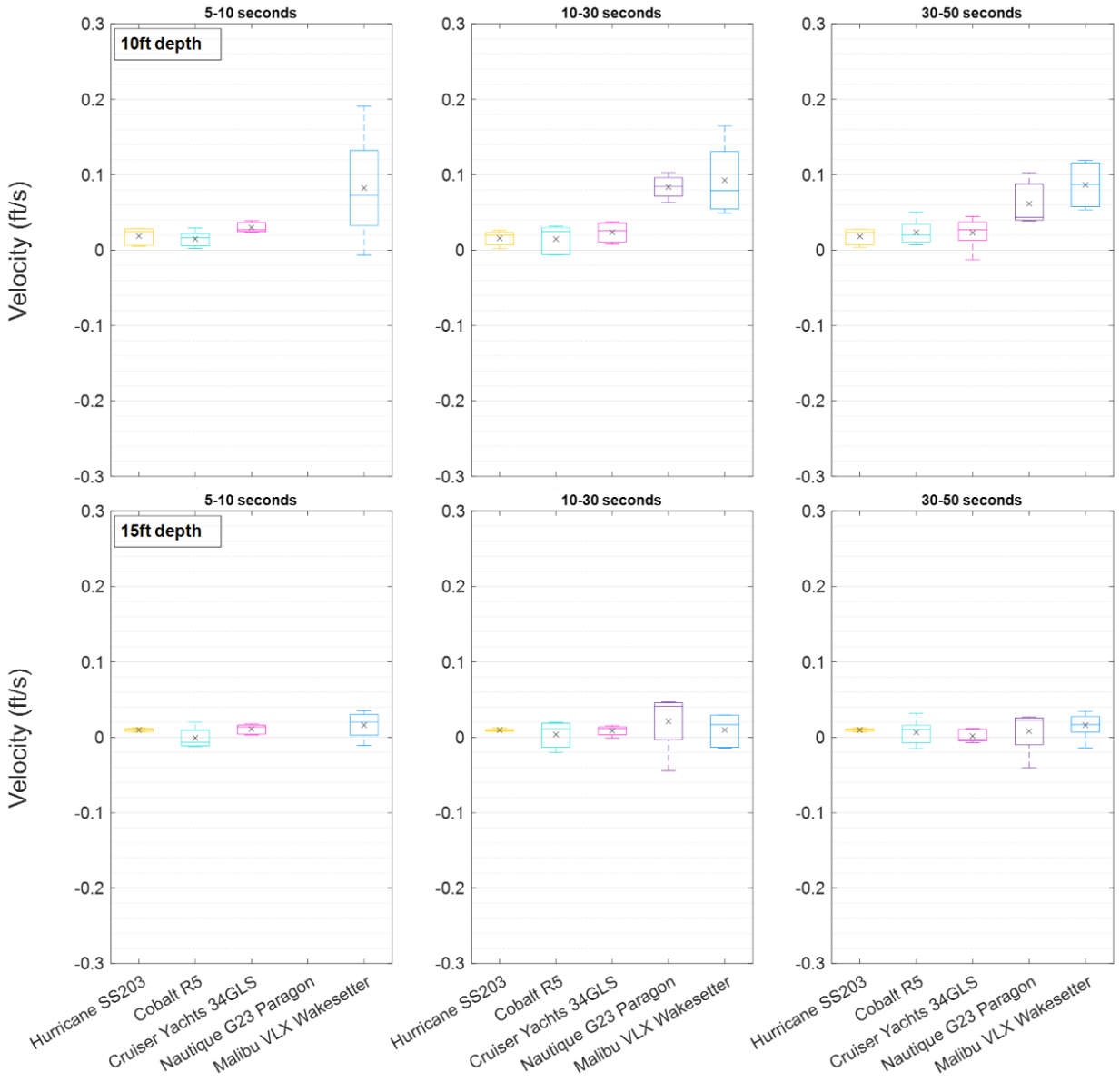

Figure 47. Boxplots (five-number summary) of the vertical (W_5) propeller wash velocities measured at 10 and 15 ft during 2022 Condition 2 boats. Positive velocities indicate upward movement.

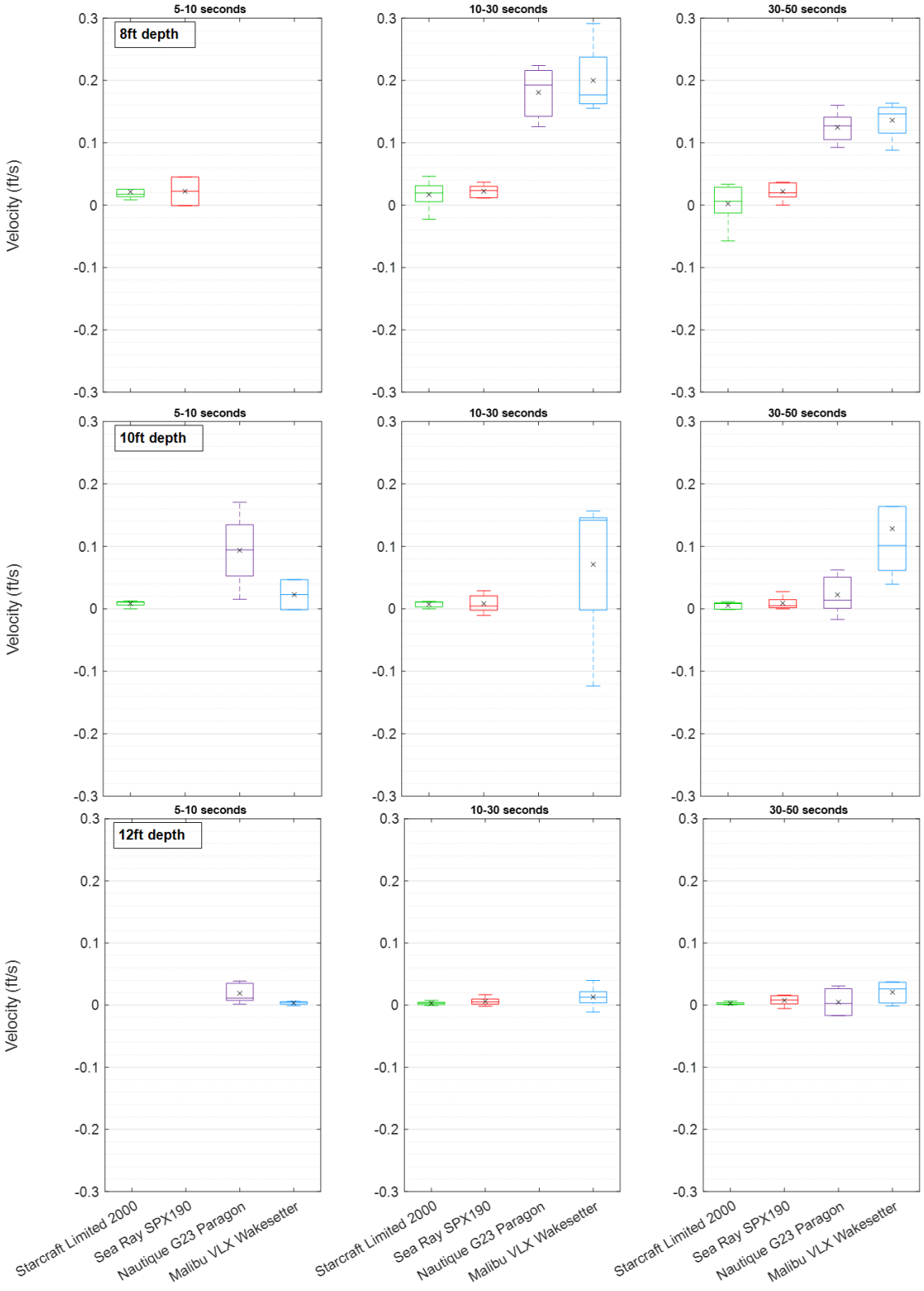

Figure 48. Boxplots (five-number summary) of the vertical (W_5) propeller wash velocities at 8, 10, and 12 ft during 2023 Condition 2 testing. Positive velocities indicate water movement in the upward direction.

7.1.4 ADV – wave velocity

7.1.4.1 Summary of overall data quality

The ADV was deployed in 16 ft of water in 2022 and 9 ft of water in 2023. The overall quality of the ADV velocity data was good, with the following exceptions:

1. The velocity data in 2023 were significantly noisier (0.22 ft/s rms) for the Nautique G23 Paragon compared to the other test boats (0.035-0.048 ft/s rms), so that the wave velocity parameters were not measurable for planing mode (Condition 1).
2. The velocity correlation filter removed several seconds of data from the 2023 Nautique G23 Paragon and Malibu VLX Wakesetter passes for semi-displacement mode (Condition 2). This may have been caused by the velocities exceeding the maximum measurable velocity of the ADV (3.3 ft/s) or excessive turbulence.
3. The bow wave velocities for the Cobalt R5 for displacement mode (Condition 2) in 2022 were similar in magnitude to the noise floor (0.03 – 0.06 ft/s) and therefore could not be reliably extracted.

7.1.4.2 Maximum velocity associated with bow waves

The highest maximum bow wave velocities were associated with the two wakeboats in semi-displacement (Condition 2) in 2023 (9 ft depth), which were 0.53 ft/s and 0.63 ft/s for the Malibu VLX Wakesetter and Nautique G23 Paragon, respectively (Table 10). These velocities exceed the critical velocity associated with the disturbance and potential resuspension of sand (Figure 49). For planing mode (Condition 1), the highest maximum bow wave velocity was produced by the Cruisers Yachts 34GLS in 2022 (16 ft depth), exceeding the 0.27 ft/s velocity threshold for disturbance and potential resuspension of coarse silt (Figure 49).

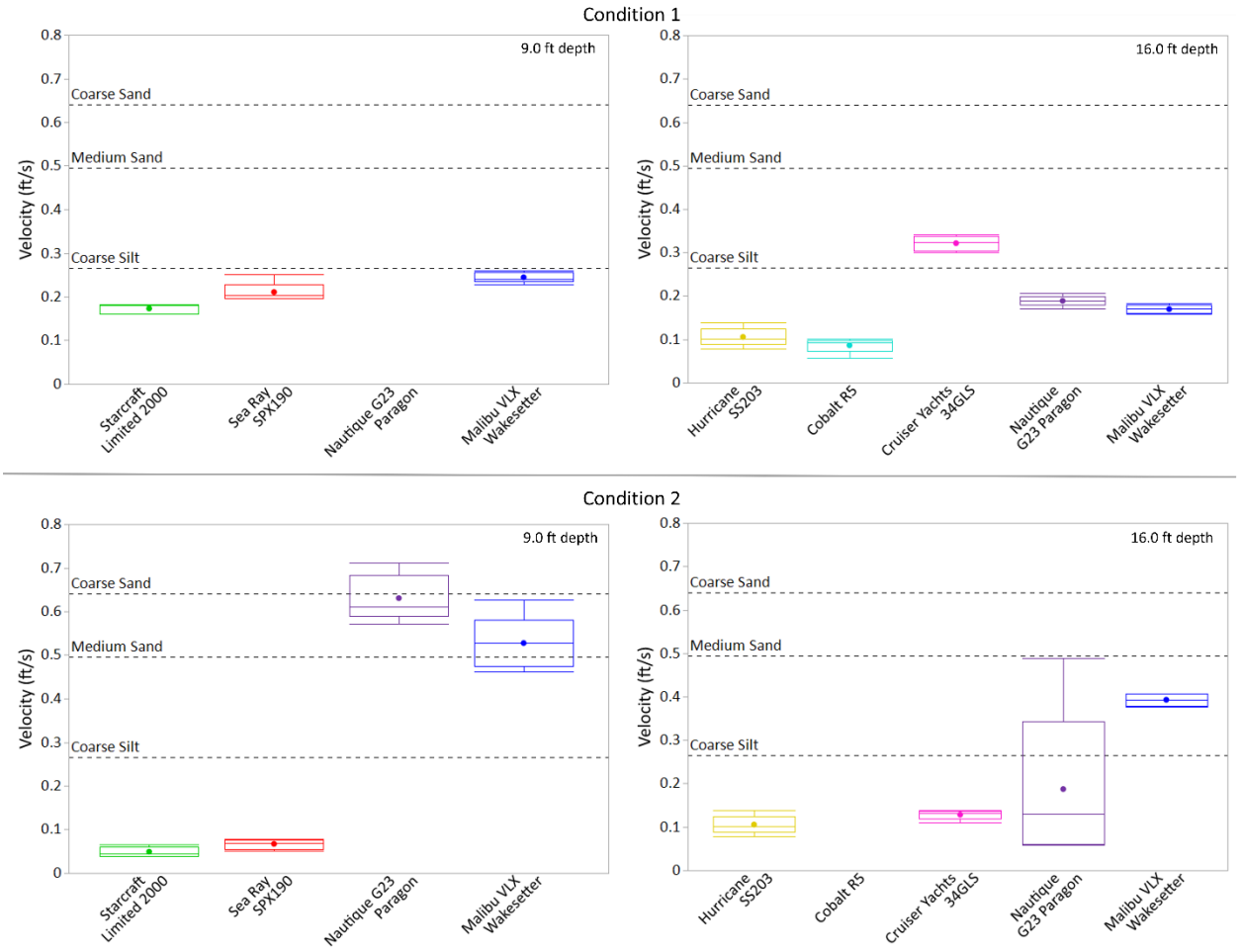

Figure 49. Boxplots (five-number summary) of the maximum bow wave velocities recorded by the ADV for boats operated in Condition 1 (top) and Condition 2 (bottom) during 2023 (left) and 2022 (right) testing. The critical velocities for disturbance and potential resuspension of coarse silt, medium sand, and coarse sand are shown as horizontal dashed lines – see Appendix for more details.

7.1.4.3 Maximum velocities associated with stern waves

The highest maximum stern wave velocities occurred at the 2023 test site (9 ft depth) and were associated with the two wakeboats in semi-displacement mode (Condition 2), with mean velocities of 1.6 ft/s and 1.2 ft/s for the Nautique G23 Paragon and the Malibu VLX Wakesetter, respectively (Table 10), which greatly exceed the critical velocity of coarse sand disturbance and resuspension potential (Figure 50). The Starcraft Limited 2000 and Sea Ray SXP190 generated mean stern wave velocities of 0.31 and 0.44 ft/s, respectively, which can disrupt coarse silt, but not medium sand.

At the 2022 test site (16 ft depth) and during Condition 2 testing, the Nautique G23 Paragon had the highest maximum stern wave velocity of 0.49 ft/s. The largest boat, the Cruisers Yachts 34GLS, produced 0.40 ft/s, while the Malibu VLX Wakesetter and Cobalt R5 generated similar mean maximum stern wave velocities of around 0.3 ft/s (Table 10). The differences in maximum stern wave velocities between boats were less distinct for planing mode (Condition 1), with all boats having mean velocities less than the 0.27 ft/s velocity threshold for disturbance and potential resuspension of coarse silt (Table 10, Figure 50).

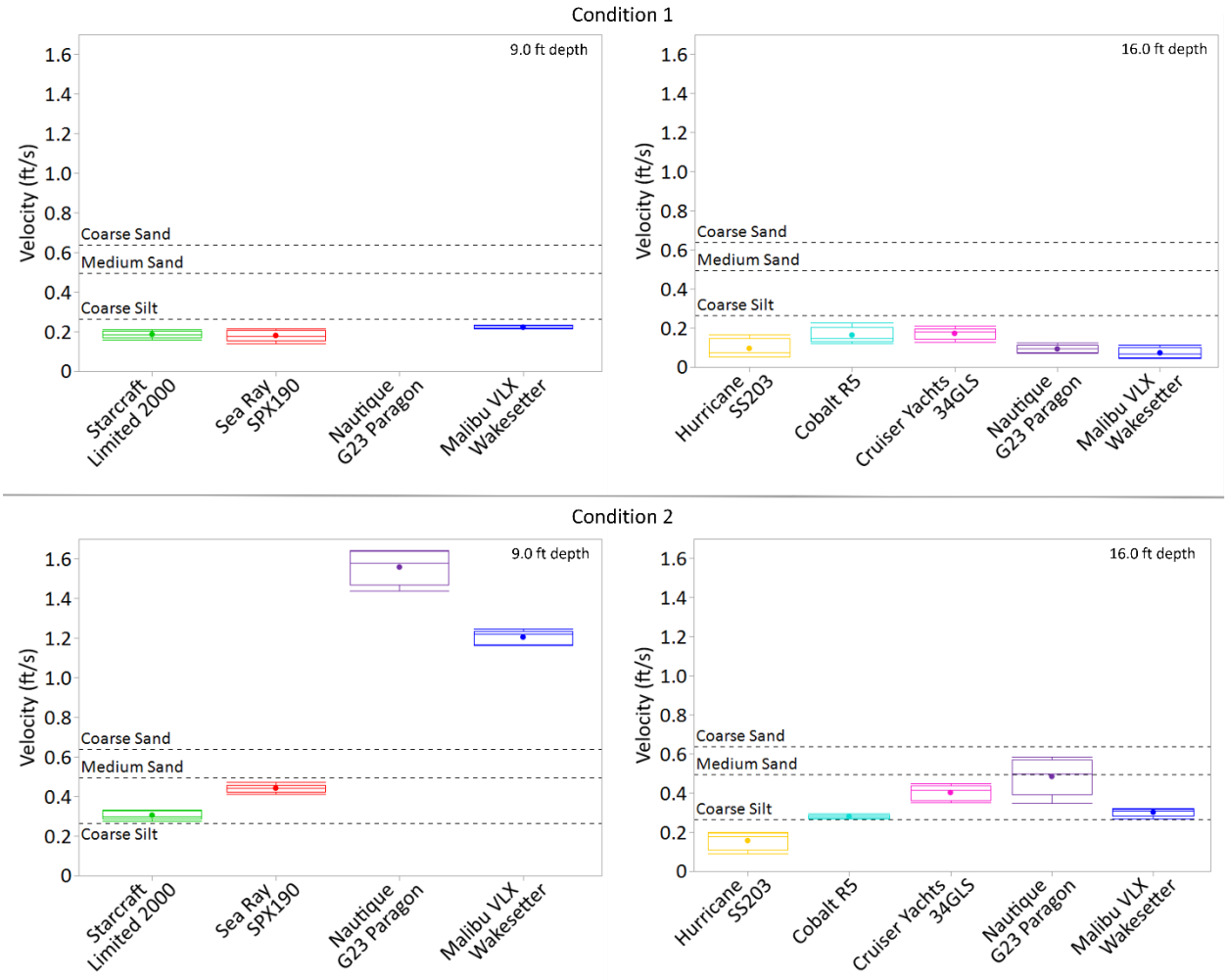

Figure 50. Boxplots (five-number summary) of the maximum stern wave velocities recorded by ADV for boats operated in Condition 1 (top) and Condition 2 (bottom) during 2023 (left) and 2022 (right) testing. The critical velocities for disturbance and potential resuspension of coarse silt, medium sand, and coarse sand are shown as horizontal dashed lines – see Appendix for more details.

7.1.4.4 Maximum velocities associated with transverse waves

At 9 ft depth (2023 site), the wakeboats had the highest transverse wave velocities that were greater than 0.27 ft/s, which can disturb and potentially resuspend coarse silt (Figure 51). The Nautique G23 Paragon and Malibu VLX Wakesetter generated mean transverse wave velocity magnitudes of 0.46 ft/s and 0.32 ft/s, respectively (Table 10). At the deeper 16 ft depth (2022 site) the same boats had mean transverse wave velocities of less than 0.2 ft/s (Table 10). At both depths, the non-wakeboats all had transverse wave velocities less than 0.1 ft/s (Table 10, Figure 51). As expected, and discussed in Section 2.1.2, the test boats did not produce measurable transverse wave velocities during planing mode (Condition 1) testing.

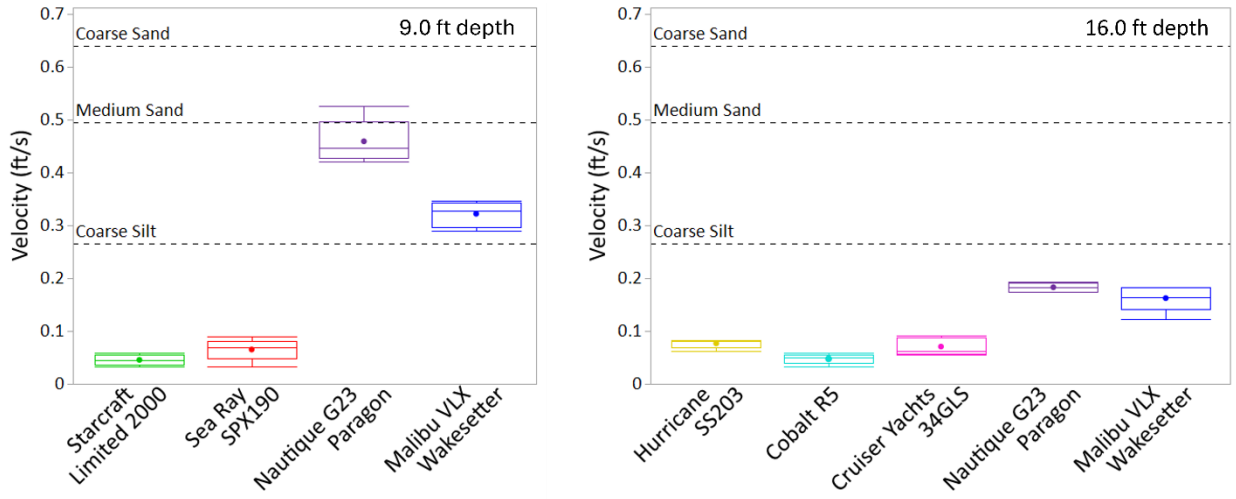

Figure 51. Boxplots (five-number summary) of the maximum transverse wave velocities recorded by the ADV for boats operated in Condition 2 during 2023 (left) and 2022 (right) testing. This was displacement mode for the non-wakeboats and semi-displacement for the wakeboats. The critical velocities for disturbance and potential resuspension of coarse silt, medium sand, and coarse sand are shown as horizontal dashed lines (see Appendix for additional description). Transverse waves were not generated in planing mode (Condition 1).

Table 10. Summary of the ADV measured mean maximum bow, stern, and transverse wave velocities. NULL entries indicate wave parameters that were not measurable. Values exceeding the 0.27 ft/s velocity threshold for disturbance and potential resuspension of coarse silt are bolded.

Boat	Depth (ft)	Condition	Maximum Bow Wave Velocity	Maximum Stern Wave Velocity	Maximum Transverse Wave Velocity
			Mean ± SD (ft/s)	Mean ± SD (ft)	Mean ± SD (ft)
[1]Hurricane SS203	16	1	0.098 ± 0.023	0.096 ± 0.050	NULL
	16	2	0.106 ± 0.022	0.157 ± 0.047	0.077 ± 0.009
[1]Cobalt R5	16	1	0.086 ± 0.017	0.164 ± 0.041	NULL
	16	2	NULL	**0.28 ± 0.009**	0.048 ± 0.009
[1]Cruiser Yachts 34GLS	16	1	**0.321 ± 0.017**	0.173 ± 0.031	NULL
	16	2	0.129 ± 0.011	**0.403 ± 0.040**	0.071 ± 0.017
[1]Nautique G23 Paragon	16	1	0.189 ± 0.013	0.093 ± 0.021	NULL
	16	2	0.187 ± 0.178	**0.485 ± 0.096**	0.183 ± 0.009
[1]Malibu VLX Wakesetter	16	1	0.170 ± 0.010	0.073 ± 0.028	NULL
	16	2	**0.393 ± 0.014**	**0.302 ± 0.021**	0.163 ± 0.024
[2]Starcraft Limited 2000	9	1	0.173 ± 0.011	0.187 ± 0.020	NULL
	9	2	0.049 ± 0.011	**0.305 ± 0.023**	0.046 ± 0.010
[2]Sea Ray SPX190	9	1	0.211 ± 0.023	0.18 ± 0.03	NULL
	9	2	0.067 ± 0.012	**0.442 ± 0.022**	0.065 ± 0.021
[2]Nautique G23 Paragon	9	1	NULL	NULL	NULL
	9	2	**0.630 ± 0.054**	**1.559 ± 0.088**	**0.460 ± 0.041**
[2]Malibu VLX Wakesetter	9	1	0.245 ± 0.012	0.223 ± 0.008	NULL
	9	2	**0.527 ± 0.063**	**1.205 ± 0.036**	**0.322 ± 0.024**

1 - 2022

2 - 2023

7.1.4.5 Relating measured maximum stern velocity to Froude number

The stern waves produced the highest maximum velocities more often than the bow waves and were measurable for all boats and all conditions, except for the noisy Nautique G23 Paragon data during planing mode (Condition 1) in 2023. Following previous studies that relate boat-generated wave sizes to Froude numbers (Sections 2.1.6 and 2.1.7), we explored the relationship of the maximum stern wave velocities to the length and depth Froude numbers (Figure 52). The highest maximum velocities occur at a length Froude number of about 0.6. The relationship of stern wave velocities to the depth Froude number shows a stronger correlation, with the maximum velocities at a depth Froude number of 1. A one-way ANOVA analysis of the maximum stern wave velocities, grouped by the seven unique depth Froude numbers, showed the depth Froude number as a strong explanatory factor (p <0.0001).

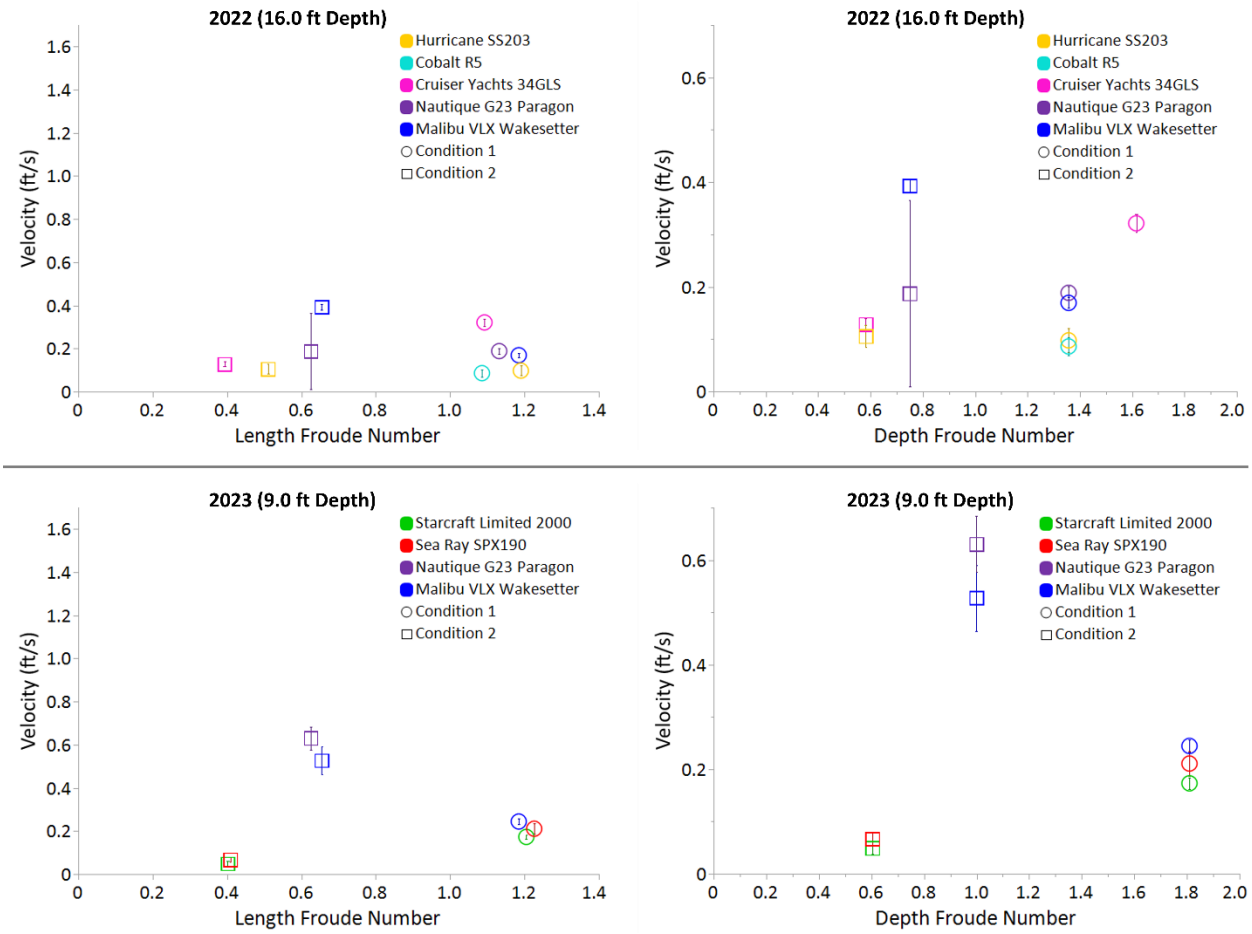

Figure 52. Mean maximum stern wave velocity versus length Froude number and depth Froude number for 2022 (top) and 2023 (bottom) testing. The error bars are the standard deviation of the five passes.

7.1.4.6 Propeller wash velocities

Propeller wash was evident in the ADV velocities only for the two wakeboats during semi-displacement (Condition 2) testing in 2023 (9 ft depth). For both boats, there was considerable variability in the propeller wash velocities between passes (Figure 53). Averaging the five passes for each boat shows that the propeller wash had similar timing and duration, but the Malibu VLX Wakesetter had higher time average velocities (Figure 53). A statistical analysis of the maximum propeller wash velocities for the five passes of each boat shows greater variation for the Nautique G23 Paragon (0.98 ft/s ± 0.31 [mean ± SD]) compared to the Malibu VLX Wakestter (1.24 ft/s ± 0.06); however, both are on the order of 1.0 ft/s (Figure 54). A paired *t*-test of the maximum velocities showed no statistically significant difference in the means between the two wakeboats (p = 0.11).

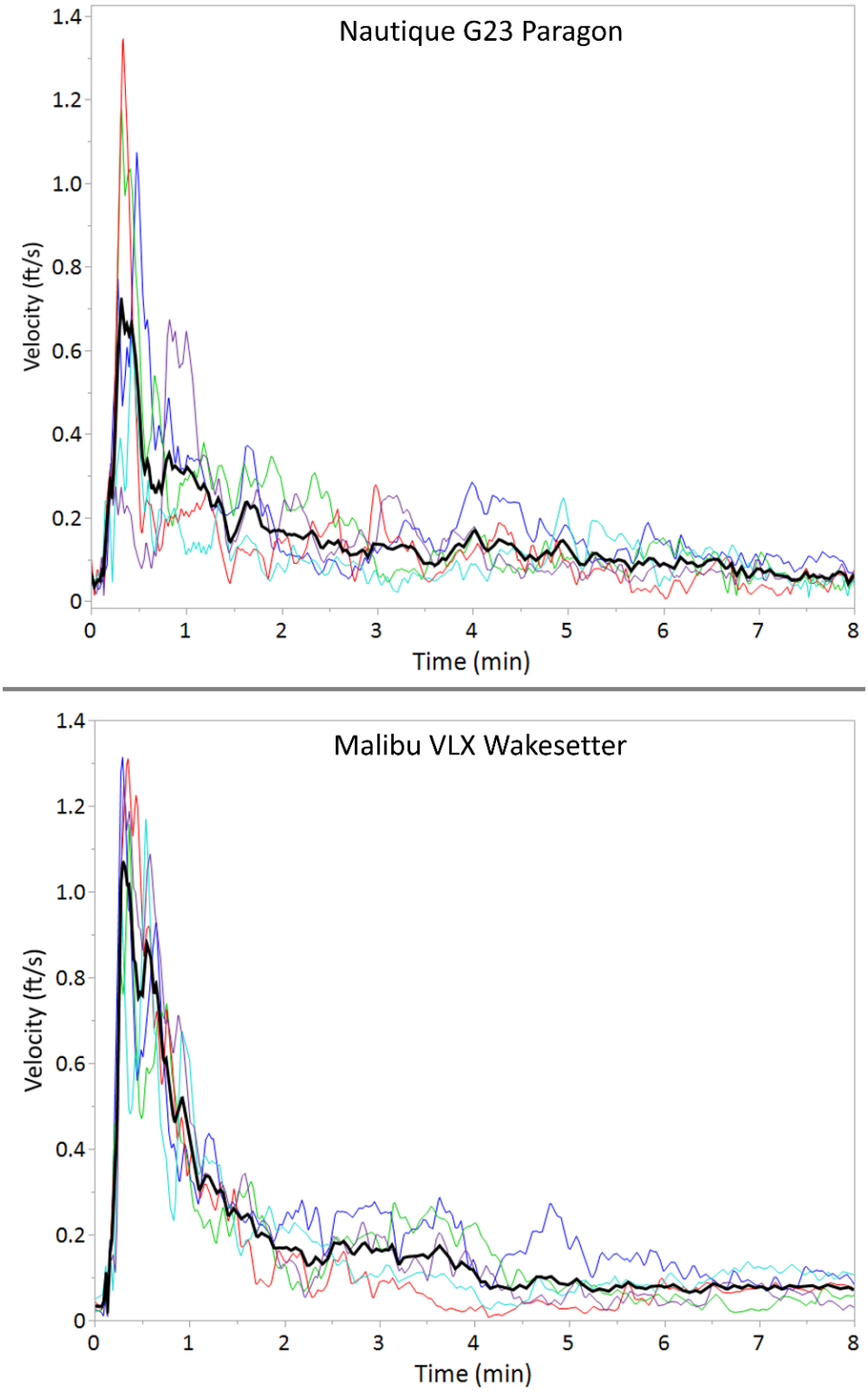

Figure 53. Time series of measured propeller wash velocity during semi-displacement mode testing of the wakeboats in 2023 (Condition 2, 9 ft depth). The black lines are the average of the five passes (colored lines).

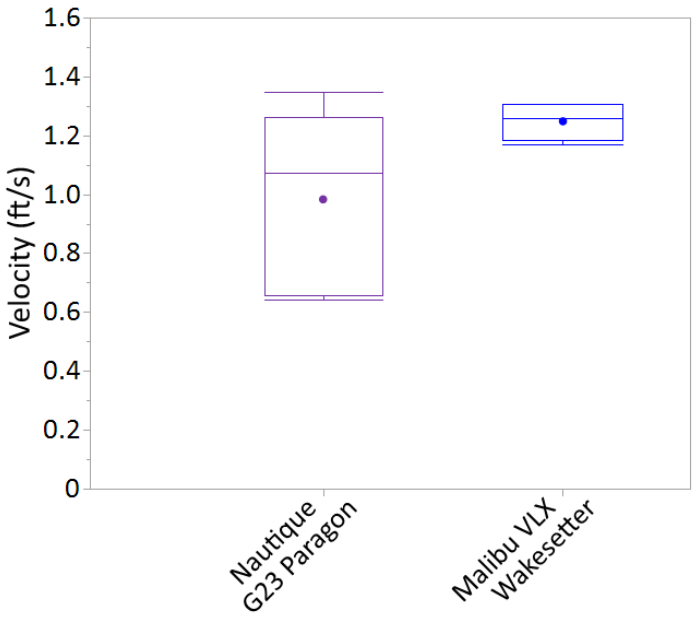

Figure 54. Boxplots (five-number summary) of the maximum propeller wash velocities for the semi-displacement mode passes made by the wakeboats in 2023 (Condition 2, 9 ft depth). The dot denotes the mean maximum velocity.

7.1.4.7 Signal amplitude (qualitative measure of suspended sediment concentrations)

The ADV signal amplitudes, a qualitative measure of suspended sediment concentration, were plotted as a time series for each test day. A 10-second moving average filter was applied to the signal amplitude for the time series plots. The 2022 (16 ft depth) data showed very little change associated with the boat passes, and the signal amplitude was in the range of 120-130 dB each day (Figure 55). The 2023 data (9 ft deep) had substantial increases in signal amplitude associated with the Condition 2 passes for the two wakeboats (Figure 56), with maximum signal amplitudes around 180 dB. Figure 57 gives the distributions of the maximum 10-second average signal amplitude for each boat and condition in 2023. It is difficult to evaluate the statistical significance of, for example, differences in signal amplitude between boats in Condition 1, due to variability in the background turbidity in the lake. However, based on paired *t*-tests, the following statements hold for the 2023 data:

1) The Condition 2 ADV signal amplitudes for the Malibu VLX Wakesetter and Nautique G23 Paragon are significantly higher than the amplitudes for the same boats in Condition 1 (p <0.001 in all cases).

2) The Condition 2 ADV signal amplitudes for the Malibu VLX Wakesetter and Nautique G23 Paragon are significantly higher than the other boats in Condition 2 (p <0.001 in all cases).
3) The Condition 2 ADV signal amplitudes for the Malibu VLX Wakesetter and Nautique G23 Paragon are not significantly different from each other (p = 0.44).

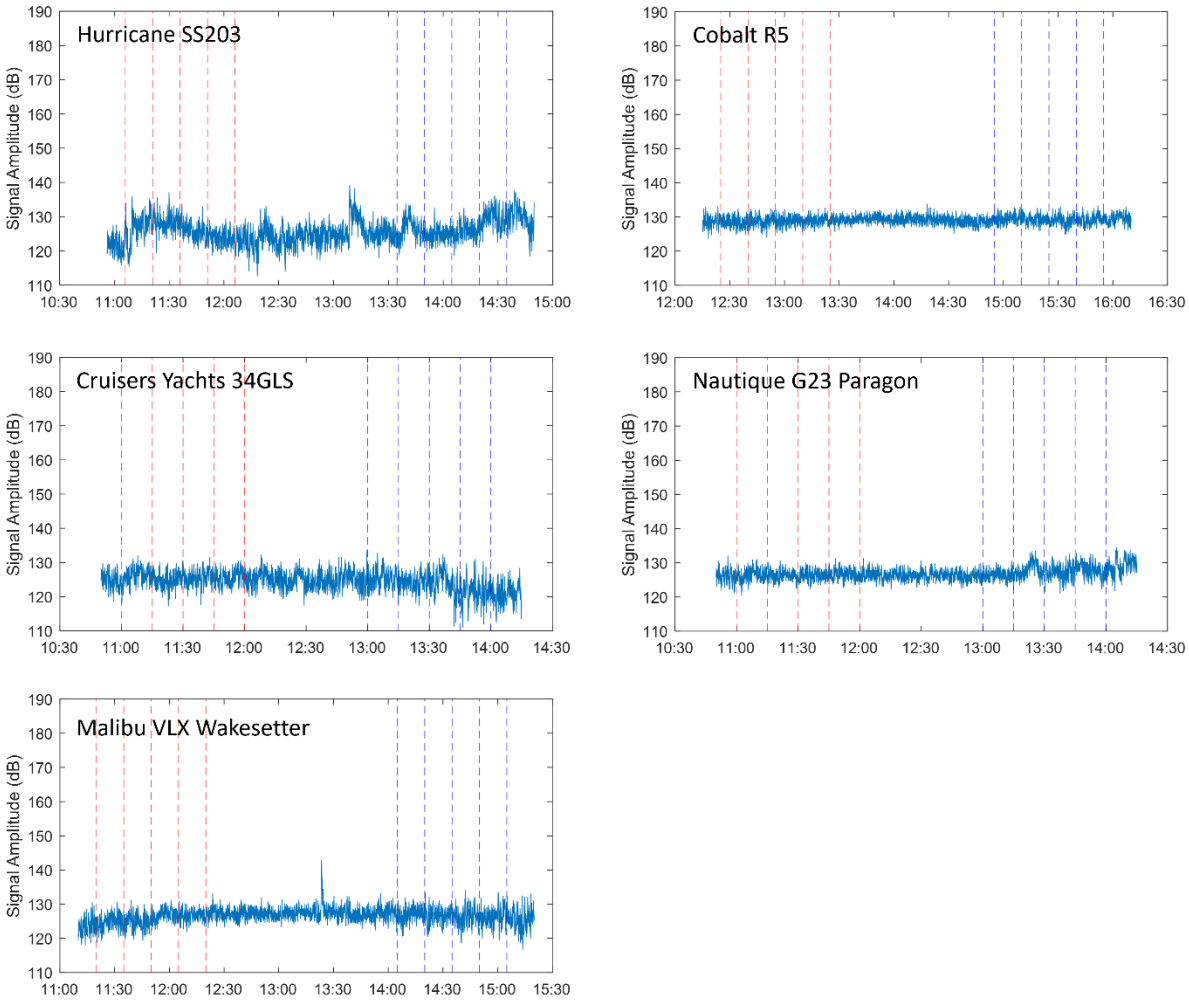

Figure 55. Time series of the ADV signal amplitude for the 2022 test boats (16 ft depth). The red and blue vertical dashed lines give the times of Condition 1 and Condition 2 passes, respectively. The signal amplitudes plotted are the average of the three beams.

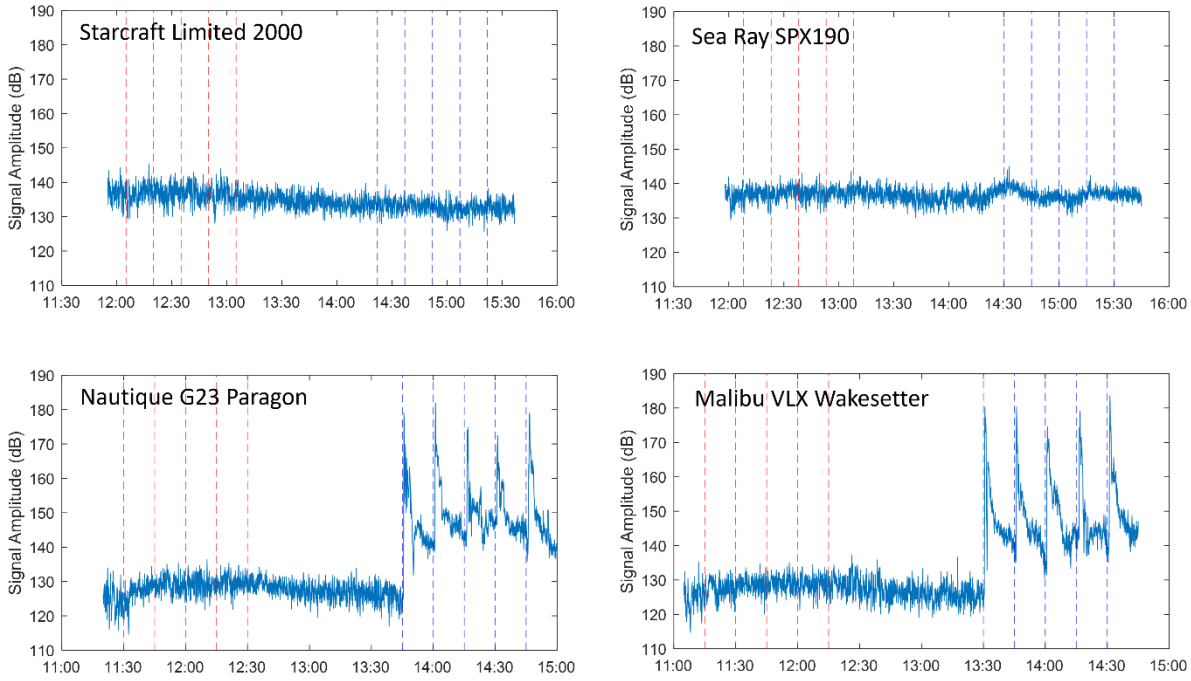

Figure 56. Time series of the ADV signal amplitude for the 2023 test boats (9 ft depth). The red and blue vertical dashed lines give the times of Condition 1 and Condition 2 passes, respectively. The signal amplitudes plotted are the average of the three beams.

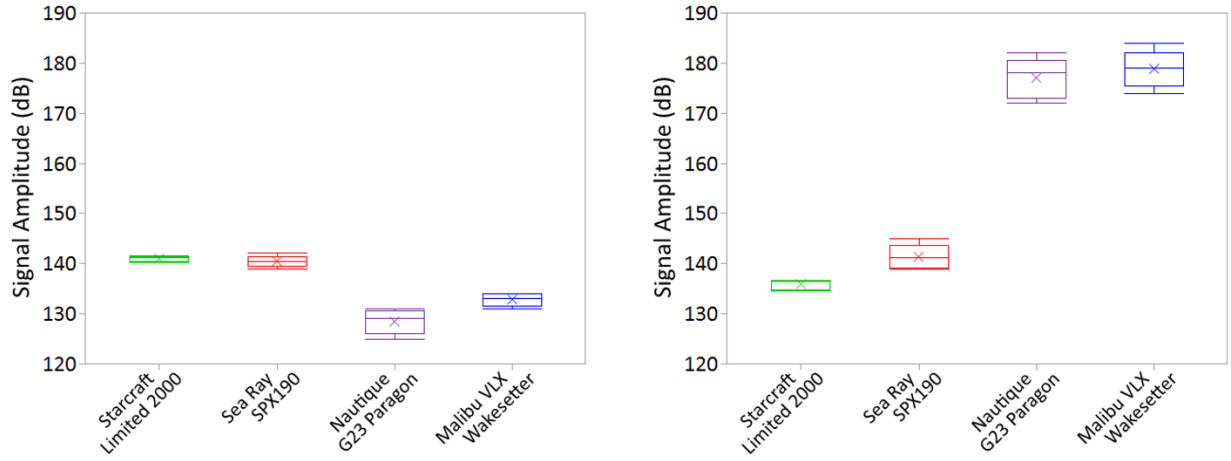

Figure 57. Boxplots (five-number summary) of the maximum 10-second average signal amplitude for Condition 1 (left panel) and Condition 2 (right panel) passes in 2023 (9 ft depth).

7.1.5 Boat hull pitch

For planing mode (Condition 1), the average hull pitch was <13° for both all boats (Figure 58). The highest overall pitch was the Malibu VLX Wakesetter during semi-displacement mode (Condition 2) in both 2022 (15.7° ± 0.2 [mean ± SD]) and 2023 (15.2° ± 0.1). The Nautique G23 Paragon had the next highest pitch, which also occurred during semi-displacement mode (2022- 13.2° ± 0.2, 2023- 14.1° ± 0.1).

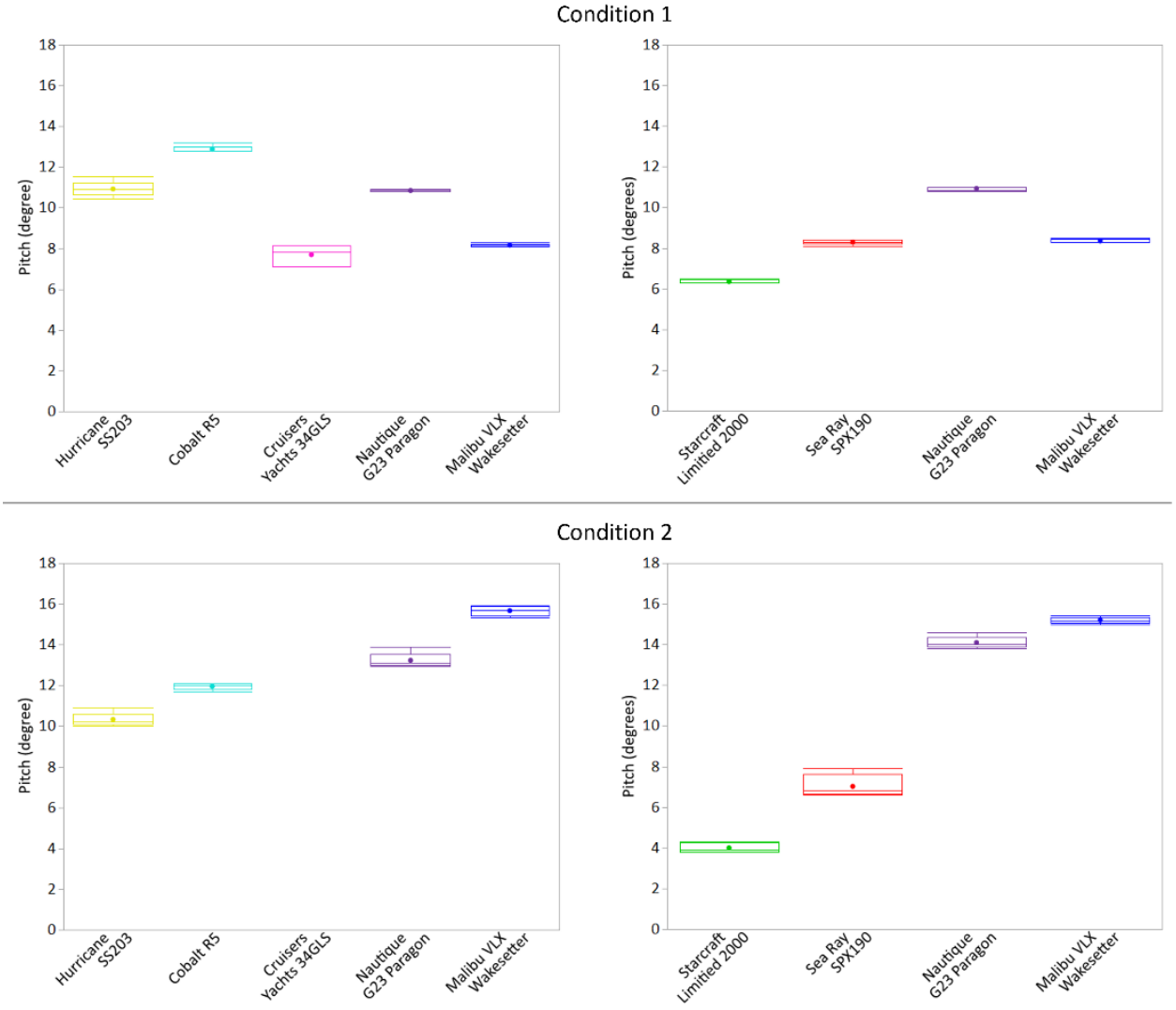

Figure 58. Boxplots (five-number summary) of the average pitch of the boats while traveling between pads during 2022 (left) and 2023 (right) testing.

7.2 Environmental impacts by recreational powerboats

7.2.1 Water quality

7.2.1.1 Temperature profiles

The water column temperature at the 27 ft pad was between 59°F and 65°F during fall 2022 testing in North Arm Bay (Figure 59). On each day of testing, the water column temperature was consistent with depth and varied by less than 3°F, indicating that the water column was not thermally stratified. The water column temperature profile followed the same trend at the shallower 16 ft pad (not shown). Historical data confirmed the bay had already completed fall turnover and was no longer thermally stratified like it is in warmer months (e.g., August).

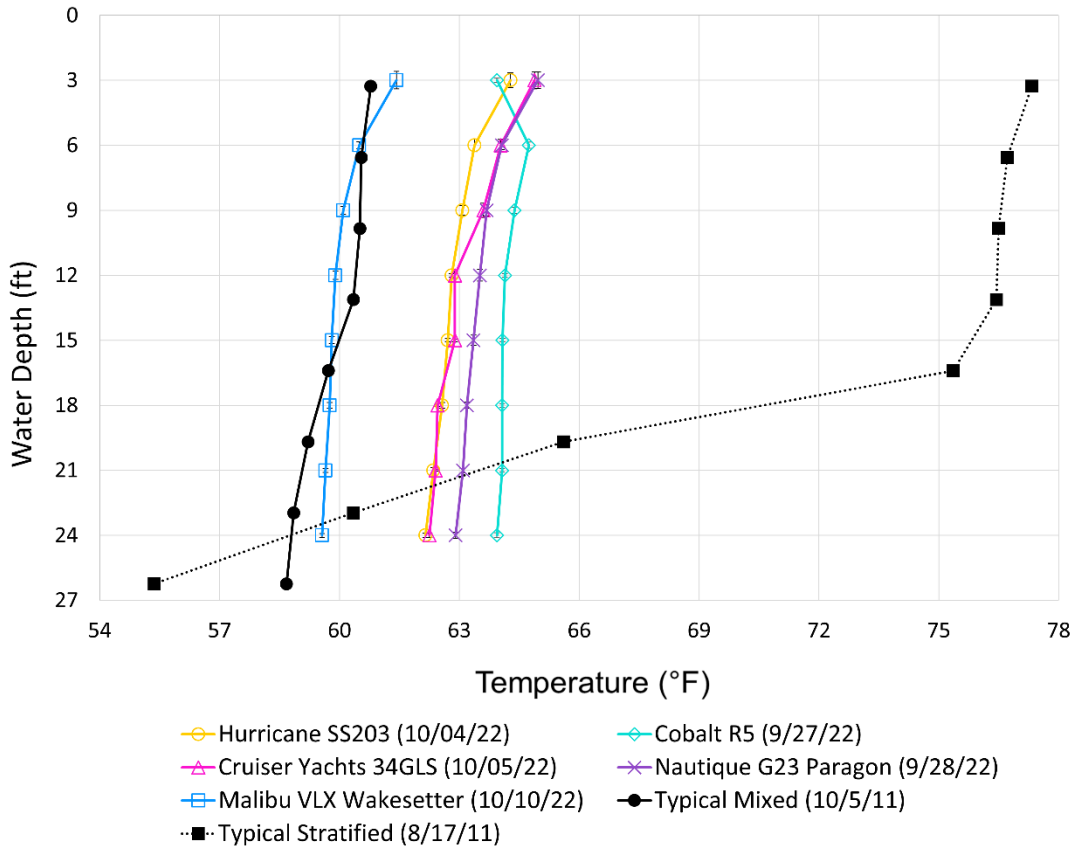

Figure 59. Average water column temperature at the 27 ft pad during fall 2022 testing in North Arm Bay. The historical data are single-point measurements taken at an unknown location in North Arm Bay and are courtesy of Minnehaha Creek Watershed District.

The water column temperature profile at the deep site (i.e., 14 ft) during the fall 2023 field campaign in Maxwell Bay was between 54°F and 68°F (Figure 60). On each of the four days of testing, the water column temperature was consistent with depth and varied by less than 1°F, and therefore not thermally stratified at the test site.

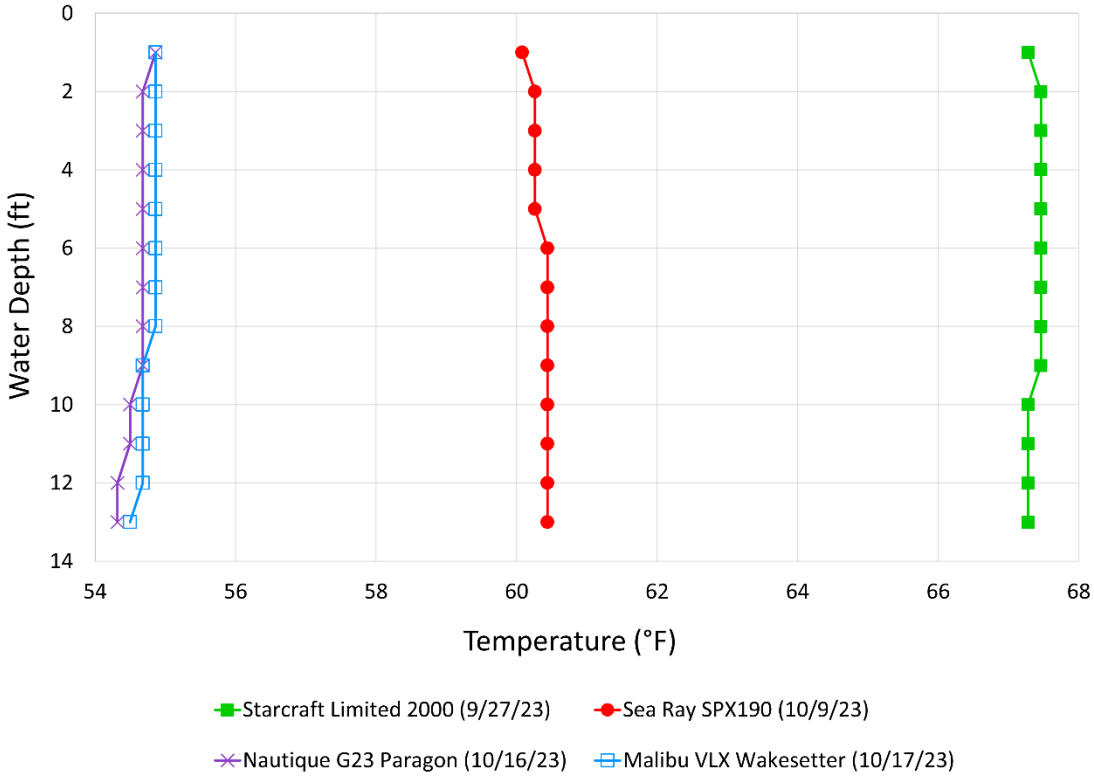

Figure 60. Water column temperature profile at Maxwell Bay during testing of the fall 2023 boats. The single-point measurements were collected at the 14 ft pad location.

7.2.1.2 Suspended solids (TSS, VSS, FSS)

To compare the impact of boat passes on background suspended solids concentrations, the pre-boat pass samples (Pre) for each year were analyzed using a two-way ANOVA to test the effect of sample date and condition (morning or afternoon). For 2022, the interaction between date and condition was significant (*p*-value = 0.0004) which indicates that the background TSS concentrations varied differently in the morning and afternoon on different sampling dates. In 2023, the effect of date (*p*-value = 0.0014), condition (*p*-value = 0.011) and the interaction between date and condition (*p*-value = 0.0011) were significant which indicates that background

TSS concentrations varied by date and varied differently between the morning and afternoon on different dates. For this reason, each condition was treated as an independent experiment and was analyzed separately.

Mixed models were used to fit the repeated measured data for each independent dataset (for each operating condition for each boat) allowing for unequal variance at different time steps. For 2022, these models tested for the effect of sampling location (16 and 27 ft), sampling depth (near-bed, mid-depth), boat pass (pre, pass, post), and the interactions between these factors. For 2023, these models tested for the effect of sampling location (9 and 14 ft), boat pass (pre, pass, post), and the interactions between these factors.

In 2022, all samples collected in North Arm Bay had relatively low TSS concentrations regardless of date, location, depth, or morning or afternoon (<10 mg/L; Figure 61). Across boats and conditions, sampling location and sampling depth were most frequently significant in 2022 (Table 11). Although boat pass had a significant effect on suspended solids for some boat operating conditions, there was not a consistent pattern with TSS (total), VSS (organic) or FSS (inorganic fraction) (Figure 61).

Suspended solids concentrations overall were slightly higher in Maxwell Bay in 2023 than in North Arm Bay in 2022, especially on the day the Sea Ray SPX190 was tested (Figure 62). On this day the average wind speeds increased from approximately 7 mph in the morning to approximately 15 mph in the afternoon which may account for some of the increase. Similar to 2022, in 2023, across boats and conditions, sampling location most frequently had a significant effect on suspended solids (Table 12). However, as the pad locations were in shallower water in 2023 than in 2022, there was a greater impact of boat pass on suspended solids. Specifically, the pre-boat pass samples were significantly less than the post-boat pass samples for the Malibu VLX Wakesetter during semi-displacement mode (Condition 2) testing (post-hoc Tukey HSD with α=0.05). For the Nautique G23 Paragon during semi-displacement testing (Condition 2), there was no significant effect of boat pass on TSS, but when only the inorganic fraction (FSS) was considered, the pre-boat pass samples were significantly less than the samples collected after the pass samples (i.e., after the first pass).

Together these samples indicate that 1) there is a high level of variation in suspended solids samples, even when collected at the same depth and within 6 inches laterally, and 2) patterns in suspended solids as a function of boat passes may be obscured by this variability. For our study, sediment resuspension was observed in video footage (Section 7.2.3); however, it was not well mixed laterally or vertically when the samples were collected, which likely led to the significant variability. Daeger et al. (2022) conducted a similar study, comparing suspended solids concentrations at 5, 10, and 15 ft water depth before and after boat passes, but pooled samples collected at different depths in the water column. They reported much higher levels of suspended solids for their shallowest case (5 ft depth), but due to their sampling scheme, likely averaged out any near lakebed suspension at deeper water depths.

Table 11. Effect test results for mixed models with unequal variances for 2022 suspended solids samples. Prob > F values of less than 0.05 are bold and considered significant. Condition 1 (C1) is planing mode and Condition 2 (C2) is displacement or semi-displacement. TSS = total suspended solids, VSS = volatile suspended solids, and FSS = fixed suspended solids.

			Location		Depth		Location*Depth		Pass		Location*Pass		Depth*Pass		Location*Depth*Pass	
			F Ratio	Prob > F	F Ratio	Prob > F	F Ratio	Prob > F	F Ratio	Prob > F	F Ratio	Prob > F	F Ratio	Prob > F	F Ratio	Prob > F
Hurricane SS203	C1	TSS	13.22	**0.001**	0.00	1.00	2.00	0.17	1.76	0.21	0.61	0.56	2.19	0.15	0.44	0.65
		VSS	1.95	0.18	1.95	0.18	0.05	0.82	1.53	0.25	1.65	0.23	4.21	**0.036**	2.98	0.08
		FSS	6.96	**0.014**	2.22	0.15	1.59	0.22	0.45	0.64	0.32	0.73	0.17	0.84	1.04	0.37
	C2	TSS	2.53	0.12	24.50	**<.0001**	4.50	**0.044**	0.03	0.97	0.10	0.90	1.46	0.25	0.10	0.90
		VSS	0.01	0.93	23.81	**<.0001**	0.01	0.93	0.11	0.90	1.89	0.19	2.11	0.16	0.47	0.63
		FSS	3.11	0.09	0.25	0.62	7.68	**0.012**	0.11	0.90	3.09	0.08	0.01	0.99	0.26	0.78
Cobalt R5	C1	TSS	0.04	0.84	1.32	0.27	18.34	**0.001**	0.33	0.73	7.02	**0.008**	0.00	1.00	1.36	0.29
		VSS	6.86	**0.021**	5.88	**0.030**	0.08	0.78	3.20	0.08	5.90	**0.016**	0.98	0.40	2.40	0.13
		FSS	5.22	**0.034**	8.58	**0.008**	24.90	**<.0001**	1.48	0.26	6.14	**0.013**	0.47	0.63	0.83	0.46
	C2	TSS	35.44	**<.0001**	2.75	0.11	8.76	**0.007**	4.03	**0.041**	0.35	0.71	2.18	0.15	5.80	**0.014**
		VSS	6.13	**0.024**	2.21	0.16	7.61	**0.013**	0.55	0.59	0.04	0.96	1.78	0.21	0.20	0.82
		FSS	23.68	**<.0001**	5.60	**0.027**	2.92	0.10	4.72	**0.026**	0.48	0.63	1.47	0.26	5.47	**0.017**
Cruisers Yachts	C1	TSS	23.86	**<.0001**	0.08	0.78	15.42	**0.0006**	0.79	0.47	11.14	**0.0004**	0.22	0.81	1.25	0.31
		VSS	7.88	**0.010**	2.49	0.13	2.49	0.13	0.15	0.86	1.98	0.17	0.24	0.79	0.24	0.79
		FSS	2.42	0.13	5.98	**0.023**	7.11	**0.014**	1.09	0.36	4.21	**0.036**	0.79	0.47	1.24	0.32
	C2	TSS	0.00	1.00	12.52	**0.002**	11.57	0.00	0.34	0.71	6.37	**0.007**	1.35	0.28	0.33	0.73
		VSS	22.23	**0.0001**	10.47	**0.004**	2.47	0.13	0.69	0.52	1.34	0.29	0.39	0.69	1.87	0.19
		FSS	16.67	**0.0005**	27.08	**<.0001**	5.39	**0.030**	1.09	0.36	4.54	**0.029**	2.25	0.14	0.30	0.75
Nautique G23 Paragon	C1	TSS	21.90	**0.0001**	0.02	0.88	2.13	0.16	0.19	0.83	1.44	0.27	0.37	0.70	2.04	0.16
		VSS	26.71	**<.0001**	0.96	0.34	9.44	**0.006**	0.28	0.76	1.29	0.30	0.08	0.93	1.89	0.19
		FSS	2.03	0.17	1.62	0.22	1.26	0.27	0.50	0.62	0.30	0.75	0.93	0.42	0.88	0.43
	C2	TSS	5.41	**0.030**	3.37	0.08	0.73	0.40	0.78	0.48	3.76	**0.049**	1.18	0.34	3.07	0.08
		VSS	1.26	0.28	4.35	0.05	0.64	0.43	0.47	0.63	0.15	0.86	0.15	0.86	2.39	0.13
		FSS	2.57	0.13	0.19	0.67	3.60	0.08	3.51	0.06	4.48	**0.031**	2.20	0.15	6.44	**0.010**
Malibu VLX Wakesetter	C1	TSS	0.00	1.00	0.02	0.90	2.10	0.16	0.61	0.56	3.85	**0.044**	2.95	0.08	2.56	0.11
		VSS	0.02	0.88	2.30	0.14	2.78	0.11	0.24	0.79	0.31	0.74	0.31	0.74	5.17	**0.020**
		FSS	0.65	0.43	8.80	**0.007**	0.29	0.59	4.13	**0.037**	14.02	**0.0004**	6.37	**0.010**	15.45	**0.0002**
	C2	TSS	17.61	**0.0003**	1.96	0.17	0.01	0.93	0.37	0.70	0.10	0.90	0.84	0.44	1.87	0.18
		VSS	6.02	**0.024**	0.82	0.38	4.82	**0.041**	1.13	0.35	0.57	0.58	0.20	0.82	1.73	0.21
		FSS	9.30	**0.007**	7.54	**0.014**	4.56	**0.048**	0.40	0.68	0.17	0.85	1.60	0.24	0.48	0.63

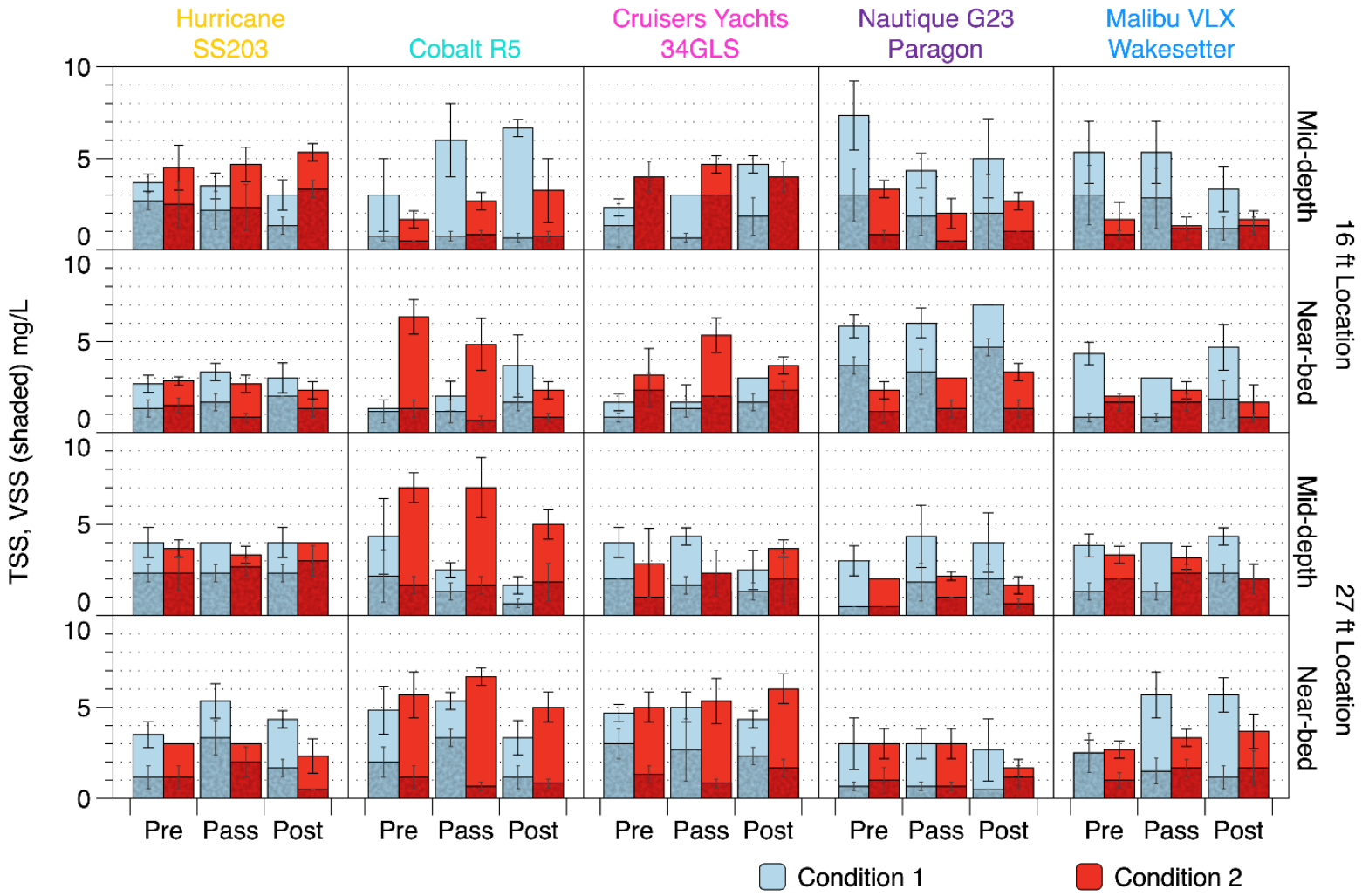

Figure 61. Total suspended solids (TSS) and volatile suspended solids (VSS; shaded) for 2022 water samples in North Arm Bay. The blue and red bars are planing mode (Condition 1), and displacement mode for the non-wakeboats and semi-displacement for the wakeboats (Condition 2), respectively. The difference between TSS and VSS is the fixed suspended solids (FSS).

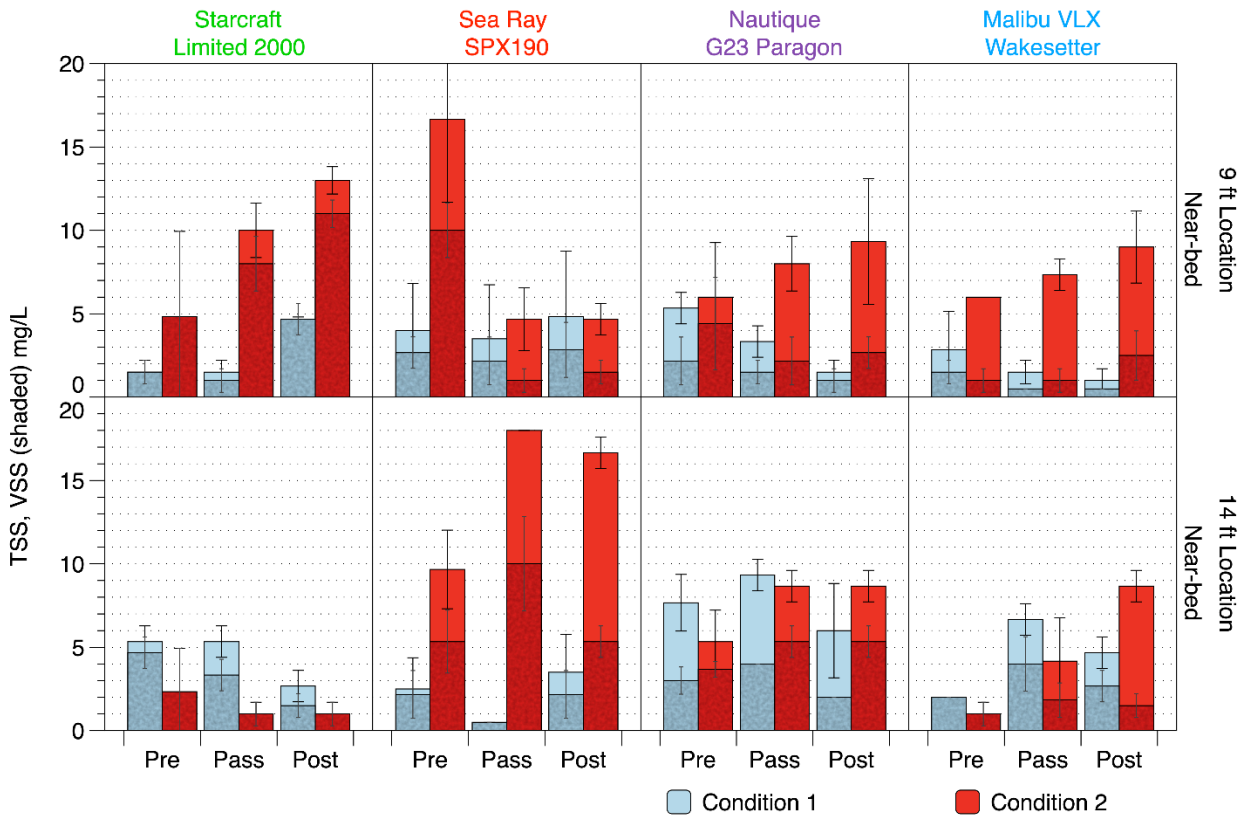

Figure 62. Total suspended solids (TSS) and volatile suspended solids (VSS; shaded) for 2023 water samples in Maxwell Bay. The blue and red bars are planing mode (Condition 1), and displacement mode for the non-wakeboats and semi-displacement for the wakeboats (Condition 2), respectively. The difference between TSS and VSS is the fixed suspended solids (FSS).

Table 12. Effect test results for mixed models with unequal variances for 2023 suspended solids samples. Prob > F values of less than 0.05 are bold and considered significant. Condition 1 (C1) is planing mode and Condition 2 (C2) is displacement or semi-displacement. TSS = total suspended solids, VSS = volatile suspended solids, and FSS = fixed suspended solids.

			Location		Pass		Location*Pass	
			F Ratio	Prob > F	F Ratio	Prob > F	F Ratio	Prob > F
Starcraft Limited 2000	C1	TSS	18.51	**0.001**	0.01	0.99	15.37	**0.002**
		VSS	2.61	0.13	1.48	0.29	15.65	**0.002**
		FSS	9.33	**0.011**	2.53	0.15	0.70	0.53
	C2	TSS	29.80	**0.003**	2.85	0.13	3.91	0.08
		VSS	20.52	**0.006**	2.31	0.18	3.08	0.12
		FSS	-	-	-	-	-	-
Sea Ray SPX190	C1	TSS	1.60	0.23	0.61	0.57	0.13	0.88
		VSS	1.64	0.23	1.18	0.36	0.29	0.76
		FSS	1.41	0.26	0.27	0.77	0.01	0.99
	C2	TSS	18.80	**0.006**	0.90	0.45	11.15	**0.008**
		VSS	8.28	**0.018**	9.22	**0.014**	12.81	**0.006**
		FSS	8.57	**0.017**	1.25	0.35	7.90	**0.022**
Nautique G23 Paragon	C1	TSS	23.44	**0.001**	2.63	0.14	2.21	0.18
		VSS	10.09	**0.016**	5.96	**0.032**	2.31	0.17
		FSS	8.86	**0.016**	0.70	0.53	0.68	0.54
	C2	TSS	0.03	0.87	1.74	0.25	0.15	0.87
		VSS	4.09	0.08	0.06	0.95	1.36	0.32
		FSS	3.87	0.09	8.49	**0.017**	2.02	0.21
Malibu VLX Wakesetter	C1	TSS	15.67	**0.004**	2.71	0.14	4.88	**0.048**
		VSS	18.75	**0.003**	0.46	0.65	3.58	0.09
		FSS	0.91	0.36	0.70	0.53	1.81	0.23
	C2	TSS	10.57	**0.011**	18.20	**0.004**	3.44	0.11
		VSS	0.01	0.92	1.03	0.40	0.74	0.51
		FSS	16.15	**0.003**	15.24	**0.005**	5.48	**0.045**

7.2.1.3 Total phosphorous

All samples collected and analyzed for total phosphorus came back as below the RAL reporting level of 0.05 mg/L, therefore no additional analysis was performed. These are typical total phosphorus values in Maxwell Bay and North Arm Bay, although much higher levels of total phosphorus have been reported. Historical total phosphorus data from September and October from Lake Minnetonka - North Arm (n=90; 2001-2018) ranged from 0.006 - 0.74 mg/L with a median value of 0.046 mg/L and from Lake Minnetonka-Maxwell Bay (n = 76; 2001-2016) ranged from 0.021-0.72 mg/L with a median of 0.045 mg/L (MPCA 2024). The water quality standard for

aquatic life and recreational use in the North Central Hardwood Forest Ecoregion in MN for total phosphorus is 0.04 mg/L, so even samples below the RAL reporting level could have levels of total phosphorus that indicate impairment.

7.2.1.4 Turbidity

At the 9 ft depth, there was a statistically significant overall increase in median turbidity (over a nine-minute window) between pre- and post-boat passes for both wakeboats during both test conditions (Figure 63). However, the turbidity difference between pre- and post- boat passes was small for planing (Condition 1; <1 FNU) compared to semi-displacement (Condition 2; ~3 FNU). There was also an increase of ~2 FNU at the 14 ft depth site for both wakeboats for semi-displacement mode (Condition 2), but this difference was only statistically significant for the Nautique G23 Paragon. There were no statistically significant ($\alpha = 0.05$) differences in turbidity between pre- and post- boat passes for the Sea Ray SPX190 for either location or condition. Valbuena et al. (2024) measured turbidity increases with boat passage of ~7 NTU in an 8.2 ft deep portion of Lake Tahoe. However, they were able to record turbidity at a much faster rate (1 Hz) and thus were able to more fully see the impact of a single boat pass. At one sample per minute (as in this study), we may have missed the maximum peak following a boat pass. In Valbuena et al. (2024), the maximum turbidity spikes following a single boat passage were on the order of 10-20 seconds in duration.

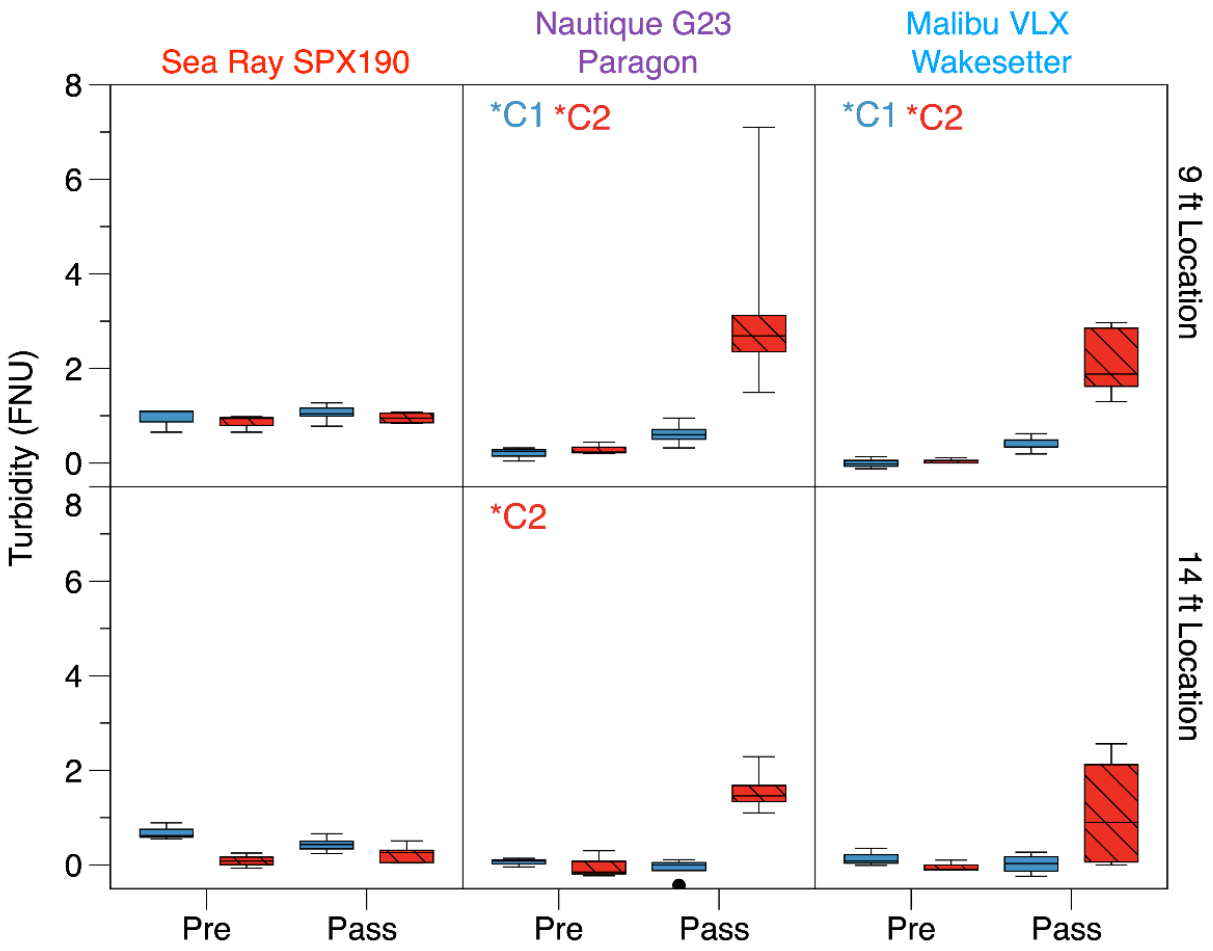

Figure 63. Boxplots (five-number summary) of the median turbidity over three 9-minute windows before boat passes (Pre) and immediately after each of the five boat passes (Pass) in Maxwell Bay in 2023. * notes a statistically significant difference for Condition 1 (C1) or Condition 2 (C2).

To compare the full distribution of turbidity measurements in pre- and post-boat pass time periods, we constructed cumulative probability plots for each boat and operating condition. These plots summarize the distribution of turbidity for each boat and condition over the time period that encompasses all five passes compared to the time period before boat passes. Specifically for semi-displacement mode (Condition 2), there is a shift toward more frequent higher turbidity measurements for both wakeboats in 2023 (Figure 64). These results may be conservative because the timeseries were filtered prior to analysis but still indicate that there are more frequent high turbidity measurements in the period post- boat passage at both 9 and 14 ft depths. This phenomenon is not visible for the Sea Ray SPX190 for any depth or operating condition.

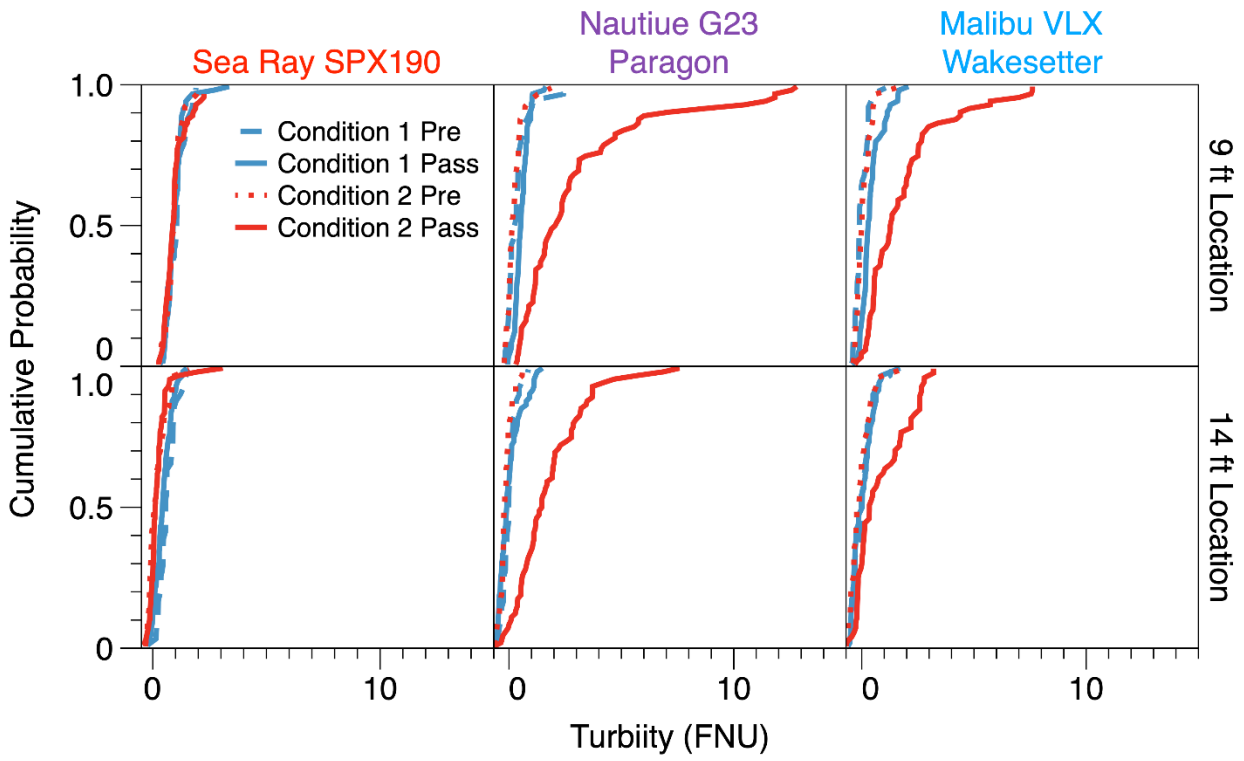

Figure 64. Cumulative probability plots of turbidity by boat and operating condition for Maxwell Bay, 2023. Blue is planing mode (Condition 1) and red is displacement mode for the Sea Ray SPX190 and semi-displacement for the wakeboats (Condition 2). Dashed lines are the pre-boat passage and solid lines are the post-boat passage.

7.2.2 Underwater videos

During the 2023 field campaign, four waterproof cameras captured underwater video at the sensor pads during boat testing (Sections 5.3.3 and 6.6). Videos of the first pass for each condition were created and can be downloaded at the University of Minnesota's digital conservancy/data repository (https://doi.org/10.13020/r7w9-dp20). Figures 65 - 68 are screenshots taken from the underwater videos of the wakeboats during semi-displacement mode (Condition 2) testing. The time of the boat pass is shown in the top corner of each camera view.

7.2.2.1 Condition 1 (planing mode) observations

- For all boats at the 9 ft depth, there was slight but distinct disturbance to the water and lakebed sediment that lasted <10 seconds and coincided with the bow and stern pressure waves. The sediment that did move appears to be decaying organic matter (detritus). There was no sediment resuspension or exhaust bubbles observed for any of the boats.

- For all boats at the 14 ft depth, there was again brief (<10 seconds) movement of water and sediment (detritus) that coincided with the bow and stern pressure waves. There was no sediment resuspension or exhaust bubbles observed for any of the boats. The detritus at this location appears to have been further along in the decay process and therefore less dense than the detritus at the 9 ft depth.

7.2.2.2 Condition 2 (displacement or semi-displacement mode) observations

- Due to loss of battery, we were not able to capture video of the Starcraft Limited 2000 during this condition.
- At both 9 and 14 ft depths, the Sea Ray SPX190 created minimal water and sediment (detritus) movement that lasted <10 seconds. Again, movement coincided with the bow and stern pressure waves. There was no resuspension of sediment or exhaust bubbles observed.
- For the Nautique G23 Paragon and Malibu VLX Wakesetter, there was significant water movement, disturbance to the lakebed, and resuspension of sediment at both 9 and 14 ft depths.
    - At the 9 ft depth (Figures 65 and 66), the flow velocities were high enough to resuspend and entrain sediments, detritus, shells, and vegetation. Some of the vegetation being carried by the currents was alive, as indicated by its vibrant green color. Vegetation fragments and root systems are seen, indicating shearing and complete uprooting. The duration of the resuspension and entrainment lasted over 15 minutes as material was still observed in the water column when the next pass occurred 15 minutes later.
    - Exhaust bubbles were observed at the 9 ft depth, but not at the 14 ft depth for both wakeboats. This is consistent with the ADCP echogram bubble extent results (Section 7.1.1).
    - At the 14 ft depth (Figures 67 and 68), the resuspended and entrained sediment (detritus) resettled after approximately 8 minutes for the Nautique G23 Paragon and 5 minutes for Malibu VLX Wakesetter. This is consistent with the ADCP echogram suspended sediment extent results (Section 7.1.2). It is evident that the

sediment that initially resuspended in the fixed frame of view was carried away by the flows, and the sediment that eventually deposited in the frame of view originated from another location.

- The connection between the bow and stern pressure waves, transverse waves, and propeller wash are particularly evident in these two videos. The generated velocities produced by the bow and stern pressure waves were short in duration but large enough to initiate movement of the lakebed material. The longer duration velocities and currents of the transverse waves and propeller wash that followed were large enough to suspend and entrain the disturbed sediments into the water column.

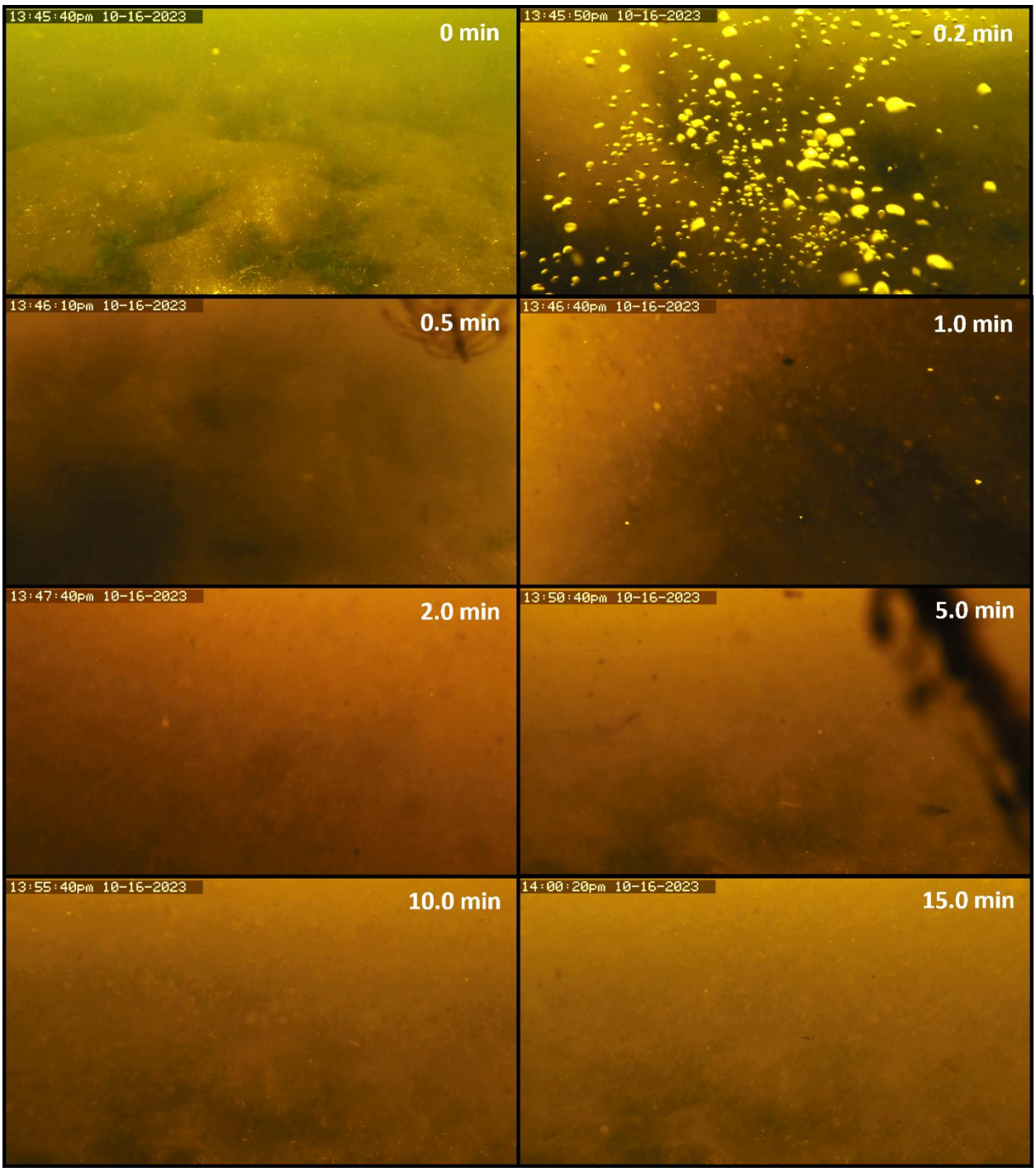

Figure 65. Screenshots taken from underwater video at 9 ft (ADV) during pass 1 of semi-displacement mode (Condition 2) testing of the Nautique G23 Paragon. The upper right image (0.2 min) verifies the presence of exhaust bubbles within the flow.

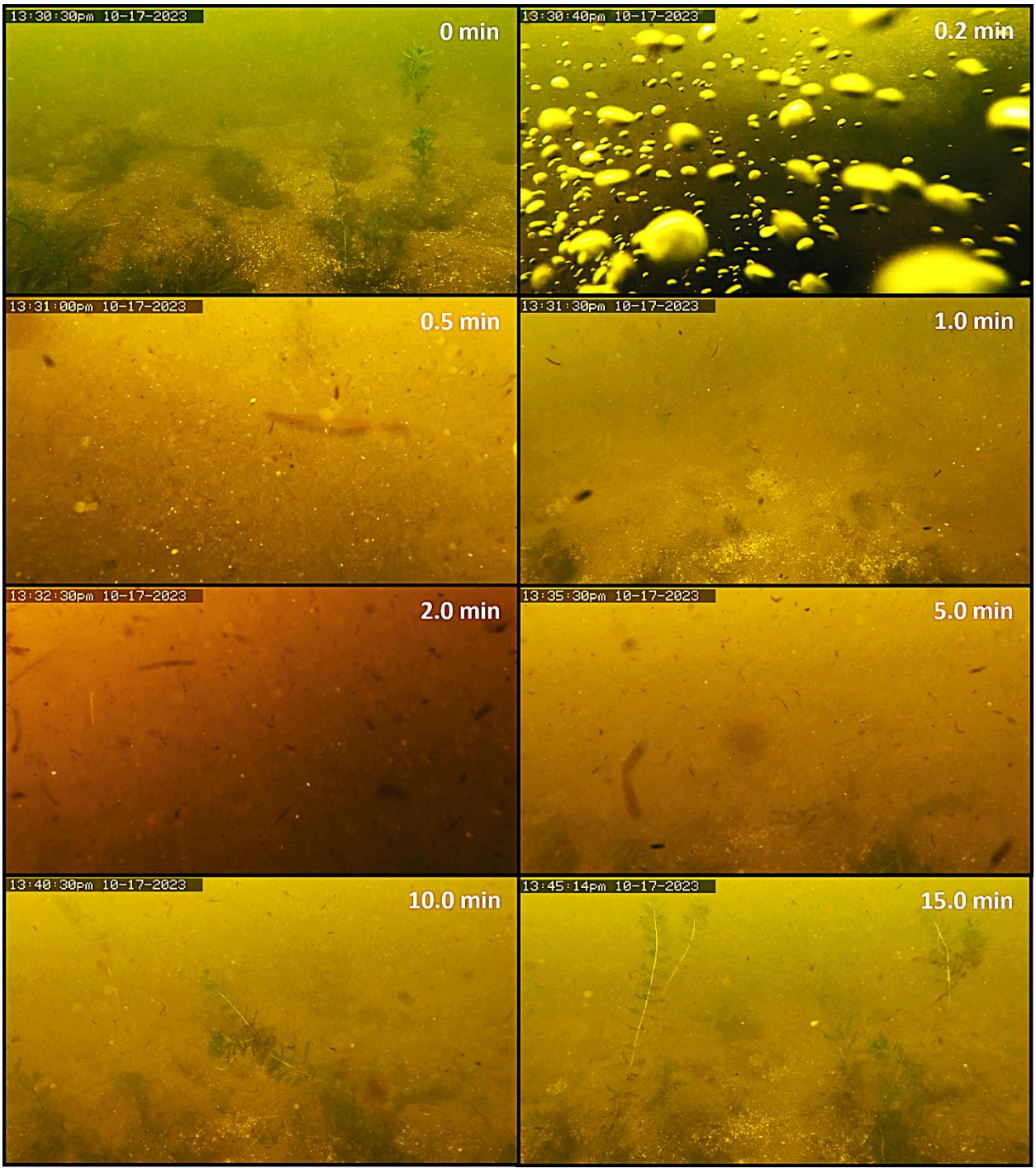

Figure 66. Screenshots taken from underwater video at 9 ft (ADV) during pass 1 of semi-displacement mode (Condition 2) testing of the Malibu VLX Wakesetter. The upper right image (0.2 min) verifies the presence of exhaust bubbles within the flow.

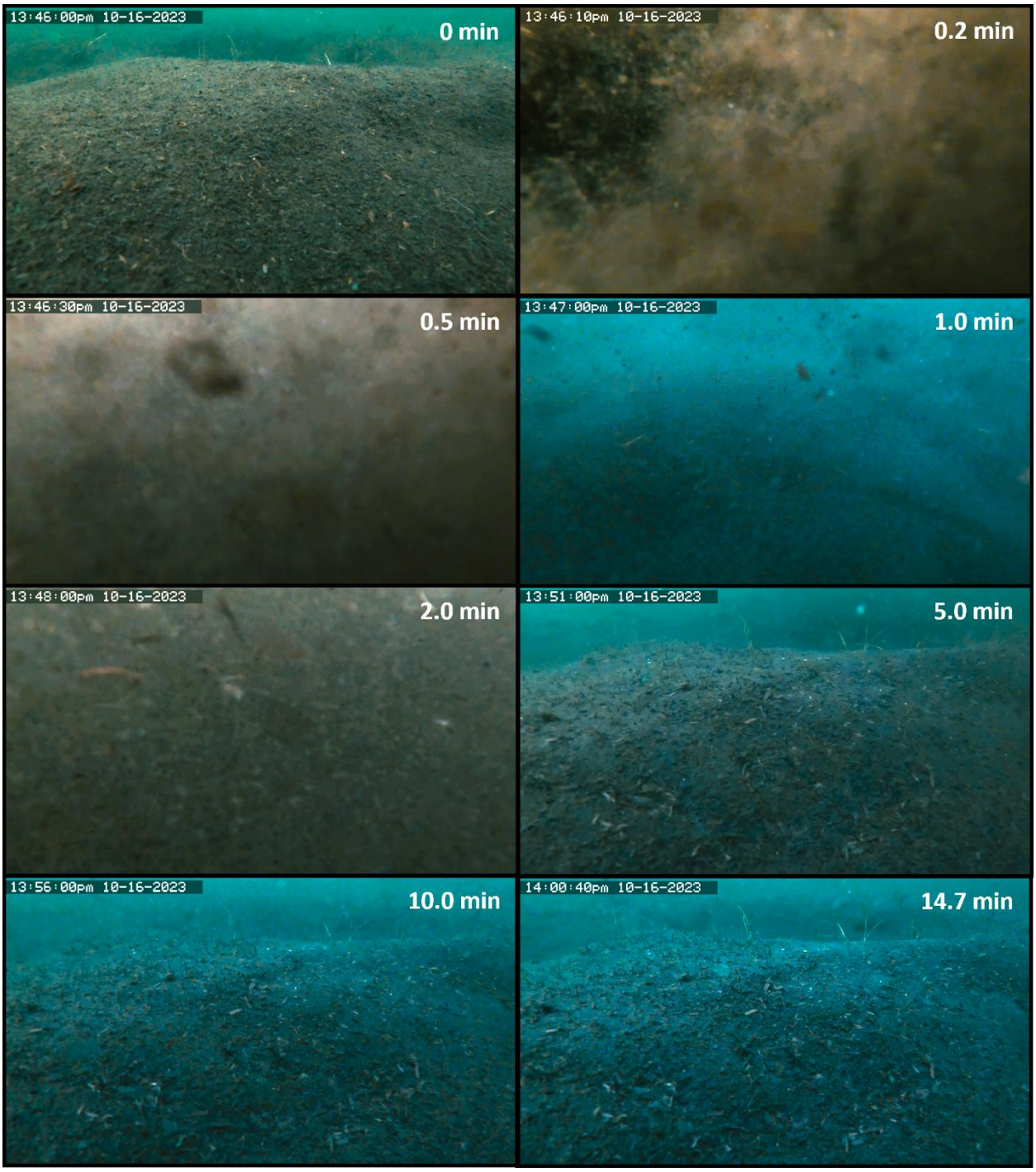

Figure 67. Screenshots taken from underwater video at 14 ft (ADCP) during pass 1 of semi-displacement mode (Condition 2) testing of the Nautique G23 Paragon.

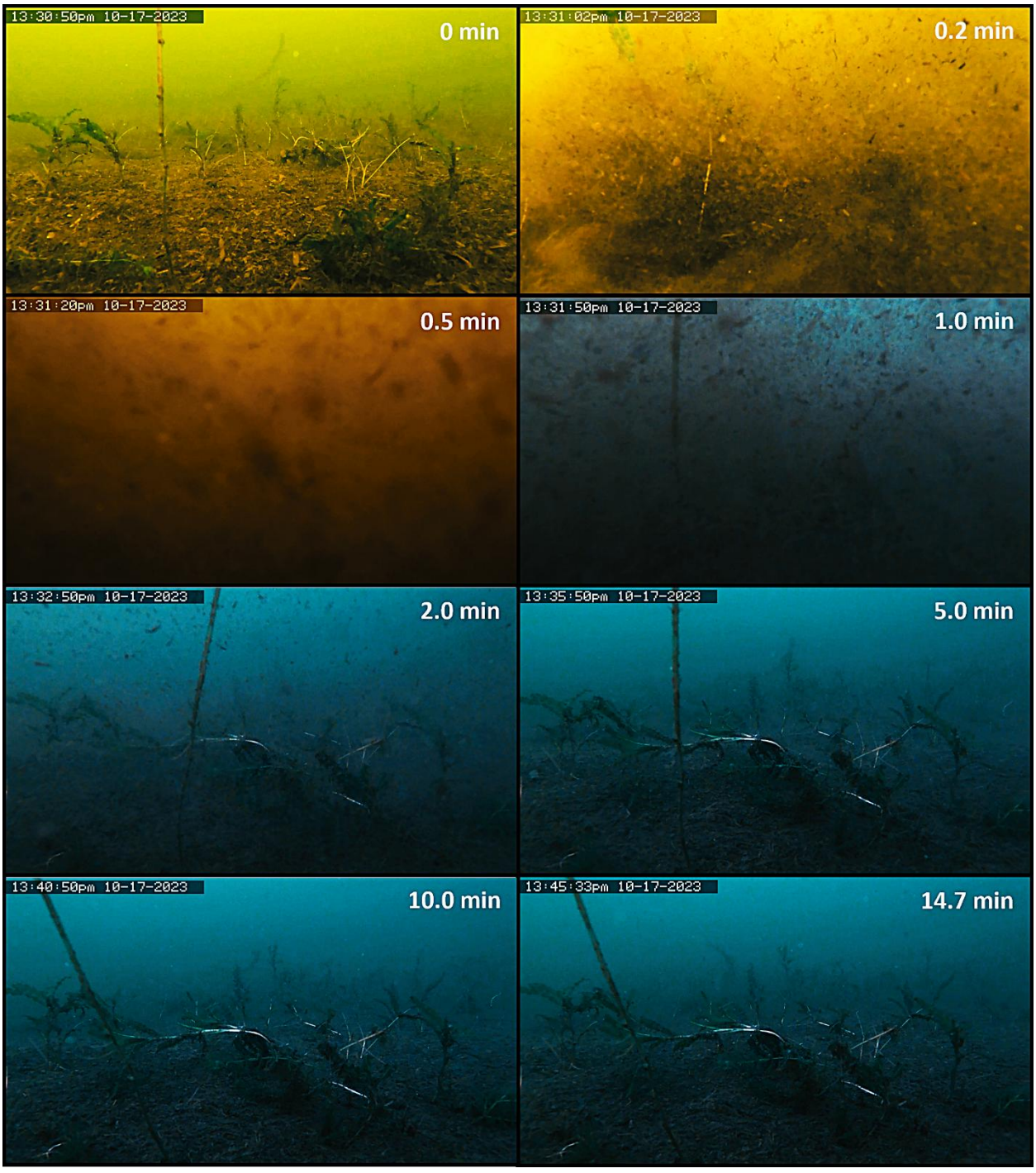

Figure 68. Screenshots taken from underwater video at 14 ft (ADCP) during pass 1 of semi-displacement mode (Condition 2) testing of the Malibu VLX Wakesetter.

7.2.3 Aerial videos

A drone was used in the 2023 field campaign to capture aerial footage during testing (Section 5.9 and 6.6). When possible, videos for each boat and test condition were created and can be downloaded at the University of Minnesota's digital conservancy/data repository (https://doi.org/10.13020/r7w9-dp20).

7.2.3.1 Condition 1 (planing mode) observations

Due to technical difficulties with the drone, we were not able to capture videos of the Starcraft Limited 2000, Sea Ray SPX190, or Nautique G23 Paragon in planing mode. The Malibu VLX Wakesetter video shows no evidence of sediment resuspension, which is consistent with the underwater video observations (Section 7.2.2.1).

7.2.3.2 Condition 2 (displacement or semi-displacement mode) observations

The videos show no sediment resuspension for the Starcraft Limited 2000 or Sea Ray SPX190. The videos of the Nautique G23 Paragon and Malibu VLX Wakesetter show significant sediment resuspension, with both boats displaying similar trends. The bathymetry at this test site has an approximate slope of 1.4%, with the water depth increasing from 9 ft to 14 ft in the direction of boat travel. For both wakeboats, the sediment plume becomes visible within 30 seconds of passing through the first set of buoys at the 9 ft water depth. For the Malibu VLX Waketter, there is also sediment resuspension clearly visible after 1.5 minutes at depths between 10 and 11 ft (Figure 69). Due to the raw video of the first pass being cut short for the Nautique G23 Paragon, we were not able to assess the sediment resuspension in relation to water depth. The next time video was captured was just before the second pass 15 minutes later, and by this time the extent of the sediment plume had increased (Figure 70). There was no observable sediment resuspension at the 14 ft site for either boat in the aerial videos; however, the underwater videos (Section 7.2.2.2) and ADCP echogram data (Section 7.1.2) do show resuspension at this depth. Furthermore, the depth that the drone camera can see into the water column is influenced by the transparency of the water, with better transparency allowing for deeper observations. The fall water transparency in Maxwell Bay has historically been 7-10 ft (UMN-LakeBrowser), so in the absence of additional data sets (e.g., echogram, underwater video, etc.), it was not possible

to determine if sediment resuspension occurred at depths deeper than the water transparency with the drone.

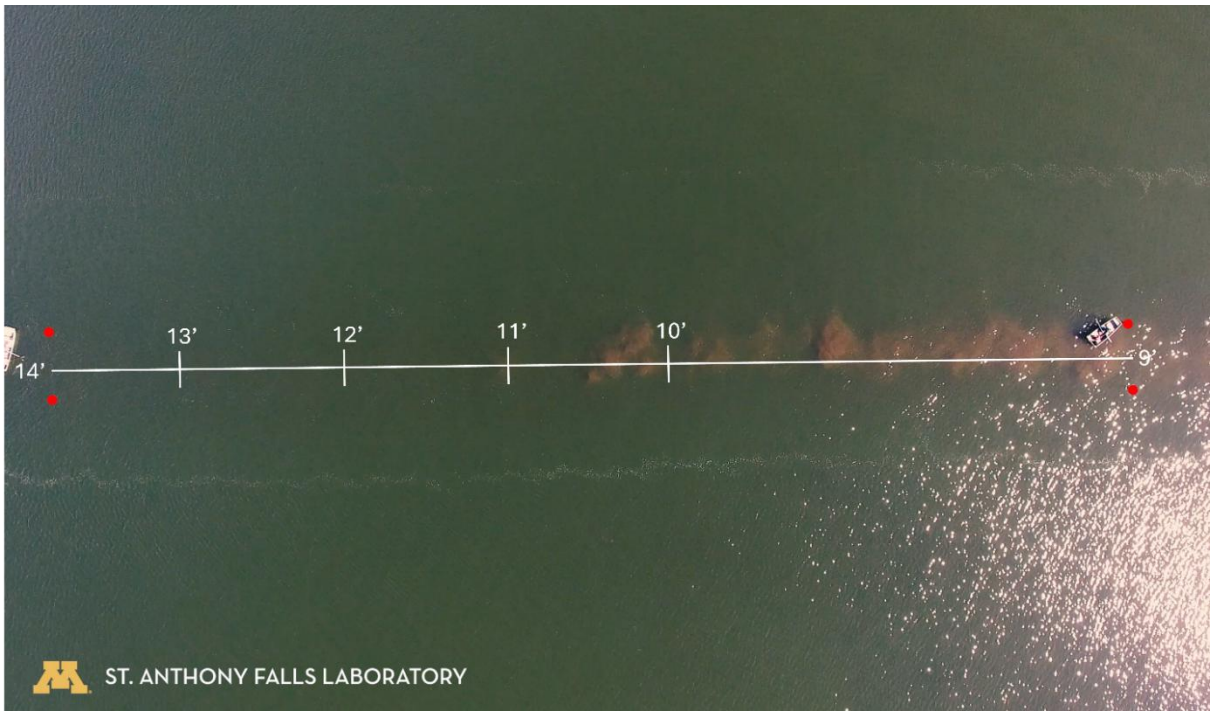

Figure 69. Drone screenshot taken 1.5 minutes after the first pass of the Malibu VLX Wakesetter during semi-displacement mode (Condition 2) testing. The sediment resuspension plume is visible at water depths of 10-11 ft.

Figure 70. Drone screenshot 15 minutes after the first pass of the Nautique G23 Paragon during semi-displacement mode (Condition 2) testing showing the extent of the resuspended sediment plume.

The resuspended sediment plume drifted and expanded with time and each subsequent pass. The increase in plume size is attributable to the following: additional sediment resuspension with each subsequent pass, the time between each pass being too short to allow the resuspended sediment to settle, and baseline currents within the lake.

To provide visual context and a sense of plume scale, a drone screenshot was taken approximately one hour after the first pass of the Malibu VLX Wakesetter (Figure 71). The straight-line distance between the ADV pad at 9 ft and the ADCP pad at 14 ft was 350 ft.

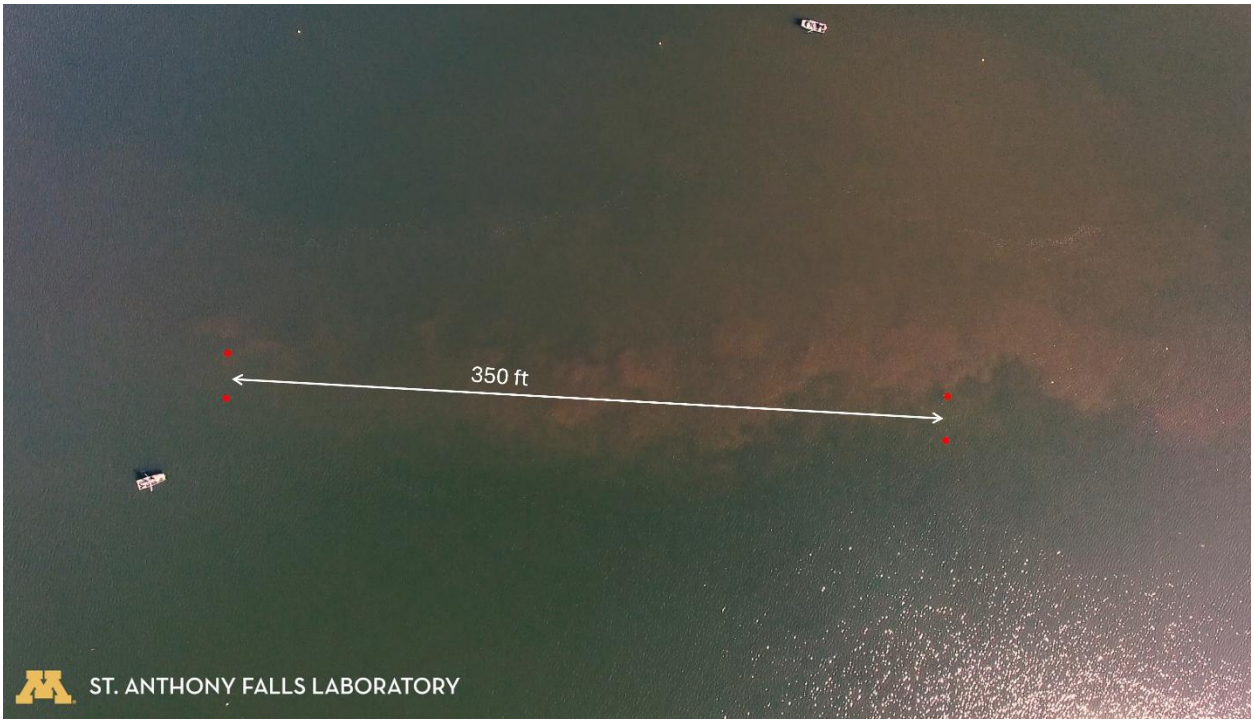

Figure 71. Drone screenshot captured approximately one hour after the first pass of the Malibu VLX Wakesetter under semi-displacement mode (Condition 2). The distance between sensor pads (red buoy goals posts) is 350 ft and provides a visual scale of the plume size.

7.2.4 Sediment characteristics

Lakebed sediment was sampled and characterized at each measurement location (Table 13, Section 6.7). The deeper ADCP sites (27 and 14 ft) were characterized as a fine muck with >20% organic matter, while the shallower ADV sites (16 and 9 ft) were characterized as a sand/gravel mix with less than 0.5% organic matter. The shallow sites had >1100 mg/kg total P compared to

approximately 300 mg/kg in the deep sites; however, the deeper sites had >13 mg/kg extractable P compared to 3-4 mg/kg in the shallow sites. As the impacts on nutrient and sediment resuspension by boats are a function not only of the water depth, but also the local sediment characteristics, these data provide context for the potential for sediment and nutrient resuspension. Due to the sampling method used (Section 5.8.4), the sediment characterization reported here is likely an underestimate of the amount of organic matter at the lakebed (e.g., detritus). Detritus is decaying organic matter that can be at various stages of decay with a broad range of particle sizes, shapes, and densities.

Table 13. Lakebed sediment characteristics at each measurement location. LOI OM is loss on ignition organic matter, Bray P is a measure of extractable phosphorus, and total P is the total phosphorus content.

			Grain Size (mm)			LOI OM (%)		Bray P (mg/kg)		Total P (mg/kg)	
Year	Site (Depth)	Texture	D_{10}	D_{50}	D_{90}	Mean	SD	Mean	SD	Mean	SD
2022	16	Sand Gravel	0.20	0.84	3.0	0.30	0.00	18.7	1.2	363	85
2022	27	Muck	N/A	N/A	N/A	20.1	0.10	4.0	1.0	1105	37
2023	9	Gravely Sand	0.15	0.37	2.1	0.40	0.00	13.7	0.60	297	72
2023	14	Muck	N/A	N/A	N/A	24.5	0.30	3.0	0.00	1408	78

8.0 DISCUSSION

8.1 Summary of hydrodynamic phenomena produced by recreational boats

The results presented here identify three distinct hydrodynamic phenomena produced by common recreational powerboats that have the potential to affect the water column and lakebed: 1) bow and stern pressure waves, 2) transverse gravity waves, and 3) propeller wash. Two instruments used in the testing collected data on water velocities produced by these three hydrodynamic phenomena - the ADV measured near-bottom horizontal velocities, and the ADCP measured the horizontal and vertical velocity profiles in the water column. The associated resuspension of lake sediment was quantified by a total of six different measurements: water samples, turbidity sondes, the ADV signal strength, the ADCP backscatter, the underwater videos, and aerial drone videos. Taken individually, each information source has limitations, but taken together, there are multiple lines of evidence that wakeboats operating in semi-displacement

mode (i.e., surfing) are capable of resuspending sediment in water depths that are greater than non-wakeboats and wakeboats operating in displacement or planing mode.

8.1.1 Bow and stern pressure waves

We document and measure the short-duration pressure waves associated with the bow and stern of a boat in motion. Although these pressure waves are only present at a fixed location for few seconds, they can penetrate deep into the water column. The hull of a boat in transit pushes water forward and down generating a bow wave. Immediately behind the boat water moves backward and up as it rebounds to fill the volume of water displaced by the hull, termed the stern wave. Because the boat hull is the source of these pressure waves, the water velocities are greatest near the surface and decrease non-linearly with water depth.

While measurements were made at fixed locations in this study, it's important to understand that the bow and stern waves move with the boat. The bow and stern waves induce velocity and pressure fluctuations directly under the boat, which is the source of divergent waves and, if present, transverse waves.

8.1.2 Transverse gravity waves

Operating a boat in displacement or semi-displacement produces transverse gravity waves behind the stern that travel in the same direction and approximate speed as the boat. Transverse waves produce orbital velocities that are largest at the water surface and decrease non-linearly with water depth. Like the bow and stern waves, the transverse waves can penetrate deep into the water column and interact with the lakebed. The velocity amplitude of transverse waves decreases with time but persist for several minutes after the boat has passed.

8.1.3 Propeller wash

Propeller wash is defined in this report as the thrust created by the rotating blades of a powerboat propeller, which accelerates water astern, forming a turbulent jet-like flow. Propeller wash is a highly complex, 3-dimensional phenomena that proved to be challenging to measure and quantify. Near the stern, the propeller wash originates as a highly turbulent, rotational jet, that is projected into the water column at an angle oblique to the water surface. Jets are a well-

studied fluid phenomenon; however, two additional conditions make the propeller wash of a recreational boat particularly challenging:

1) Engine exhaust bubbles – for the boats studied here and most modern recreational boats in use today, exhaust gases are vented directly into the propeller wash via vents/manifolds and carried along in the turbulent flows. Because the bubbles are gas-filled and compressible, they help dissipate the energy within the propeller wash (Chanson, 1996). Bubbles are also buoyant and, because they become distributed throughout the wash, they give buoyancy to the propeller wash, causing an upwelling effect in the water column.

2) Crossflow effects – The propeller wash jet is moving with the boat and the impact of this is vastly different than if the jet were stationary. This situation is analogous to a stationary vertical smokestack where wind flows horizontally across the top of the stack (Figure 72a). Figure 72 also shows several examples of crossflow from other applications.

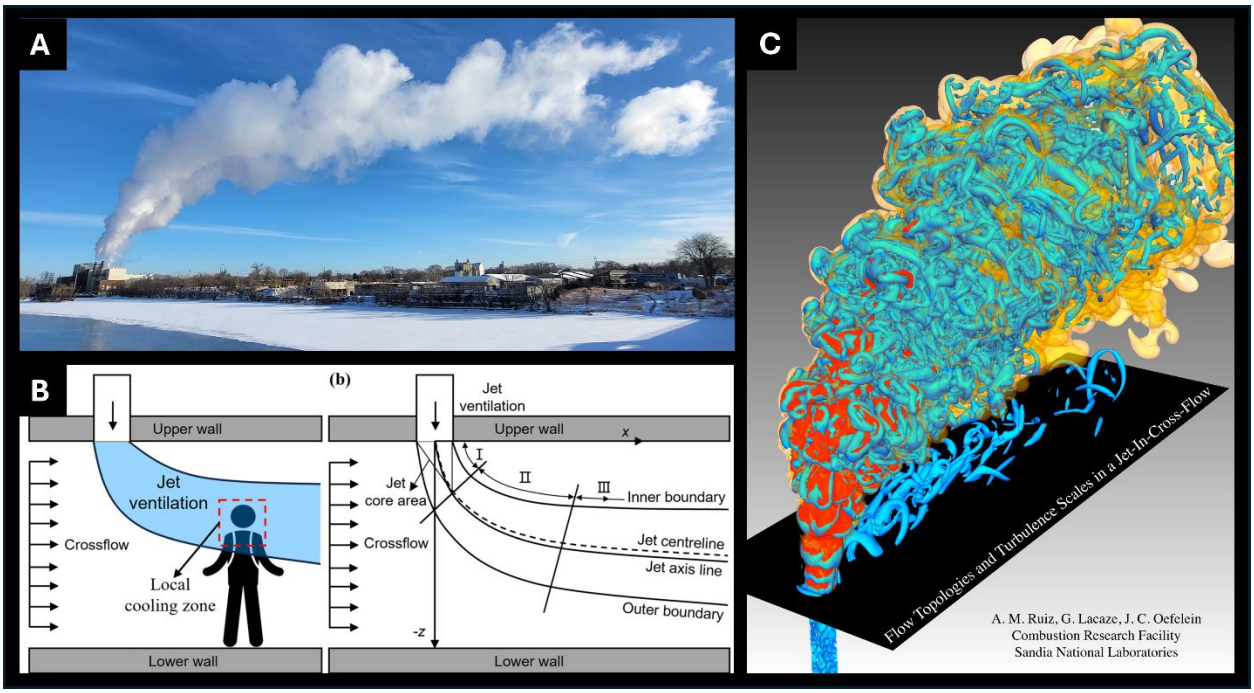

Figure 72. A) Water vapor emitted from a vertical stack that is met with a horizontal crossflow of wind. B) An example of a HVAC ventilation jet (air) and crossflow within confined mine spaces (Wang et al. 2024). C) A numerical simulation of a fluid jet within a crossflow (Ruiz et al. 2014).

For a recreational boat, the source creating the propeller wash jet (i.e., rotating propeller) is moving within stationary or quiescent water, resulting in the flow bending in the direction opposite of the boat's direction of travel. We simulated this crossflow effect in a laboratory flume to visualize this process (Figure 73). No quantifiable measurements were taken. To replicate a boat in motion, a shaft and propeller were attached to a motor which was secured to a carriage that moved down a flume of quiescent water at varying speeds. To show the propeller wash, minus exhaust bubbles, pink clay was fed down the shaft and through the propeller blades. When in motion, it was clear there was a crossflow effect that limited the penetration depth of the propeller wash (pink dotted line); however, when stationary, like a fixed jet in quiescent water, there were no crossflow effects observed, and the propeller wash followed the trajectory of the shaft angle (red dashed line). Another significant observation was that at faster simulated speeds (e.g., planing mode- Condition 1) the crossflow effect became more apparent, where the pink clay tracer did not penetrate the quiescent water as deeply as compared to when slower speeds were simulated (e.g., displacement or semi-displacement- Condition 2).

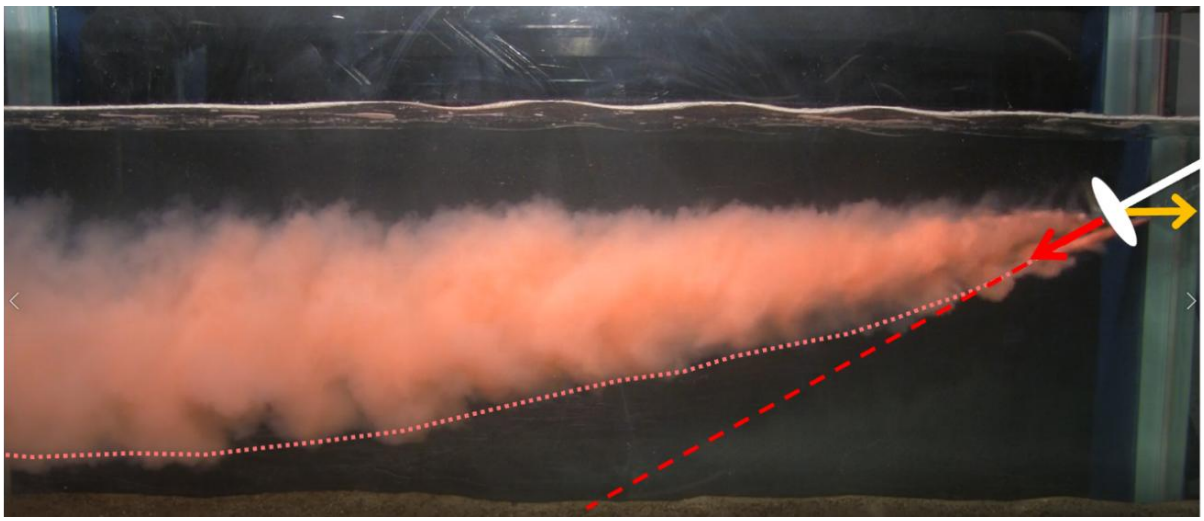

Figure 73. Image from a visual demonstration conducted at St. Anthony Falls Lab, showing a moving propeller wash jet (pink plume) through a quiescent tank of water. The jet bends in the direction opposite of boat travel (pink dotted line). The yellow vector notes the direction of travel. The position of the propeller and shaft angle is shown in white. The red arrow and dashed line indicate the alignment of the shaft and direction of the propeller wash jet when stationary.

Ray (2020) modelled boat propeller wash by simulating a stationary, non-buoyant jet penetrating a quiescent fluid. This approach is oversimplified as it does not consider the effects of the buoyant

exhaust bubbles or crossflow, resulting in an overprediction of the penetration depth of the propeller wash (i.e., 33 ft). Fay et al. (2022) performed CFD simulations of a stationary boat with a crossflow and was able to capture the crossflow effect of the jet. The reliability of the simulations, however, is uncertain because no validation information was provided in the article and modeled water velocities below 2 ft/s were omitted from the figure (see Section 3.1 for more details).

8.1.4 Integrating the hydrodynamic phenomena

Figure 74 illustrates the three phenomena at the full spatial scale of the impacts at a moment in time. (1) Bow and stern pressure waves are brief yet have the potential to generate substantial velocities that can initiate the motion of bottom sediments. (2) Transverse waves form behind the boat and dissipate in amplitude with time/distance from the boat. Our data shows transverse waves produce orbital motions that extend well into the water column and persist for 60-90 seconds when operating in Condition 2. (3) The turbulent propeller wash is projected downward into the water column and the crossflow effect caused by the moving boat bends the jet in the opposite direction of boat travel, limiting the depth of penetration. Propeller wash velocities dissipate as the area impacted by the propeller wash expands. Buoyancy from the dispersed exhaust bubbles within the propeller wash create an upwelling effect that brings the wash toward the water surface. Regardless of boat or condition, our data shows the bubbles persisted in the water column for approximately 150 seconds (Section 7.1.1, Figures 32 and 33), except for the Cruisers Yachts GLS34 during displacement mode (Condition 2) when the bubbles persisted for nearly 225 seconds.

Using the speeds of the boats during Condition 2 testing, we provide a rough estimate of the moving spatial window associated with the propeller wash bubbles. Because the bubbles persisted at a fixed position (i.e., ADCP) for 150 seconds and the wakeboats were driven at 11.6 mph (17 ft/s), this equates to a total bubble impact length of ~2550 ft (850 yds). For the non-wakeboats the boat speeds were ~8 mph (11.7 ft/s), which results in a bubble impact length of ~1400 ft (470 yds).

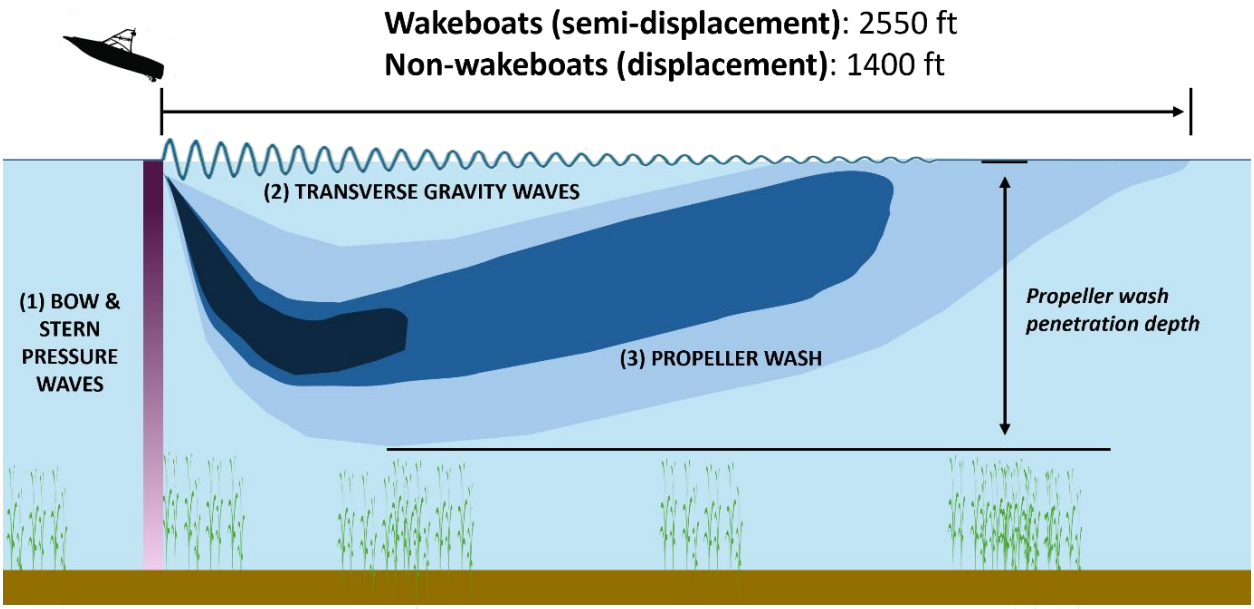

Figure 74. Illustration showing the full spatial extent of hydrodynamic phenomena formed during Condition 2 testing, which was displacement mode for the non-wakeboats and semi-displacement mode for wakeboats.

8.2 Summary of environmental impacts by recreational powerboats

8.2.1 Sediment – resuspension and entrainment within the water column

The various data and visual observations of this study provide insight into the hydrodynamic processes leading to the resuspension of sediment in the water column. Velocities generated by the bow and stern pressure waves are short-lived with a single forward and backward motion. Even for non-wakeboats in displacement mode (Condition 2), these forces are enough to move detritus and cause vegetation to sway. Higher bow/stern pressure velocities from heavier boats, mode of operation (e.g., speed and hull pitch), and shallower water depths, result in greater potential for bottom sediment disruption.

Bow and stern pressure waves of the recreational boats tested, however, were not sufficient to cause sustained sediment resuspension at the depths studied here. We observe that both the orbital transverse waves and turbulent propeller wash are the mechanisms that resuspend, entrain, and transport sediment. If the propeller wash penetrates to the lakebed, like it did in 2023 at the 9 ft location during semi-displacement (Condition 2) testing of the wakeboats, it can directly cause sediment scour and resuspension, as well as vegetation shearing and complete

uprooting. The work presented here shows that wakeboats in semi-displacement mode (surfing) produce all three phenomena at greater magnitudes than the test boats in planing mode and the non-wakeboats in displacement mode. Thus, they have the highest potential for resuspension and entrainment of sediment, especially if the activity is consistently carried out in the same location, which is supported by our data (i.e., 5 repeated passes) and Yousef (1978).

Repeat boat passage had a significant effect on concentrations of suspended solids for some boat operating conditions in water depths 14 ft or less (2023 measurements); however, there were no consistent effects of boat passage on total suspended solids (TSS), organic solids (VSS), or inorganic solids (FSS) concentrations in depths 16 ft and greater (2022 measurements). Both wakeboats during semi-displacement (Condition 2) showed an increase in inorganic suspended solids (FSS) concentrations between pre-boat pass and post-boat pass samples and, for the Malibu VLX Wakesetter, this was also true for total suspended solids concentrations (TSS).

There was an increase in background turbidity of 2-3 FNU between pre- and post-boat passes at the 9 ft and 14 ft depths for both wakeboats for semi-displacement mode (Condition 2). The differences were only statistically significant for the Nautique G23 Paragon. The 2022 and 2023 sampling campaigns, along with underwater video footage, indicate that the plume of suspended solids after boat passage is highly variable spatially and temporally, as evidenced by both the variation in suspended solids concentrations collected simultaneously at the same depth and within 6 inches laterally, and the temporal variation of turbidity measurements. This variability may obscure actual impacts of boat passage on suspended sediment concentrations from single boat passes. Multiple boat passes are expected to have a cumulative impact during heavy traffic periods (Bilkovic et al. 2019).

8.2.2 Consideration of aquatic vegetation and vertical impacts of recreation boats

There is a broad variety of aquatic vegetation found in lakes. For rooted vegetation, the height the plant extends above the lakebed will depend on species, time of year, and environmental parameters like lakebed composition, water clarity, lake depth and local climate.

This study documents the depth of penetration for various hydrodynamic phenomena reference from the water surface. The depth to the top of aquatic vegetation is also an important

consideration, but it was not directly studied here. Bow and stern waves, transverse waves, and propeller wash can all interact with aquatic vegetation, causing the vegetation to be pushed, pulled, twisted and lifted from the generated velocities within the water column. If the forces are great enough, damage can occur to the vegetation including stripping of leaves, breaking of stems, or even uprooting.

The underwater videos recorded at both the ADV and ADCP sites in 2023 document damage to vegetation, specifically from the wakeboats in semi-displacement (surfing) mode (https://doi.org/10.13020/r7w9-dp20). These sites were not heavily vegetated at the time of the study, but we observed damage to the sparse aquatic vegetation including stem stripping and breaking as well as uprooting. The relative contributions of the bow/stern waves, transverse waves, and propeller wash to plant damage is an area for future study.

8.3 Guidance for depth of operation to limit impacts on the lake environment

This study generated a wealth of data quantifying the hydrodynamic phenomena affecting the water column beneath various recreational boats in motion. Data from two field seasons, seven boats, four study sites, and multiple sensor systems including underwater and aerial video, provide the information needed to inform science-based guidance on the minimum operational depth that recreational powerboats, under typical modes of operation, should maintain to minimize impacts to the lakebed. For practical reasons, operating depth recommendations are considered in 5 ft depth increments measured from the water surface (i.e., 5, 10, 15, 20 ft, etc.).

8.3.1 Condition 1 (planing mode) – synthesis of results

The boat speeds during planing mode ranged between 21 and 25 mph. The maximum exhaust bubble depths were less than 10 ft for all boats. The ADCP results show estimated threshold depths for bow and stern pressure waves- the water depths at which the pressure wave velocities decrease to levels that no longer exceed the critical velocity for disturbance and potential resuspension of coarse silts (0.3 ft/s). This threshold depth was 9.5 ft or less for all boats, except the Cruisers Yachts 34GLS, which required a depth of 13 ft. The Cruisers Yachts 34GLS was by far the largest boat tested, weighing over 14,500 lb, having an overall length and width of about 36 and 12 ft, respectively, and powered by two 380-horsepower engines. The size of this boat is

uncommon on most Minnesota inland lakes. At the 2022 ADV site where the water depth was 16 ft, the measured bow and stern velocities were less than 0.2 ft/s for all boats, except the Cruisers Yachts 34GLS bow wave (0.32 ft/s). In 2023, the ADV bow and stern velocities at the 9 ft site were less than 0.25 ft/s for all boats. Underwater video from 2023 testing shows the bow and stern pressure waves of all boats causing brief but distinct disturbance to decaying organic matter (detritus) on the lakebed at both the 9 ft and 14 ft depth sites.

While propeller wash velocities were likely very high within the initial moments of the propeller wash jet for all boats in planing mode, the ADCP and ADV propeller wash velocities outside this intense region were minimal or not measurable. The ADCP propeller wash velocities were near zero at depths ≥10 ft in 2022, and depths ≥8 ft in 2023. The ADV propeller wash velocities were too small to measure in both 2022 (16 ft) and 2023 (9 ft).

The water samples were highly variable and show no clear evidence of increased suspended solids for either year. In 2023, there was a minimal increase in turbidity at the 9 ft depth for the wakeboats during this condition; however, the increase was minimal (<1 FNU change). Finally, the ADCP echograms show no evidence of sediment resuspension either year.

Key takeaways to establish guidance on operating depth for planing mode are:

- The maximum penetration depths of the exhaust bubbles were <10 ft.
- Some of the bow and stern pressure wave velocities were large enough to disturb lower density sediments (e.g., detritus, silt) at depths >10 ft; however, the absence of transverse waves and minimal propeller wash velocities at depths ≥10 ft prevented the sediments from resuspending and entraining in the water column.
- There was no evidence of increased suspended solids that would be a cause for concern.

8.3.1.1 Recommended depth of operation for planing mode

It is recommended that recreational boats, like the ones studied here, operate in 10 ft of water or greater when planing to minimize impacts on the lakebed.

8.3.2 Condition 2 non-wakeboats (displacement mode) - synthesis of results

The boat speeds of the non-wakeboats during displacement mode (Condition 2) ranged between 7 and 9 mph. The maximum bubble depth for the Hurricane SS203 and Starcraft Limited 2000 (deck boats) and the Sea Ray SXP190 (smallest bowrider) was 5-6 ft. The maximum bubble depths for the larger bowriders, Cobalt R5 and Cruisers Yachts 34GLS, was 9 and 10 ft, respectively. One possible explanation for this observation is that these two boats had dual propellers that contra-rotate, which may have sheared the bubbles to a smaller size with less buoyancy force, resulting in deeper penetration of the bubbles.

Near the lakebed (16 ft depth) in 2022, the measured ADV bow wave velocities were relatively small (0.11 – 0.13 ft/s), and the stern wave velocities were quite a bit larger (0.16 – 0.4 ft/s). The same was true at the lakebed (9 ft depth) in 2023, where the measured ADV bow wave velocities were small (<0.1 ft/s) and the stern wave velocities were significantly larger (0.31 – 0.44 ft/s). The stern wave velocities measured by the ADCP were consistently higher than bow wave velocities, thus the threshold depths were deeper for the stern waves. In 2022, the threshold depth for the horizontal stern waves was 13 ft for the Hurricane SS203 and Cobalt R5, and around 10 ft for the vertical direction of the stern waves. The threshold depths for the largest test boat, Cruisers Yachts 34GLS, were 18 ft (horizontal) and 12.5 ft (vertical). Looking closer at the ADCP measured horizontal stern wave velocities through the water column for the Cruisers Yachts 34GLS, Figure 37 shows substantial velocities of around 1.0 ft/s at 10 ft, which decrease to around 0.45 ft/s at 15 ft. In 2023, the threshold depth was 8.5 ft (horizontal) and 6.0 ft (vertical) for the Starcraft Limited 2000, and 10 ft (horizontal) and 6 ft (vertical) for the Sea Ray SPX190.

Transverse waves were produced by the non-wakeboats in displacement mode. At a water depth of 16 ft, the maximum transverse wave velocities at the lakebed measured by the ADV in 2022 were 0.08, 0.05, and 0.07 ft/s for the Hurricane SS203, Cobalt R5, and Cruisers Yachts 34GLS, respectively. In 2023 (9 ft depth), the maximum transverse wave velocity was 0.05 ft/s for the Starcraft Limited 2000 and 0.07 ft/s for the Sea Ray SPX190. For both years, the maximum vertical transverse wave velocities measured by the ADCP were around 0.1 ft/s or less at a water depth of 10 ft.

While propeller wash velocities were likely very high within the initial moments of the propeller wash jet, the measured ADCP and ADV propeller wash velocities outside this intense region were minimal for the non-wakeboats in displacement mode. For both test years, the propeller wash velocities measured by the ADCP were near zero at 10 ft depth. Similarly, propeller wash was not evident from the ADV measurements at both the 16 ft (2022) and 9 ft (2023) water depths.

Even though some of the measured bow and stern pressure wave velocities were quite large (e.g., Cruisers Yatchs 34GLS, Sea Ray SPX190) and enough to briefly disturb the lakebed during this condition, the transverse wave and propeller wash velocities were not large enough to resuspend and entrain bottom sediments. For example, in 2023 near the lakebed (9 ft depth), the Sea Ray SPX190 generated a mean maximum horizontal stern wave velocity of 0.44 ft/s, as measured by the ADV. The underwater video shows that this stern wave velocity caused sediment to briefly (3-8 seconds) move laterally along the bed; however, the transverse wave and propeller wash velocities at this location were minimal (~0.1 ft/s or less), and the sediment did not resuspend. This reinforces the important role that transverse waves and propeller wash play in resuspending, entraining, and transporting lakebed material.

This study did not test the wakeboats in displacement mode. However, like the non-wakeboats, wakeboats also routinely operate in displacement mode. The Malibu VLX Wakesetter is very similar to the Cobalt R5 bowrider when its wake-enhancing technologies are not in use. For example, they both have deep V-shaped planing hulls and the Cobalt R5 and Malibu VLX Wakesetter have similar dry weights of 4,880 and 4,200 lb, respectively. As mentioned above, the Cobalt R5 did not generate hydrodynamic phenomena that were a cause for concern at depths ≥10 ft. Therefore, when operating in displacement mode, there is no reason to suspect that the hydrodynamic phenomena would be any different, whether generated by a wakeboat or non-wakeboat of similar total weights.

Like in planing mode (Condition 1), the water samples in displacement mode (Condition 2) were highly variable and show no clear evidence of increased suspended solids for either year. The ADCP echograms also showed no evidence of sediment resuspension either year. There was no

difference in turbidity between pre- and post- boat passes for the Sea Ray SPX190 at either depth in 2023.

Key takeaways to establishing guidance on operating depth for displacement mode are:

- The maximum penetration depths of the exhaust bubbles were <10 ft.
- The bow and stern pressure wave velocities were large enough to disturb sediments at depths >10 ft; however, the transverse wave and propeller wash velocities were minimal at depths ≥10 ft, which prevented these sediments from being resuspended and entrained in the water column.
- There was no evidence of increased suspended solids or turbidity that would be a cause for concern.

8.3.2.1 Recommended depth of operation for non-wakeboats and wakeboats in displacement mode

It is recommended that recreational boats, like the ones studied here, operate in 10 ft of water or greater when in sustained displacement mode (e.g., slow cruising) to minimize impacts on the lakebed.

For most recreational boat users, traveling in waters less than 10 ft deep is unavoidable. For example, going through channels, getting to and from boat lifts, docks, and launches, etc. In these scenarios it is recommended to go as slow as possible (i.e., slower than the displacement speeds tested here), to minimize the magnitude of the bow and stern pressure waves. Minimizing the potential for initial sediment movement is key to preventing its suspension. It is also recommended, and already a common practice for many, to trim the motor up if possible, when in shallow water to direct the propeller wash jet away from the lakebed.

8.3.3 Condition 2 wakeboats (semi-displacement mode- surfing) – synthesis of results

The boat speed of the wakeboats during semi-displacement mode (Condition 2) was 11.6 mph. During this mode of operation, the ballast tanks were full, yielding a total weight of 9,400 lb for the Nautique G23 Paragon and 7,890 lb for Malibu VLX Wakesetter. The hull pitch of the wakeboats were the highest of all test boats. The hull pitch of the Nautique G23 Paragon was 13.2 and 14.1 degrees in 2022 and 2023, respectively, and 15.2 and 15.7 degrees for Malibu VLX

Wakesetter. This transitional speed and the magnitudes of boat weight and hull pitch, cause maximum hull resistance that creates the large wake waves needed for wakesurfing.

The bubble penetration depth reached 10-12 ft. The bubble depths were confirmed visually with the underwater videos that were captured in 2023, showing exhaust bubbles at the 9 ft ADV location, but not at the 14 ft ADCP location.

In 2022, the ADV at a depth of 16 ft measured maximum horizontal bow velocities of 0.19 ft/s and 0.39 ft/s for the Nautique G23 Paragon and Malibu VLX Wakesetter, respectively. The maximum horizontal stern wave velocities were 0.49 ft/s for the Nautique G23 Paragon and 0.30 ft/s for the Malibu VLX Wakesetter. The velocities were considerably higher at the 2023 ADV site where the water depth was 9 ft. The maximum horizontal velocities for the Nautique G23 Paragon were 0.63 ft/s (bow) and 1.56 ft/s (stern). Similarly, the velocities for the Malibu VLX Wakesetter were 0.53 ft/s (bow) and 1.21 ft/s (stern). The ADCP stern wave velocities through the water column were consistently higher than bow wave velocities, thus the threshold depths are deeper for the stern waves. In 2022, the stern wave threshold depths for the Nautique G23 Paragon were 22.5 ft for horizontal velocities and 15.0 ft for vertical velocities. In the same year, the horizontal velocity data was poor for the Malibu VLX Wakesetter and therefore a depth was not determined; however, the depth for the vertical velocity was 14.5 ft. In 2023, ADCP data was only measured down to 12.5 ft due to the shallower water depth. The horizontal stern wave velocities at 12.5 ft were far greater than the 0.3 ft/s threshold for coarse silt disturbance for both wakeboats, with the velocities being 1.2 ft/s and 0.9 ft/s for the Nautique G23 Paragon and Malibu VLX Wakesetter, respectively. The 2023 underwater videos clearly show the brief, yet intense, bow and stern pressure wave velocities that initiated the motion of lakebed sediment and vegetation at both 9 and 14 ft depths.

The 2022 ADCP data show that the Nautique G23 Paragon generated vertical transverse wave velocities of 0.22 and 0.21 ft/s at 10 and 15 ft depths, respectively. The Malibu VLX Wakesetter generated slightly lower velocities of 0.17 and 0.12 ft/s at 10 and 15 ft depths, respectively. By 20 ft the vertical transverse wave velocities had dropped to <0.1 ft/s for both boats. Because the propeller wash and associated exhaust bubbles were substantial and occupied much of the water

column at the 2023 ADCP site (14 ft depth), quality transverse wave data was not obtained until roughly 25 seconds after the boat had passed, and even then, only the vertical data was usable. The vertical transverse wave velocities for both boats after 25 seconds were around 0.1 ft/s at 8 ft that decreased to near zero at 12 ft, but likely larger velocities were present in the initial moments after the boat pass. At the 16 ft ADV site in 2022, the maximum horizontal transverse wave velocities at the lakebed were 0.18 ft/s and 0.16 ft/s for the Nautique G23 Paragon and Malibu VLX Wakesetter, respectively. At the 9 ft ADV site in 2023, the maximum horizontal transverse wave velocities at the lakebed were 0.46 ft/s for the Nautique G23 Paragon and 0.32 ft/s for the Malibu VLX Wakesetter. At both 2023 depths, the underwater video shows the back-and-forth movement of the orbital transverse waves with suspended lakebed materials entrained within.

The wakeboats had measurable ADV propeller wash velocities at the 9 ft site in 2023. The maximum horizontal propeller wash velocities at the lakebed were 0.98 ft/s and 1.24 ft/s for the Nautique G23 Paragon and Malibu VLX Wakesetter, respectively. For both boats, the average horizontal propeller wash velocities at this location were above 0.1 ft/s for 4-5 minutes. The ADV was not able to measure a propeller wash signal at the 16 ft ADV site in 2022. At the ADCP site in 2023, the vertical propeller wash velocities were measured for both boats that showed upwelling (i.e., water moving towards the water surface). The mean upwelling velocities varied between 0.12 and 0.2 ft/s at 8 ft depth, that decreased to between 0.02 and 0.12 ft/s at 10 ft depth. In 2022, the ADCP also measured vertical propeller wash upwelling velocities for both boats that were between 0.06 ft/s and 0.1 ft/s at 10 ft, and near zero at 15 ft.

It is not possible to discern whether the transverse waves or propeller wash were the main influence of sustained sediment resuspension and entrainment; however, the transverse waves had deeper penetration and larger velocities. Propeller wash velocities were large immediately abaft but quickly decreased at depths below the maximum penetration depth of the jet (Figure 74). Both hydrodynamic phenomena and their impacts on the lakebed were captured in the underwater and aerial videos that were collected in 2023.

The 2023 ADCP echogram data shows resuspension of bottom sediment at a depth of 14 ft for only the wakeboats during this condition. The mean maximum suspension height off the lakebed was 5.7 and 4.3 ft for the Nautique G23 Paragon and Malibu VLX Wakesetter, respectively. The underwater video shows that the resuspended bottom sediment at this location appears to be decaying organic matter (detritus). At the shallower 9 ft depth, the underwater video documents significant disruption to the lakebed. The flow velocities were large enough to resuspend sediment, shells, and vegetation- some of which were sheared and uprooted. The aerial drone videos during 2023 testing show a visible sediment plume develop from 10 to 11 ft water depths, with the plume only increasing in size with time and each subsequent boat pass.

Despite significant variability in suspended sediment concentrations and turbidity measurements, fixed (inorganic) suspended solids concentrations increased from samples collected before boat passes to after 5 passes across locations (9 and 14 ft depth) in 2023. There was also a shift toward more frequent higher turbidity measurements in the period post- boat passage at both depths in 2023. The median turbidity over 9-minute windows increased from <1 FNU pre- boat pass to ~3 FNU at the 9 ft depth and ~ 2 FNU at the 14 ft depth post- boat passage.

Key takeaways to establish guidance on operating depth for wakeboats in semi-displacement mode (surfing) are:

- The maximum penetration depths of the exhaust bubbles were 10-12 ft.
- The bow and stern pressure wave velocities were large enough to disturb lakebed sediments to depths of approximately 20 ft.
- Transverse wave velocities between 0.12 - 0.21 ft/s were generated at a depth of 15-16 ft. By 20 ft deep the transverse wave velocities had decreased to near zero.
- Propeller wash velocities were significant at depths coinciding with the exhaust bubbles (~10 ft). The measured velocities were moving towards the water surface (upwelling), which likely played a significant role in the sustained sediment suspension and entrainment. The velocities quickly decreased outside this intense region and by 15 ft they were near zero.

- At both depths in 2023, there was a small increase in turbidity of 2-3 FNU between pre- and post-boat passes.
- At a depth of 14 ft, the underwater video and ADCP echogram data confirmed that lakebed sediment (detritus) had resuspended.

8.3.3.1 Recommended depth of operation for wakeboats in semi-displacement (surfing) mode

It is recommended that wakeboats operate in 20 ft of water or greater when in semi-displacement (surfing) mode to minimize impacts to the lake bottom.

8.3.4 Recommendation for locations with aquatic vegetation

The velocities generated by both non-wakeboats and wakeboats have the potential to damage aquatic vegetation. The depth recommendations provided above are specified relative to the lake bottom, but just as easily could be relative to the top of the aquatic vegetation. Since vegetation grows throughout the open-water season, this is a more difficult recommendation to specify. In general, boats should avoid areas of the lake with aquatic vegetation to minimize damage.

8.4 Limitations of this research and future needs

Boats tested – This study tested two deck boats with outboard motors, three bowriders with stern drive motors, and two wakeboats with inboard motors. While these boats are representative of typical recreational powerboats in most Minnesota lakes, we recognize there are other types (e.g., pontoons, jet boats, etc.), manufacturers, and models in operation. Furthermore, as recreational boating continues to gain popularity, so does the evolution of boats (e.g., engine horsepower, wave manipulating technologies, etc.). Additional research that includes different types of recreational powerboats is needed.

Lakebed substrates and study locations – Four test sites were used in this study, each with a different water depth. However, the sediment composition at the deeper ADCP sites (27 and 14 ft) were similar, characterized as fine muck with >20% organic matter. The sediments at the shallower ADV sites (16 and 9 ft) were also similar, characterized by a sand/gravel mix with less than 0.5% organic matter. The study was constrained to a limited number of tests sites and substrates. In general, coarse lakebed material will require higher velocities to resuspend and entrain. Fine grain inorganic sediment, detritus, or “muddy” bottoms are examples of substrates

that will require less velocities to resuspend and entrain. Additional research that incorporates more lakebed substrates is needed.

Wind waves and powerboat hydrodynamic phenomena on sediment focusing - Over time, lake sediments sort such that finer and lighter materials that are easier to suspend accumulate in lower energy locations (deeper depths), and coarser and heavier materials that can persist in higher energy locations remain in shallower depths. This is known as sediment focusing. If the velocities generated by wind waves and lake currents were once the primary energy sources for sediment redistribution within a lake, how has this been altered by powerboat hydrodynamic phenomena, including wakeboats in surfing mode that produce higher velocities that extend deeper into the water column? Research into the vertical impacts of wind waves and boat waves on sediment focusing is a potentially important area of research.

Impacts to aquatic vegetation – As mentioned previously, this study did not directly examine the impacts of these hydrodynamic phenomena on aquatic vegetation, however, this remains a vitally important area of study. Our underwater videos show that the high velocities generated by wakeboats in semi-displacement mode (Condition 2- surfing) can damage living aquatic vegetation. Aquatic plants may also serve to dampen energy from wind and boats waves, thus protecting lakebed materials from resuspending. Additional research is needed that specifically examines recreational boating activities and their impact on various types of aquatic vegetation.

Limited data within propeller wash - A large effort was undertaken to extract useful data from within the most intense region of the propeller wash jet, which occurs immediately aft of the stern, but in the end, it was not possible with the ADCP. This was due to the acoustic signal attenuating in the exhaust bubbles, localized high velocities, and turbulence.

Impacts of recreational boating on lake temperature and mixing – Our fieldwork was conducted in the fall after the lake bays had already completed turnover and therefore were no longer thermally stratified. The impact that boat hydrodynamics have on thermally stratified waters is an important limnological topic that should be the focus of future research.

Boat propeller wash in crossflows – This study illustrates the effect of crossflow on propeller wash penetration depth. Jets in crossflow is an area studied in fundamental fluid mechanics, but there

is limited research in applications associated with non-stationary, rotational jets, like those of a recreational boat propeller. Additionally, the injection of exhaust gas into the jet adds additional complexity through energy dissipation and buoyancy. This topic has both complex physics and important applications that warrant further study.

Longer hiatus between boat passes – This study implemented a 15-minute hiatus between individual boat passes. The underwater video shows that during semi-displacement (Condition 2, 9 ft depth) testing of the wakeboats, sediment remained suspended in the water column when the next pass occurred 15 minutes later. Future research should consider implementing a longer hiatus between individual passes.

Overall impact of recreational boating on lake water quality – The various quantitative and qualitative measures of sediment resuspension by recreational boats demonstrate convincingly that boats, under certain circumstances, can generate local plumes of resuspended sediment that may persist for minutes to hours. As evidenced by the variability in our turbidity and suspended solids samples, these plumes can be very heterogeneous and single point samples in space or time may miss the impact. While we observed significant effects of individual boat passes on suspended solids and turbidity, the overall impact of heavy boat traffic on lake water quality was not quantified in this study, especially in comparison to other sources of sediment and nutrients, such as stream inflows and wind-wave resuspension. To fully capture the spatial and temporal variability of suspended sediment plumes, future research should deploy instrumentation with sampling rate of at least 2-3 samples/minute and an array of instrumentation at different depths and at different distances from the boat track.

9.0 REFERENCES

Ahmed, M. R., Faizal, M., Prasad, K., Cho, Y.-J., Kim, C.-G., & Lee, Y.-H. (2010). Exploiting the orbital motion of water particles for energy extraction from waves. Journal of Mechanical Science and Technology, 24, 943–949. https://doi.org/10.1007/s12206-010-0203-0

Alexander, M. T., & Wigart, R. C. (2013). Effect of motorized watercraft on summer nearshore turbidity at Lake Tahoe, California–Nevada. Lake and Reservoir Management, 29(4), 247–256. https://doi.org/10.1080/10402381.2013.840704

Anthony, J. L., & Downing, J. A. (2003). Physical impacts of wind and boat traffic on Clear Lake, Iowa, USA. Lake and Reservoir Management, 19(1), 1–14. https://doi.org/10.1080/07438140309353984

Asplund, T. R. (2000). The effects of motorized watercraft on Aquatic Ecosystems. Wisconsin Department of Natural Resources. PUBL-SS-948-00, Madison.

Asplund, T. R., & Cook, C. M. (1997). Effects of motor boats on submerged aquatic macrophytes. Lake and Reservoir Management, 13(1), 1–12. https://doi.org/10.1080/07438149709354290

ASTM. (2017). Standard test methods for particle-size distribution (gradation) of soils using sieve analysis. D6913/D6913M—17.

Barrett, J. C., Grossman, G. D., & Rosenfeld, J. (1992). Turbidity-induced changes in reactive distance of rainbow trout. Transactions of the American Fisheries Society, 121(4), 437–443. https://doi.org/10.1577/1548-8659(1992)121<0437:TICIRD>2.3.CO;2

Baud, A., Jenny, J.-P., Francus, P., & Gregory-Eaves, I. (2021). Global acceleration of lake sediment accumulation rates associated with recent human population growth and land-use changes. Journal of Paleolimnology, 66, 453–467. https://doi.org/10.1007/s10933-021-00217-6

BAW -Bundesanstalt für Wasserbau. (2011). BAW Code of Practice: Principles for the design of bank and bottom protection for inland waterways. Karlsruhe, Germany.

Beachler, M. M., & Hill, D. F. (2003). Stirring up trouble? resuspension of bottom sediments by recreational watercraft. Lake and Reservoir Management, 19(1), 15–25. https://doi.org/10.1080/07438140309353985

Bilkovic, D., Mitchell, M., Davis, J., Andrews, E., King, A., Mason, P., Herman, J., Tahvildari, N., & Davis, J., (2017). Review of boat wake wave impacts on shoreline erosion and potential solutions for the Chesapeake Bay. STAC Publication Number 17-002, Edgewater, Maryland.

Bilkovic, D., Mitchell, M., Davis, J., Herman, J., Andrews, E., King, A., Mason, P., Tahvildari, N., Davis, J., & Dixon, R. (2019) Defining boat wake impacts on shoreline stability toward management and policy solutions. Ocean and Coastal Management, 182, 104945. https://doi.org/10.1016/j.ocecoaman.2019.104945

Canfield, D. E. Jr., Langeland, K. A., Linda, S. B., & Haller, W. T. (1985). Relations between water transparency and maximum depth of macrophyte colonization in lakes. Journal of Aquatic Plant Management, 23, 25-28.

Chambers, P. A., & Kaiff, J. (1985). Depth distribution and biomass of submersed aquatic macrophyte communities in relation to secchi depth. Canadian Journal of Fisheries and Aquatic Sciences, 42(4), 701–709. https://doi.org/10.1139/f85-090

Chanson, H. (1996). Air Bubble Entrainment in Free-Surface Turbulent Shear Flows. Academic Press Limited. Elsevier.

Combs, S. M., & Nathan, M. V. Soil Organic Matter. p. 53-58. In Recommended Chemical Soil Test Procedures for the North Central Region. North Central Regional Research Publication No. 221 (Revised). Jan. 1998. Missouri Agricultural Experiment Station SB 1001.

Daeger, A., Bosch, N. S., & Johnson, R. (2022). Impacts of nutrient and sediment resuspension by various watercraft across multiple substrates, depths, and operating speeds in Indiana's largest natural lake. Proceedings of the Indiana Academy of Science, 130(2), 112–122.

Doig, L. E., North, R. L., Hudson, J. J., Hewlett, C., Lindenschmidt, K.-E., & Liber, K. (2017). Phosphorus release from sediments in a river-valley reservoir in the northern Great Plains of North America. Hydrobiologia, 787(1), 323–339. https://doi.org/10.1007/s10750-016-2977-2

Faltinsen, O. M. (2006). Hydrodynamics of high-speed marine vehicles. Cambridge University Press. https://doi.org/10.1017/CBO9780511546068

Fang, X., Jiang, L., Jacobson, P. C., Stefan, H. G., Alam, S. R., & Pereira, D. L. (2012). Identifying cisco refuge lakes in Minnesota under future climate scenarios. Transactions of the American Fisheries Society, 141(6), 1608-1621. https://doi.org/10.1080/00028487.2012.713888

Fay, E. M., Gunderson, A., & Anderson, A. (2022). Numerical study of the impact of wake surfing on inland bodies of water. Journal of Water Resource and Protection, 14(03), 238–272. https://doi.org/10.4236/jwarp.2022.143012

Fischenich, J. C. (2001). Stability thresholds for stream restoration materials, U.S. Army Engineer Research and Development Center (ERDC), Vicksburg, Mississippi, Technical Note No. EMRRP-SR-29.

Fleit, G., & Baranya, S. (2021). Acoustic measurement of ship wave–induced sediment resuspension in a large river. Journal of Waterway, Port, Coastal, and Ocean Engineering, 147(2), 04021001. https://doi.org/10.1061/(ASCE)WW.1943-5460.0000627

Ford, D. E., & Stefan, H. G. (1980). Thermal predictions using integral energy model. Journal of the Hydraulics Division, 106(1), 39–55. https://doi.org/10.1061/JYCEAJ.0005358

Francis, J., Nohner, J., Bauman, J., & Gunderman, B. (2023). A literature review of wake boat effects on aquatic habitat. Michigan Department of Natural Resources, Fisheries report 37, Lansing.

Frank K., Beagle, D. & Denning, J. Phosphorus. p.21-29. In Recommended Chemical Soil Test Procedures for the North Central Region. North Central Regional Research Publication No. 221 (Revised). Jan. 1998. Missouri Agricultural Experiment Station SB 1001.

Gardner, M. B. (1981). Effects of turbidity on feeding rates and selectivity of bluegills. Transactions of the American Fisheries Society, 110(3), 446–450. https://doi.org/10.1577/1548-8659(1981)110<446:EOTOFR>2.0.CO;2

Garrad, P. N., & Hey, R. D. (1987). Boat traffic, sediment resuspension and turbidity in a Broadland river. Journal of Hydrology, 95(3), 289–297. https://doi.org/10.1016/0022-1694(87)90007-2

Green, M. O., & Coco, G. (2014). Review of wave-driven sediment resuspension and transport in estuaries. Reviews of Geophysics, 52(1), 77-117. https://doi.org/10.1002/2013RG000437

Gucinski, H. (1982). Sediment suspension and resuspension from small-craft induced turbulence. U.S. Environmental Protection Agency, Report 600/3-82-084, Annapolis, Maryland.

Hamill, G. A., Johnston, H. T., & Stewart, D. P. (1999). Propeller wash scour near quay walls. Journal of Waterway, Port, Coastal, and Ocean Engineering, 125(4), 170–175. https://doi.org/10.1061/(ASCE)0733-950X(1999)125:4(170)

Hamilton, D., & Mitchell, S. (1997). Wave-induced shear stresses, plant nutrients and chlorophyll in seven shallow lakes. Freshwater biology, 38(1), 159-168. https://doi.org/10.1046/j.1365-2427.1997.00202.x

Horne, A. J., & Goldman, C. R. (1994). Limnology, 2nd Edition. McGraw Hill.

Hoverson, D., & McGinley, P. (2007). Waves, wind, watercraft and water clarity: a study of sediment resuspension in Clark Lake. Center for Watershed Science and Education, University of Stevens Point.

Irvine, K. N., Droppo, I. G., Murphy, T. P., & Lawson, A. (1997). Sediment resuspension and dissolved oxygen levels associated with ship traffic: implications for habitat remediation. Water Quality Research Journal, 32(2), 421–438. https://doi.org/10.2166/wqrj.1997.027

Jacobson, P. C., Stefan, H. G., & Pereira, D. L. (2010). Coldwater fish oxythermal habitat in Minnesota lakes: influence of total phosphorus, July air temperature, and relative depth. Canadian Journal of Fisheries and Aquatic Sciences, 67(12), 2002–2013. http://doi.org/10.1139/F10-115

Kumar, P. P., & Premchand, M. (2015). Numerical investigation of the influence of water depth on ship resistance. International Journal of Computer Applications, 116(17), 10–17. https://doi.org/10.5120/20427-2750

Lackenby, H. (1963). The effect of shallow water on ship speed. Shipbuilder and Marine Engine Builder, 70, 446–450.

Larsson, L., & Raven, H. C. (2010). Ship resistance and flow. Published by The Society of Naval Architects and Marine Engineers, SNAME, The Principles of Naval Architecture Series, ISBN: 978-0-939773-76-3.

Lewis, E V. ed. *Principles of Naval Architecture, Vol. I & 2*. New York, 1941.

Liao, Q., Wang, B., & Wang, P.-F. (2015). In situ measurement of sediment resuspension caused by propeller wash with an underwater particle image velocimetry and an acoustic doppler velocimeter. Flow Measurement and Instrumentation, 41, 1–9. https://doi.org/10.1016/j.flowmeasinst.2014.10.008

Liddle, M. J., & Scorgie, H.R.A. (1980). The effects of recreation on freshwater plants and animals: A review. Biological Conservation, 17(3), 183-206. https://doi.org/10.1016/0006-3207(80)90055-5

Macfarlane, G.J. (2012) Marine vessel wave wake: Focus on vessel operations within sheltered waterways, PhD thesis, University of Tasmania.

Macfarlane, G.J. (2018). Wave wake study: HB4099 motorboat working group. University of Tasmania, Australian Maritime College, Report 18WW01, Launceston.

Macfarlane, G.J. (2025), Wakesurfing, Wakeboarding, and Waterskiing: A Comparison of Wake Characteristics. River Research and Applications. https://doi.org/10.1002/rra.4438

Malibu Boat (2020) How to Make a Perfect Wake or Wave with Power Wedge III, website: https://www.malibuboats.com/news/2018-news/power-wedge, accessed June 2021.

Marr, J., Riesgraf, A., Herb, W., Lueker, M., Kozarek, J., & Hill, K. (2022). A field study of maximum wave height, total wave energy, and maximum wave power produced by four recreational boats on a freshwater lake. St. Anthony Falls Project Report No. 600, University of Minnesota, Minneapolis.

Maynord, S. T. (2000). Physical forces near commercial tows. Interim Report for the Upper Mississippi River – Illinois Waterway System Navigation Study, U.S. Army Corps of Engineers, ENV Report 19, Vicksburg, Mississippi.

Minnesota Department of Natural Resources (2024). Lake Survey Report: Minnetonka (27013300). Retrieved from: https://www.dnr.state.mn.us/lakefind/showreport.html?downum=27013300

Mosisch, T. D., & Arthington, A. H. (2004). Impacts of recreational power-boating on freshwater ecosystems. R. Buckley (Ed.), Environmental Impacts of Ecotourism, CABI Publishing, Oxford, pp. 125–154.

Mueller, H., Hamilton, D. P., & Doole, G. J. (2016). Evaluating services and damage costs of degradation of a major lake ecosystem. Ecosystem Services, 22, 370–380. https://doi.org/10.1016/j.ecoser.2016.02.037

Murphy, K. J., Willby, N. J., & Eaton, J. W. (1995). Ecological impacts and management of boat traffic on navigable inland waterways. The Ecological Basis for River Management, 42, 427–442.

Nedohin, D. N., & Elefsiniotis, P. (1997). The effects of motor boats on water quality in shallow lakes. Toxicological & Environmental Chemistry, 61(1–4), 127–133. https://doi.org/10.1080/02772249709358479

Niemistö, J., Tamminen, P., Ekholm, P., & Horppila, J. (2012). Sediment resuspension: rescue or downfall of a thermally stratified eutrophic lake? Hydrobiologia, 686(1), 267–276. https://doi.org/10.1007/s10750-012-1021-4

Nikora, V. I., & Goring, D.G. (2002). Fluctuations of suspended sediment concentration and turbulent sediment fluxes in an open-channel flow. Journal of Hydraulic Engineering, 128(2), 214-224. https://doi.org/10.1061/(ASCE)0733-9429(2002)128:2(214)

Nortek (2017). Signature principles of operation. Nortek Manuals. N3015-025 1. release

Orihel, D. M., Baulch, H. M., Casson, N. J., North, R. L., Parsons, C. T., Seckar, D. C. M., & Venkiteswaran, J. J. (2017). Internal phosphorus loading in Canadian fresh waters: A critical review and data analysis. Canadian Journal of Fisheries and Aquatic Sciences, 74(12), 2005–2029. https://doi.org/10.1139/cjfas-2016-0500

Ortiz, D. A., Meyer, M., Daulton, T., & Kovar, B. (2024). The effects of wake boats on lake ecosystem health: a literature review. Wisconsin's Green Fire, Rhinelander, Wisconsin.

Osborne, P. D., MacDonald, N. J., & Parkinson, S. (2012). Sediment transport in response to wave groups generated by high-speed vessels. Coastal Sediments' 07, 110–123. https://doi.org/10.1061/40926(239)9

Pelley, J. (2016). Taming Toxic Algae Blooms. ACS Central Science, 2(5), 270–273. https://doi.org/10.1021/acscentsci.6b00129

Qin, B., Hu, W., Gao, G., Weiping, H., Guang. G., Luo, L., & Zhang, J. (2004). Dynamics of sediment resuspension and the conceptual schema of nutrient release in the large shallow Lake Taihu, China. Chinese Science Bulletin, 49(1), 54–56. https://doi.org/10.1007/BF02901743

Rabaud, M., & Moisy, F. (2014). Narrow ship wakes and wave drag for planing hulls. Ocean Engineering, 90, 34–38. https://doi.org/10.1016/j.oceaneng.2014.06.039

Ray, A. (2020). Analyzing threats to water quality from motorized recreation on Payette Lake, Idaho. Big Payette Lake Water Quality Council, Valley County, Idaho.

Raymond, S., Galvez, R. (2015). Impact of lake navigation—sediment suspension study: Lake Masson and Sand Lake cases. Laval University, Quebec.

Riley, E. T., & Prepas, E. E. (1984). Role of internal phosphorus loading in two shallow, productive lakes in Alberta, Canada. Canadian Journal of Fisheries and Aquatic Sciences, *41*(6), 845-855. https://doi.org/10.1139/f84-101

Ruiz, A., Lacaze, G., & Oefelein, J. (2014). Flow topologies and turbulence scales in a jet in cross flow. Combustion Research Facility, Sandia National Laboratories. https://doi.org/10.1103/APS.DFD.2014.GFM.P0072

Sagerman, J., Hansen, J. P., & Wikström, S. A. (2020). Effects of boat traffic and mooring infrastructure on aquatic vegetation: a systematic review and meta-analysis. Ambio, 49, 517-530. https://doi.org/10.1007/s13280-019-01215-9

Savitsky, D., & Morabito, M. (2010). Surface wave contours associated with the forebody wake of stepped planing hulls. Marine Technology and SNAME news, 47(1), 1–16. https://doi.org/10.5957/mtsn.2010.47.1.1

Schindler, D. W. (1977) Evolution of phosphorus limitation in lakes: natural mechanisms compensate for deficiencies of nitrogen and carbon in eutrophied lakes. Science, 195(4275), 260–2622.

Schlichting, O. (1934). Ship resistance in water of limited depth-resistance of sea-going vessels in shallow water. Jahrbuch der STG, 35, 127–148.

Smarts, M. M., Radar, R. R., Nielsen, D. N., & Claflin, T. O. (1985). The effect of commercial and recreational traffic on the resuspension of sediment in Navigation Pool 9 of the Upper Mississippi River. Hydrobiologia, 126(3), 263–274. https://doi.org/10.1007/BF00007504

State of Maine. (2024). An act to implement the recommendation in the Department of Inland Fisheries and Wildlife's Report on wake boats. Legislative Document No. 2284, HP 1472.

State of Vermont. (2024). Environmental Protection Rule, Chapter 32, Vermont Use of Public Water Rules, State of Vermont, Agency of Natural Resources, Department of Environmental Conservation, https://dec.vermont.gov/document/vermont-use-public-waters-rules

Stuart-Smith, R D., Richardson, A. M. M., & White, R. W. G. (2004). Increasing turbidity significantly alters the diet of brown trout: a multi-year longitudinal study. Journal of fish biology, 65, 376–388.

Symonds, A., Britton, G., Donald, J., & Loehr, H. (2016). Predicting propeller wash and bed disturbance by recreational vessels at marinas. Bulletin of the Permanent International Association of Navigation Congress PIANC, 70–80.

Tandon, H. L. S., Cescas, M. P., & Tyner, E. H. (1968). An acid-free vanadate-molybdate reagent for the determination of total phosphorus in soils. Soil Science Society of America Journal, 32(1), 48-51. https://doi.org/10.2136/sssaj1968.03615995003200010012x

Tang, C., Li, Y., He, C., & Acharya, K. (2020). Dynamic behavior of sediment resuspension and nutrients release in the shallow and wind-exposed Meiliang Bay of Lake Taihu. Science of the Total Environment, 708, 135131. https://doi.org/10.1016/j.scitotenv.2019.135131

Tavakoli, S., Shaghaghi, P., Mancini, S., De Luca, F., & Dashtimanesh, A. (2022). Wake waves of a planing boat: an experimental model. Physics of Fluids, 34(3). https://doi.org/10.1063/5.0084074

Terra Vigilis Environmental Services Group. (2022). Water quality and wave impact study: phase 2 report. https://www.safewakes.org/_files/ugd/2936a3_e64f2cd98fcb49c9b060fa11a959fbd0.pdf

Terra Vigilis Environmental Services Group. (2024). Lake Waramaug Shallow Water Environment Wave Impact Study, Final Report.

Trebitz, A. S., Brazner, J. C., Brady, V. J., Axler, R., & Tanner, D. K. (2007). Turbidity tolerances of Great Lakes coastal wetland fishes. North American Journal of Fisheries Management, 27(2), 619–633. https://doi.org/10.1577/M05-219.1

University of Minnesota (2024). LakeBrowser: Minnetonka-Maxwell Bay (Hennepin). Retrieved from: https://lakes.rs.umn.edu/#27013320

Valbuena S.A., Bombardelli F.A., & Schladow S.G. (2020). Boat induced sediment resuspension and water clarity in shallow flows. River Flow 2020 10th Conference on Fluvial Hydraulics, 1333–1341.

Valbuena, S.A., Schladow, S.G., & Bombardelli, F.A. (2024). Boat effects on lake water clarity and the efficacy of a no-wake zone policy. Lake and Reservoir Management, 41, 16-33. https://doi.org/10.1080/10402381.2024.2388540

Velasco, D. W., Lefevre, D., Gojak, C., Nylund, S., Hutton, B., Zakardjian, B., Mahiouz, K., Bezile, A., & Heyndrickx, C. (2021). Performance evaluation of a combined ADCP-scientific echosounder system. *OCEANS: San Diego–Porto*, San Diego, California, USA, 1-10. http://doi.org/10.23919/OCEANS44145.2021.9706094

Wang, J., Jiang, C., Zhou, X., Yu, S., & Bai, G. (2024). Experimental study on flow characteristics of jet ventilation in crossflow in confined mine spaces. Scientific Reports, 14, 8022. https://doi.org/10.1038/s41598-024-58267-5.

Wang, P. F., Rivera, I., Richter, K., Liao, Q., Farley, K., Chen, H.-C., Germano, J., Markillie, K., & Gailani, J. (2016). Evaluation of resuspension from propeller wash in DoD harbors. Technical Report 3049, Project ER-201031.

Wei, M., Chiew, Y. M., & Cheng, N.-S. (2020). Recent advances in understanding propeller jet flow and its impact on scour. Physics of Fluids, 32(10), 101–303. https://doi.org/10.1063/5.0023266

Wetzel, R. G. (2001). *Limnology: lake and river ecosystems*. gulf professional publishing.

Weyhenmeyer, G. A. (1998). Resuspension in lakes and its ecological impact- a review. Ergebnisse Der Limnologie, 51, 185–200.

Yousef, Y.A., McLellon, W. M., Fagan R. H., Zebuth, H. H., & Larrabee, C. R. (1978). Mixing effects due to boating activities in shallow lakes. U.S. Department of Interior, Office of Water Research and Technology, Technical Report ESEI No. 78-10.

Yousef, Y.A., McLellon, W. M., & Zebuth, H. H. (1980). Changes in phosphorus concentrations due to mixing by motorboats in shallow lakes. Water Research, 14(7), 841-852.

10.0 APPENDIX

The following information supplements St. Anthony Falls Laboratory Project Report 604, "*A Field Study of Recreational Powerboat Hydrodynamics and their Impacts on the Water Column and Lakebed*."

ADCP tilt verification

The ADCP was attached to a pad and placed on the lakebed. The method of deployment is discussed in Section 5.3. During data analysis, the pitch and roll of the ADCP sensor was examined. Pitch is a measure of the deviation of the sensor, in degrees, about the y-axis and Roll is the deviation in degrees about the x-axis. The ADCP records the pitch and roll continually during deployment. The two measurements describe the tilt of orientation of the sensor. Table A1 summarizes the pitch and roll for each boat testing in this campaign. The data verifies that the sensor was not excessively tilted during testing.

Table A1. Summary of pitch and roll of the ADCP as deployed.

Boat	Year	Pitch (degrees) Mean ± SD (ft)	Roll (degrees) Mean ± SD (ft)
Hurricane SS 203	2022	7.07 ± 0.02	1.54 ± 0.01
Cobalt R5	2022	-0.60 ± 0.02	1.48 ± 0.01
Cruisers Yachts 34 GLS	2022	2.77 ± 0.04	0.41 ± 0.01
Nautique G23 Pragagon	2022	1.91 ± 0.02	1.46 ± 0.01
Malibu VLX Wakesetter	2022	5.46 ± 0.02	-1.33 ± 0.01
Starcraft Limited 2000	2023	1.96 ± 0.02	-3.01 ± 0.01
Sea Ray SPX 190	2023	-1.18 ± 0.02	0.54 ± 0.01
Nautique G23 Pragagon	2023	-0.83 ± 0.01	-0.88 ± 0.01
Malibu VLX Wakesetter	2023	-1.89 ± 0.01	0.26 ± 0.01

Acoustic Doppler Current Profiler (ADCP) – principles of operation

Several publications exist that provide necessary details and background information on the design and principle of operation of ADCP technologies. In this study, a Signature 1000+ developed by Nortek was used (Nortek 2025); however, ADCP technologies are developed by a range of manufacturers, and all use a similar design and are based on similar principles.

Figure A1 illustrates an idealized single beam from an ADCP. The ADCP is not shown but is located at the bottom and narrowest part of the beam. Sound is produced by a single transceiver, which is capable of sending and receiving a sound signal. The sound is focused and travels nominally along the beam axis toward the water surface. Sound is reflected back to the transceiver as it collides with particles within the water column and this sound is precisely recorded (amplitude and frequencies) at the ADCP.

Each beam is divided into vertical measurement bins and the height of each bin is a user-specified parameter. For 2022 data, the bin height was set at 5.0 cm and in 2023 the bin height was 2.0 cm. The distance between the face of the ADCP and an individual measurement bin is defined as the *range*. The ADCP also has a *blanking distance*, which is the distance from the device to the first measurement point, of 10 cm.

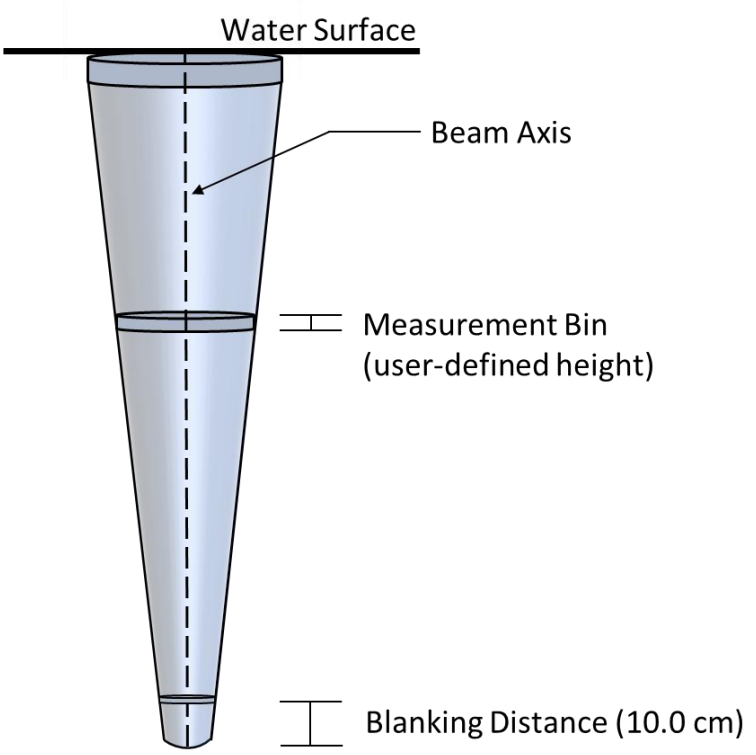

Figure A1. Schematic of a single beam generated by the ADCP where the ADCP is at the bottom of the beam (narrowest portion). Sound is emitted from a single ADCP transceiver and travels nominally along the beam axis.

Figure A2 illustrates the 5-beam arrangement for a bottom mounted, upward looking Nortek ADCP. The center beam, Beam 5, is oriented vertically upward. Beams 1 through 4 are tilted 25 degrees from vertical and located 90 degrees from one another. For the data campaign discussed in this report, Beams 1 and 3 were oriented in the direction of boat travel and Beams 2 and 4 were perpendicular to the boat travel direction. Other details of the ADCP placement and pad design can be found in Section 5.3 of the report.

During data collection, the ADCP Signature 1000 was set to Burst mode with HR enabled on all 5 beams. All beams emitted a pair of very quick sound bursts, referred to as a pulse coherent burst mode rather than broadband mode sometimes used with ADCPs. As shown in Figure A1, this outgoing sound is focused in a narrow beam and travels along the axis of each of the five beams. Particles in the water column serve as reflectors for the acoustic signal and allow the device to estimate the beam-wise velocity of the water. In this study, the ADCP was programmed to sample as fast as possible, which was 4 Hz, when using all 5 beams and with echo-sounder mode enabled. This meant that a pulse coherent burst was emitted every ¼ second.

The transformation from beam-wise velocities to Cartesian (UVW) velocities of the ADCP assumes homogeneous water velocity in all beam bins of a certain range. The composite diameter of the four beams at a specific range represents a *measurement disk*. The diameter of the disk grows larger with the range of the measurement. Three disks are illustrated in Figure A2.

The assumption of uniform flow conditions across a disk is critical to the processing of the measured data and allows the accurate transformation of measured data from beam-wise velocities to Cartesian velocities, U, V, and W. Details on this transformation can be found in the references cited above. In short, pairs of beams 180 degrees apart can be used to calculate the vertical velocity, W, and one horizontal velocity, either U or V, assuming homogenous velocity within each disk.

The resulting transformed velocities are U_{13}, V_{24}, W_{13}, W_{24}, where the subscript indicates the dependency of the calculated velocity on the beam coordinates. For example, U_{13} is dependent solely on the Beam 1 and Beam 3 velocities, etc. A small difference between W_{13} and W_{24} would be indicative of a homogenous disk or sample volume. The center vertical beam also gives a

beam-wise velocity, which is another measurement of the vertical velocity, W_5 and requires no transformation.

In most instances of ADCP analysis with steady state wave or mean flows, the assumption of homogeneous spatial flow within the measurement disk along with temporal averaging is assumed for the transformation from beam coordinates to cartesian coordinates (i.e., XYZ coordinates). This is a reasonable assumption with our observed transverse waves. However, for our other flows of interest, the jet-like prop wash phenomenon and the fast-moving initial bow and stern waves, this homogenous spatial flow assumption for all fours beams was not likely valid. This is especially true with respect to beams 2 and 4, used for Y direction velocity calculations, because they were directed away from the boat track line. Our approach was limited to direct measurements of the beam velocities and combining only beams 1 and 3 (used for X direction velocity calculations) and beam 5 (which was the Z direction velocity). Our pre-processing of the ADCP data included evaluation of data quality of beam-wise velocity data points and any data not meeting quality assurance requirements through correlation or amplitude values were eliminated from the analysis. See report Section 6.2 for details on our data filtering process.

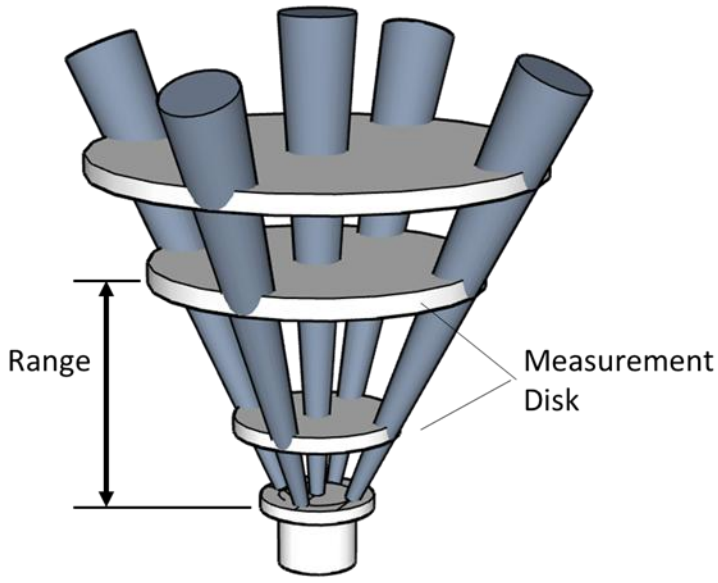

Figure A2. Schematic of an upward projecting ADCP illustrating the five-beam orientation.

Acoustic Doppler Profiler (ADV) – methods for relating wave and propeller wash velocities to sediment resuspension

Quantifying propeller wash turbulence and bed shear stress

The velocity field generated from propeller wash is a relatively short-duration phenomenon involving high-frequency turbulent fluctuations superimposed on lower frequency variation in the mean velocities. The velocity field resulting from propeller wash has a mean that varies slowly over time, but also has significant turbulent fluctuations. Empirical relationships have been developed that relate the turbulent fluctuations in a flow field to corresponding shear stresses within the water column, which can be used to estimate the ability of the flow to resuspend sediment (Biron et al. 2004, Kim et al. 2000). Both Reynolds stress and turbulent kinetic energy (TKE) have been used to quantify near-bed shear stress. Biron et al. (2004) found TKE to be a more robust estimator of shear stress in complex flow fields. Previous studies of sediment resuspension due to near-bed velocity fields have separated the turbulent fluctuations from slowly varying mean velocities (Koch and Chanson, 2008) and wave-induced velocities (Bian et al. 2018, Cannon et al. 2022, Egan et al. 2019, Hansen and Reidenbach 2012).

In our analyses, we explored using the frequency domain methods given by Bricker and Monismith (2007) to separate turbulent fluctuations from wave-induced velocities to estimate the maximum Reynolds stress for each boat pass. We found the results to be unreliable, mainly because the transient wave amplitudes of the transverse waves gave a distinct, but not dominant, peak in the frequency domain. Based on Biron et al. (2004), we chose to use TKE as the measure of turbulence and its ability to resuspend sediment. The TKE calculations were performed as follows:

1) For each boat pass, the filtered velocity signals (U, V, W) were processed in 10-second intervals, starting three seconds after the stern wave signal.
2) The turbulent fluctuations were separated from the wave-induced velocities in the time domain by subtracting the estimated wave-induced velocity (report Figure 27) from the U velocity signal.

$$U^* = U - \widetilde{U} \qquad \text{(A.1)}$$

where $\widetilde{U}$ is the wave-induced velocity. Since the wave velocity $\widetilde{U}$ is derived from the pressure signal of the ADV, it was assumed that the wave velocity is in the U-direction with negligible components in the V and W direction.

3) U*, V, and W were then passed through a noise de-spiking filter (Parsheh et al. 2010)
    a. Turbulent kinetic energy for each 10-second interval was then calculated as:

$$TKE = \frac{\sum_{i=1}^{n}\left[\left(U_i^* - \overline{U^*}\right)^2 + (V_i - \overline{V})^2 + (W_i - \overline{W})^2 \right]}{2\,n} \quad \text{(A.2)}$$

where n is the number of samples, and the overbar indicates the mean velocity for the 10-second sample.

4) For each pass, the maximum 10-second value of TKE was recorded.
5) The corresponding maximum turbulent shear stress was calculated as (Biron et al. 2004):

$$\theta_{pw} = 0.19\,\rho\,TKE, \quad \text{(A.3)}$$

where ρ is the density of water.

To estimate the ability of propeller wash turbulence to resuspend sediment of different sizes, the turbulent shear stress was calculated using Equations A.2 and A.3 for each boat pass, a. These turbulent shear stresses were then compared to the critical shear stresses given in Table 1 of Fischenich (2001) and reproduced below in Table A1.

Quantifying wave-generated shear stress and sediment resuspension potential

Water waves visible at the surface extend vertically into the water column equal to about half of their wavelength. Interaction of the wave and the lakebed can generate bottom velocities and shear stress capable of resuspending sediment into the water column. In addition to sediment resuspension by wind-driven waves (Green and Coco 2014), bottom shear stresses and sediment resuspension by boat-generated waves have also been studied in the context of barge navigation on large rivers (Fleit and Baranya 2021, Garcia et al. 1998, Rodriguez et al. 2002, Maynord 1990). Rodr ı´guez et al. (2002) used tow tests of scale model river barges to characterize the bottom shear stresses due to the bow and stern waves. Fleit and Baranya (2021) used field measurements to find relationships between ship-induced waves and suspended sediment concentrations in the Danube River.

We chose the methods given by Green and Coco (2014) and Green and MacDonald (2001) to explore the ability of boat-generated waves (bow, stern, transverse) to resuspend sediment. The previously described methods were used to find the maximum velocity magnitude associated with the bow wave, the stern wave, and transverse waves. These three wave velocities can be related to shear stresses and the potential for sediment resuspension by the wave-induced skin friction (Θ_w) and the friction factor (f_w):

$$\theta_w = \frac{0.5\rho f_w U_w^2}{(\rho_s - \rho)} \quad \text{(A.4)}$$

$$f_w = e^{(5.21*(\frac{2.5D_{50}}{d_w})^{0.194}} - 5.977 \quad \text{(A.5)}$$

$$d_w = \frac{TU_w}{2\pi} \quad \text{(A.6)}$$

where ρ and ρ_s are the densities of water and sediment, respectively, U_w is the near-bottom wave-induced velocity, D_{50} is the median sediment diameter, d_w is the near-bottom wave orbital excursion amplitude, and T is the wave period. Θ_w is a dimensionless quantity with a threshold value of 0.056, e.g., sediment resuspension is predicted for Θ_w >0.056 (Green and Coco 2014).

The studies described by Green and Coco (2014) considered wind-generated waves only – the applicability of these methods to boat-generated waves hasn't been explored to date, but the analysis provides a starting point for estimating the potential for sediment resuspension by boat-generated waves. Using Equations A.4, A.5, and A.6, the wave velocity required to resuspend different sediment size classes were created (Table A2). The particle classes and sizes follow Fischenich (2001).

Table A2. Critical wave velocities, calculated from equations A.4-A.6, and critical shear stresses, taken from Fischenich (2001), for different particle sizes. The minimum particle size gives the lower limit of the size range for each particle class.

Particle Class	Minimum Particle Size (in)	Critical Wave Velocity (ft/s)	Critical Shear Stress (Pa)
Medium Silt	0.001	0.20	0.05
Coarse Silt	0.002	0.26	0.05
Fine Sand	0.005	0.38	0.14
Medium Sand	0.01	0.50	0.19
Coarse Sand	0.02	0.64	0.29
Very Coarse Sand	0.04	2.12	0.48
Very Fine Gravel	0.08	3.18	1.44
Fine Gravel	0.16	8.49	2.87

Bubble Depth Limits – Wakeboats by test year

The Nautique G23 Paragon and Malibu VLX Wakesetter were the only boats tested in both 2022 and 2023. In terms of bubble extent, the 2022 and 2023 echogram data were highly repeatable for both test conditions (Figure A3). For each boat and condition, a pooled *t*-test was used to evaluate the statistical significance of the average maximum bubble limit depth between years (Table A3). For Condition 1, the years for both boats were not statistically significant (Nautique G23 Paragon; *p*-value = 0.0616, Malibu VLX Wakesetter; *p*-value = 0.9029). For Condition 2, the years were not statistically significant for the Nautique G23 Paragon (*p*-value = 0.4865) but were statistically significant for the Malibu VLX Wakesetter (*p*-value = 0.0179). However, when the years were combined for Condition 2 and the wakeboats were compared, the means were not significantly different from each other (*p*-value = 0.5053). Because of the data analysis described here, we decided to combine the 2022 and 2023 echogram data in the report.

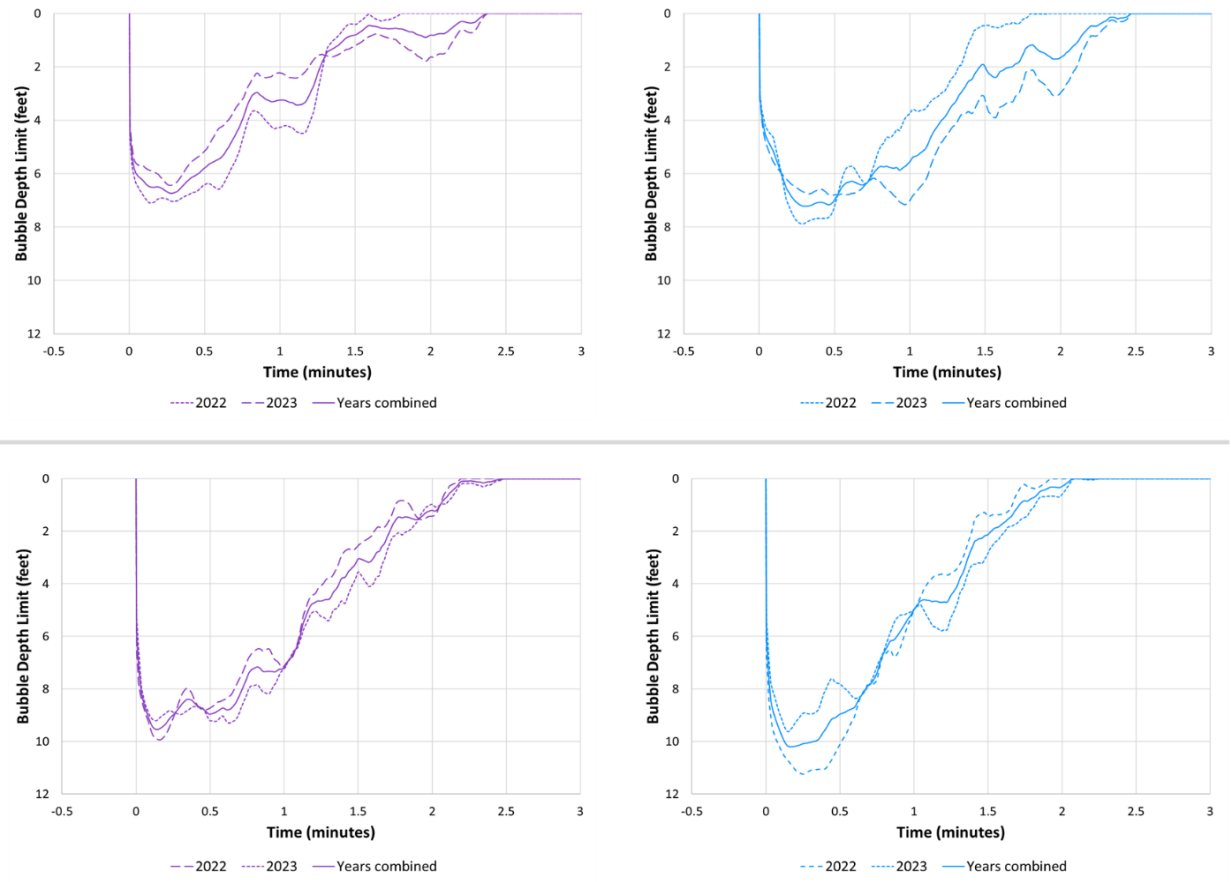

Figure A3. 5-second moving average of the bubble depth limit for the Nautique G23 Paragon (purple) and Malibu VLX Wakesetter (blue) during 2022 and 2023 testing. The top frames are planing mode (Condition 1) and the bottom frames are semi-displacement mode (Condition 2).

Table A3. The average maximum bubble depth limit values of the 99th percentile for the wakeboats in planing mode (Condition 1) and semi-displacement mode (Condition 2). A statistically significant difference between years using a pooled *t*-test (α <0.05) is denoted by (✳).

Boat	Condition	2022 Mean ± SD (ft)	2023 Mean ± SD (ft)	Pooled *t*- test (*p*- value)
Nautique G23 Paragon	Conditon 1	8.4 ± 1.4	6.9 ± 0.3	0.0616
	Condition 2	11.2 ± 1.8	10.5 ± 1.1	0.4865
Malibu VLX Wakesetter	Conditon 1	8.4 ± 0.5	8.3 ± 0.8	0.9029
	Condition 2	12.1 ± 1.2	10.4 ± 0.5	0.0179✳

ADCP bow and stern wave regression analysis coefficients and statistics

The following tables contain the regression information when performing the logarithmic fit to the form:

$$d = b1 + b2 \ln U \quad \text{(A.7)}$$

where *d* is the distance from bottom and *U* is velocity in the direction of interest.

Table A4. Horizontal (U_{13}) regression analysis information for ADCP bow and stern wave data

Test Year	Boat	Condition	Wave	b1	p-value1	standard error1	b2	p-value2	standard error2	RMSE	R_2	regression shown in report Figure 37
2022	Hurricane SS203	1	Bow	-3.86	2.24E-121	2.41E-02	0.11	7.65E-72	2.24E-03	0.01	0.96	Yes
		1	Stern	-3.84	1.20E-90	5.93E-02	0.09	1.18E-36	4.97E-03	0.02	0.76	Yes
2022	Cobalt R5	1	Bow	-3.31	4.59E-72	2.88E-02	0.08	9.36E-31	3.38E-03	0.01	0.89	Yes
		1	Stern	-4.15	1.47E-140	1.61E-02	0.14	1.67E-106	1.21E-03	0.00	0.99	Yes
2022	Cruisers Yachts 34GLS	1	Bow	-2.88	8.58E-69	2.35E-02	0.09	2.20E-35	3.15E-03	0.01	0.94	Yes
		1	Stern	-4.28	2.10E-54	1.27E-01	0.15	4.72E-24	1.08E-02	0.04	0.67	Yes
2022	Nautique G23 Paragon	1	Bow	-2.87	2.30E-49	3.74E-02	0.06	1.10E-13	6.03E-03	0.01	0.71	Yes
		1	Stern	-3.29	1.26E-80	5.79E-02	0.08	1.23E-30	5.14E-03	0.03	0.72	Yes
2022	Malibu VLX Wakesetter	1	Bow	-3.38	9.10E-116	1.62E-02	0.09	8.52E-65	1.75E-03	0.01	0.97	Yes
		1	Stern	-5.99	1.80E-70	1.36E-01	0.27	3.30E-42	1.19E-02	0.05	0.82	Yes
2022	Hurricane SS203	2	Bow	-5.60	4.30E-152	3.62E-02	0.19	1.51E-110	2.60E-03	0.03	0.98	Yes
		2	Stern	-3.36	1.88E-122	2.24E-02	0.16	2.12E-93	2.02E-03	0.02	0.98	Yes
2022	Cobalt R5	2	Bow	-4.99	1.25E-79	9.10E-02	0.18	1.77E-49	6.77E-03	0.02	0.87	Yes
		2	Stern	-3.95	1.02E-40	9.39E-02	0.19	1.10E-30	7.43E-03	0.02	0.93	Yes
2022	Cruisers Yachts 34GLS	2	Bow	-4.03	6.77E-169	1.87E-02	0.17	2.31E-138	1.37E-03	0.01	0.99	Yes
		2	Stern	-2.39	1.25E-107	2.26E-02	0.14	1.57E-91	1.87E-03	0.05	0.98	Yes
2022	Nautique G23 Paragon	2	Bow	-3.48	6.57E-102	2.31E-02	0.13	2.59E-66	2.32E-03	0.01	0.97	Yes
		2	Stern	-1.82	4.67E-27	5.45E-02	0.09	1.70E-08	1.22E-02	0.03	0.62	Yes
2022	Malibu VLX Wakesetter	2	Bow	-3.56	2.94E-27	1.21E-01	0.02	5.38E-01	2.50E-02	0.01	0.01	No
		2	Stern	-1.73	6.55E-20	3.04E-02	0.02	1.31E-01	1.05E-02	0.01	0.14	No
2023	Starcraft Limited 2000	1	Bow	-2.50	6.02E-67	3.53E-02	0.12	1.31E-22	8.37E-03	0.02	0.75	Yes
		1	Stern	-2.80	1.65E-111	3.31E-02	0.15	2.00E-57	5.27E-03	0.02	0.87	Yes
2023	Sea Ray SPX190	1	Bow	-2.39	2.84E-78	2.17E-02	0.19	1.91E-45	5.28E-03	0.01	0.95	Yes
		1	Stern	-2.71	1.55E-149	1.75E-02	0.17	1.70E-100	2.71E-03	0.01	0.97	Yes
2023	Nautique G23 Paragon	1	Bow	-1.56	6.35E-16	9.51E-02	-0.18	1.70E-06	2.93E-02	0.02	0.56	No
		1	Stern	-2.03	8.88E-121	1.40E-02	0.14	5.72E-76	2.56E-03	0.02	0.96	Yes
2023	Malibu VLX Wakesetter	1	Bow	-2.19	5.53E-70	1.77E-02	0.16	4.47E-39	4.71E-03	0.01	0.95	Yes
		1	Stern	-2.33	2.12E-70	3.71E-02	0.16	1.14E-39	6.45E-03	0.03	0.88	Yes
2023	Starcraft Limited 2000	2	Bow	-4.59	1.15E-189	1.97E-02	0.37	3.84E-154	2.79E-03	0.01	0.99	Yes
		2	Stern	-2.99	3.49E-19	2.09E-01	0.31	3.40E-14	2.96E-02	0.07	0.69	Yes
2023	Sea Ray SPX190	2	Bow	-4.32	5.88E-170	2.12E-02	0.37	4.17E-138	3.14E-03	0.01	0.99	Yes
		2	Stern	-2.20	7.00E-02	2.43E-01	0.24	8.19E-02	3.16E-02	0.07	0.98	Yes
2023	Nautique G23 Paragon	2	Bow	-1.96	1.43E-84	2.17E-02	0.20	6.15E-59	4.55E-03	0.04	0.96	Yes
		2	Stern	0.02	2.71E-01	2.17E-02	0.09	2.82E-09	8.75E-03	0.02	0.85	Yes
2023	Malibu VLX Wakesetter	2	Bow	-1.90	1.91E-56	3.03E-02	0.17	1.26E-30	7.69E-03	0.02	0.89	Yes
		2	Stern	-0.16	1.51E-16	1.39E-02	0.06	4.42E-20	3.85E-03	0.03	0.79	Yes

Table A5. Vertical (W_5) regression analysis information for ADCP bow and stern wave data

Test Year	Boat	Condition	Wave	b1	p-value1	standard error1	b2	p-value2	standard error2	RMSE	R^2	regression shown in report Figure 38
2022	Hurricane SS203	1	Bow	-4.95	1.16E-110	5.87E-02	0.17	5.00E-70	4.53E-03	0.01	0.92	Yes
		1	Stern	-4.23	7.29E-125	4.33E-02	0.12	1.41E-71	3.14E-03	0.03	0.91	Yes
2022	Cobalt R5	1	Bow	-4.74	6.03E-97	6.14E-02	0.14	1.50E-49	5.28E-03	0.01	0.87	Yes
		1	Stern	-4.01	1.10E-82	8.24E-02	0.09	1.20E-32	5.67E-03	0.03	0.68	Yes
2022	Cruisers Yachts 34GLS	1	Bow	-3.56	9.83E-78	2.59E-02	0.17	5.50E-51	3.40E-03	0.01	0.98	Yes
		1	Stern	-2.99	6.04E-95	1.61E-02	0.13	3.50E-71	1.50E-03	0.01	0.99	Yes
2022	Nautique G23 Paragon	1	Bow	-4.16	1.93E-61	8.07E-02	0.13	2.87E-23	9.05E-03	0.01	0.72	Yes
		1	Stern	-4.37	2.48E-143	2.70E-02	0.17	5.90E-107	2.11E-03	0.02	0.98	Yes
2022	Malibu VLX Wakesetter	1	Bow	-4.12	8.77E-97	4.34E-02	0.11	1.61E-47	4.11E-03	0.01	0.89	Yes
		1	Stern	-4.19	1.23E-157	1.69E-02	0.13	1.35E-110	1.39E-03	0.01	0.99	Yes
2022	Hurricane SS203	2	Bow	-5.80	5.48E-103	8.87E-02	0.23	1.52E-70	6.38E-03	0.04	0.91	Yes
		2	Stern	-4.28	3.24E-174	1.67E-02	0.18	2.95E-143	1.25E-03	0.02	0.99	Yes
2022	Cobalt R5	2	Bow	-4.40	2.51E-94	7.35E-02	0.15	6.58E-59	5.15E-03	0.04	0.88	Yes
		2	Stern	-5.17	5.00E-67	1.22E-01	0.22	9.65E-42	9.60E-03	0.02	0.83	Yes
2022	Cruisers Yachts 34GLS	2	Bow	-3.78	2.37E-147	2.69E-02	0.16	1.37E-117	1.92E-03	0.04	0.98	Yes
		2	Stern	-3.45	1.11E-94	2.66E-02	0.16	2.30E-68	2.65E-03	0.01	0.98	Yes
2022	Nautique G23 Paragon	2	Bow	-4.10	7.46E-85	5.30E-02	0.18	2.26E-52	5.31E-03	0.03	0.92	Yes
		2	Stern	-3.24	6.52E-114	3.03E-02	0.17	3.37E-92	2.56E-03	0.05	0.98	Yes
2022	Malibu VLX Wakesetter	2	Bow	-4.53	9.86E-31	1.67E-01	0.15	9.77E-07	2.67E-02	0.01	0.40	No
		2	Stern	-3.24	3.32E-123	2.12E-02	0.16	1.90E-96	1.91E-03	0.02	0.99	Yes
2023	Starcraft Limited 2000	1	Bow	-4.05	2.97E-93	4.97E-02	0.32	1.49E-59	8.87E-03	0.04	0.93	Yes
		1	Stern	-4.15	9.43E-111	5.88E-02	0.34	8.46E-78	8.59E-03	0.06	0.92	Yes
2023	Sea Ray SPX190	1	Bow	-3.90	2.36E-91	5.09E-02	0.33	4.02E-61	8.90E-03	0.04	0.93	Yes
		1	Stern	-3.65	1.39E-115	4.26E-02	0.30	7.99E-82	6.62E-03	0.04	0.94	Yes
2023	Nautique G23 Paragon	1	Bow	-3.96	4.46E-09	2.91E-01	0.53	1.07E-03	1.27E-01	0.01	0.57	No
		1	Stern	-3.41	5.32E-114	3.49E-02	0.33	2.33E-87	5.86E-03	0.04	0.97	Yes
2023	Malibu VLX Wakesetter	1	Bow	-3.64	1.58E-37	1.36E-01	0.35	6.93E-17	3.12E-02	0.07	0.65	Yes
		1	Stern	-4.07	3.18E-107	5.47E-02	0.38	8.74E-79	8.59E-03	0.05	0.94	Yes
2023	Starcraft Limited 2000	2	Bow	-4.19	6.68E-176	2.72E-02	0.32	8.52E-138	3.59E-03	0.02	0.98	No
		2	Stern	-3.98	8.67E-118	4.90E-02	0.34	3.20E-86	7.17E-03	0.06	0.94	Yes
2023	Sea Ray SPX190	2	Bow	-3.83	4.21E-170	2.21E-02	0.31	4.69E-135	3.13E-03	0.03	0.99	Yes
		2	Stern	-4.97	6.88E-84	8.95E-02	0.42	2.19E-51	1.54E-02	0.05	0.87	Yes
2023	Nautique G23 Paragon	2	Bow	-2.88	2.88E-63	4.69E-02	0.37	1.42E-45	1.11E-02	0.04	0.94	Yes
		2	Stern	-2.69	1.32E-69	4.23E-02	0.40	1.44E-56	9.33E-03	0.04	0.96	Yes
2023	Malibu VLX Wakesetter	2	Bow	-3.28	5.77E-34	1.00E-01	0.47	2.73E-20	2.99E-02	0.04	0.84	Yes
		2	Stern	-2.80	2.51E-63	5.49E-02	0.34	8.35E-44	1.19E-02	0.05	0.91	Yes

Table A6. Weather data obtained from Flying Cloud Airport, Eden Prairie, Minnesota, located 11 miles from the study site. Wind speed, wind direction, and air temperature are one-hour averages. Pre- indicates the hour immediately preceding testing of each condition, and Dur- indicates an hour during testing of each condition.

Test Year	Boat	Condition	Start Time	Stop Time	Wind Speed (mph)	Wind Direction (degrees)	Air Temperature (°F)
2022	Hurricane SS203	Pre- 1	10/4/22 10:06	10/4/22 11:06	10	350	76
		Dur- 1	10/4/22 11:06	10/4/22 12:07	13	10	80
2022	Hurricane SS203	Pre- 2	10/4/22 12:33	10/4/22 13:33	14	0	79
		Dur- 2	10/4/22 13:33	10/4/22 14:34	9	0	77
2022	Cobalt R5	Pre- 1	9/27/22 11:26	9/27/22 12:26	14	180	58
		Dur- 1	9/27/22 12:26	9/27/22 13:25	12	180	59
2022	Cobalt R5	Pre- 2	9/27/22 13:56	9/27/22 14:56	13	170	59
		Dur- 2	9/27/22 14:56	9/27/22 15:56	12	200	59
2022	Cruisers Yatchs 34GLS	Pre- 1	10/5/22 10:00	10/5/22 11:00	5	290	70
		Dur- 1	10/5/22 11:00	10/5/22 12:00	10	110	70
2022	Cruisers Yatchs 34GLS	Pre- 2	10/5/22 12:00	10/5/22 13:00	9	110	69
		Dur- 2	10/5/22 13:00	10/5/22 13:59	5	260	71
2022	Nautique G23 Paragon	Pre- 1	9/28/22 10:00	9/28/22 11:00	3	Variable	57
		Dur- 1	9/28/22 11:00	9/28/22 12:00	3	Variable	59
2022	Nautique G23 Paragon	Pre- 2	9/28/22 12:35	9/28/22 13:35	8	310	60
		Dur- 2	9/28/22 13:35	9/28/22 14:35	9	330	62
2022	Malibu VLX Wakesetter	Pre- 1	10/10/22 10:20	10/10/22 11:20	8	10	67
		Dur- 1	10/10/22 11:20	10/10/22 12:20	12	350	69
2022	Malibu VLX Wakesetter	Pre- 2	10/10/22 13:05	10/10/22 14:05	9	10	71
		Dur- 2	10/10/22 14:05	10/10/22 15:06	8	20	71
2023	Starcraft Limited 2000	Pre- 1	9/27/23 11:05	9/27/23 12:05	9	260	70
		Dur- 1	9/27/23 12:05	9/27/23 13:05	5	270	71
2023	Starcraft Limited 2000	Pre- 2	9/27/23 13:24	9/27/23 14:24	5	250	71
		Dur- 2	9/27/23 14:24	9/27/23 15:26	5	250	72
2023	Sea Ray SPX190	Pre- 1	10/9/23 11:09	10/9/23 12:09	14	130	55
		Dur- 1	10/9/23 12:09	10/9/23 13:08	13	140	56
2023	Sea Ray SPX190	Pre- 2	10/9/23 13:32	10/9/23 14:32	9	150	56
		Dur- 2	10/9/23 14:32	10/9/23 15:31	15	140	56
2023	Nautique G23 Paragon	Pre- 1	10/16/23 10:31	10/16/23 11:31	6	0	56
		Dur- 1	10/16/23 11:31	10/16/23 12:31	8	130	57
2023	Nautique G23 Paragon	Pre- 2	10/16/23 12:46	10/16/23 13:46	7	320	59
		Dur- 2	10/16/23 13:46	10/16/23 14:46	8	110	61
2023	Malibu VLX Wakesetter	Pre- 1	10/17/23 10:15	10/17/23 11:15	7	210	61
		Dur- 1	10/17/23 11:15	10/17/23 12:15	7	230	63
2023	Malibu VLX Wakesetter	Pre- 2	10/17/23 12:30	10/17/23 13:30	7	340	65
		Dur- 2	10/17/23 13:30	10/17/23 14:31	6	0	65

References

Bian, C., Liu, Z., Huang, Y., Zhao, L., & Jiang, W. (2018). On estimating turbulent Reynolds stress in wavy aquatic environment. Journal of Geophysical Research: Oceans, 123(4), 3060-3071. http:/doi.org/10.1002/2017JC013230

Biron, P. M., Robson, C., Lapointe, M. F., & Gaskin, S. J. (2004). Comparing different methods of bed shear stress estimates in simple and complex flow fields. Earth Surface Processes and Landforms, 29(11), 1403-1415. http://doi.org/10.1002/esp.1111

Bricker, J. D., & Monismith, S. G. (2007). Spectral wave–turbulence decomposition. Journal of Atmospheric and Oceanic Technology, 24(8), 1479-1487. https://doi.org/10.1175/JTECH2066.1

Cannon, D., Kibler, K. M., Kitsikoudis, V., Medeiros, S. C., & Walters, L. J. (2022). Variation of mean flow and turbulence characteristics within canopies of restored intertidal oyster reefs as a function of restoration age. Ecological Engineering, 180, 106678. http://doi.org/10.1016/j.ecoleng.2022.106678

Egan, G., Cowherd, M., Fringer, O., & Monismith, S. (2019). Observations of near-bed shear stress in a shallow, wave-and current-driven flow. Journal of Geophysical Research: Oceans, 124(8), 6323-6344. https://doi.org/10.1029/2019JC015165

Fischenich, J. C. (2001). Stability thresholds for stream restoration materials, U.S. Army Engineer Research and Development Center (ERDC), Vicksburg, Mississippi, Technical Note No. EMRRP-SR-29.

Fleit, G., & Baranya, S. (2021). Acoustic measurement of ship wave–induced sediment resuspension in a large river. Journal of Waterway, Port, Coastal, and Ocean Engineering, 147(2), 04021001. https://doi.org/10.1061/(ASCE)WW.1943-5460.0000627

Garcia, M. H., Admiraal, D. M., Rodriguez, J. F., and Lopez, F. (1998). Navigation-induced bed shear stresses: laboratory measurements, data analysis and field application. Civil Engineering Studies, Hydraulic Engineering Series No. 56, University of Illinois at Urbana-Champaign.

Green, M. O., & Coco, G. (2014). Review of wave-driven sediment resuspension and transport in estuaries. Reviews of Geophysics, 52(1), 77-117. https://doi.org/10.1002/2013RG000437

Green, M. O., & MacDonald, I. T. (2001). Processes driving estuary infilling by marine sands on an embayed coast. Marine Geology, 178(1-4), 11-37. https://doi.org/10.1016/S0025-3227(01)00188-8

Hansen, J. C. R., & Reidenbach, M. A. (2012). Wave and tidally driven flows in eelgrass beds and their effect on sediment suspension. Marine Ecology Progress Series, 448, 271-287. https://doi.org/10.3354/meps09225

Kim, S. -C., Friedrichs, C. T., Maa, J. P.-Y., & Wright, L. D. (2000). Estimating bottom stress in tidal boundary layer from acoustic Doppler velocimeter data. Journal of Hydraulic Engineering, 126(6), 399-406. https://doi.org/10.1061/(ASCE)0733-9429(2000)126:6(399)

Koch, C., & Chanson, H. (2008). Turbulent mixing beneath an undular bore front. Journal of Coastal Research, 24(4), 999-1007. https://doi.org/10.2112/06-0688.1

Maynord, S.T. (1990). Velocities induced by commercial navigation. U.S. Army Engineer Research Waterways Experiment Station, Technical Report No. HL-90-15, Vicksburg, Mississippi.

Nortek (2025). Guide to understanding adcps. Retrieved from: https://www.nortekgroup.com/knowledge-center/wiki/guide-to-understanding-adcps

Parsheh, M., Sotiropoulos, F., & Porté-Agel, F. (2010). Estimation of power spectra of acoustic-doppler velocimetry data contaminated with intermittent spikes. Journal of Hydraulic Engineering, 136(6), 368-378. https://doi.org/10.1061/(ASCE)HY.1943-7900.0000202

Rodriguez, J. F., Admiraal, D. M., López, F., & Garcia, M. H. (2002). Unsteady bed shear stresses induced by navigation: laboratory observations. Journal of Hydraulic Engineering, 128(5), 515-526.